

# **SINGLE-PHASE CONVECTIVE HEAT TRANSFER AND PRESSURE DROP COEFFICIENTS IN CONCENTRIC ANNULI**

**Warren Reece van Zyl**

**25227531**

**30 June 2013**

---



University of Pretoria

**University of Pretoria**

Department of Mechanical

and Aeronautical Engineering

Supervisors:      Dr J Dirker  
                                 Prof J.P Meyer

## Abstract

Varying diameter ratios associated with smooth concentric tube-in-tube heat exchangers are known to have an effect on its convective heat transfer capabilities. Much literature exists for predicting the inner tube's heat transfer coefficients, however, limited research has been conducted for the annulus and some of the existing correlations are known to have large errors.

Linear and nonlinear regression models exist for determining the heat transfer coefficients, however, these are complex and time consuming methods and require much experimental data in order to obtain accurate solutions. A direct solution to obtain the heat transfer coefficients in the annulus is sought after.

In this study a large dataset of experimental measurements on heat exchangers with annular diameter ratios of 0.483, 0.579, 0.593 and 0.712 was gathered. The annular diameter ratio is defined as the ratio of the outer diameter of the inner tube to the inner diameter of the outer tube. Using various methods, the data was processed to determine local and average Nusselt numbers in the turbulent flow regime. These methods included the modified Wilson plot technique, a nonlinear regression scheme, as well as the log mean temperature difference method. The inner tube Reynolds number exponent was assumed to be a constant 0.8 for both the modified Wilson plot and nonlinear regression methods. The logarithmic mean temperature difference method was used for both a mean analysis on the full length of the heat exchanger, and a local analysis on finite control volumes. Friction factors were calculated directly from measured pressure drops across the annuli.

The heat exchangers were tested for both a heated and cooled annulus, and arranged in a horizontal counter-flow configuration with water as the working medium. Data was gathered for Reynolds numbers (based on the hydraulic diameter) varying from 10 000 to 28 000 for a heated annulus and 10 000 to 45 000 for a cooled annulus. Local inner wall temperatures which are generally difficult to determine, were measured with thermocouples embedded within the wall. Flow obstructions within the annuli were minimized, with only the support structures maintaining concentricity of the inner and outer tubes impeding flow.

Energy balances between 2% and 4.5%, for the heated and cooled annulus respectively, were achieved. The logarithmic mean temperature difference results differed from those of the linear and nonlinear regression schemes by up to 4% and 7% for a heated and cooled annulus respectively. Differences from recently published correlations were between 14% and 7% for the heated and cooled annulus respectively. Local heat transfer analyses showed larger heat transfer coefficients at the annulus inlet and decreasing towards the outlet by 50% of the inlet value. Measured wall temperatures deviated from those predicted by the linear regression method by a maximum of 1.5°C, and 2.5°C for the nonlinear regression scheme.

Friction factors showed a stronger dependence on annular ratio than is accounted for by recently published correlations. Lower annular ratios produced larger friction factors with a maximum difference of 13% between friction factors from the smallest annular diameter ratio of 0.483 and largest annular diameter ratio of 0.712. Larger friction factors were obtained for a cooled annulus.

## **Publications in Journals and Conferences**

Van Zyl, W.R., Dirker, J. & Meyer, J.P., Single-Phase Convective Heat Transfer and Pressure Drop Coefficients in Concentric Annuli, Heat Transfer Engineering, accepted November 2012.

Van Zyl, W.R., Dirker, J. & Meyer, J.P., Single-Phase Heat Transfer and Pressure Drop Coefficients in Smooth Concentric Annuli, Proceeding of the Ninth International Conference on Heat Transfer, Fluid Mechanics and Thermodynamics (HEFAT 2012), Malta, pp 753 – 762, 16 – 18 July 2012,.

## Acknowledgements

The following people and institutions have made invaluable contributions to my work and I would like to thank them for their continuous help and support:

Dr J. Dirker for his relentless contributions and guidance without which the completion of this study would have been a far more daunting undertaking.

Prof J.P Meyer for invaluable insight and knowledge in the field of heat transfer.

Mr M. Ntuli for constantly leading me in the right direction and willingly parting his knowledge and experience with this study.

Mr D. Gouws who offered his hand and advice with all aspects involving experimentation and laboratory practices; and his ability to identify a problem before it happened.

Mr N. Smit for his vast knowledge in manufacturing processes and his commitment to helping me.

Mr K. Ntombeni for being an extra set of hands when two were just not enough, as well as his experience and knowledge in manufacturing heat exchangers.

To my family: my Mother, who is my tower of strength and can always offer me motivation even at the hardest of times. My father; whom without I could never be the person I am today and who will willingly give up anything to come to my aid. My two brothers and best friends: Dylan and Linton. You have always been there for me in every aspect of life, from day one. You laid the foundations in my life and made me not have to look far for my role models.

Lastly to my friends and colleagues who stood by me through it all, I can never thank you enough.

# Contents

Abstract .....	i
Publications in Journals and Conferences .....	iii
Acknowledgements .....	iv
List of Figures.....	viii
List of Tables .....	xi
Nomenclature .....	xii
1 Introduction .....	1
1.1 Introduction .....	1
1.2 Objectives .....	2
1.3 Layout of Report .....	2
1.3.1 Notation .....	3
2 Literature Study .....	4
2.1 Existing Nusselt Number Correlations .....	4
2.2 Numerical Methods to Determine Heat Transfer Correlations .....	10
2.3 Wilson Plot Method (Linear Regression Analysis) .....	11
2.4 Khartabil and Christensen Method (Nonlinear Regression Analysis).....	11
2.5 Friction Factors .....	12
2.6 Spacers and Tube Concentricity .....	15
2.7 Annulus Entry Lengths.....	15
2.8 Equivalent Diameters .....	15
3 Experimental Setup .....	17
3.1 Introduction .....	17
3.2 Experimental Facility.....	17

3.3	Test Sections .....	20
3.4	Inner Tube Construction .....	21
3.5	Inner Tube Inlet and Outlet Sections .....	24
3.6	Outer Tube.....	26
3.7	Complete Heat Exchanger Test Section .....	28
3.8	Insulation .....	29
4	Data Reduction.....	32
4.1	Introduction .....	32
4.2	LMTD Method for the Mean Heat Transfer Coefficient .....	32
4.3	LMTD Method for the Local Heat Transfer Coefficient .....	34
4.4	Modified Wilson Plot Method (1969) .....	36
4.5	Khartabil and Christensen Method (1992).....	36
4.6	Energy Balance.....	37
4.7	Friction Factors .....	37
5	Data Analysis.....	38
5.1	Introduction .....	38
5.2	Mean Heat Transfer .....	39
5.3	Inner Tube Reynolds Number Exponent .....	41
5.4	Wall Temperature Analysis .....	45
5.5	Local Heat Transfer Rates.....	48
5.6	Energy Balance.....	54
5.7	Friction Factor .....	55
5.8	Colburn j-Factor .....	57
5.9	Other Test Section Results .....	62
5.10	Conclusion.....	64
6	Influence of Annular Diameter Ratio .....	65

6.1	Introduction .....	65
6.2	Mean Heat Transfer .....	65
6.3	Friction Factors .....	71
6.4	Colburn j-Factor .....	72
6.5	Modified Wilson Plot and Khartabil and Christensen Coefficients .....	76
6.6	Conclusion .....	79
7	Conclusion.....	80
7.1	Heat Transfer .....	80
7.2	Friction Factor.....	81
7.3	Influence of Annular Diameter Ratio .....	82
8	References .....	83

## Appendices

A	The Wilson Plot Method.....	A.1
A.1	Introduction.....	A.1
A.2	The Modified Wilson Plot Technique Explained.....	A.1
A.3	Comparison of Modified Wilson Plot Wall Temperatures to Measured Wall Temperatures.....	A.14
A.4	Heat Transfer Coefficient Analysis.....	A.20
B	Khartabil and Christensen Nonlinear Regression.....	B.1
B.1	Introduction.....	B.1
B.2	The Nonlinear regression method explained.....	B.1
B.3	Comparison of Khartabil and Christensen Wall Temperatures to Measured Wall Temperatures.....	B.11
B.4	Heat Transfer Coefficient Analysis.....	B.16
C	Test Section Results	
C.1	Introduction.....	C.1
C.2	Annular diameter Ratio 0.482.....	C.1



C.3	Annular Diameter Ratio 0.579.....	C.7
C.4	Annular Diameter Ratio 0.712.....	C.13
C.5	Energy Balance.....	C.18
C.6	Summary.....	C.19
C.7	Discussion.....	C.21
D	Uncertainty Analysis.....	D.1
D.1	Introduction.....	D.1
D.2	Cause and Types of Experimental Errors.....	D.1
D.3	Generalized Uncertainty Analysis Methods.....	D.2
D.4	Quantifying Uncertainties.....	D.4

## List of Figures

Figure 2.1: Ratio of the experimental Nusselt numbers of Petukhov and Roizen (1964) and Leung et al (1962) to the Nusselt numbers of Equation (2.21). Extracted from Gnielinski (2009). .....	9
Figure 2.2: Ratio of the experimental Nusselt numbers of Dirker and Meyer (2004) to the Nusselt numbers of Equation(2.21). Extracted from Gnielinski (2009). .....	10
Figure 2.3: Friction factors calculated using the correlations of Table 2.3.....	14
Figure 3.1: Schematic representation of the experimental facility used. ....	18
Figure 3.2: Cross section of the heat exchanger test section showing the diameters of the inner tube and outer tube. ....	21
Figure 3.3: Three methods used for attaching thermocouples to the inner tube wall used in Ntuli et al (2011)..	22
Figure 3.4: Cross section of the inner tube wall showing the method used to attach the thermocouples. ....	23
Figure 3.5: Bush used to reattach the two ends of the inner tube.....	23
Figure 3.6: Schematic representation of the reconstructed inner tube and respective thermocouple attachments. (Not drawn to scale) .....	24
Figure 3.7: a) Inlet and Outlet sections for the inner tube. b) Circumferential locations of thermocouples attached to the inner tube inlet and outlet sections. ....	25
Figure 3.8: Spacer used to hold the inner tube and annulus concentric.....	27
Figure 3.9: Schematic of a completed heat exchanger with dimensions provided in Table 3.5. ....	28
Figure 4.1: Heat exchanger divided into nine control volumes to calculate the local heat transfer. ....	34
Figure 4.2: A single control volume used to calculate the local heat transfer.....	35
Figure 5.1: Reynolds numbers for both the inner tube and annulus for a a) cooled b) heated annulus. ....	38
Figure 5.2: Nusselt numbers for cooling of the annulus with an annular diameter ratio of 0.593. ....	39
Figure 5.3: Heat transfer coefficients for heating of the annulus with an annular diameter ratio of 0.593. ....	40
Figure 5.4: Ratio of Nusselt numbers with different inner Reynolds number exponents using the modified Wilson plot method. ....	43
Figure 5.5: Ratio of Nusselt numbers with different Inner Reynolds number exponents using the nonlinear regression method. ....	43
Figure 5.6: Wall temperature profiles for the inner tube fluid, inner tube wall and annulus wall for a cooled annulus with low inner tube flow rates and a) low annular flow rates b) high annular flow rates...	46
Figure 5.7: Wall temperature profiles for the inner tube fluid, inner tube wall and annulus wall for a cooled annulus with high inner tube flow rates and a) low annular flow rates b) high annular flow rates..	46
Figure 5.8: Wall temperature profiles for the inner tube fluid, inner tube wall and annulus wall for a heated annulus with low inner tube flow rates and a) low annular flow rates b) high annular flow rates...	47
Figure 5.9: Wall temperature profiles for the inner tube fluid, inner tube wall and annulus wall for a heated annulus with high inner tube flow rates and a) low annular flow rates b) high annular flow rates..	47

Figure 5.10: Local LMTD Nusselt numbers for control volumes 1 – 9, compared to the mean LMTD heat transfer coefficients and those calculated from Dirker and Meyer (2004) and Gnielinski (2009) for the case of cooling the annulus. .... 50

Figure 5.11: Local LMTD Nusselt numbers for control volumes 1 – 9, compared to the mean LMTD heat transfer coefficients and those calculated from Dirker and Meyer (2004) and Gnielinski (2009) for the case of heating the annulus. .... 51

Figure 5.12: Local Nusselt numbers as a function of axial distance along the heat exchanger length for various  $Re_{DhLocal}$  and  $Re_i = 20\ 000$  for a cooled annulus..... 52

Figure 5.13: Local Nusselt numbers as a function of axial distance along the heat exchanger length for various  $Re_{DhLocal}$  and  $Re_i = 30\ 000$  for a cooled annulus. .... 53

Figure 5.14: Local Nusselt numbers as a function of axial distance along the heat exchanger length for various  $Re_{DhLocal}$  and  $Re_i = 19\ 000$  for a heated annulus. .... 53

Figure 5.15: Local Nusselt numbers as a function of axial distance along the heat exchanger length for various  $Re_{DhLocal}$  and  $Re_i = 24\ 000$  for a heated annulus..... 54

Figure 5.16: Energy balance for both heating and cooling of the annulus..... 55

Figure 5.17: Diabatic friction factors for a heated and cooled annulus, compared to the correlations of Blasius, Jones and Leung (1981), Kaneda et al (2003) and Gnielinski (2009). .... 56

Figure 5.18: Nusselt numbers obtained using the modified Wilson plot technique for a heated and cooled annulus for an annular diameter ratio of 0.593..... 57

Figure 5.19: Colburn j-factors for both a heated and cooled annulus for an annular diameter ratio of 0.593. ... 59

Figure 5.20: Comparison of the friction factor and Colburn j-factor for a heated and cooled annulus. .... 60

Figure 5.21: Ratio of Colburn j-factor to experimental friction factor. .... 61

Figure 6.1: Comparison of Nusselt numbers for various annular diameter ratios at  $Re_{Dh} = 10\ 000$  for a cooled annulus..... 66

Figure 6.2: Comparison of Nusselt numbers for various annular diameter ratios at  $Re_{Dh} = 25\ 000$  for a cooled annulus..... 67

Figure 6.3: Comparison of Nusselt numbers for various annular diameter ratios at  $Re_{Dh} = 10\ 000$  for a heated annulus. .... 67

Figure 6.4: Comparison of Nusselt numbers for various annular diameter ratios at  $Re_{Dh} = 25\ 000$  for a heated annulus. .... 68

Figure 6.5: General trends present in Nusselt numbers as a function of annular diameter ratio for a heated and cooled annulus..... 69

Figure 6.6: Comparison of Nusselt numbers obtained from the modified Wilson plot method for various annular diameter ratios at  $Re_{Dh} = 10\ 000$ , for a heated and cooled annulus..... 70

Figure 6.7: Comparison of Nusselt numbers obtained from the modified Wilson plot method for various annular diameter ratios at  $Re_{Dh} = 25\ 000$ , for a heated and cooled annulus..... 70

Figure 6.8: Friction factors for various annular diameter ratios for a heated and cooled annulus with  $Re_{Dh} = 10\ 000$  and  $Re_i = 20\ 000$ . .... 71

Figure 6.9: Friction factors for various annular diameter ratios for a heated and cooled annulus with  $Re_{Dh} = 20\ 000$  and  $Re_i = 20\ 000$ . ..... 72

Figure 6.10: The relationship between the Colburn  $j$ -factor and annular diameter ratio for a cooled annulus with  $Re_{Dh} = 10\ 000$ . ..... 73

Figure 6.11: The relationship between the Colburn  $j$ -factor and annular diameter ratio for a cooled annulus with  $Re_{Dh} = 25\ 000$ . ..... 74

Figure 6.12: The relationship between the Colburn  $j$ -factor and annular diameter ratio for a heated annulus with  $Re_{Dh} = 10\ 000$ . ..... 75

Figure 6.13: The relationship between the Colburn  $j$ -factor and annular diameter ratio for a heated annulus with  $Re_{Dh} = 25\ 000$ . ..... 75

Figure 6.14: Comparison of Colburn  $j$ -factors for a heated and cooled annulus with  $Re_{Dh} = 25\ 000$ . ..... 76

Figure 6.15: Sieder and Tate type equation coefficients a)  $C_i$ , b)  $C_o$ , and c)  $P$ , obtained from the modified Wilson plot technique of Briggs and Young (1969), for various annular diameter ratios for a heated and cooled annulus. .... 77

Figure 6.16: Sieder and Tate type equation coefficients a)  $C_i$ , b)  $C_o$ , and c)  $P$ , obtained from the Khartabil and Christensen (1992) method, for various annular diameter ratios for a heated and cooled annulus. 78

## List of Tables

<i>Table 2.1: Equations available from literature describing the Nusselt number in a smooth concentric annulus for forced convection in fully developed turbulent flow. Adapted from Dirker and Meyer (2005).....</i>	<i>7</i>
<i>Table 2.2: Equations from recent publications describing the Nusselt number in a smooth concentric annulus for forced convection.....</i>	<i>8</i>
<i>Table 2.3: Equations available in literature describing the friction factor in a smooth concentric annulus for forced convection.....</i>	<i>13</i>
<i>Table 3.1: Components present in the experimental facility and their useful working ranges.....</i>	<i>19</i>
<i>Table 3.2: Tube diameters and annular diameter ratios for the four heat exchangers tested.....</i>	<i>21</i>
<i>Table 3.3: Dimensions of the two bushes used on the two inner tubes. Refer to Figure 3.5 for a description of the dimension parameters.....</i>	<i>24</i>
<i>Table 3.4: Maximum distance between spacers for the associated inner tubes.....</i>	<i>27</i>
<i>Table 3.5: Dimensions of all four heat exchangers (refer to Figure 3.9 for labels).....</i>	<i>29</i>
<i>Table 3.6: Theoretical heat loss using 25mm and 50mm thick insulation with <math>D_{oo} = 28.58\text{mm}</math> and maximum temperature gradient of <math>10^{\circ}\text{C}</math>.....</i>	<i>30</i>
<i>Table 3.7: Theoretical heat loss using 25mm and 50mm thick insulation with <math>D_{oo} = 34.93\text{mm}</math> and maximum temperature gradient of <math>10^{\circ}\text{C}</math>.....</i>	<i>30</i>
<i>Table 5.1: Legend used In Figure 5.6 to Figure 5.9.....</i>	<i>45</i>
<i>Table 5.2: Coefficient of determination for wall temperature curve fits.....</i>	<i>49</i>
<i>Table 5.3: Constants <math>C_1</math>, <math>C_2</math> and <math>C_3</math> for the polynomial curves fitted through the experimental Colburn <math>j</math>-factors.....</i>	<i>58</i>
<i>Table 5.4: Constant <math>C_4</math>, <math>C_5</math> and <math>C_6</math> used in the polynomial given in Equation (5.8).....</i>	<i>61</i>
<i>Table 5.5: Percentage difference comparison of <math>Nu</math>, <math>f</math>, and the <math>j</math>-factor for a heated and cooled annulus.....</i>	<i>62</i>
<i>Table 5.6: Percentage difference for <math>Nu_{wp}</math> and <math>f</math> when compared to the correlations of Gnielinski (2009).....</i>	<i>63</i>
<i>Table 5.7: Mean and maximum energy balances.....</i>	<i>63</i>

## Nomenclature

$A_i$	Cross Sectional Area of Inner Tube	$m^2$
$A_o$	Cross Sectional Area of Annulus	$m^2$
$A_s$	Outer Heat Transfer Surface of the Inner Tube	$m^2$
$a$	Annular Diameter Ratio ( $D_1/D_o$ )	-
$C_p$	Specific Heat	$kJ/Kg.K$
$C_i$	Inner Tube Correlation Coefficient	-
$C_o$	Outer Tube Correlation Coefficient	-
$CV$	Control Volume	-
$C_1$	Constant for Colburn j-factor Curve Fit	-
$C_2$	Constant for Colburn j-factor Curve Fit	-
$C_3$	Constant for Colburn j-factor Curve Fit	-
$C_4$	Constant for Ratio of Friction Factor and Colburn j-factor Curve Fit.	-
$C_5$	Constant for Ratio of Friction Factor and Colburn j-factor Curve Fit.	-
$C_6$	Constant for Ratio of Friction Factor and Colburn j-factor Curve Fit.	-
$D_1$	Outer Diameter of Inner Tube	$m$
$D_o$	Inner Diameter of Outer Tube	$m$
$D_{ib}$	Inner Diameter of Bush	$m$
$D_{oo}$	Outer Diameter of the Outer Tube	$m$
$E$	Modulus of Elasticity	$GPa$
$eb$	Energy Balance Error	-
$F_{ann}$	Factor taking into account the annular diameter ratio in Equation (2.2)	-
$f$	Friction Factor	-
$g$	Gravitational Acceleration	$m/s^2$
$h$	Heat Transfer Coefficient	$W/m^2K$
$I_x$	Second Moment of Perpendicular to the Axial Direction	$m^4$
$j$	Colburn j-factor	-
$k$	Thermal Conductivity	$W/mK$
$k_1$	Factor in Equation(2.2)	-

$K$	Factor to take into account the temperature dependence of fluid properties	-
$L$	Tube Length	m
$L_b$	Length of Inner Tube Connector Bush	m
$L_{hx}$	Heat Transfer Length	m
$L_{dP}$	Pressure Drop Length	m
$L_i$	Length of Inner Tube	m
$L_{ij}$	Length of Inner Tube Inlet/Outlet Sections	m
$L_{max}$	Maximum Distance Between Annulus Supports	m
$L_{TIW}$	Distance Between Inner Tube Thermocouples	m
$L_{TO}$	Distance Between Outer Tube Thermocouples	m
$L_{TO1}$	Distance of Annulus Inlet and Outlet to the Inner tube Inlet and Outlet	m
$L_{spacer}$	Distance Between Spacers	m
$L_{unsupported}$	Unsupported Axial length of Tube	m
$M$	Inner Tube Mass per Meter	kg/m
$\dot{m}$	Mass Flow Rate	kg/s
$N$	Number of Data Points	-
$N_{cv}$	Number of Control Volumes	-
$N_i$	Number of Thermocouples on the Inner Tube	-
$n$	Prandtl Number Exponent	-
$Nu$	Nusselt Number	-
$\overline{Nu}$	Mean Nusselt Number	-
$\Delta p$	Pressure Drop	Pa
$P$	Annulus Reynolds Number Exponent	-
$P_i$	Inner Tube Reynolds Number Exponent	-
$Pr$	Prandtl Number	-
$\dot{Q}$	Heat Transfer Rate	W
$\overline{Q}$	Mean Heat Transfer Rate	W
$\dot{Q}_{loss}$	Heat Lost to Surroundings	W
$Re$	Reynolds Number	-
$\overline{Re}$	Mean Reynolds Number	-
$Re^*$	Modified Reynolds Number	-
$R^2$	Coefficient of Determination	-

$r_h$	Hydraulic radius	m
$T$	Temperature	°C
$T_b$	Bulk Annulus Temperature	°C
$\bar{T}$	Mean Temperature	°C
$\hat{T}$	Predicted Temperature	°C
$T_{LMTD}$	Log Mean Temperature Difference	°C
$V$	Average Velocity	m/s
$w$	Distributed Load	N/m
$x$	Axial Coordinate Along Heat Exchanger	m
$y$	Vertical Direction Perpendicular to the Heat Exchanger Length	-
$y_\delta$	Vertical Displacement	m
$z$	Exponent in Equation (2.5)	-

## Greek Symbols

$\mu$	Viscosity	kg/m. s
$\rho$	Density	kg/m <sup>3</sup>
$\tau$	Ratio of Friction Factor and Colburn j-factor	-
$\zeta$	Factor in Equation (2.15)	-

## Subscripts

CV	Control Volume
Dh	Based on the Hydraulic Diameter
$f$	Based on Film Temperature, $T_f = \frac{1}{2}(T_b + T_{w,o})$
i	Inner
ii	Inner tube inlet
ins	Referring to the insulation
io	Inner tube outlet
j	Index
LMTD	Based on the Logarithmic Mean Temperature Difference Method
Local	Referring to a Control Volumes Local Property
mean	Referring to a Property Calculated Using Mean Values Over the Heat



## Exchanger Test Section Length

o	Outer/Annular
oi	Annular inlet
oo	Annular outlet
Pi	Based on a Range of Inner Reynolds Number Exponents
ratio	Ratio of Nusselt Numbers
w	Inner Tube Wall
o	Annulus side
$\infty$	Ambient
0.8	Based on a Inner Reynolds Number Exponent of 0.8

# Chapter 1

## Introduction

### 1.1 Introduction

Convection heat transfer is the main heat transfer mechanism in most heat exchangers used for a wide range of applications. These include small scale applications such as cooling of electronic equipment to much larger scale applications such as cooling plants in electricity generation. Whatever the application may be, the convection heat transfer mechanism needs to be thoroughly understood in order to optimally design heat exchangers.

One of the simplest types of heat exchanger is a tube-in-tube heat exchanger. This consists of a smooth annular passage with an inner tube held concentrically inside an outer tube. A counter flow configuration is normally used for these heat exchangers.

In the design of such heat exchangers, one needs to determine the physical dimensions in order to provide sufficient, heating or cooling of the fluid within the restriction of the available pumping power. This is done by determining the heat transfer coefficients and friction factors associated with the heat exchanger. Over the years much work has been performed to understand the heat transfer mechanisms within smooth tube-in-tube heat exchangers, and attempts have been made to develop correlations for predicting the Nusselt numbers as a function of the Reynolds number. Some existing correlations are reported by Dirker and Meyer (2004) to be inconsistent with each other and it has been found that some heat transfer predictions from these may differ by up to 20% depending on the Reynolds number. Much attention is given to the effect that the annular diameter ratio has on the heat transfer and pressure drop within the annulus.

## 1.2 Objectives

Possible reasons for inconsistencies in the existing correlations in the literature was investigated experimentally. Heat transfer and pressure drop data for test sections for various annular diameter ratios was gathered. The test facility used was designed specifically to accommodate different heat exchanger test sections. All work done in this study was performed in a fully turbulent flow regime with Reynolds numbers based on the hydraulic diameter between 10 000 and 40 000. The main objectives of this study were:

- To determine the mean Nusselt numbers over the entire heat exchanger test section length using various methods presented in the literature.
- To calculate friction factors directly from measured pressure drops across the pressure drop length.
- To compare the different methods of calculating the mean heat transfer from experimental data.
- To accurately measure the inner and outer tube wall temperatures.
- To determine the local heat transfer over finite control volumes spaced equally over the heat exchanger length. By using the local heat transfer the effect of axial location on the heat transfer was investigated.
- To investigate the effects of the annular diameter ratio on heat transfer and friction factors.

## 1.3 Layout of Report

The main text consists of seven chapters. These include Chapter 2, the literature survey. Chapter 3 explains the experimental facility and test sections used. Chapter 4 introduces the methods used to analyze the experimental data. Chapter 5 presents the results for the test section with an annular diameter ratio of 0.593. Chapter 6 presents a comparison of all four annular diameter ratios. Chapter 7 concludes all the results. Appendix A provides the methods used in implementing the modified Wilson plot technique of Briggs and Young (1915). Appendix B shows how the nonlinear regression of Khartabil and Christensen (1915) is implemented. Appendix C provides the results of the heat exchangers

not included in the texts main body. Appendix D investigates the uncertainties on the system and results.

### **1.3.1 Notation**

Four annular diameter ratios were investigated for the case of both a heated and cooled annulus. All figures presenting results of a cooled annulus are in blue with a heated annulus presented in red.

Nomenclature declared in the main text document and are which are used in the Appendices are not declared again in the Appendices. Nomenclature which only appears in the Appendices are declared in separate nomenclature lists for each Appendix.

# Chapter 2

## Literature Study

### 2.1 Existing Nusselt Number Correlations

Due to the complexities of turbulent flow, up to now no analytical correlations for predicting Nusselt numbers have been developed, unlike the laminar flow regime where theoretical correlations have been developed. It is thus required that experimental data in the turbulent regime is used to obtain a correlation, as explained by Gnielinski (2009). Correlations for predicting the Nusselt number in the annulus for various flow properties and mediums are summarized in Table 2.1(extracted from Dirker and Meyer (2004)). Here Equation (2.15)of Pethukov and Roizen (1964), however, was altered from the original publication of Dirker and Meyer (2004) as Gnielinski (2009) suggests that it was originally based on the hydraulic diameter. These correlations correspond to the Dittus-Boelter form of the equation and with an exception of a few, depend on the annular diameter ratio of the heat exchanger. The annular diameter ratio ( $a$ ) is the ratio of the outer diameter of the inner tube to the inner diameter of the outer tube.

$$a = \frac{D_1}{D_o} \tag{2.1}$$

An annular diameter ratio of 0.0 would suggest an outer tube with a thin wire as an inner tube and an annular diameter ratio of 1.0 would suggest a parallel plate geometry. Gnielinski (2009) reports that the direction of heat flux (heating or cooling of the annulus) influences the heat transfer of the heat exchanger as the physical fluid properties will change as they are temperature dependent. No direct investigations that deal specifically with this are available; this is evident from the correlations in Table 2.1. These equations often give erroneous results when applied to cases where the limiting range of the diameter ratio is exceeded according to Davis (1943). To rectify this, Equation (2.9) of Davis (1943) was then created for a wide range of diameter ratios.

Dirker and Meyer (2004) compared the correlations of Table 2.1 for arbitrary values of the diameter ratio and Prandtl numbers. Neither of these equations were found to be in close agreement with each other and the results produced Nusselt numbers within 20% of the average predicted values. Equation (2.11) proposed by Foust and Christian (1940) produced Nusselt numbers of order of magnitude 3 times greater than the other equations.

More recent equations to predict the Nusselt number within an annulus are presented in Table 2.2. Equation (2.20) proposed by Dirker and Meyer (2004) produced Nusselt numbers accurate to within 3% from their experimental data.

Most recently Gnielinski (2009) modified a semi-empirical correlation available for fully developed tube flow to accommodate annular ducts. The modification as explained by Gnielinski (2009) for annular ducts is necessary for two reasons:

- 1 The friction factor in annular ducts differs from tubes due to the different velocity profiles of the fluid, and thus the friction factor depends on the diameter ratio.
- 2 More accurate data made available recently would lead to a more accurate correlation.

Using several sets of experimental data to derive a correlation, Gnielinski (2009) proposed Equation (2.21), repeated here:

$$Nu_{Dh} = \frac{\left(\frac{f}{8}\right) Re_{Dh} Pr_o}{k_1 + 12.7 \sqrt{\frac{f}{8} (Pr_o^{2/3} - 1)}} \left[ 1 + \left(\frac{D_h}{L}\right)^{2/3} \right] F_{ann} K \quad (2.2)$$

Where  $k_1$  is given as:

$$k_1 = 1.07 + \frac{900}{Re_{Dh}} - \frac{0.63}{(1 + 10Pr_o)} \quad (2.3)$$

The correction factor for the dependence of fluid properties on temperature is given for liquids as:

$$K = \left( \frac{Pr}{Pr_w} \right)_o^{0.11} \quad (2.4)$$

For gases the correction factor reads:

$$K = \left( \frac{T_b + 273.15}{T_w + 273.15} \right)_o^z \quad (2.5)$$

Where  $z = 0$  for a cooled annulus and differs for a heated annulus, depending on the fluid used. Gnielinski (2009) correlated data using  $z = 0.45$  in the range  $0.5 < \frac{T_b}{T_w} < 1.0$ . For carbon dioxide and steam in the same range, Gnielinski (2009) suggests  $z$  should be approximately equal to 0.15. The factor to take into account the annular diameter ratio dependence ( $F_{ann}$ ), is given as:

$$F_{ann} = 0.75a^{-0.17} \quad (2.6)$$

The friction factor ( $f$ ) is calculated using:

$$f = (1.8 \log_{10} Re^* - 1.5)^{-2} \quad (2.7)$$

And the modified Reynolds number is:

$$Re^* = Re_{Dh} \frac{(1 + a^2) \ln a + (1 - a^2)}{(1 - a)^2 \ln a} \quad (2.8)$$

Lu and Wang (2008) experimentally determined correlations for tube-in-tube heat exchangers for three different flow orientations: horizontal flow, upward flow and downward flow. The Nusselt number correlation for the horizontal flow is provided in Equation (2.22).

Swamee *et al* (2008) presented Equation (2.23) where they used fundamental equations of heat transfer and a Sieder and Tate type correlation as well as an equivalent hydraulic diameter. Swamee *et al* (2008) used Equation (2.23) to optimally design tube diameters and flow rates for a tube-in-tube heat exchanger.

**Table 2.1: Equations available from literature describing the Nusselt number in a smooth concentric annulus for forced convection in fully developed turbulent flow. Adapted from Dirker and Meyer (2005)**

Author(s)	Correlation	Equation	Diameter ratio range ( $\alpha$ )	Reynolds number range ( $Re_{Dh}$ )	Working fluid
Davis(1943)	${}^1 Nu_{Dh} = 0.038\alpha^{-0.15} \left(\frac{1}{\alpha} - 1\right)^{0.2} Re_{Dh}^{0.8} Pr_o^{1/3} \left(\frac{\mu}{\mu_w}\right)^{0.14}$	(2.9)	0.000147 – 0.847	Not Specified	All media
McAdams(1954)	$Nu_{Dh} = 0.03105\alpha^{-0.15} \left(\frac{1}{\alpha} - 1\right)^{0.2} Re_{Dh}^{0.8} Pr_o^{1/3} \left(\frac{\mu}{\mu_w}\right)^{0.14}$	(2.10)	0.000147 – 0.847	Not Specified	All media
Foust and Christian(1940)	${}^1 Nu_{Dh} = \frac{0.04\alpha}{(\frac{1}{\alpha} + 1)^{0.2}} Re_{Dh}^{0.8} Pr_o^{0.4}$	(2.11)	0.543 – 0.833	3,000 – 60,000	Water
McAdams(1954)	$Nu_{Dh} = 0.023 Re_{Dh}^{1/3} \left(\frac{\mu}{\mu_w}\right)^{0.14}$	(2.12)	Not specified	Not Specified	Not specified
Monrad and Pelton(1942)	${}^2 Nu_{Dh} = 0.023 \left[ \frac{2 \ln \frac{1-\alpha^{-2}+1}{\alpha-\alpha^{-2} \ln \frac{1}{\alpha}}}{\alpha-\alpha^{-2} \ln \frac{1}{\alpha}} \right] Re_{Dh}^{0.8} Pr_o^{1/3}$	(2.13)	0.606, 0.408, 0.0588	12,000 – 220,000	Water, air
Wiegand et al.(1945)	${}^2 Nu_{Dh} = 0.023\alpha^{-0.45} Re_{Dh}^{0.8} Pr_o^{1/3} \left(\frac{\mu}{\mu_w}\right)^{0.14}$	(2.14)	0.1 – 1	Not Specified	Fluids: $\mu_{material} \leq 2\mu_{water}$
Kays and Leung (1963)	Results listed in tables for various conditions		0 – 1	$10^4 - 10^6$	Not specified
Petukhov and Roizen(1964)	$Nu_{Dh} = \frac{0.06759\alpha^{-0.16}}{\left(\frac{1}{\alpha} + 1\right)^{0.2}} \zeta Re_{Dh}^{0.8}$ Where $\zeta = 1 + 1.75 \left[ \frac{\frac{1-\alpha}{\alpha}}{\left(\frac{1}{\alpha} - 1\right) Re_{Dh}} \right]^{0.6}$ $\zeta = 1$ for $\alpha \leq 0.2$	(2.15)	0.07 – 1	$10^4 - 3 \times 10^5$	Air
Dittus and Boelter(1930)	${}^2 Nu_{Dh} = 0.023 Re_{Dh}^{0.8} Pr_o^{1/3}$	(2.16)	Not Specified	> 10 000	Not specified
Stein and Begell(1958)	$Nu_{Dh,f} = 0.0200\alpha^{-0.5} Re_{Dh,f}^{0.8} Pr_f^{1/3}$	(2.17)	0.812, 0.684, 0.59	30,000 – 390,000	Water
Crookston et al.(1968)	$Nu_{Dh} = 0.23\alpha^{-1/4} Re_{Dh}^{3/4} Pr_o^{1/3}$	(2.18)	0.1, 0.0625, 0.0323	17,000 – 100,000	Air

<sup>1</sup> Original equations rewritten as to have the Reynolds and Nusselt numbers based on the hydraulic diameter.  $D_h = D_o - D_1$ .

<sup>2</sup> The exponent  $n$  in Equations (2.13), (2.14) and (2.16) is equal to 0.4 for a heated annulus and 0.3 for a cooled annulus.



Table 2.2: Equations from recent publications describing the Nusselt number in a smooth concentric annulus for forced convection.

Author(s)	Correlation	Equation	Diameter ratio range ( $\alpha$ )	Reynolds number range ( $Re_{Dh}$ )	Working fluid
Gnielinski (1993)	$Nu_{Dh} = \frac{\left(\frac{f}{8}\right) Re_{Dh} Pr_o}{1 + 12.7 \sqrt{\frac{f}{8} (Pr_o^{2/3} - 1)}} \left[ 1 + \left(\frac{D_h}{L_{hx}}\right)^{2/3} \right] F_{ann} K$ $F_{ann} = 0.75 \alpha^{-0.17}$ $K = \left(\frac{Pr_o}{Pr_w}\right)^{0.11}$	(2.19)	Not Specified	2300 - $10^6$	Water
Dirker and Meyer (2004)	$Nu_{Dh} = C_o Re_{Dh}^{1/3} Pr_o^{0.14} \left(\frac{\mu}{\mu_w}\right)^{0.14}$ $P = 1.013 e^{-0.067/\alpha}$ $C_o = \frac{0.003 \alpha^{1.86}}{0.063 \alpha^{-3} - 0.0674 \alpha^{-2} + 2.225/\alpha - 1.157}$	(2.20)	0.3125 – 0.588	4000 - 30 000	Water
Gnielinski (2009)	$Nu_{Dh} = \frac{\left(\frac{f}{8}\right) Re_{Dh} Pr_o}{k_1 + 12.7 \sqrt{\frac{f}{8} (Pr_o^{2/3} - 1)}} \left[ 1 + \left(\frac{D_h}{L}\right)^{2/3} \right] F_{ann} K$ $k_1 = 1.07 + \frac{900}{Re_{Dh}} - \frac{0.63}{(1 + 10 Pr_o)}$ $K = \left(\frac{Pr_o}{Pr_w}\right)^{0.11} \text{ for liquids}$ $K = \left(\frac{T_b}{T_w}\right)^z \text{ for gases with } z = 0 \text{ for cooling}$ $z = 0.45 \text{ for } 0.5 < \frac{T_b}{T_w} < 1.0$ $F_{ann} = 0.75 \alpha^{-0.17}$ $f = (1.8 \log_{10} Re^* - 1.5)^{-2}$ $Re^* = Re_{Dh} \frac{(1 + \alpha^2) \ln \alpha + (1 - \alpha^2)}{(1 - \alpha)^2 \ln \alpha}$	(2.21)	Not Specified	Not Specified	All media
Lu and Wang (2008)	$Nu_{Dh} = 0.0022 Re_{Dh}^{1.09} Pr_o^{0.4}$	(2.22)	0.795	> 3 000	Water
Swamee et al (2008)	$Nu_{Dh} = \frac{0.027}{(1 + 1/\alpha)^{0.2}} Re_{Dh}^{0.8} Pr_o^{1/3} \left(\frac{\mu}{\mu_w}\right)^{0.14}$	(2.23)	Not specified	Not Specified	Not specified

Equation (2.21) was compared to existing experimental data, and it was shown in Gnielinski (2009) that there was good agreement with data obtained from Petukhov and Roizen (1964) and Kays and Leung (1963) with air as the working fluid and a heated annulus. This data was predicted accurately within  $\pm 5\%$ . Figure 2.1 shows a comparison of Equation (2.21) with the experimental data of Petukhov and Roizen (1964) and Leung et al (1963). Here the experimentally obtained Nusselt numbers are divided by the Nusselt numbers obtained from the correlation in Equation (2.21), thus unity would represent an exact correlation for Petukhov and Roizen (1964). The data of Kays and Leung (1963) is multiplied by 0.7 to separate the data on the same axis. However, when compared to the data of Dirker and Meyer (2004), where the working fluid was water, depending on the diameter ratio an error of up to  $\pm 15\%$  was observed. Figure 2.2 shows the comparison of the experimental data of Dirker and Meyer (2004) with Equation (2.21). Here again, the experimentally obtained Nusselt numbers are divided by the Nusselt numbers obtained from the correlation in Equation (2.21).

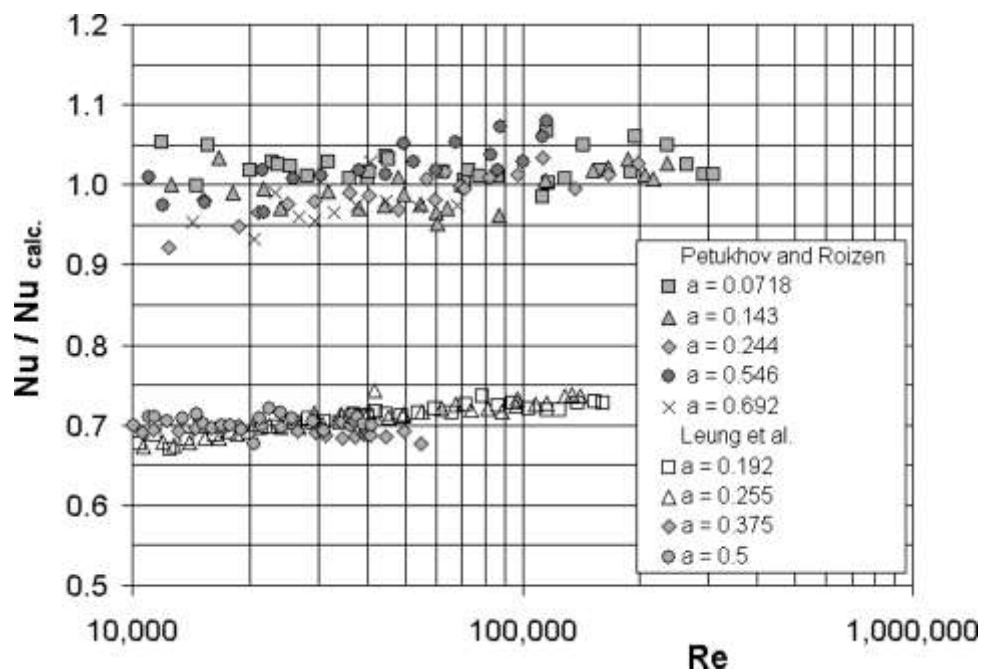


Figure 2.1: Ratio of the experimental Nusselt numbers of Petukhov and Roizen (1964) and Leung et al (1962) to the Nusselt numbers of Equation (2.21). Extracted from Gnielinski (2009).

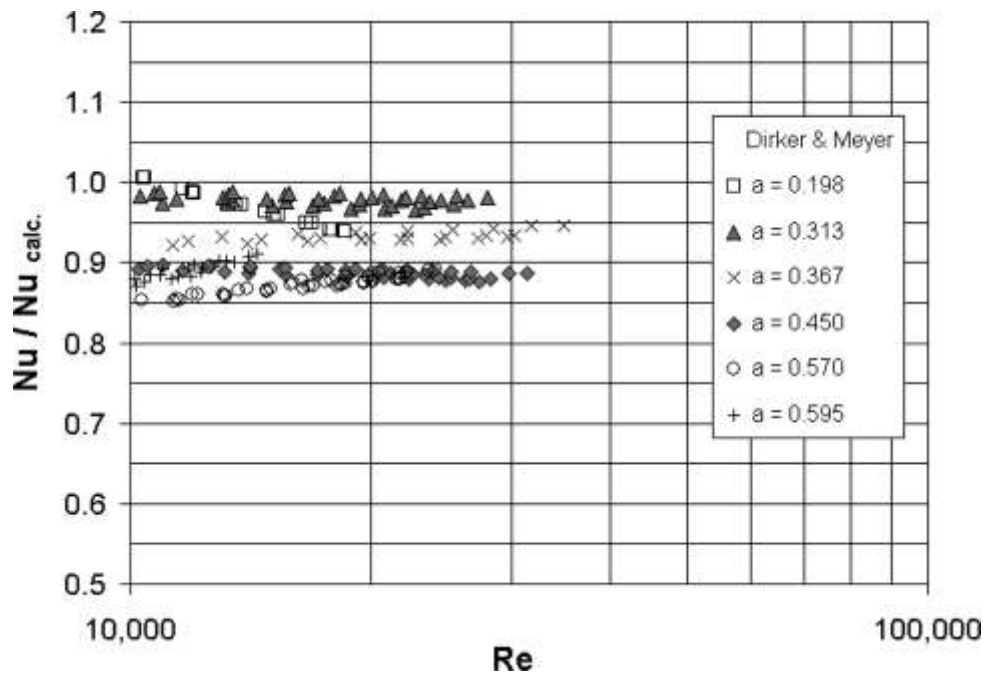


Figure 2.2: Ratio of the experimental Nusselt numbers of Dirker and Meyer (2004) to the Nusselt numbers of Equation(2.21). Extracted from Gnielinski (2009).

## 2.2 Numerical Methods to Determine Heat Transfer Correlations

When physical properties of a fluid are evaluated at the bulk temperature alone and no allowance is made for the temperature variation across the heat exchanger, it is reported by Stein and Begell (1958) that large variations may occur in the heat exchanger analysis. The best heat transfer correlations occur for the case where the wall temperatures at both the inner and outer fluids are determined. This allows for variations in all physical properties, and although Stein and Begell (1958) propose that using the bulk temperature may be suitable for industrial applications, it is however not suitable for the case where correlation derivation is required.

Heat transfer coefficients and wall temperatures may be found by direct measurement of the temperature drop across the wall separating the inner tube and annulus. This method works well for a single resistance heated tube where the thermocouples may be attached to the wall without affecting the flow in the vicinity of the thermocouple. However, according to Briggs and Young (1969), for the case where a fluid flows over the thermocouples, as occurs in a tube-in-tube heat exchanger. It is impossible to have sufficient thermocouples attached to the inner tube wall without considerably affecting the flow in the annulus.

### 2.3 Wilson Plot Method (Linear Regression Analysis)

The technique originally developed by Wilson (1915) for determining individual thermal resistance from the overall resistance for a steam condenser was modified by Briggs and Young (1969) to determine heat transfer coefficients from a linear regression model for a single phase tube-in-tube heat exchanger. This model allows the average inner and outer wall temperatures of the inner tube to be determined without the use of thermocouples and direct measurement on the outer wall of the inner tube. The reasons for the modifications of Briggs and Young (1969) were due to the evident limitations of the original Wilson (1915) method. These limitations for smooth concentric annuli are listed below as stated in Shah (1990):

1. The fluid flow rates in the inner tube and the logarithmic mean temperature difference must be kept constant.
2. The exponent for the Reynolds number in the annulus is presumed to be known and constant (Wilson (1915) used 0.82). However this exponent is a function of the Prandtl and Reynolds number and will thus vary.
3. Test data must exist only in one flow regime (turbulent or laminar).
4. Variations in fluid properties in the annulus are not taken into account.

The modification presented by Briggs and Young (1969) eliminates limitations 1, 2 and 4. Briggs and Young (1969) based their regression analysis on the Sieder and Tate (1936) equations for calculating the Nusselt number, where the inner tube Reynolds number exponent is 0.8. Wilson (1915) used a value of 0.82 for the inner tube Reynolds number exponent, which was obtained through a trial and error procedure. The method of Briggs and Young (1969) is discussed in more detail in Appendix A.

### 2.4 Khartabil and Christensen Method (Nonlinear Regression Analysis)

A scheme for determining heat transfer correlations in tube-in-tube heat exchangers using a nonlinear regression analysis was proposed by Khartabil and Christensen (1992). This scheme involves a nonlinear regression model and can be used on similar data sets to the

method proposed by Briggs and Young (1969). The linear regression model is an approximate and does not always converge to an optimum value for the unknown parameters according to Khartabil and Christensen (1992). The nonlinear scheme according to Khartabil and Christensen (1992) is guaranteed to converge if a solution exists.

This nonlinear regression model is complex and requires much experimental data in order to converge to an accurate solution for the heat transfer coefficient, according to Khartabil and Christensen (1992). Thus, direct solutions with sufficient accuracy to obtain the heat transfer coefficient are sought after. This method is discussed in more detail in Appendix B.

## 2.5 Friction Factors

Many correlations exist which accurately describe the friction factors within a circular tube. Theoretical derivations for laminar flow in annular ducts also exist, however, there is less certainty with regard to turbulent friction factors in annular ducts. Quarmby (1967) explored the available literature for friction factors in annular ducts and found there was much discrepancy between the available methods. Table 2.3 provides a summary of some known methods of calculating friction factors for annular ducts as well as their general dependence on various parameters. According to Monrad and Pelton (1940) it is clear that the friction factors for annular ducts are of a greater magnitude than those in a tube, and will decrease less with an increasing Reynolds number.

Kaneda et al (2003) performed direct numerical simulations (DNS) on flow inside and an annulus and proposed Equation (2.25) which is based on wall shear stresses.

Jones and Leung (1981) compares available data for friction factors in annuli and reports that the scatter for turbulent flow in these data is approximately -25% to +35% and many data points disagree with the standard Colebrook equation (Equation (2.24)) for smooth circular tubes modified for annular ducts:

$$\frac{1}{\sqrt{f}} = 2.0 \log_{10} Re_{Dh} \sqrt{f} - 0.8 \quad (2.24)$$

Table 2.3: Equations available in literature describing the friction factor in a smooth concentric annulus for forced convection.

Author(s)	Correlation	Equation	Diameter ratio range ( $a$ )	Reynolds number range ( $Re_{Dh}$ )	Working fluid
Kaneda et al (2003)	$\frac{f}{8} = \left[ 1.61 + \frac{1}{0.436} \ln \left( \frac{Re_{Dh}}{\sqrt{8/f}} \right) - \frac{550}{Re_{Dh} \sqrt{f/8}} \right]^{-2}$	(2.25)	0.0 – 1.0	> 10 000	Not specified
Jones and Leung (1981)	$\frac{1}{\sqrt{f}} = 2 \log_{10} Re^* \sqrt{f} - 0.8$ $Re^* = Re_{Dh} \frac{(1 + a^2) \ln a + (1 - a^2)}{(1 - a)^2 \ln a}$	(2.26)	0.0 – 1.0	10 000 – 1,000,000	Based on other authors data.
Gnielinski (2009)	$\frac{1}{\sqrt{f}} = 1.8 \log_{10} Re^* - 1.5$	(2.27)	Not specified	Not specified	All Media
Blasius (Extracted from Cengel (2006))	$f = 0.3164 Re_{Dh}^{-0.25}$	(2.28)	Not specified	Not specified	All Media

In many of these cases, extensive laminar data attest to the adequacy of the experimental techniques. This disagreement is well known and has been the subject of numerous studies. Jones and Leung (1981) explain that it is not enough to base friction factors on the hydraulic diameter alone of the annular duct for both laminar and turbulent flow; instead, a dependence on the annular diameter ratio is necessary as it has a considerable effect on the friction factors. Jones and Leung (1981) proposed Equation (2.26).

Comparing a large number of experimental data on friction factors of annular flows, Gnielinski (2009) found Equation (2.27) to best fit the data. Gnielinski (2009) modified the Reynolds number here to accommodate flow within an annulus.

The well known friction factor in smooth tubes of Blasius is provided in Equation (2.28), where the Reynolds number is modified to a Reynolds number based on the hydraulic diameter for annular flow.

Friction factors calculated using the correlations in Table 2.3 for an annular diameter ratio of 0.593 over a Reynolds number range of  $10\,000 < Re_{Dh} < 45\,000$  is shown in Figure 2.3.

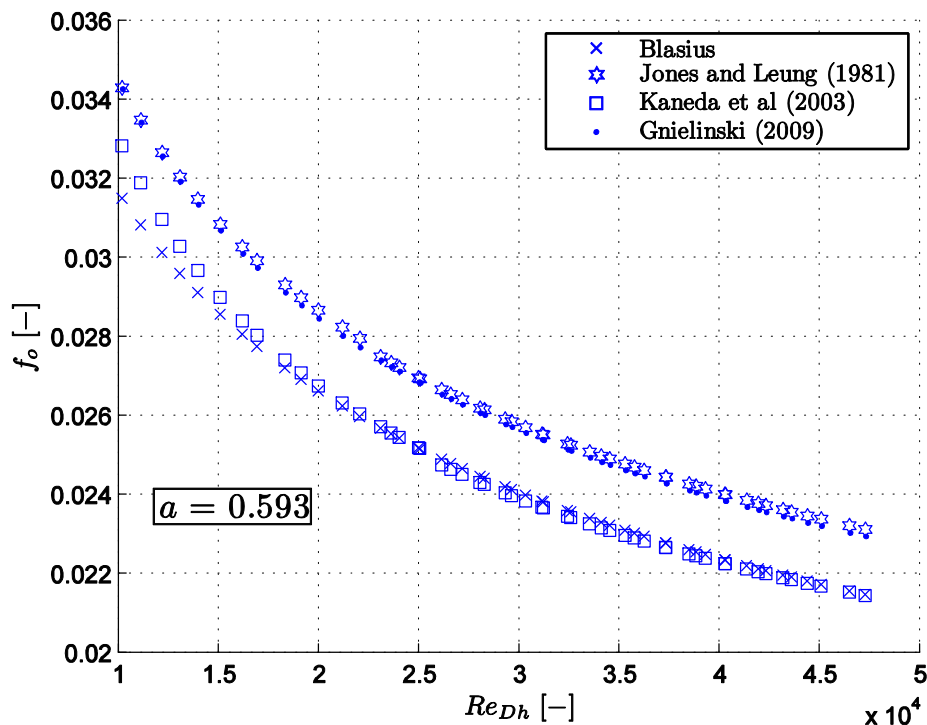


Figure 2.3: Friction factors calculated using the correlations of Table 2.3.

Figure 2.3 shows discrepancies between the friction factors predicted by the available correlations. The correlations of Jones and Leung (1981) and Gnielinski (2009) are in good

agreement, while the correlations of Blasius and Kaneda et al (2003) show agreement with each other. A 10% discrepancy is however present between the two sets.

## 2.6 Spacers and Tube Concentricity

Olson and Sparrow (1963) used four brass rods cylindrical in shape with a 1.6mm diameter to keep the annulus and inner tube concentric. Experimental results obtained by them show that these rods increased pressure gradients for at least 150 strut diameters downstream of the flow. Olson and Sparrow (1963) later repeated these tests to observe that if the rods were constructed with an aerodynamic shape the pressure gradient was unaffected.

## 2.7 Annulus Entry Lengths

The entry length in the annulus is required to allow the fluid to obtain a fully developed hydrodynamic profile. Rothfus et al (1955) originally proposed that the entry length for an annulus was far larger than that for a tube, they suggested  $200D_h$ . Later developments by Brighton and Jones (1964) showed that the hydrodynamic profiles were unchanged from  $34.5D_h$ . This was later confirmed by Quarmby (1967). Thermal entry lengths for a tube are described in Cengel (2005) to be ten times the tube diameter.

## 2.8 Equivalent Diameters

Many of the existing correlations for both the Nusselt numbers and friction factors (Table 2.1, Table 2.2 and Table 2.3) use a method of substituting an equivalent diameter to accommodate the annular passage. This equivalent diameter is a value four times the hydraulic radius ( $r_h$ ). The hydraulic radius is defined as the cross sectional area of flow divided by the wetted perimeter. For annular spaces this is given by Equation (2.29), extracted from Monrad and Pelton (1942).

$$r_h = \frac{\frac{\pi D_o^2}{4} - \frac{\pi D_1^2}{4}}{\pi(D_1 + D_o)} = \frac{D_o - D_1}{4} \quad (2.29)$$



Therefore,  $D_h = D_o - D_1$ .

Another method used, but less frequently, is similar to the hydraulic diameter with the exception that the equivalent diameter is based on the heated or cooled area rather than the wetted perimeter and results in Equation (2.30), extracted from Monrad and Pelton (1942).

$$D_h = \frac{D_1^2 - D_o^2}{D_o} \quad (2.30)$$

Although there are many applications of Equation (2.29) and Equation (2.30) in heat transfer, little work has been done to justify the use of either of these procedures according to Monrad and Pelton (1942). They also suggest that the only comprehensive study on these equivalent diameters was done by Foust and Christian (1940), where it was concluded that neither of these methods are accurate.

# Chapter 3

## Experimental Setup

### 3.1 Introduction

The experimental setup consisted of an experimental facility as well as the four test sections. The layout of the experimental facility and how it operates are discussed here. Useful working ranges of the experimental facility are provided. The experimental facility accommodated four heat exchanger test sections that were tested for both a heated and cooled annulus. The manufacturing of the test section components are also discussed here. The procedure of assembling the components to create the finished test sections are discussed in detail.

### 3.2 Experimental Facility

The experimental facility was a closed loop system designed in such a way as to accommodate heat exchangers of different sizes; as well as allowing for easy removal and addition of different heat exchangers.

A schematic representation of the experimental facility is shown in Figure 3.1. Block **i** represents the cold water supply and block **ii** represents the warm water supply. Warm or cold water could be directed to flow either through the inner tube or annulus. This allowed the annulus to be either heated or cooled. The inner tube and annulus loops are separated showing the different instruments used in the experimental facility. Figure 3.1 in its current configuration would thus represent a heat exchanger set up where the annulus is being cooled. If the cold water supply (**i**) is connected to the annulus loop and the hot water supply (**ii**) is connected to the inner tube loop, the heat exchanger configuration would be that of a heated annulus.

Cold water was stored in a 1 000 ℓ tank (item 2) and connected to a 16 kW cooling unit (item 1). Valves (items 4a and 4b) were used to control fluid flow, to either the test section

or returned to the storage tank in a bypass line. Water in the inner tube was pumped using a positive displacement pump (item 3a) with a maximum flow rate of 1 900 ℓ/h. The flow rate was controlled using a vector drive coupled to the pump motor. Pulsations in the flow were damped using a 4 ℓ accumulator (item 5a). Fluid flow rates were obtained with a Coriolis flow meter (item 6a) with an effective range of 54.5 ℓ/h – 2 180 ℓ/h. The water passed through the inner tube of the test section (item 10) and returned to the storage tank. A non-return valve (item 7a) was used to avoid back flow.

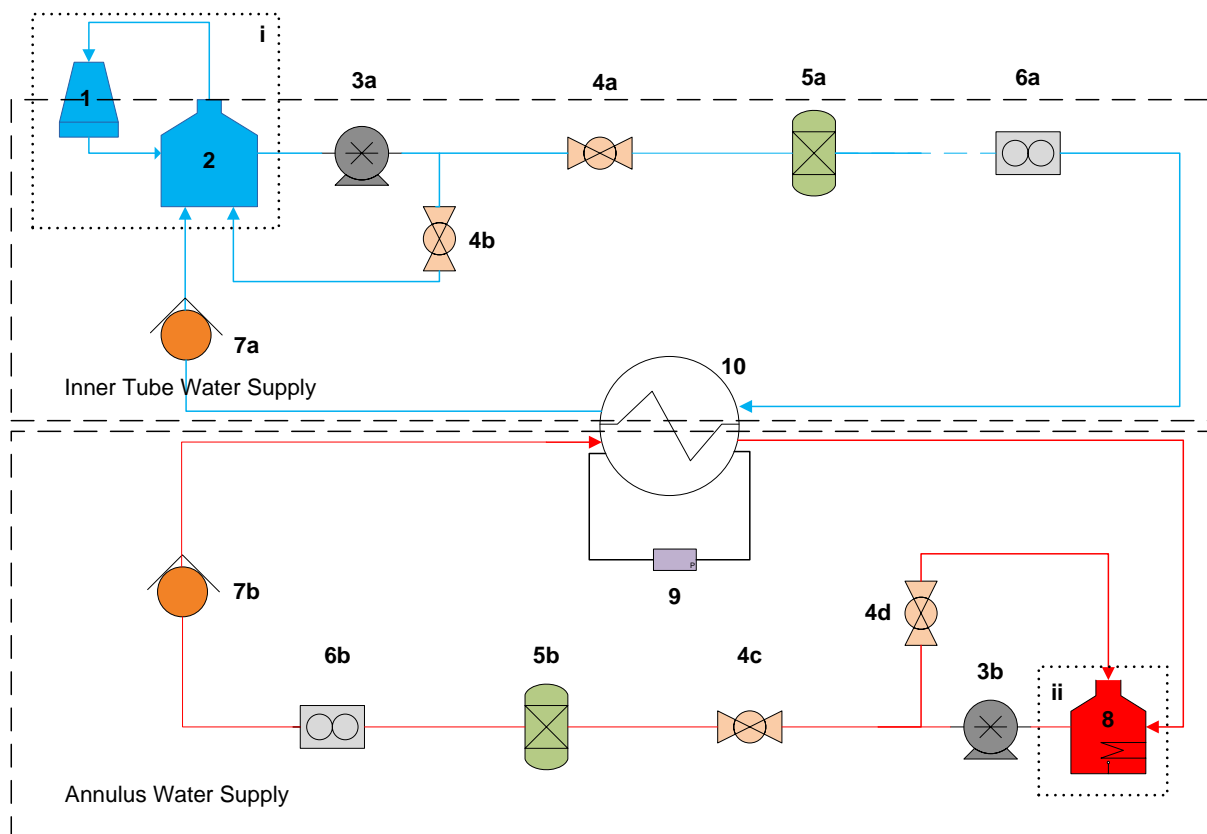


Figure 3.1: Schematic representation of the experimental facility used.

The hot water loop was equipped with a 600 ℓ storage tank (item 8) and heated with a 12 kW electrical resistance heater. The water was pumped using a 6 000 ℓ/h centrifugal pump. Valves (items 4c and 4d) were used to control fluid flow, to either the test section or returned to the storage tank in a bypass line. The flow rate was controlled using a vector drive coupled to the pump motor. Pulsations in the flow were damped using a 10 ℓ accumulator (item 5b). A Coriolis flow meter (item 6b) with a range from 170 ℓ/h – 6 800 ℓ/h

was fitted to measure the flow rate. The water passed through the test section (item 10). A non-return valve (item 7b) was used to prevent back flow.

Three pressure transducers with interchangeable diaphragms (item 9) were connected to the inlet and outlet of the annulus. The three pressure transducers were calibrated from 0 kPa to 22 kPa, 0 kPa to 35 kPa and 0 kPa to 140 kPa with accuracies of 0.25% of their full scale values. Each diaphragm used with the differential pressure transducer was calibrated using a dead weight system. All thermocouples were calibrated against a Pt100 with a manufacturer specified uncertainty of 0.1°C.

Using National Instruments data acquisition systems and labview software, the outputs to the pumps and inputs from the flow meters and pressure transducers were controlled and monitored remotely with an on-site computer. Table 3.1 provides necessary technical data of the components shown in Figure 3.1.

**Table 3.1: Components present in the experimental facility and their useful working ranges.**

<b>Item</b>	<b>Description</b>
<b>1</b>	16 kW cooling unit.
<b>2</b>	1 000ℓ storage tank for cold water.
<b>3(a)</b>	Positive displacement pump (Cemo SP 3) <ul style="list-style-type: none"> <li>• A maximum flow rate of 1 900 ℓ/h.</li> <li>• Maximum flow rate occurs at 1 750 rpm with a 1m supply head.</li> <li>• Power rating at this maximum flow rate 0.24 kW.</li> </ul>
<b>3(b)</b>	Multistage centrifugal pump (Grundfos CR 15) <ul style="list-style-type: none"> <li>• A maximum flow rate of 6 000 ℓ/hr.</li> <li>• Maximum flow rate occurs at 2 900 rpm with a 1m supply head.</li> <li>• Power rating at this maximum flow rate 5 kW.</li> </ul>
<b>4(a-d)</b>	Ball valves.
<b>5(a)</b>	Accumulator <ul style="list-style-type: none"> <li>• 4 ℓ.</li> <li>• Damps out flow resulting in a standard deviation of 1.51 e-04 kg/s. (taken from 100 readings at a constant flow rate).</li> </ul>

Table 3.1 Continued

<b>5(b)</b>	Accumulator <ul style="list-style-type: none"> <li>• 10 ℓ</li> <li>• Damps out flow resulting in a standard deviation of 1.48 e-04 kg/s. (taken from 100 readings at a constant flow rate).</li> </ul>
<b>6(a)</b>	Coriolis flow meter <ul style="list-style-type: none"> <li>• 0.015 – 0.603 kg/s (54.5 – 2 180 ℓ/h)</li> </ul> Manufacturer specified uncertainty of 0.1% of full scale value.
<b>6(b)</b>	Coriolis flow meter <ul style="list-style-type: none"> <li>• 0.047 – 1.883 kg/s (170 – 6 800 ℓ/h)</li> </ul> Manufacturer specified uncertainty of 0.1% of full scale value.
<b>7(a-b)</b>	Non-return valve.
<b>8</b>	600ℓ storage tank fitted with a 12 kW electrical resistance heater
<b>9</b>	Differential pressure transducer with interchangeable diaphragms for different pressure ranges. <ul style="list-style-type: none"> <li>• 0 – 22 kPa Manufacturer specified uncertainty of 0.25% of full scale value.</li> <li>• 0 – 35 kPa Manufacturer specified uncertainty of 0.25% of full scale value.</li> <li>• 0 – 140 kPa Manufacturer specified uncertainty of 0.25% of full scale value.</li> </ul>
<b>10</b>	Heat exchanger (Test section).

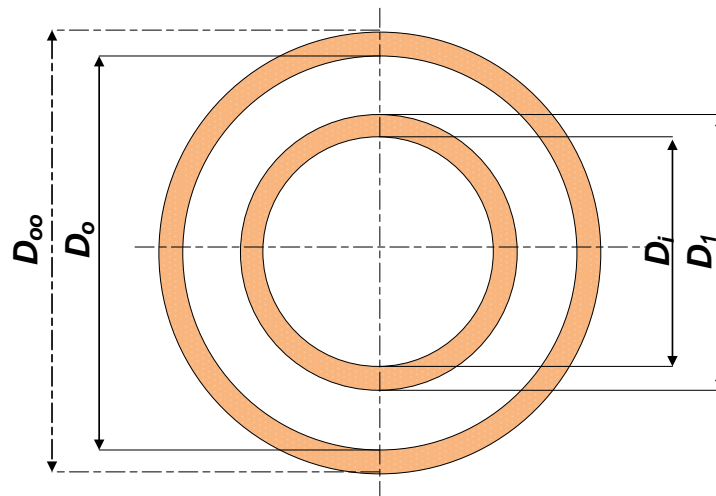
### 3.3 Test Sections

A total of four heat exchangers were built and tested, with annular diameter ratios of 0.483, 0.579, 0.593 and 0.712.

The test sections consisted of an inner tube and annulus. Two outer tubes and two inner tubes with different diameters were constructed. Alternating the outer tubes and inner tubes resulted in four annular diameter ratios. Table 3.2 provides the various tube diameters (shown in Figure 3.2) and corresponding annular diameter ratios. Tube Diameters were measured with a vernier caliper with an uncertainty on the measurement of 20 $\mu$ m.

**Table 3.2: Tube diameters and annular diameter ratios for the four heat exchangers tested.**

Heat exchanger	$D_i$ (mm)	$D_1$ (mm)	$D_o$ (mm)	$D_{oo}$ (mm)	$a (D_1/D_o)$
1	14.46	15.88	32.89	34.93	0.483
2	17.63	19.05	32.89	34.93	0.579
3	14.46	15.88	26.76	28.58	0.593
4	17.63	19.05	26.76	28.58	0.712


**Figure 3.2: Cross section of the heat exchanger test section showing the diameters of the inner tube and outer tube.**

### 3.4 Inner Tube Construction

The inner tubes were constructed from 5.5m long hard drawn copper tubes with diameters shown in Table 3.2. To measure temperatures along the length of the inner tubes, nine stations with two T-type thermocouples at each station were attached within the inner tube wall. Each station was 550mm apart with the thermocouples attached at 180° spacing around the periphery. Adding additional thermocouples at each station minimized measurement uncertainties at the station. Having four thermocouples at a station resulted in uncertainties of 0.053°C, whereas a single thermocouple had uncertainties of 0.106°C.

Three methods of attaching the thermocouples to the inner tube walls were investigated. Figure 3.3 shows the three methods. In Figure 3.3 a) the thermocouples were attached to

the wall of the inner tube with solder. The thermocouples in Figure 3.3 b) were attached to the wall as in Figure 3.3 a), however, insulation was added around the junction. In Figure 3.3 c) a groove is machined in the inner tube wall where the thermocouple was fixed within the wall without any protrusions.

The protruding solder from the thermocouple attachment in Figure 3.3 a) may be act as a fin creating heat transfer enhancement and producing inaccurate temperature results. The attachment in Figure 3.3 b) with the insulation around the protrusion produced more accurate results, however, still may have acted as a fin and disturbed flow within the annulus. Figure 3.3 c) produced the most accurate results as it had no temperature disturbances from fin effects and did not affect the fluid flow as the thermocouple was fixed within the tube wall. This method was used in this study.

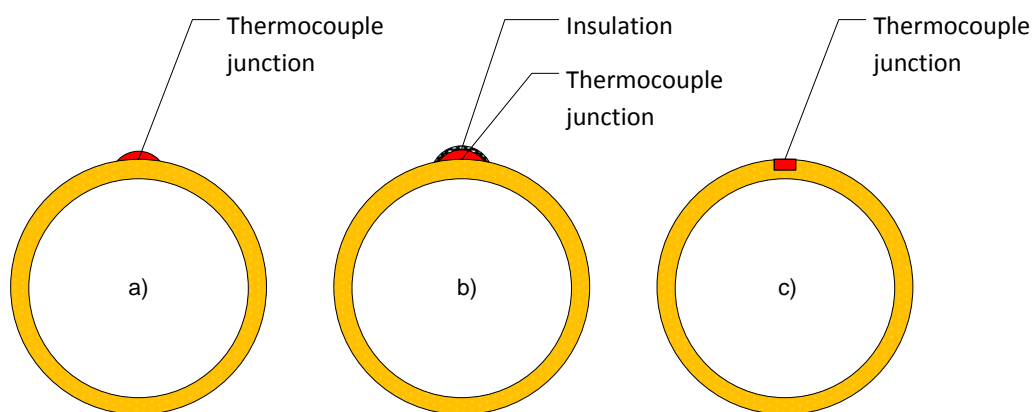


**Figure 3.3:** Three methods used for attaching thermocouples to the inner tube wall used in Ntuli et al (2011).

The attachment of the thermocouples within the inner tube wall was achieved by machining a groove into the tube wall and soldering the thermocouple junctions within the groove. The thermocouples were fed through 1.2mm diameter holes drilled through the inner tube wall and retrieved at the ends of the inner tubes. Figure 3.4 shows a cross section of an inner tube with the attached thermocouples. The Teflon-based insulation was stripped from the thermocouple leads to a length of 3mm. This resulted in 3mm junctions which were set flush with the tube walls in the machined grooves and were soldered into place. The tube walls at each station were finely sanded to remove any protrusions from the outer wall at the connection point.

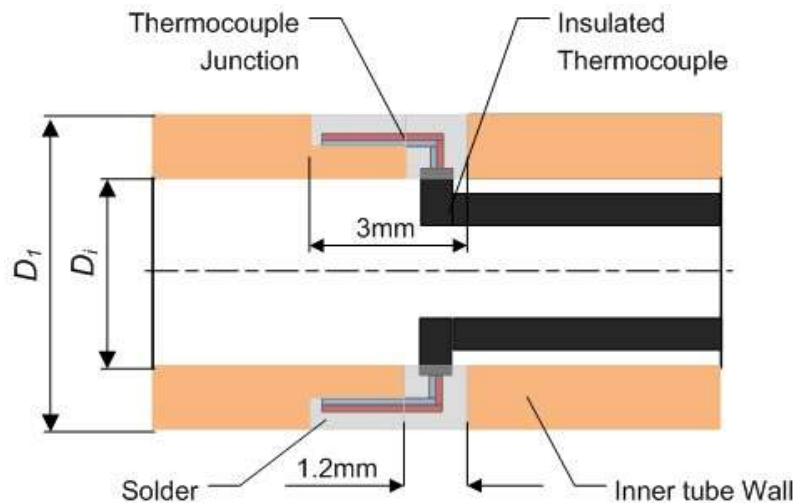


Figure 3.4: Cross section of the inner tube wall showing the method used to attach the thermocouples.

The tubes were parted near the centre to simplify feeding the thermocouples through. The tube sections were 2.475m and 3.025m long with the longer section accommodating an additional thermocouple station. To avoid having excessive thermocouple wire in the inner tube and unnecessarily long thermocouple wires, ten thermocouples were fed through one end of the tube and eight through the other. With all the thermocouples attached to the tubes and fed through to the tube ends, the tubes were reattached using copper bushes which fit inside the inner tubes. The two ends of the tubes were placed concentric to the bush and soldered together. An aligning jig was constructed to ensure the two ends of each of the inner tubes were held concentric while they are soldered together. Figure 3.5 shows the bush used, along with the associated dimensions of the bush for the two inner tubes described in Table 3.3.

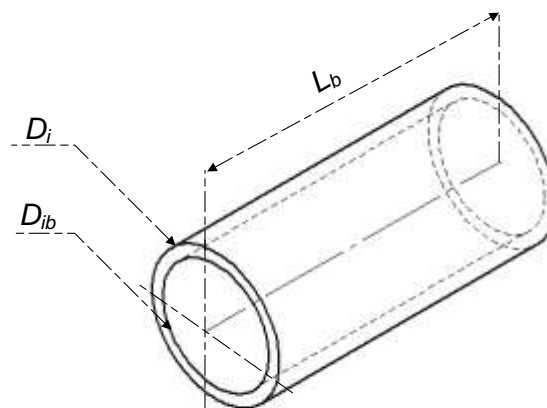


Figure 3.5: Bush used to re-attach the two ends of the inner tube.



**Table 3.3:** Dimensions of the two bushes used on the two inner tubes. Refer to Figure 3.5 for a description of the dimension parameters.

Inner tube number	$D_1$ (mm)	$D_i$ (mm)	$D_{ib}$ (mm)	$L_b$ (mm)
1	15.88	14.46	13.00	40
2	19.05	17.63	16.00	40

Figure 3.6 shows the final reconstruction of an inner tube (not drawn to scale) with the thermocouples attached and fed through the tube.

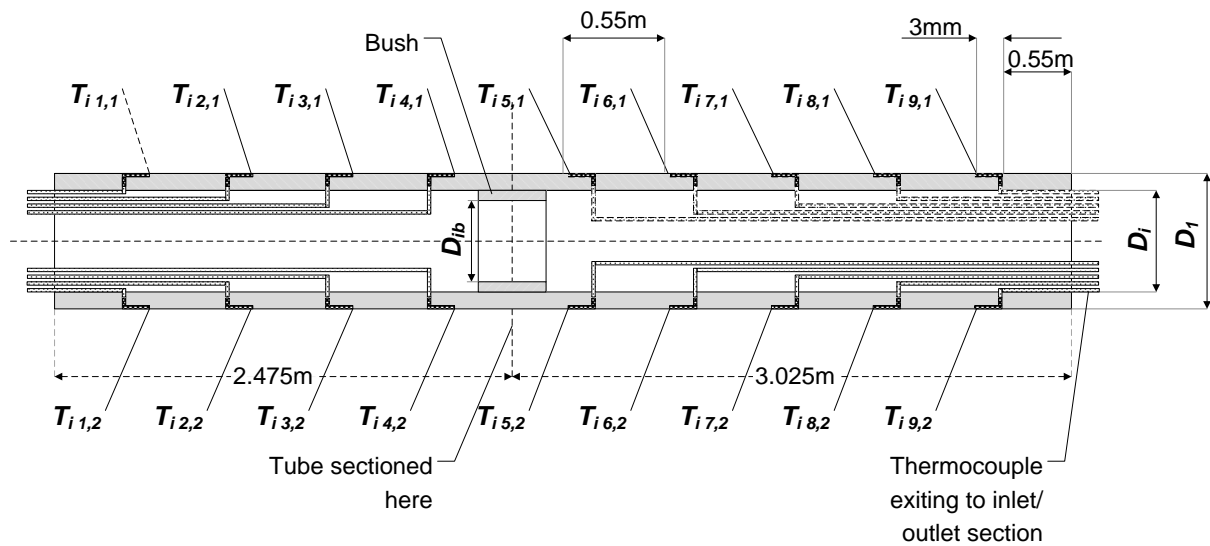


**Figure 3.6:** Schematic representation of the reconstructed inner tube and respective thermocouple attachments. (Not drawn to scale)

### 3.5 Inner Tube Inlet and Outlet Sections

The inlet and outlet sections for the inner tubes were constructed separately from hard drawn copper with diameters equal to those of the inner tube and lengths of 80mm. These sections were used as exit-ports for the thermocouple leads from the inner tubes. The inlet and outlet sections were connected to the inner tubes with straight compression couplings.

Each inlet and outlet section had two connections for the thermocouples to exit the tube. These connections were constructed by silver soldering a 6.35mm diameter tube onto the outer wall of the inlet and outlet sections. A 5mm hole was drilled through the wall of each

inlet and outlet sections allowing the thermocouple leads to exit. Straight compression couplings were silver soldered to the ends of these exit connections. A total of five thermocouples could be fitted through these exit connections.

Thermocouples were also attached to the inlet and outlet sections to measure the inner tube inlet and outlet temperatures respectively. Four thermocouples were equally spaced around the circumference of the inlet and outlet sections in order to improve the accuracy of these measurements. Figure 3.7 a) shows a representation of an inlet/outlet section, and Figure 3.7b) shows the circumferential locations of the thermocouples.

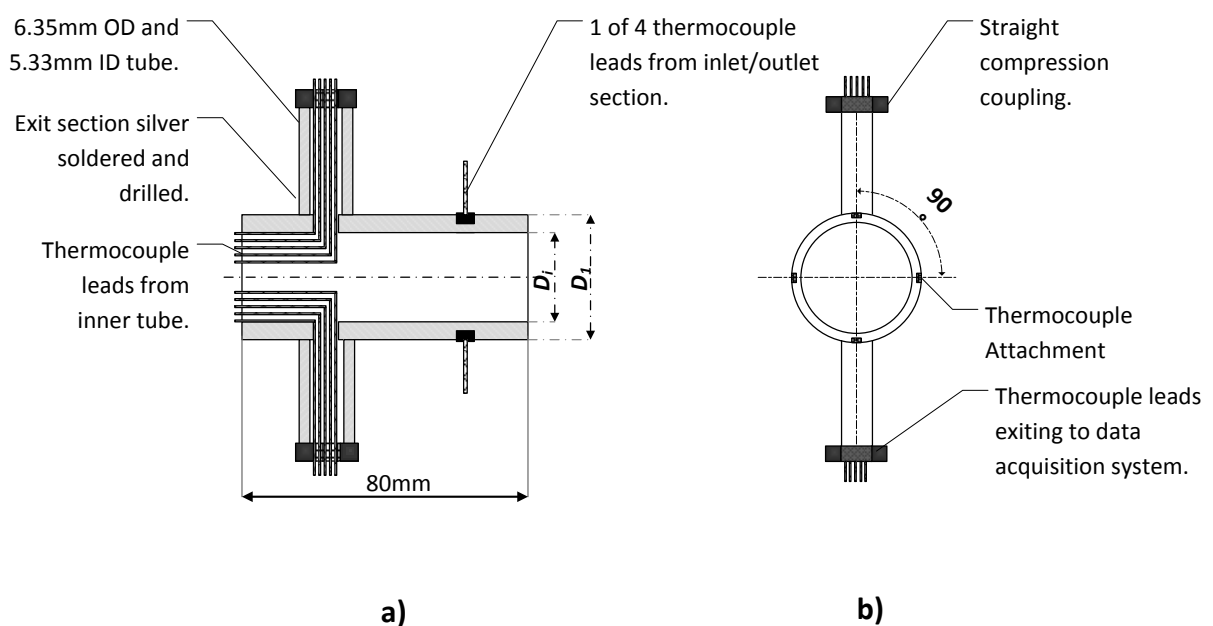


Figure 3.7: a) Inlet and Outlet sections for the inner tube. b) Circumferential locations of thermocouples attached to the inner tube inlet and outlet sections.

### 3.6 Outer Tube

Two outer tubes were constructed from hard drawn copper tube with inner and outer diameters provided in Table 3.2. The 5m long outer tube was split into eight modular sections of 625mm each, which were attachable and detachable from each other using straight compression couplings. This allowed one outer tube to be used with the two different inner tubes thus resulting in the four annular diameter ratios provided in Table 3.2. To measure the local temperatures over the length of the annulus, thermocouples were placed on the outer wall of the outer tube at intervals of 550mm along the axial length. Four thermocouples were placed at 90° intervals around the circumference of the inlet and outlet to measure the annulus inlet and outlet temperatures.

Due to the lengths of the heat exchanger, sagging of the tubes was expected. This could be rectified by inserting additional spacers. However, by increasing the number of spacers, flow obstruction within the annulus is increased. A bending analysis was performed on the inner tube where a maximum allowable vertical displacement of the inner tube of 1mm was used.

The vertical deflection of a circular cross section is given in Shigley and Budynas (2004) (Table A.9.7) as:

$$y_{\delta} = \frac{wx}{24EI_x} (2l_{\text{unsupported}}x^2 - x^3 - L_{\text{unsupported}}^3) \quad (3.1)$$

Where  $x$  is the distance along the tube length and  $L_{\text{unsupported}}$  is the total unsupported tube length. The second moment of area  $I_x$  is given in Shigley and Budynas (2004) Table A.18 as:

$$I_x = \frac{\pi}{64} (D_1^4 - D_i^4) \quad (3.2)$$

With the modulus of elasticity for copper given in Shigley and Budynas (2004) Table A.5 as  $E = 119 \times 10^9$  Pa. The distributed load,  $w$ , is the weight of the inner tube given as:

$$w = Mg \quad (3.3)$$

Where  $M$  is the mass of the tube per meter and  $g$  the gravitational acceleration.

With Equation (3.1) and Equation (3.2) an iterative process is used to determine the maximum distance between the spacers to ensure the inner tube does not vertically deflect

more than 1mm. The maximum distance between the spacers ( $L_{max}$ ) for the two inner tubes is provided in Table 3.4.

**Table 3.4: Maximum distance between spacers for the associated inner tubes**

Inner Tube	$D_1$ (mm)	$D_i$ (mm)	$L_{max}$ (m)
1	15.88	14.46	1.33
2	19.05	17.63	1.45

The maximum distance between the spacers is 1.33m for inner tube 1 and 1.45m for inner tube 2. However due to space constraints and fixed tube sizes the distance between the spacers was chosen as 635mm. This distance would ensure that the maximum vertical displacement of 1mm will not be exceeded.

To ensure that the annuli were concentric, spacers manufactured by modifying the compression fittings were used. Stainless steel pins with a diameter of 0.8mm were fixed concentrically to screws located on the compression fittings equally spaced at  $120^\circ$  apart. The screws were adjustable thus allowing the spacers to be used with various inner tube diameters. Figure 3.8 shows the spacers located on the compression fittings, holding the inner and outer tube concentric.

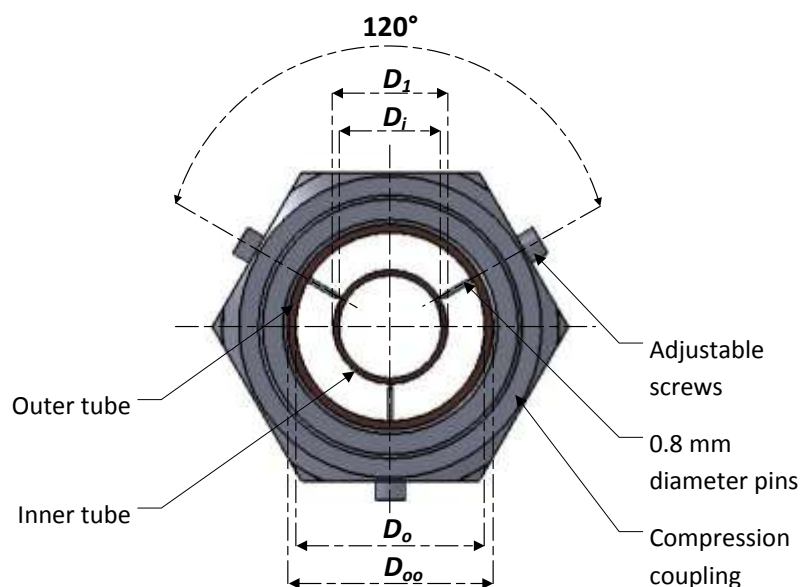


**Figure 3.8: Spacer used to hold the inner tube and annulus concentric.**

To ensure that the tubes were held concentric during assembly, a locator cylinder 30mm long was manufactured from wood with inner diameter  $D_1$  and outer diameter  $D_o$ . During assembly of the heat exchanger this locator piece was pulled through the annulus after each compression fitting is fastened and the locating pins set in place. This ensured concentricity of the annulus and inner tube.

Pressure drops across the annulus length were measured by means of pressure taps fixed on the outer walls of the annuli. The pressure taps were located as close to the inlets and outlets of the annuli as possible. Two pressure taps 180° apart were located at the inlet and two at the outlet of each annulus. The two pressure taps at each end were joined, effectively taking the average pressure drop at the two radial locations.

### 3.7 Complete Heat Exchanger Test Section

A representation of the completed heat exchanger with the inner tube, outer tube, pressure taps, as well as the inner tube inlet and outlet sections is provided in Figure 3.9 (not drawn to scale) with all associated dimensions for all for heat exchangers provided in Table 3.5.

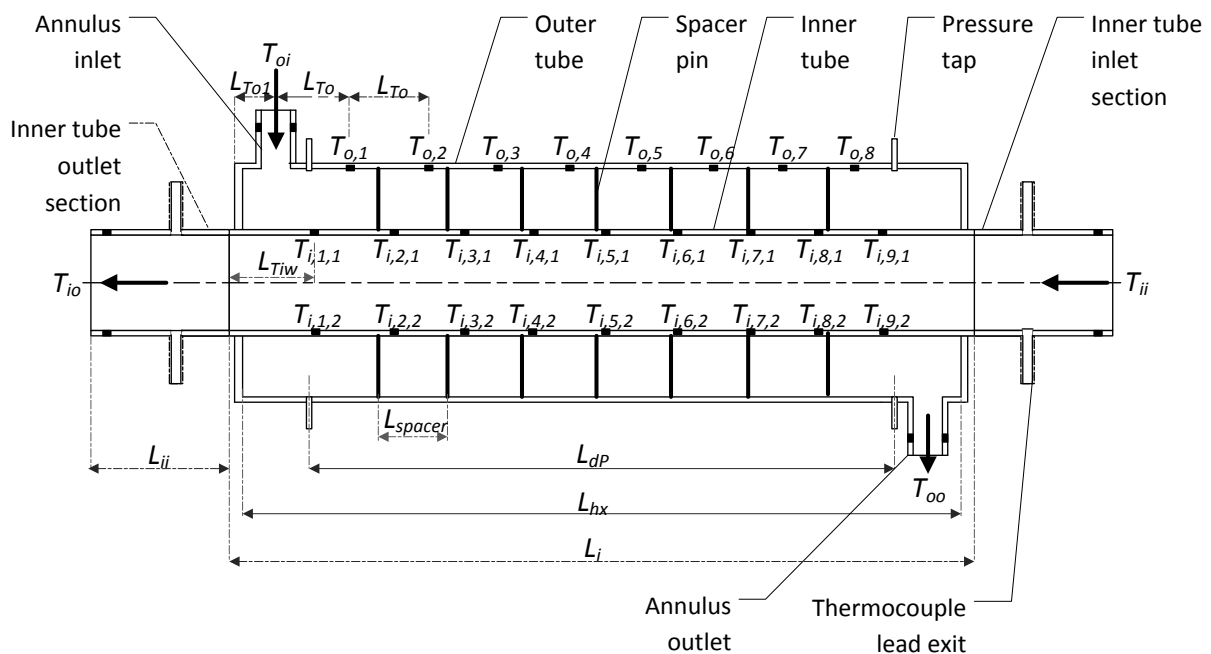


Figure 3.9: Schematic of a completed heat exchanger with dimensions provided in Table 3.5.

Table 3.5: Dimensions of all four heat exchangers (refer to Figure 3.9 for labels).

<b>Annular ratio</b>	$L_{To1}$ (m)	$L_{To}$ (m)	$L_{Tiw}$ (m)	$L_{ii}$ (m)	$L_{dp}$ (m)	$L_{hx}$ (m)	$L_{spacer}$ (m)	$L_i$ (m)
<b>0.48</b>	0.08	0.55	0.55	0.08	4.79	4.85	0.675	5.50
<b>0.58</b>	0.28	0.55	0.55	0.08	4.98	5.30	0.675	5.50
<b>0.59</b>	0.08	0.55	0.55	0.08	4.79	4.85	0.675	5.50
<b>0.71</b>	0.05	0.55	0.55	0.08	5.00	5.06	0.675	5.50

Lengths greater than 0.25m were measured with a measuring tape with uncertainties of 1mm of the measurements. Lengths smaller than 0.25m were measured with a vernier caliper with uncertainties on the measurement of  $2\mu\text{m}$ .

### 3.8 Insulation

The inlets and outlets were insulated using armafex, which is an elastomeric foam with a thermal conductivity of 0.036 W/m.K at 23°C. The heat loss through the armafex is calculated using a generalized equation for the heat loss through a cylinder given in Equation (3.4).

$$\dot{Q}_{loss} = 2\pi k_{ins} L_{hx} \frac{T_{oo} - T_{\infty}}{\ln(D_{ins}/D_{oo})} \quad (3.4)$$

Where  $T_{\infty}$  is the ambient temperature and  $D_{ins}$  the outer diameter of the insulation. A maximum heat loss will occur at a maximum temperature difference of 35°C across the insulation. This value was obtained as the hot water in the tube reaches a maximum of approximately 55°C and an ambient temperature reaches a minimum of approximately 20°C. Using the 25mm and 50mm thick armafex and the annulus outer wall diameter, the theoretical heat loss through the insulation for the 5m length of the heat exchanger is calculated and listed in Table 3.6 and Table 3.7.

The total heat exchange rate between the annulus fluid and the inner tube fluid was calculated using Equation (3.5).

$$\dot{Q}_o = \dot{m}_o C p_o (T_{oi} - T_{oo}) \quad (3.5)$$

With a minimum mass flow rate in the annulus of  $0.3 \text{ kg/s}^1$ , a minimum  $C p_o$  of  $4181.0 \text{ KJ/Kg.}^\circ\text{C}$ , and a minimum  $T_{oi} - T_{oo}$  of  $10^\circ\text{C}^2$ ; the minimum heat transfer in the heat exchanger is calculated as  $12.54 \text{ kW}$ . The percentage of this heat lost to the surroundings is shown in Table 3.6 and Table 3.7 for  $D_{oo} = 28.58\text{mm}$  and  $D_{oo} = 34.93\text{mm}$  respectively.

Table 3.6: Theoretical heat loss using 25mm and 50mm thick insulation with  $D_{oo} = 28.58\text{mm}$  and maximum temperature gradient of  $10^\circ\text{C}$ .

Insulation thickness (mm)	Annulus heat loss ( $\dot{Q}_{loss}$ ) (W)	Maximum percentage heat lost to heat exchanged (%)
25	33.11	0.26
50	22.33	0.18

Table 3.7: Theoretical heat loss using 25mm and 50mm thick insulation with  $D_{oo} = 34.93\text{mm}$  and maximum temperature gradient of  $10^\circ\text{C}$ .

Insulation thickness (mm)	Annulus heat loss ( $\dot{Q}_{loss}$ ) (W)	Maximum percentage heat lost to heat exchanged (%)
25	37.59	0.3
50	24.74	0.2

To achieve better energy balances the 50mm thick insulation was used for both outer tubes.

1The minimum flow rate is chosen as it will result in lower heat transfer rate.

2A minimum temperature difference is chosen here as it will result in a lower heat transfer

2A minimum temperature difference is chosen here as it will result in a lower heat transfer rate.

The total length of 5m for the heat transfer length was chosen due to the fact that the maximum tube length commercially available is 5.5m. A larger heat exchange length will produce larger temperature differences across the length of the tube ( $T_{ii} - T_{io}$  and  $T_{oi} - T_{oo}$ ). These larger temperature differences produce larger heat transfer values, thus reducing the uncertainties.



# Chapter 4

## Data Reduction

### 4.1 Introduction

Various approaches were used to determine the mean heat transfer coefficients for tube-in-tube heat exchangers. These include the logarithmic mean temperature method (LMTD), the modified Wilson plot method of Briggs and Young (1969) and the method of Khartabil and Christensen (1992). The LMTD method was used to calculate both mean and local heat transfer coefficients. Local calculations were focused on finite control volumes along the length of the heat exchanger while with the mean methods, the heat transfer coefficients were calculated over the entire heat transfer length of the heat exchanger. In the following sections each method is discussed in more detail.

The convection within the heat exchanger was assumed to be forced and effects from free convection are ignored. Axial conduction within the inner and outer tube was neglected. These assumptions were made due to the high turbulence within the inner tube and annulus as Reynolds numbers were in excess of 10 000.

### 4.2 LMTD Method for the Mean Heat Transfer Coefficient

The LMTD method truly reflects the exponential decay of the local temperature difference and is considerably more accurate than using the arithmetic mean fluid temperature.

$\Delta T_{LMTD}$  for an annulus is defined in Equation (4.1):

$$\Delta T_{LMTD} = \frac{(\bar{T}_w - T_{oi}) - (\bar{T}_w - T_{oo})}{\ln[(\bar{T}_w - T_{oi})/(\bar{T}_w - T_{oo})]} \quad (4.1)$$

Where  $\bar{T}_w$  is the mean surface temperature along the length of the inner tube wall. The mean surface temperature is used as the heat transfer coefficients to be calculated are the mean values over the length of the heat exchanger test section.

$\bar{T}_w$  is calculated as:

$$\bar{T}_w = \frac{1}{N_i} \sum_{j=1}^{N_i} T_{i,j} \quad (4.2)$$

With  $T_i$  the local temperatures of the inner tube wall and  $N_i$  the number of thermocouple measurement stations along the tube wall (in this study 18 were used). The overall heat transfer to the annulus fluid is calculated as:

$$\dot{Q}_o = \dot{m}_o C_{p_o} (T_{o_o} - T_{o_i}) \quad (4.3)$$

Where  $C_{p_o}$  is obtained at the bulk temperature using the fluid property correlations of Popiel and Wojtkowiak (1998) provided in Appendix A.3.2. The overall heat transfer to the inner tube fluid is calculated as:

$$\dot{Q}_i = \dot{m}_i C_{p_i} (T_{i_o} - T_{i_i}) \quad (4.4)$$

Where  $C_{p_i}$  is obtained at the bulk temperature using the fluid property correlations of Popiel and Wojtkowiak (1998) provided in Appendix A.3.2. The mean heat transfer rate is then:

$$\bar{Q} = \frac{\dot{Q}_o + \dot{Q}_i}{2} \quad (4.5)$$

The annulus heat transfer coefficient is then calculated as:

$$h_{o,LMTD,mean} = \frac{\bar{Q}}{A_s \Delta T_{LMTD}} \quad (4.6)$$

Where  $A_s$  is the heat exchange area calculated as:

$$A_s = \pi D_1 L_{hx} \quad (4.7)$$

The heat transfer coefficient is calculated at several Reynolds numbers, where the Reynolds number is defined as:

$$Re_o = \frac{\rho_o V_o D_h}{\mu_o} \quad (4.8)$$

Or more conveniently to accommodate the measured mass flow rates:

$$Re_o = \frac{\dot{m}_o D_h}{\mu_o A_o} \quad (4.9)$$

Where  $\rho_o$  and  $\mu_o$  are calculated at the bulk temperature using the fluid property equations of Appendix A.3.2.

### 4.3 LMTD Method for the Local Heat Transfer Coefficient

The local heat transfer is calculated by dividing the heat exchanger into control volumes along the heat exchange length. Figure 4.1 shows the division of the heat exchanger into nine control volumes.

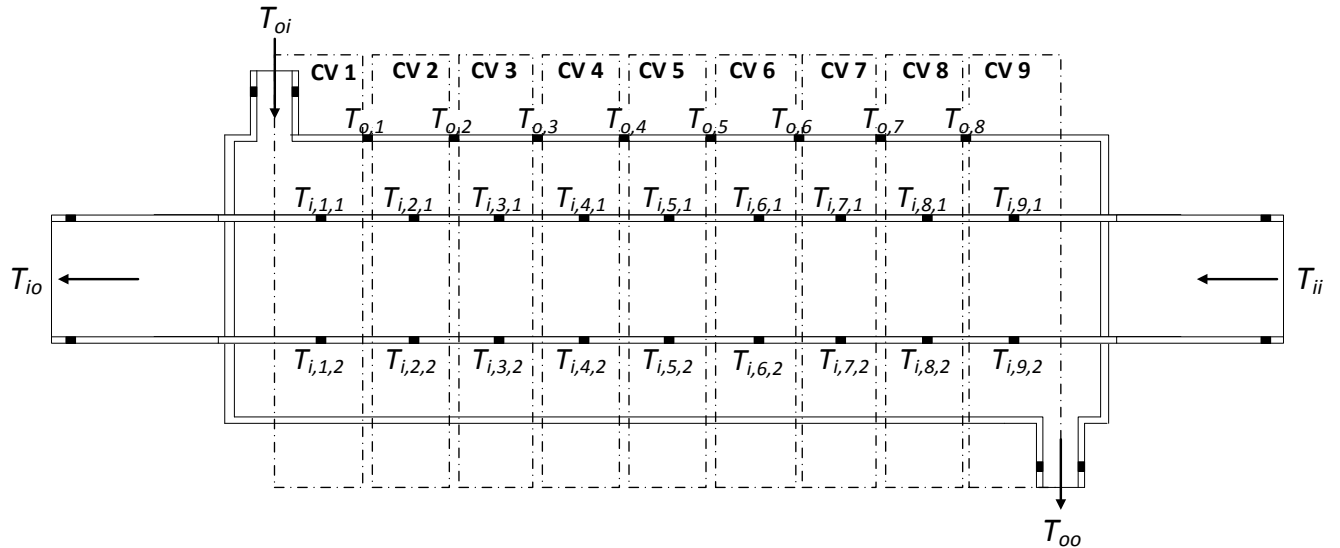


Figure 4.1: Heat exchanger divided into nine control volumes to calculate the local heat transfer.

The heat transfer of each control volume could then be calculated using the LMTD method.

The local LMTD is calculated as:

$$\Delta T_{LMTD,CV,j} = \frac{T_{oi,CV,j} - T_{oo,CV,j}}{\ln\left[\frac{(T_{w,CV,j} - T_{oo,CV,j})}{(T_{w,CV,j} - T_{oi,CV,j})}\right]} \quad (4.10)$$

Here the subscript CV refers to the associated local property of control volume  $j$ , and subscripts  $oi$  and  $oo$  refer to the inlet and outlet of the annular control volume respectively as is discussed below:

The temperatures required to calculate the  $\Delta T_{LMTD,CV,j}$  are then:

$$T_{oi,CV,j} = T_{o,j-1} \quad (4.11)$$

$$T_{oo,CV,j} = T_{o,j} \quad (4.12)$$

$$T_{w,CV,j} = (T_{i,j,1} + T_{i,j,2})/2 \quad (4.13)$$

for  $j = 1 \dots 9$ .

With the exception of the control volumes located at the annulus inlet and outlet, where the following should be used:

$$T_{oi,CV,1} = T_{oi} \quad (4.14)$$

$$T_{oo,CV,9} = T_{oo} \quad (4.15)$$

Figure 4.2 represents a single control volume showing the associated temperatures.

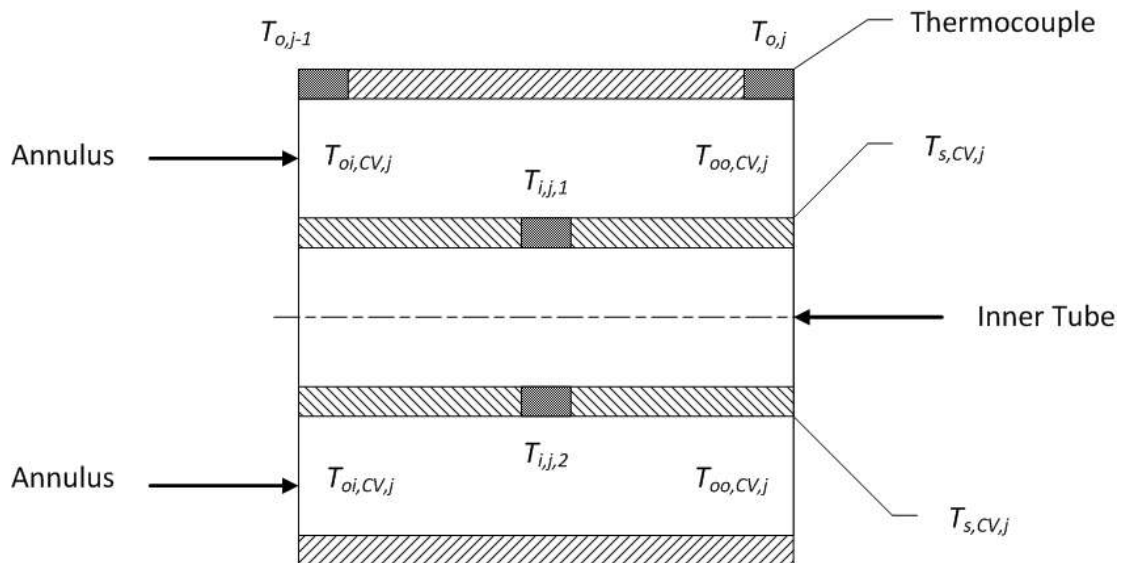


Figure 4.2: A single control volume used to calculate the local heat transfer.

The rate of heat transfer for each control volume is approximated as:

$$\dot{Q}_{o,CV,j} = \dot{m}_o C_{p_o,CV,j} (T_{oo,CV,j} - T_{oi,CV,j}) \quad (4.16)$$

With  $T_{oi,CV,j} = T_{o,j-1}$  and  $T_{oo,CV,j} = T_{o,j}$ , and  $C_{p_o,CV,j}$  is calculated using the equations of Appendix A.3.2 at the local bulk temperature given as:

$$T_{b,CV} = \frac{T_{oi,CV,j} + T_{oo,CV,j}}{2} \quad (4.17)$$

The heat transfer coefficient for each control volume is:

$$h_{o,LMTD,CV,j} = \frac{\dot{Q}_{o,CV,j}}{A_{s,CV,j} \Delta T_{LMTD,CV,j}} \quad (4.18)$$

The local Reynolds number for each control volume is:

$$Re_{o,CV,j} = \frac{\dot{m}_{o,CV,j} D_h}{\mu_{o,CV,j} A_o} \quad (4.19)$$

Where  $\mu_{o,CV,j}$  is calculated at the local bulk temperature using the equations of Appendix A.3.2.

#### 4.4 Modified Wilson Plot Method (1969)

The modified Wilson plot method of Briggs and Young (1969) is a linear regression analysis used to calculate heat transfer coefficients in the annulus of tube-in-tube heat exchangers. This method only requires inlet and outlet temperatures, as well as the mass flow rates of the fluid in the inner tube and annulus. The modified Wilson plot method predicts the average inner tube wall temperatures. The modified Wilson plot technique of Briggs and Young (1969) is provided in Appendix A. This method calculates the values of  $C_i$ ,  $C_o$ , and  $P$  which are different for each annular ratio and direction of heat flux. These values are used to calculate Nusselt numbers using the Sieder and Tate type equations:

$$Nu_i = \frac{h_i D_i}{k_i} = C_i Re_i^{0.8} Pr_i^{\frac{1}{3}} \left( \frac{\mu}{\mu_w} \right)_i^{0.14} \quad (4.20)$$

$$Nu_{Dh} = \frac{h_o D_h}{k_o} = C_o Re_{Dh}^P Pr_o^{\frac{1}{3}} \left( \frac{\mu}{\mu_w} \right)_o^{0.14} \quad (4.21)$$

An investigation into the use of the exponent 0.8 used in Equation (4.20) is provided in section 5.3.

#### 4.5 Khartabil and Christensen Method (1992)

The nonlinear regression method of Khartabil and Christensen (1992) uses a similar data set to that of the modified Wilson plot method. The steps taken to calculate the heat transfer coefficient in the annulus of the heat exchanger using the method of Khartabil and Christensen (1992) is provided in Appendix B. The values of  $C_i$ ,  $C_o$  and  $P$  were calculated

from this method and used in the Sieder and Tate type equations (Equation (4.20) and Equation (4.21)) to obtain Nusselt numbers.

## 4.6 Energy Balance

To quantify the proficiency of the heat exchangers and measurement devices, energy balances are calculated by comparing the heat transfer in the inner tube and annulus, given by:

$$eb = \frac{\dot{Q}_i - \dot{Q}_o}{(\dot{Q}_i + \dot{Q}_o)/2} \quad (4.22)$$

Where  $\dot{Q}_i$  is given as

$$\dot{Q}_i = \dot{m}_i c_{p_i} (T_{ii} - T_{io}) \quad (4.23)$$

## 4.7 Friction Factors

The friction factors for the annuli were calculated from the experimentally obtained pressure drop across the annulus length. The friction factor is defined as:

$$f = \frac{2D_h \Delta p}{\rho_o L_{dp} V_o^2} \quad (4.24)$$

Here  $\Delta p$  is the measured pressure drop over the pressure drop length  $L_{dp}$ , and  $V_o$  the average fluid velocity in the annulus given as:

$$V_o = \frac{\dot{m}_o}{\rho_o A_o} \quad (4.25)$$

# Chapter 5

## Data Analysis

### 5.1 Introduction

Using the methods of Chapter 4 the data from the heat exchanger test section with an annular diameter ratio 0.593 is analyzed here. The analyses of heat exchangers with annular diameter ratios 0.482, 0.579 and 0.712 are provided in Appendix C, and a comparison of all the annular diameter ratios is provided in Chapter 6. The effect of altering the annular diameter ratio on both the Nusselt numbers and friction factors were also investigated and reported on later.

The experimental procedure followed was to keep the inlet temperatures to both the inner tube and annulus constant. The flow rates in the inner tube were held constant while altering the annulus flow rates through a spectrum. This procedure was repeated for various inner tube flow rates, obtaining data across a large range of Reynolds number combinations. The resulting Reynolds number combinations are shown in Figure 5.1.

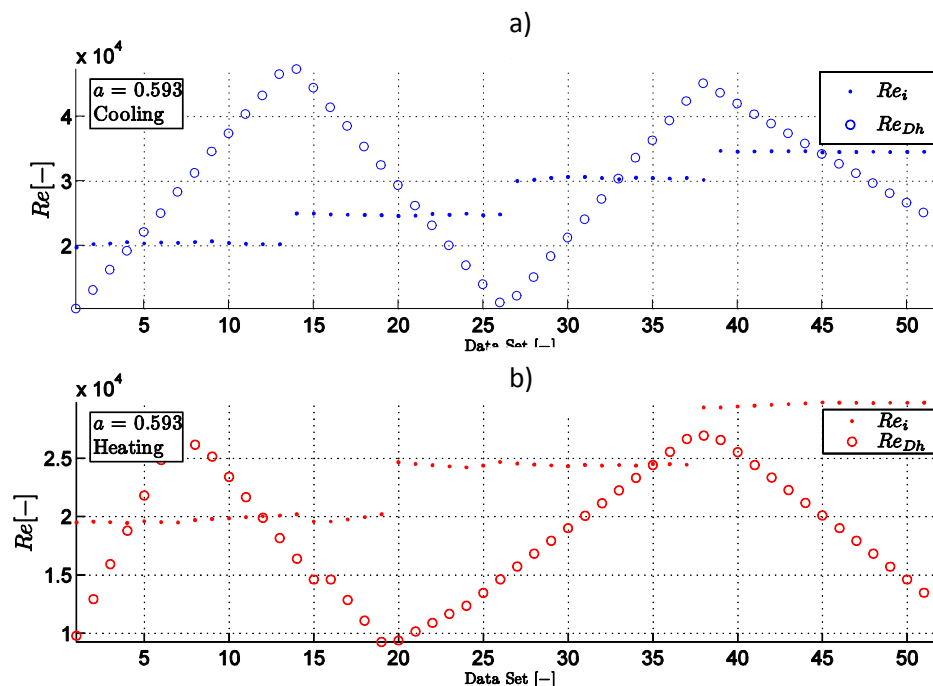


Figure 5.1: Reynolds numbers for both the inner tube and annulus for a) cooled b) heated annulus.

## 5.2 Mean Heat Transfer

The mean heat transfer coefficient was calculated using the three methods of Chapter 4; namely the mean LMTD method, modified Wilson plot method and the nonlinear regression method of Khartabil and Christensen (1992). The experimental results were compared to the correlations of Dittus and Boelter (1930) (Equation (2.16)), Dirker and Meyer (2004) (Equation (2.20)), Gnielinski (2009) (Equation (2.21)) and Swamee et al (2008) (Equation (2.23)). Figure 5.2 and Figure 5.3 show the Nusselt numbers for the case of cooling and heating the annulus respectively.

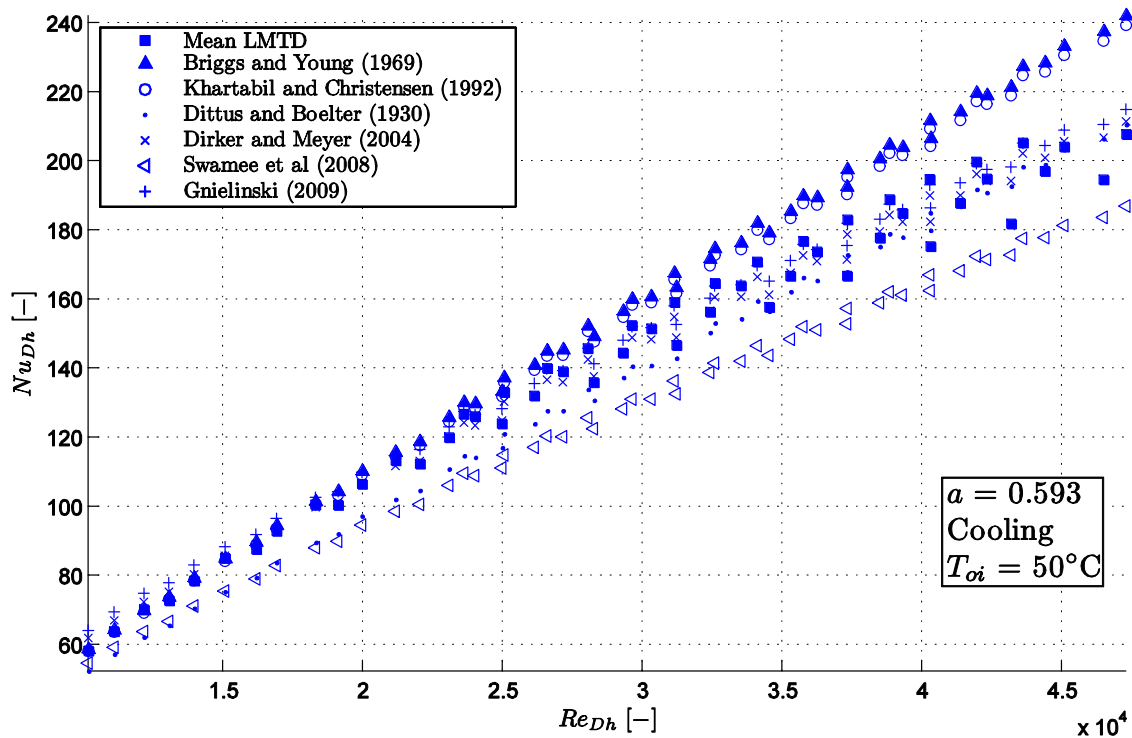


Figure 5.2: Nusselt numbers for cooling of the annulus with an annular diameter ratio of 0.593.

For a cooled annulus close agreement was found to exist between the results obtained with the linear and nonlinear regression methods. The correlations of Gnielinski (2009), Dirker and Meyer (2004), Dittus and Boelter (1930) and Swamee et al (2008) seem to under predict these methods. The mean LMTD results agree well with the linear and nonlinear regression results for annular Reynolds numbers lower than 20 000. For annular Reynolds numbers higher than this, a scatter in the LMTD results is observed. On closer inspection it is found that this scatter is directly linked to the spectrum of inner Reynolds numbers used. The mean LMTD data points on the lower edge of the scatter band in Figure 5.2 corresponded to



test conditions at the lowest inner tube Reynolds number, while the mean LMTD points at the upper edge of the scatter band corresponded to test conditions at the highest inner tube Reynolds number. The difference between the regression methods results and the Gnielinski (2009) and Dirker and Meyer (2004) correlations were up to 10%.

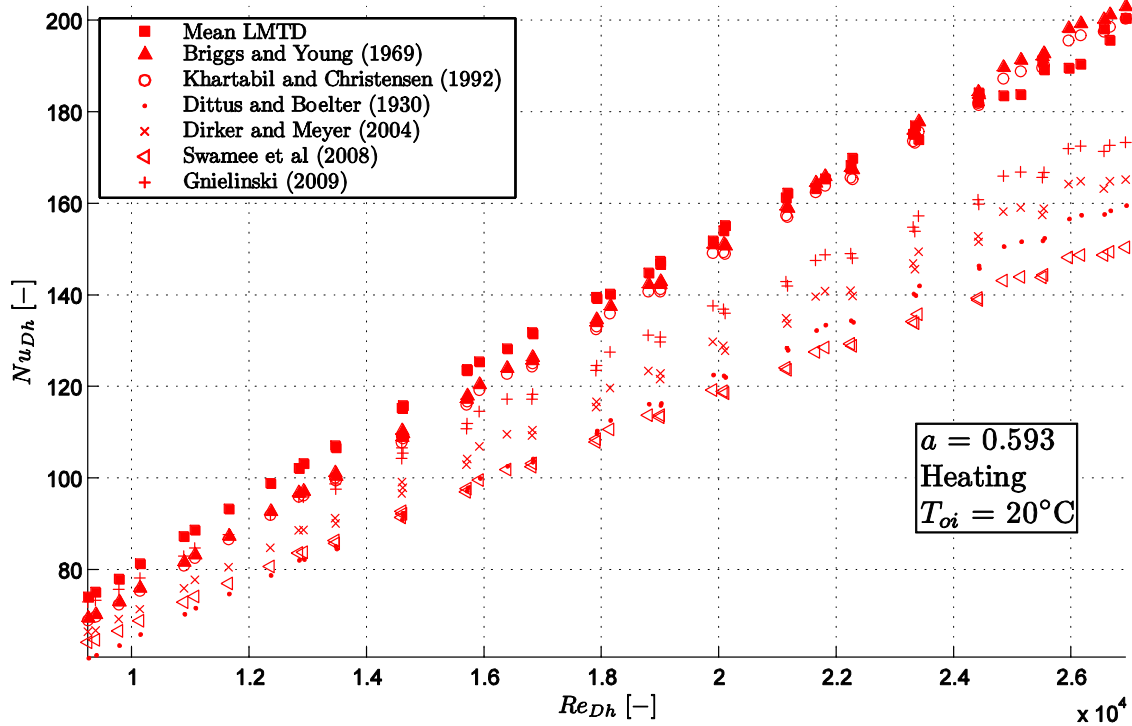


Figure 5.3: Heat transfer coefficients for heating of the annulus with an annular diameter ratio of 0.593.

For a heated annulus, it was observed that there is a close agreement between the mean Nusselt numbers obtained via the linear regression, nonlinear regression and the LMTD methods for almost all annular Reynolds numbers tested. The deviation of the LMTD-based Nusselt numbers (as was the case with a cooled annulus) could not be verified for the heated case due to a smaller range of annular Reynolds numbers under consideration. The difference between the regression methods results and the Gnielinski (2009) and Dirker and Meyer (2004) correlations were up to 8% and 15%

Similar analyses were performed on other heat exchanger test sections with  $a = 0.483$ ,  $a = 0.579$  and  $a = 0.712$ ., for a cooled and heated annulus. The results of these are provided in Appendix C. In section 6 the effect of altering the annular diameter ratio on the mean Nusselt number for specific Reynolds numbers in the annulus and inner tube is investigated.

The experimental Nusselt numbers for the case of a heated annulus are on average 35 % larger than the Nusselt numbers of a cooled annulus. This discrepancy is caused by the different Prandtl numbers that occur as a result of the fluid temperatures of the heated and cooled annulus. This is investigated in further detail in section 5.8.

Uncertainties for the Nusselt number were calculated in Appendix D using the method of Kline and McClintock (1953).

### 5.3 Inner Tube Reynolds Number Exponent

The methods of Briggs and Young (1969) and Khartabil and Christensen (1992) assume the Reynolds number exponent of the inner tube ( $P_i$ ) to be constant. They suggest a value of 0.8, shown in Equation (4.20) which was based on the Sieder and Tate (1936) form of the equation. The original method of Wilson (1915) used a value of 0.82 for  $P_i$ . In this study 0.8 was used for the exponent of the Reynolds number, as the Sieder and Tate (1936) form of the equation included the effects of the viscosity ratio of the bulk fluid to the fluid at the inner tube wall, whereas Wilson (1915) omitted the viscosity ratio effects.

In the studies of Briggs and Young (1969) and Khartabil and Christensen (1992) the inner tube was smooth and free of obstructions. In this study, the thermocouples fed through the inner tube occupied 8.61% of the inner tube cross sectional area of test sections 1 and 3; and 5.79% of the inner tube cross sectional area of test sections 2 and 4. This may alter the inner tube Reynolds number exponent of 0.8 and result in different mean Nusselt numbers. By altering the exponent between 0.8 and 0.82 the effects on the Nusselt numbers of the annulus for the modified Wilson plot and nonlinear regression methods were investigated. This is given mathematically as:

$$Nu_i = \frac{h_i D_i}{k_i} = C_i Re_i^{P_i} Pr_i^{\frac{1}{3}} \left( \frac{\mu}{\mu_w} \right)_i^{0.14} \quad (5.1)$$

for  $0.8 \leq P_i \leq 0.82$

The annular Nusselt numbers calculated from the modified Wilson plot method and nonlinear regression scheme are calculated using the modified expression for the inner tube

Nusselt number given in Equation (5.1). The resulting annulus Nusselt numbers are denoted by  $Nu_{Dh,0.8}$ , for  $P_i = 0.8$ , and  $Nu_{Dh,P_i}$  for  $0.8 \leq P_i \leq 0.82$ . This is given mathematically as:

$$Nu_{Dh,0.8} = Nu_{Dh} \text{ for } P_i = 0.8. \quad (5.2)$$

$$Nu_{Dh,P_i} = Nu_{Dh} \text{ for } 0.8 < P_i \leq 0.82 \quad (5.3)$$

An averaged ratio of the Nusselt numbers with an altered exponent ( $Nu_{Dh,P_i}$ ) to the Nusselt numbers with an exponent of 0.8 ( $Nu_{Dh,0.8}$ ) were used to observe the effects of altering  $P_i$ .

The averaged ratio is defined in Equation (5.4) below:

$$Nu_{Dh,ratio} = \frac{1}{N} \sum_{j=1}^N \frac{(Nu_{Dh,P_i})_j}{(Nu_{Dh,0.8})_j} \quad (5.4)$$

for  $0.8 \leq P_i \leq 0.82$

Where  $N$  is the number of data points captured.

The influence of the Reynolds number exponent of the inner tube, in the Sieder and Tate equation, was investigated for a range of values between 0.8 and 0.82. The modified Wilson Plot and nonlinear regression methods were used for this range of  $P_i$  values. Figure 5.4 and Figure 5.5 show the ratio of Nusselt numbers obtained from altered  $P_i$  values to Nusselt numbers obtained with a  $P_i$  value of 0.8 (refer to Equation (5.4)), using the modified Wilson plot and nonlinear regression methods respectively.

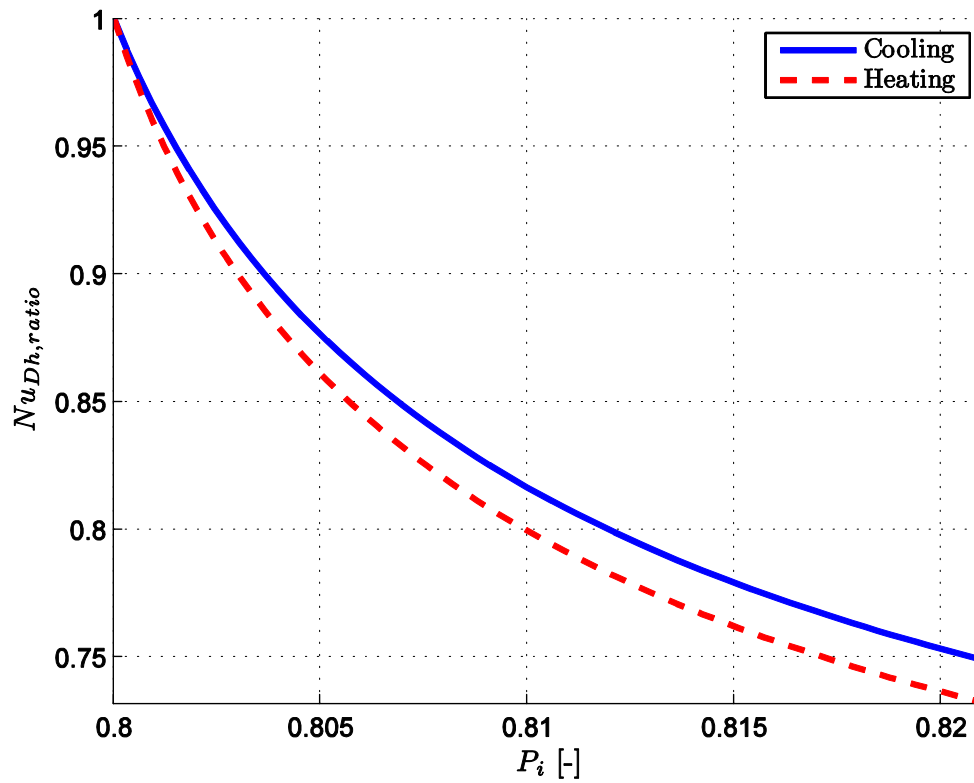


Figure 5.4: Ratio of Nusselt numbers with different inner Reynolds number exponents using the modified Wilson plot method.

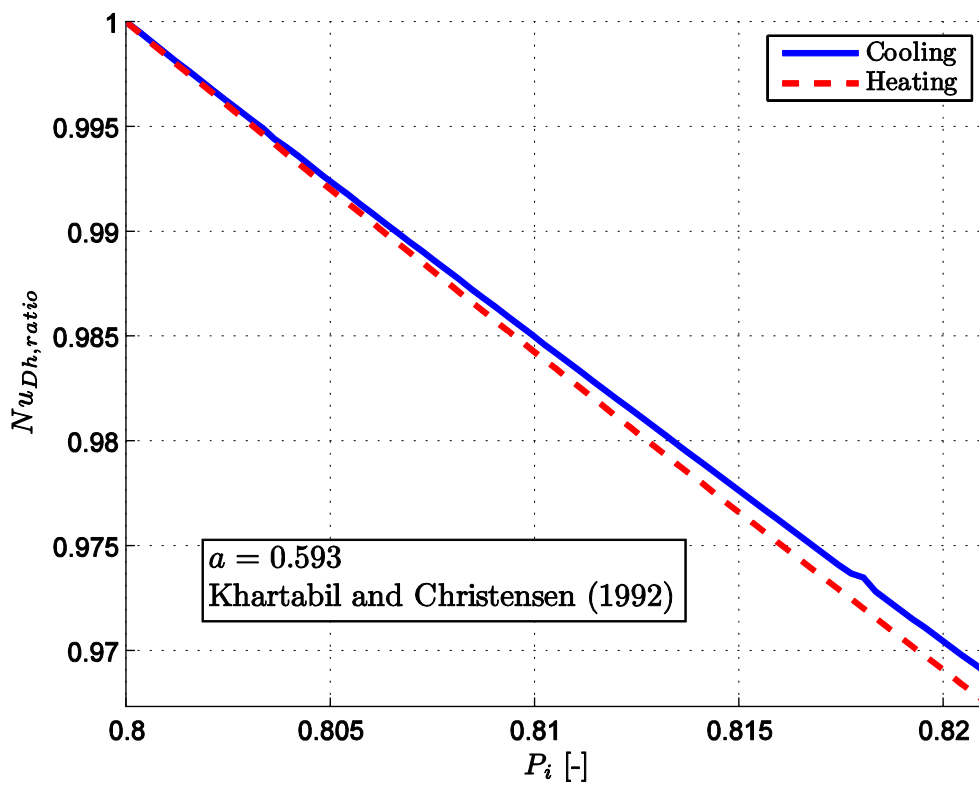


Figure 5.5: Ratio of Nusselt numbers with different Inner Reynolds number exponents using the nonlinear regression method.











Figure 5.4 shows that by increasing  $P_i$  from 0.8 to 0.82 there is a decrease in the Nusselt number in the annulus by up to 30% if the modified Wilson plot is used. The nonlinear regression scheme is influenced less by changes in  $P_i$ . In Figure 5.5 the nonlinear regression scheme shows a maximum decrease in Nusselt number of 3% if  $P_i$  is increased from 0.8 to 0.82.

Altering the value of  $P_i$  to 0.82 would result in a 30% Nusselt number decrease using the modified Wilson plot method and a 3% Nusselt number decrease in the nonlinear regression method. This would result in a large disagreement between the modified Wilson plot and the nonlinear regression method. Based on the fact that at  $P_i = 0.8$  both regression methods give similar results, it is thus assumed that a constant  $P_i$  value of 0.8 is suitable for this study.

## 5.4 Wall Temperature Analysis

A temperature profile along the axial length of the test section, for both the inner tube and outer tube wall is shown in Figure 5.6 to Figure 5.9. This temperature profile is shown for both high and low Reynolds numbers in the inner tube and annulus. Table 5.1 provides the legend and description of the plots given in Figure 5.6 to Figure 5.9.

Table 5.1: Legend used In Figure 5.6 to Figure 5.9.

Cooled annulus	Description	Heated annulus
	Inner tube inlet and outlet temperatures with a linear curve fitted to these two points.	
	The inner tube wall temperatures, with a second order polynomial curve fitted through these points.	
	The outer tube wall temperatures as well as the annulus inlet and outlet temperatures with a second order polynomial curve plotted through these points.	
	The flow direction in the inner tube.	
	The flow direction in the annulus.	

The annular inlet and inner tube outlet are located at  $x = 0$ ; and the annulus outlet and inner tube inlet are located at  $x = L_{hx}$ . Figure 5.6 a) and b) are plotted at low  $Re_i$  with Figure 5.7a) and b) plotted at a high  $Re_i$ .

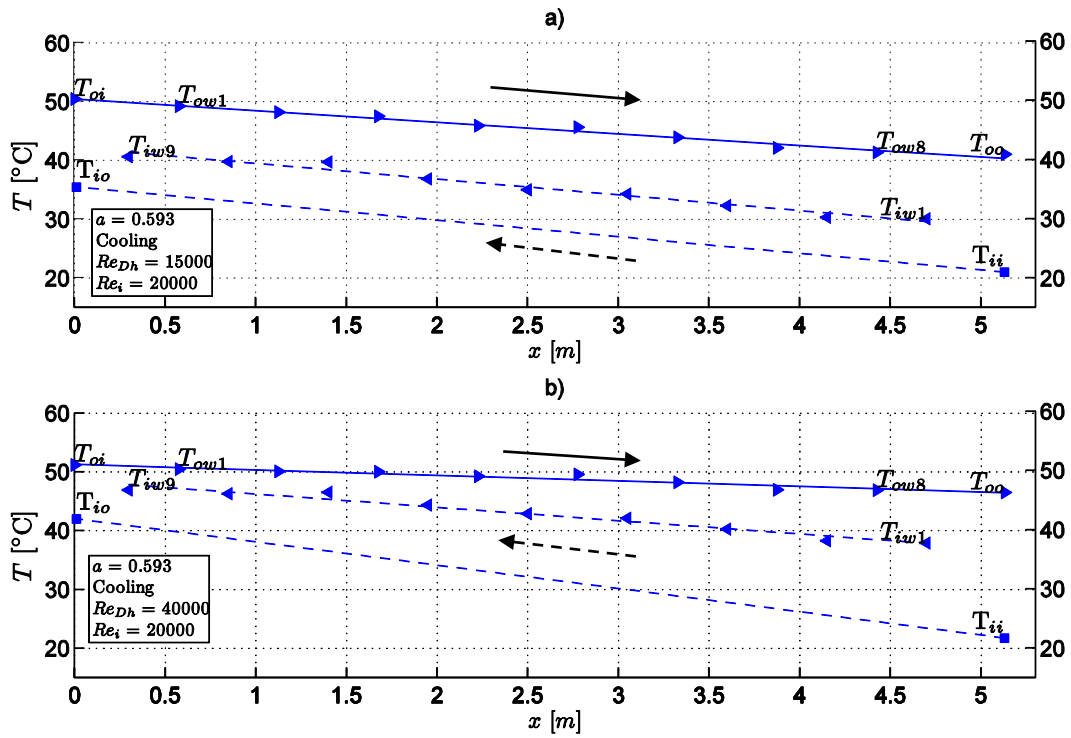


Figure 5.6: Wall temperature profiles for the inner tube fluid, inner tube wall and annulus wall for a cooled annulus with low inner tube flow rates and a) low annular flow rates b) high annular flow rates.

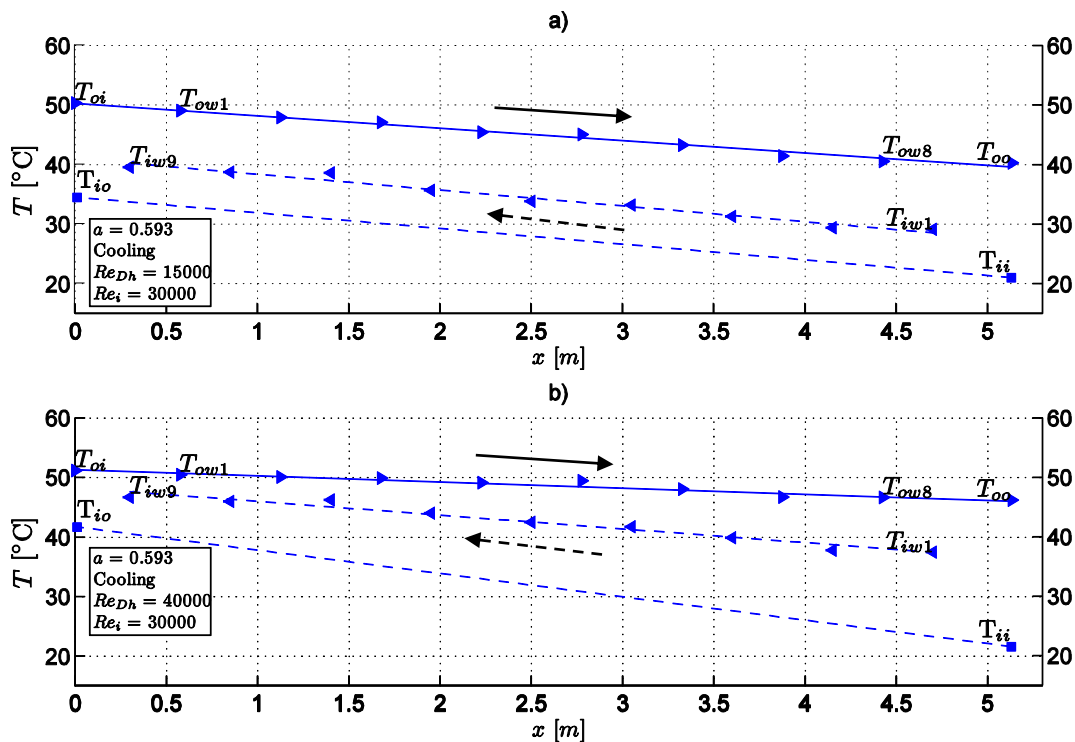


Figure 5.7: Wall temperature profiles for the inner tube fluid, inner tube wall and annulus wall for a cooled annulus with high inner tube flow rates and a) low annular flow rates b) high annular flow rates.

Figure 5.8 a) and b) and Figure 5.9 a) and b) are for a low and high  $Re_i$  respectively, for a heated annulus.

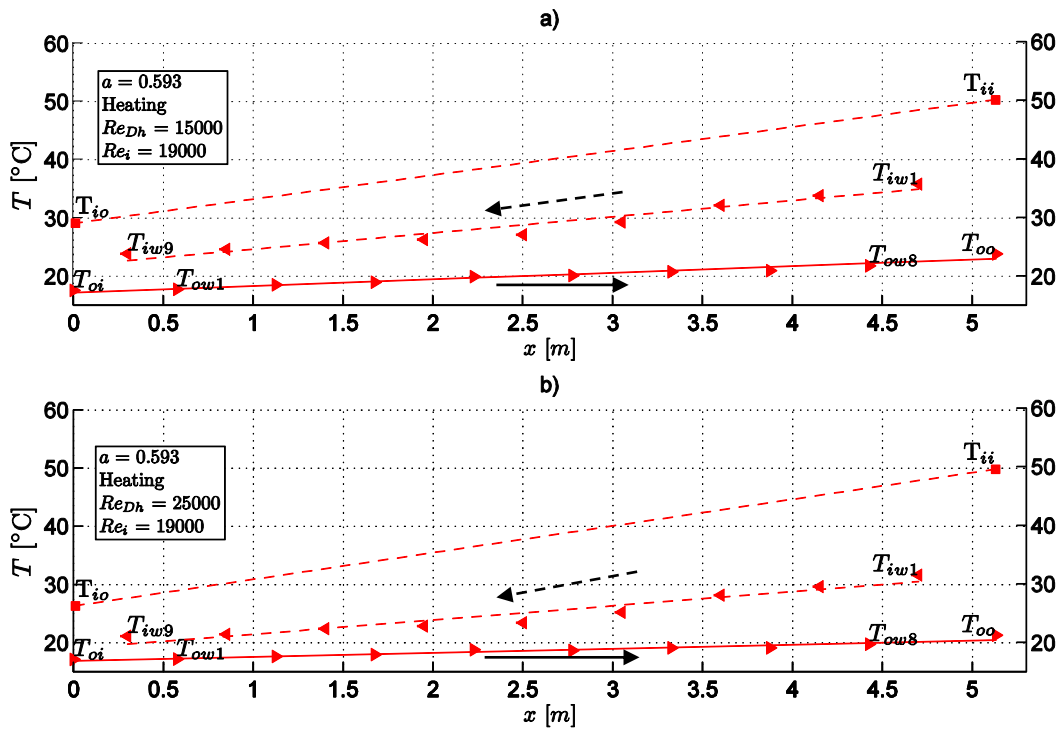


Figure 5.8: Wall temperature profiles for the inner tube fluid, inner tube wall and annulus wall for a heated annulus with low inner tube flow rates and a) low annular flow rates b) high annular flow rates.

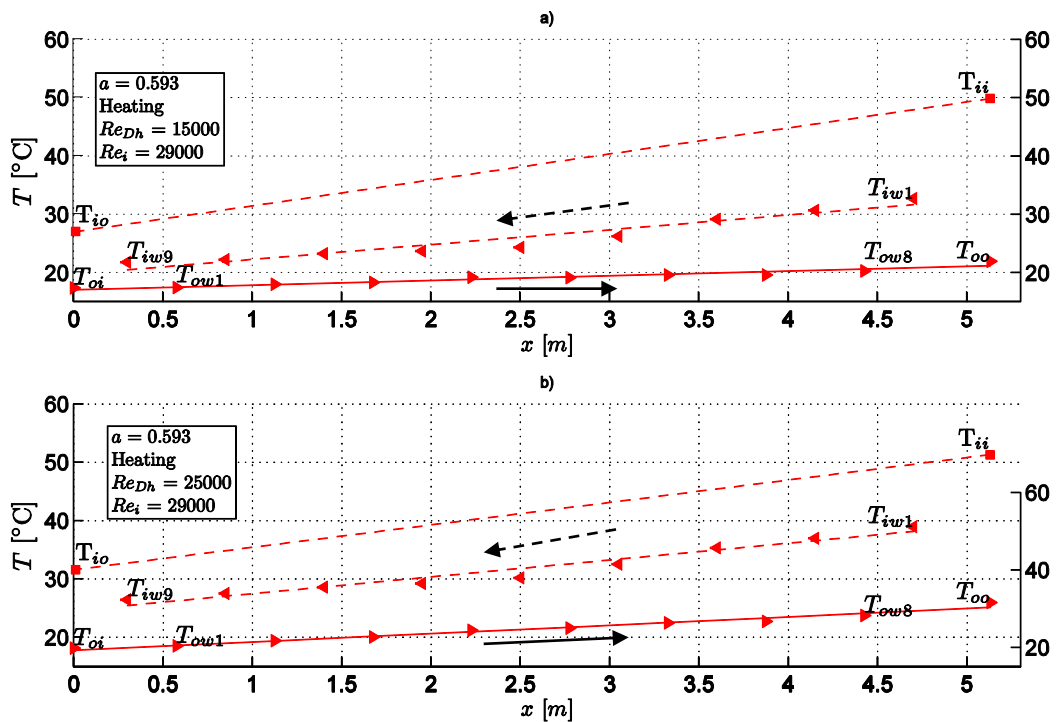


Figure 5.9: Wall temperature profiles for the inner tube fluid, inner tube wall and annulus wall for a heated annulus with high inner tube flow rates and a) low annular flow rates b) high annular flow rates



## 5.5 Local Heat Transfer Rates

Calculating the local Nusselt numbers using the experimental wall temperatures resulted in errors larger than 100% when compared to the mean Nusselt numbers. A sensitivity analysis showed that an error of the inner tube wall temperature of 0.8°C results in a local Nusselt number error in excess of 130%. As a result of this high sensitivity to temperature errors, a second order polynomial fitted curve as in Figure 5.6 to Figure 5.9 was applied to each of the test runs and the wall temperatures from these curve fits were used to calculate the local Nusselt numbers.

A maximum deviation from the fitted curve of 1.2°C occurs at  $x = 2.6\text{m}$  for a heated annulus with  $Re_{Dh} = 25\ 000$  and  $Re_i = 29\ 000$ . The annulus inlet and outlet temperatures ( $T_{oi}$  and  $T_{oo}$ ) are within 0.3°C of the fitted curve of the annulus wall temperatures. Uncertainties of the thermocouples at the inlet and outlet as well as the wall temperatures are given in Appendix D. The measured inlet and outlet temperatures of both the annulus and inner tube result in uncertainties of 0.053°C. The inner tube wall temperatures and outer tube wall temperature measurements had uncertainties of 0.075°C and 0.106°C respectively.

A method of determining the ‘Goodness of fit’ of a curve to experimental data is by calculating the coefficient of determination ( $R^2$ ) of the fitted curve, as explained in Gujarati and Porter (2009). An  $R^2$  value of 1.0 would represent a perfect fit where the function in terms of the independent variable  $x$  (axial distance along the test section) is able to predict the dependent variable  $T$  (temperature) with 100% accuracy. An  $R^2$  value of 0.0 would suggest the fitted curve is unable to predict any of the points. Equation (5.5) was used to calculate the coefficient of determination.

$$R^2 = 1 - \frac{\sum_{i=1}^7 [(T_i - \hat{T}_i)^2]}{\sum_{i=1}^7 [(T_i - \bar{T})^2]} \quad (5.5)$$

Where  $T_i$  is the measured temperature,  $\hat{T}_i$  the temperature predicted by the curve fit and  $\bar{T}$  the mean of the measured temperatures. The coefficient of determination for the inner tube and annulus wall temperature curve fits were calculated for each test run. The average coefficient of determination for both the inner tube and annulus wall for both a heated and cooled annulus are shown in Table 5.2.

Table 5.2: Coefficient of determination for wall temperature curve fits.

Cooling		Heating	
$\bar{R}_i^2$ (-)	$\bar{R}_o^2$ (-)	$\bar{R}_i^2$ (-)	$\bar{R}_o^2$ (-)
0.938	0.940	0.934	0.936

The coefficient of determinations of Table 5.2 show that the curve fits will predict about 93% of the wall temperatures to within 0.075°C and 0.106°C for the inner tube and outer tube walls respectively.

The mean measured inner wall temperatures were also compared to those predicted by the modified Wilson plot method of Briggs and Young (1969) and the nonlinear regression analysis of Khartabil and Christensen (1992). The average difference of the mean measured wall temperatures to those predicted by Briggs and Young (1969) and Khartabil and Christensen (1992), were 0.46°C and 1.69°C respectively. These temperature differences are discussed in more detail in Appendix A and Appendix B for the Briggs and Young (1969) and Khartabil and Christensen (1992) methods.

Using the fitted wall temperatures the local LMTD method presented in Chapter 4 was used to calculate local Nusselt numbers for each control volume (control volumes were arranged as in Figure 4.1). The local Nusselt numbers in Figure 5.10 and Figure 5.11 are compared to the mean Nusselt numbers calculated using the mean LMTD method, as well as the correlation of Dirker and Meyer (2004) and Gnielinski (2009) for a cooled and heated annulus respectively. In Figure 5.10 and Figure 5.11 the local Nusselt numbers are a function of the local Reynolds numbers on the abscissa and the mean Nusselt numbers a function of the mean Reynolds numbers.

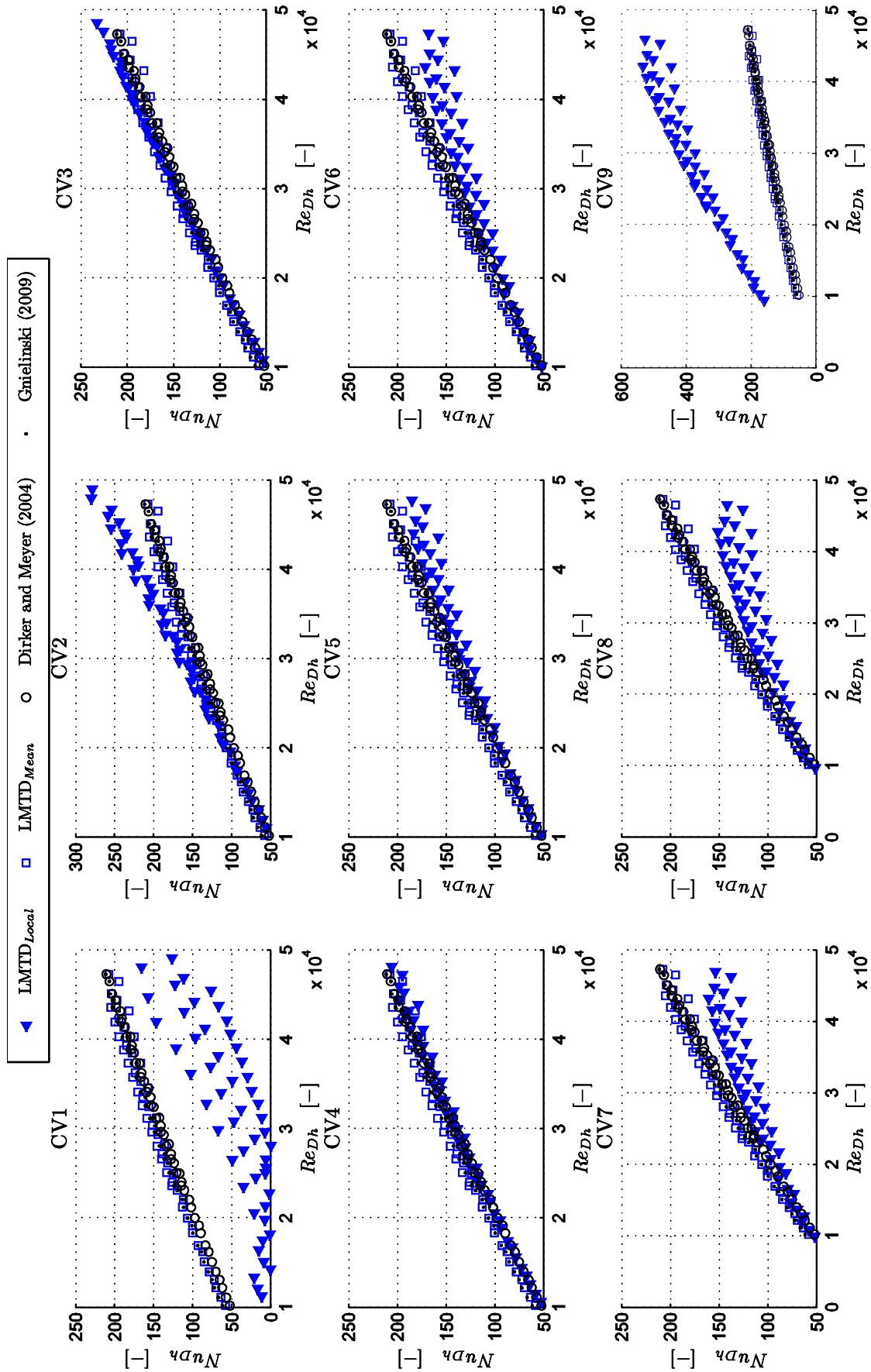


Figure 5.10: Local LMTD Nusselt numbers for control volumes 1 – 9, compared to the mean LMTD heat transfer coefficients and those calculated from Dirker and Meyer (2004) and Gnielinski (2009) for the case of cooling the annulus.

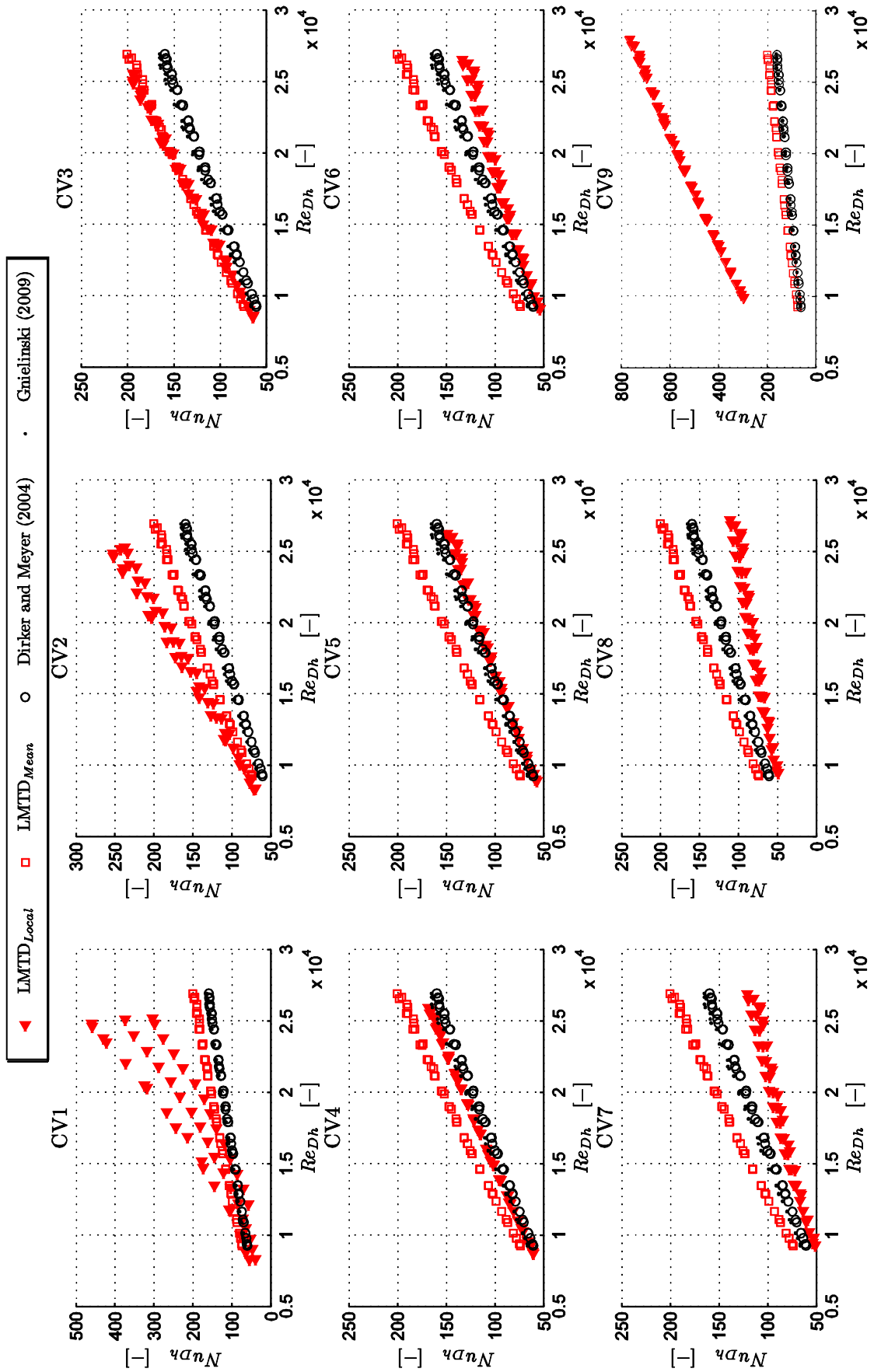


Figure 5.11: Local LMTD Nusselt numbers for control volumes 1 – 9, compared to the mean LMTD heat transfer coefficients and those calculated from Dirker and Meyer (2004) and Gnielinski (2009) for the case of heating the annulus.

Large deviations occur at control volumes 1 and 9. This is possibly due to the unstructured flow at the annulus inlet and outlet. The control volumes located nearer to the annulus inlet show a higher local Nusselt number, with a decrease towards the annulus outlet.

The uncertainties on the local Nusselt numbers were calculated using the method of Kline and McClintock (1953) shown in Appendix D. The resulting uncertainties of the local Nusselt numbers were on average 7.5% and 4.7% for a cooled and heated annulus respectively.

The local Nusselt numbers are presented in Figure 5.12 to Figure 5.15 as a function of axial length along the tube for various values of  $Re_{DhLocal}$ . Figure 5.12 and Figure 5.14 are for the case of a low  $Re_i$  value and Figure 5.13 and Figure 5.15 for a high  $Re_i$  value. As experimental measurements were not taken at precisely the same values of  $Re_{DhLocal}$  for each control volume, the local Nusselt numbers were obtained via a linear interpolation process between the neighboring local Nusselt numbers at each specified  $Re_{DhLocal}$  value.

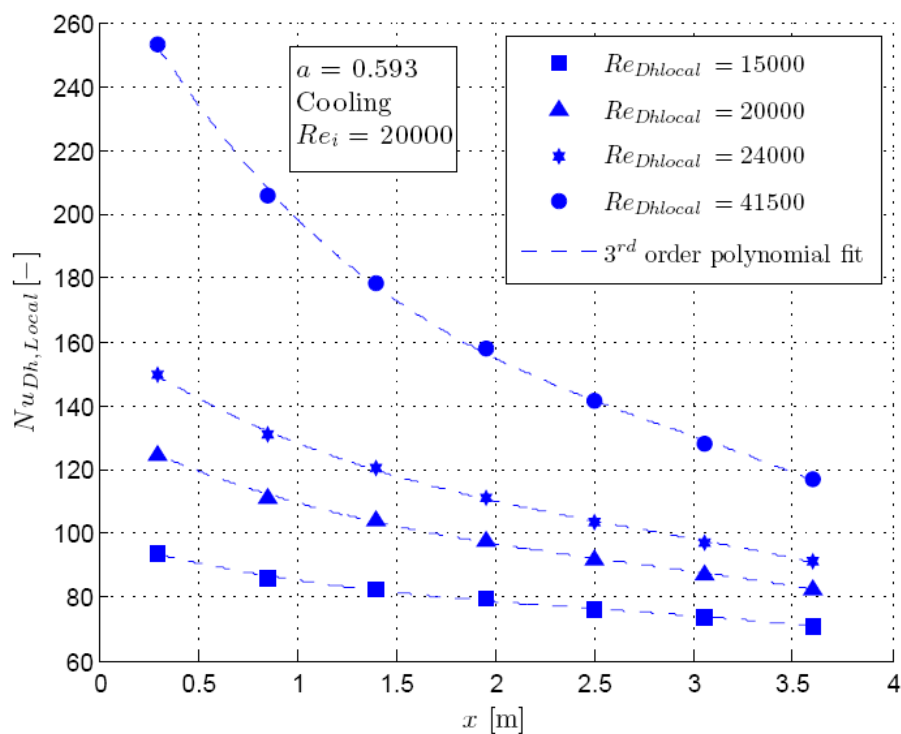


Figure 5.12: Local Nusselt numbers as a function of axial distance along the heat exchanger length for various  $Re_{DhLocal}$  and  $Re_i = 20\,000$  for a cooled annulus.

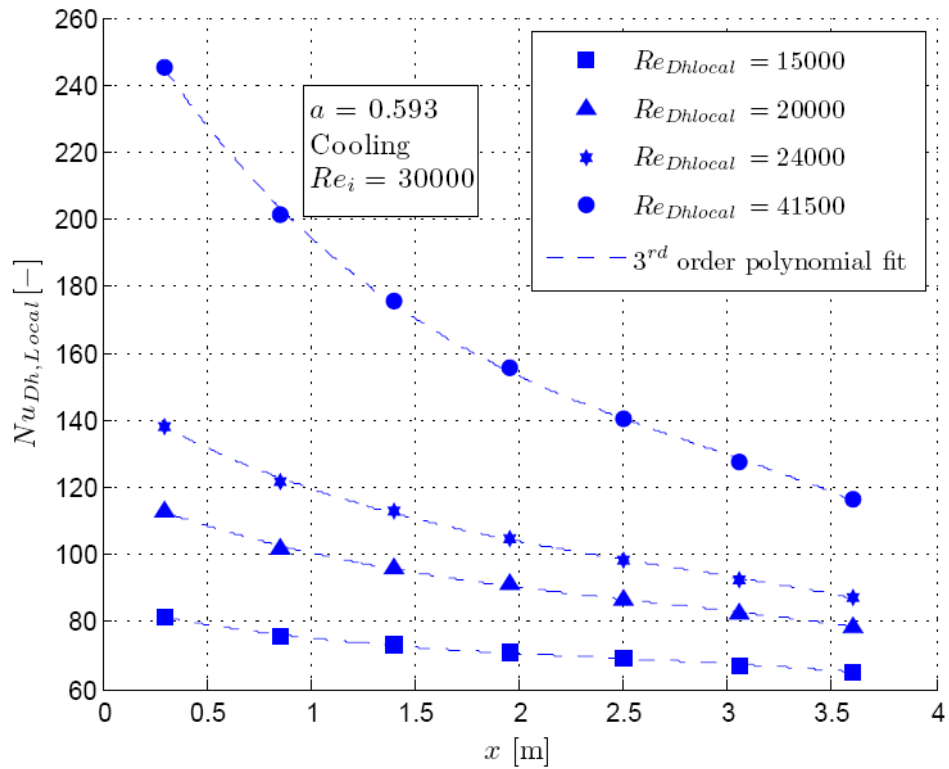


Figure 5.13: Local Nusselt numbers as a function of axial distance along the heat exchanger length for various  $Re_{DhLocal}$  and  $Re_i = 30\,000$  for a cooled annulus.

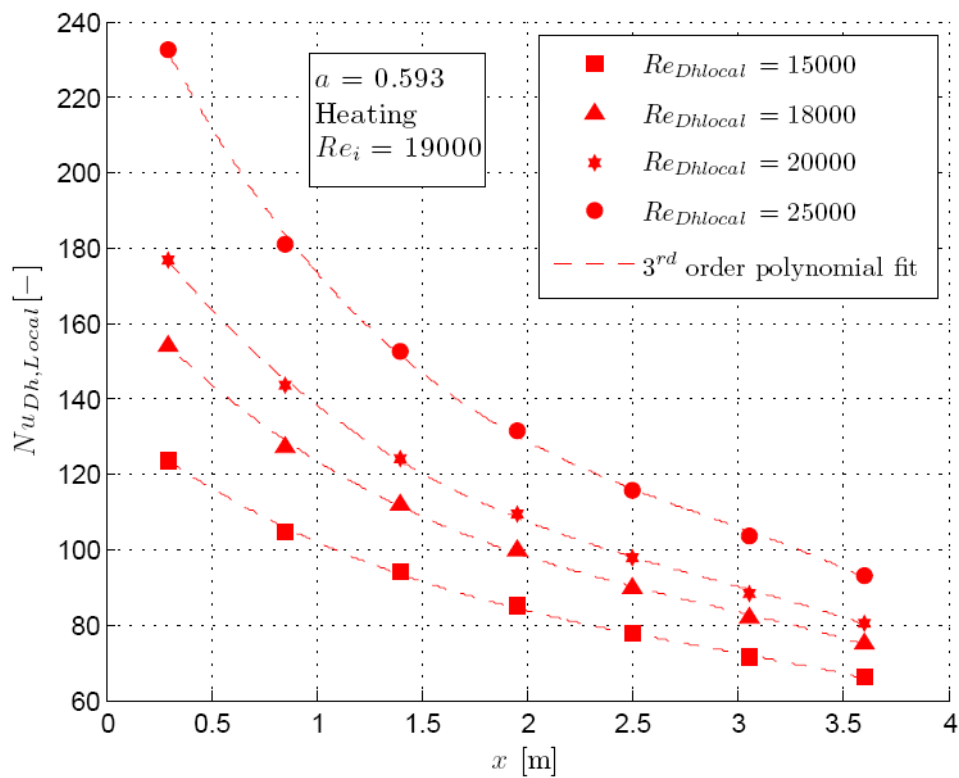


Figure 5.14: Local Nusselt numbers as a function of axial distance along the heat exchanger length for various  $Re_{DhLocal}$  and  $Re_i = 19\,000$  for a heated annulus.

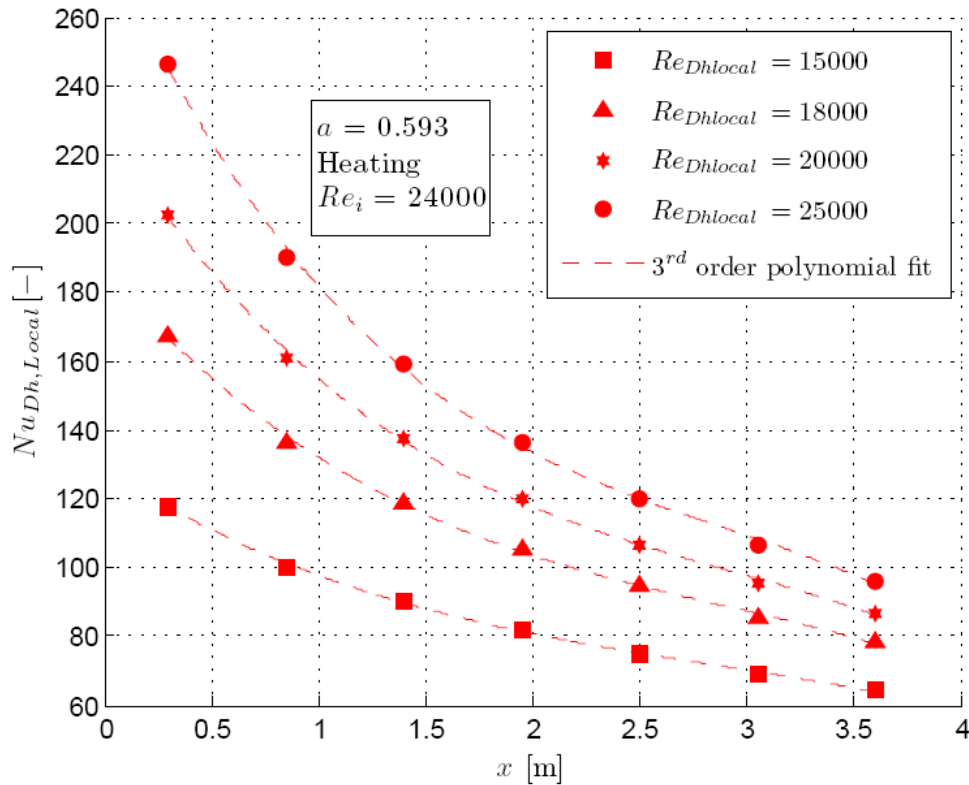


Figure 5.15: Local Nusselt numbers as a function of axial distance along the heat exchanger length for various  $Re_{Dh,local}$  and  $Re_i = 24\,000$  for a heated annulus.

Figure 5.12 to Figure 5.15 suggest that at the entrance to the annulus larger local Nusselt numbers exist, and a decrease towards the annulus outlet. Larger differences in the local Nusselt numbers, from the annulus inlet to outlet, are found for larger  $Re_{Dh,local}$  values.

## 5.6 Energy Balance

The energy balance calculated in Equation (4.22) for each test run, as well as the mean energy balance for both a heated and cooled annulus are shown in Figure 5.16.

For the case of the cooled annulus, it is expected that the energy balance error ( $eb$ ) would be higher as it is difficult to completely avoid losing heat to the surroundings, even with adequate insulation. This is due to the large temperature differences between the outer tube wall and surroundings. The mean energy balance error for a cooled annulus is 1.8% with a maximum of 3.7%. Heating of the annulus produced lower energy balance errors with a mean of 0.8% and a maximum of 1.4%.

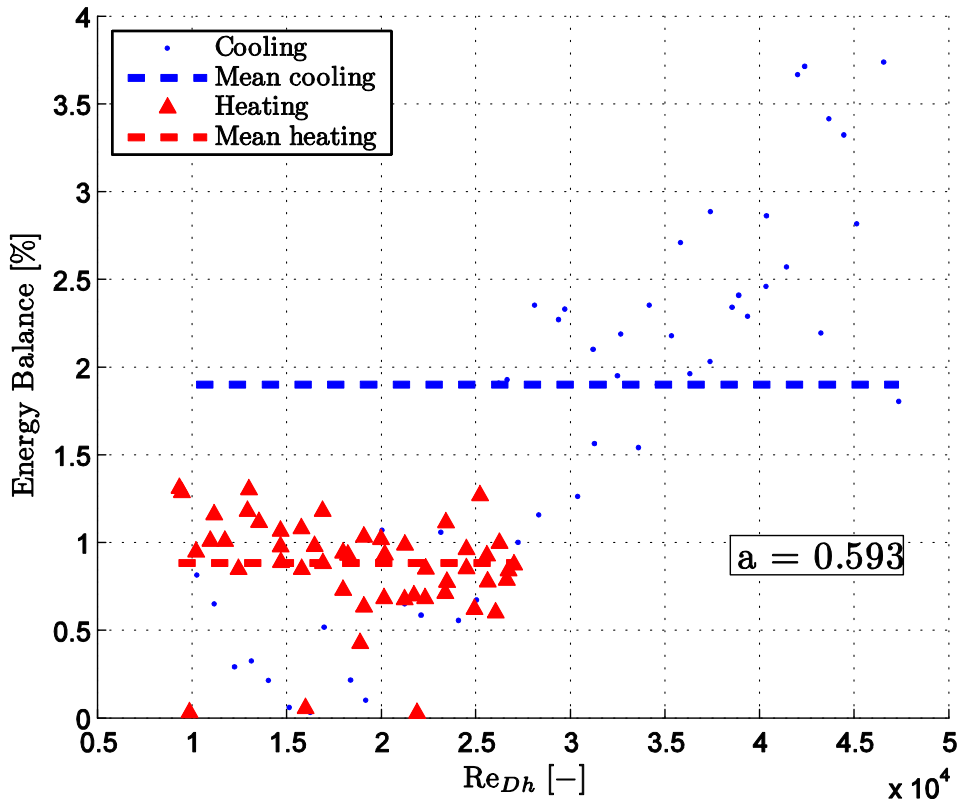


Figure 5.16: Energy balance for both heating and cooling of the annulus.

### 5.7 Friction Factor

The friction factors calculated over the pressure drop length of the heat exchanger are shown in Figure 5.17. The friction factors are for both a heated and cooled annulus. The experimental friction factors are compared to those predicted by the equations of Blasius, Jones and Leung (1981), Kaneda et al (2003) and Gnielinski (2009).

The friction factors for a cooled annulus are within 4% of the Gnielinski (2009) and Jones and Leung (1981) correlations. The correlations of Blasius and Kaneda et al (2003) under predict the friction factors by up to 10%. For a heated annulus slightly lower friction factors are observed than those of a cooled annulus and are within 1.5% of the Gnielinski (2009) and Jones and Leung (1981) correlations. The correlations of Blasius and Kaneda et al (2003) under predict the friction factors by up to 8%.



The friction factor uncertainties are calculated in Appendix D. The resulting average uncertainties for a cooled and heated annulus are 1.6% and 0.7% of the friction factor respectively.

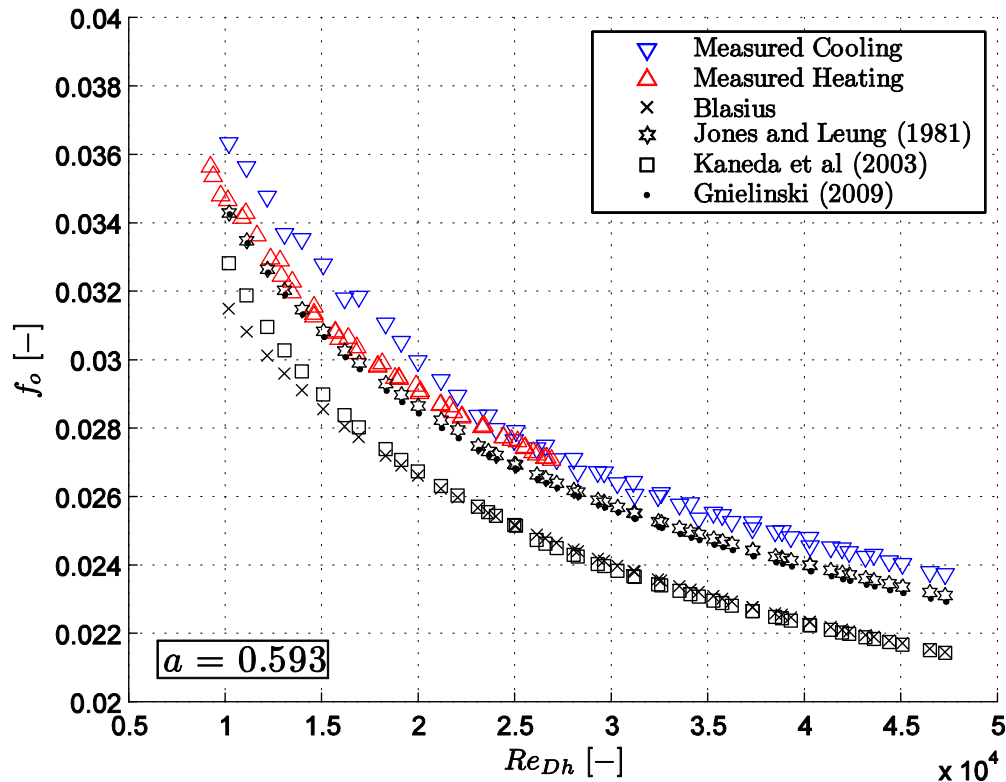


Figure 5.17: Diatomic friction factors for a heated and cooled annulus, compared to the correlations of Blasius, Jones and Leung (1981), Kaneda et al (2003) and Gnielinski (2009).

The larger friction factors may be attributed to non-concentricity present in the connection of the outer tube sections. During the construction of the heat exchanger much effort was taken to assemble the outer tube concentric to the inner tube as explained in section 3. After the heat exchanger was assembled the concentricity of the inner and outer tube may have been lost.

The coupling used to hold the outer tubes concentric had sections 15mm long that formed part of the annulus wall. These were machined to have equal inner diameters to that of the outer tube. These sections may have had a higher surface roughness, which would result in larger friction factors. In section 6 friction factor results of Ntuli *et al* (2010) are investigated. The results of Ntuli *et al* (2010) also show larger friction factors than is predicted in the literature.

## 5.8 Colburn j-Factor

The Nusselt numbers obtained for a heated annulus were on average 35% larger than those of a cooled annulus. The Nusselt numbers obtained using the modified Wilson plot technique, for both a heated and cooled annulus are shown in Figure 5.18. The results of the modified Wilson plot technique were used in this investigation as it produced the most accurate wall temperature predictions when compared to the experimental results (see Appendix A). It is also the most widely used in literature.

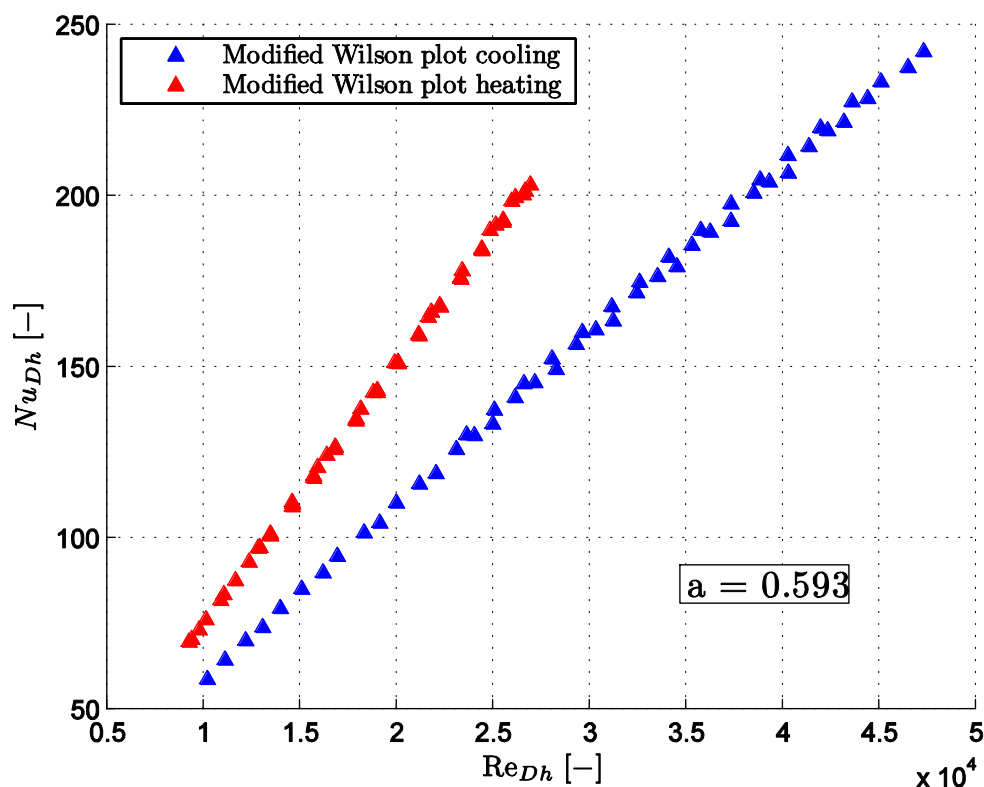


Figure 5.18: Nusselt numbers obtained using the modified Wilson plot technique for a heated and cooled annulus for an annular diameter ratio of 0.593.

The discrepancy in Nusselt numbers between a heated and cooled annulus warranted an investigation into the Colburn j-factor. It would be more accurate to represent the heat transfer results in terms of the Colburn j-factor, as this would neglect the effects of the Prandtl number on the heat transfer results. The Prandtl numbers of the annulus fluid for a heated and cooled annulus would differ as a result of the different mean annulus fluid temperatures.

The Colburn  $j$ -factor is defined as:

$$j = \frac{Nu_{Dh}}{Pr_o^{2/3} Re_{Dh}} \quad (5.6)$$

The results of the Colburn  $j$ -factor are plotted on a logarithmic scale in Figure 5.19 for both a heated and cooled annulus. A polynomial curve with the form given in Equation (5.7) was fitted to the Colburn  $j$ -factors for a heated and cooled annulus. The polynomial curves are also shown on Figure 5.19.

$$j = C_1 Re_{Dh}^2 + C_2 Re_{Dh} + C_3 \quad (5.7)$$

The constants  $C_1$ ,  $C_2$  and  $C_3$  for a heated and cooled annulus and all annular diameter ratios are provided in Table 5.3.

Table 5.3: Constants  $C_1$ ,  $C_2$  and  $C_3$  for the polynomial curves fitted through the experimental Colburn  $j$ -factors.

Annular diameter ratio ( $a$ )	Cooling			Heating		
	$C_1$	$C_2$	$C_3$	$C_1$	$C_2$	$C_3$
<b>0.482</b>	1.74e-13	-2.01e-08	2.69e-03	3.71e-13	-2.74e-08	2.56e-03
<b>0.579</b>	8.72e-14	-1.14e-08	2.48e-03	4.89e-13	-3.14e-08	2.55e-03
<b>0.593</b>	1.22e-13	-1.18e-08	2.40e-03	5.85e-14	-5.50e-09	2.19e-03
<b>0.712</b>	-1.95e-14	3.55e-10	2.28e-03	2.39e-13	-1.36e-08	2.22e-03

The constant  $C_1$  show an overall decreasing trend for an increasing annular diameter ratio.  $C_2$  shows an overall increasing trend with an increasing annular diameter ratio while  $C_3$  remains fairly constant across the annular diameter ratio range. The polynomial curves fitted all the Colburn  $j$ -factor results within 5%.

A plot of the Colburn  $j$ -factors for the test sections with annular diameter ratios  $a = 0.482$ ,  $a = 0.579$  and  $a = 0.712$  are provided in Appendix C.

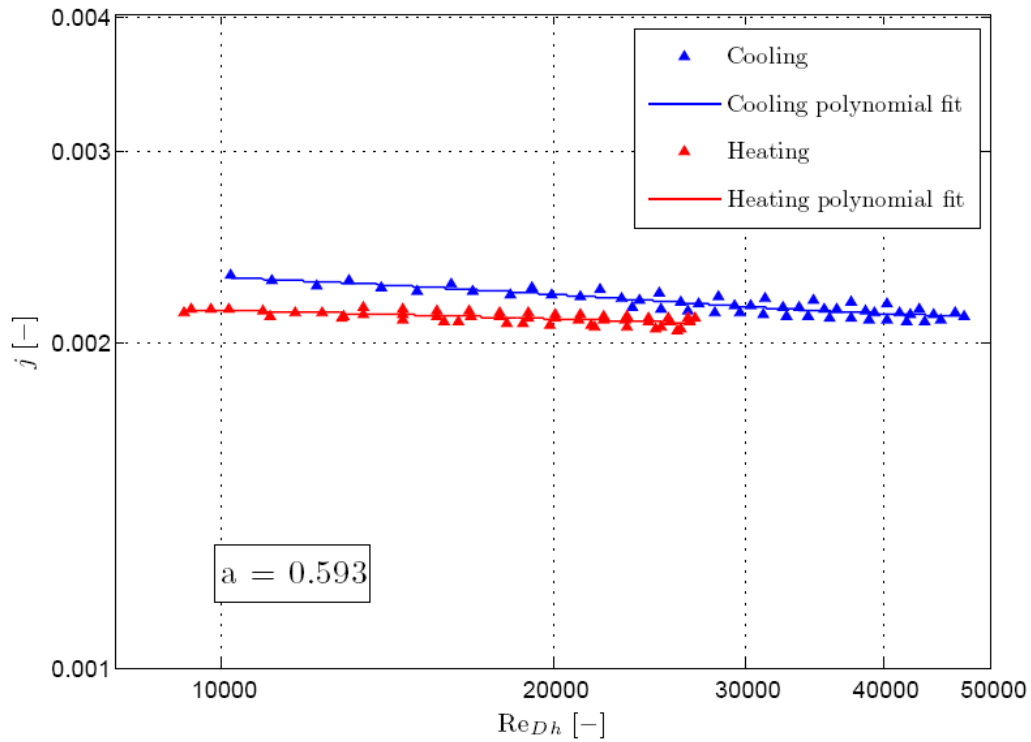


Figure 5.19: Colburn j-factors for both a heated and cooled annulus for an annular diameter ratio of 0.593.

The average percentage difference between the Colburn j-factors for a heated and cooled annulus is 2.6% for an annular diameter ratio of 0.593.

The percentage difference between a heated and cooled annulus for the Nusselt numbers are on average eight times larger than the percentage difference of the Colburn j-factor. This indicates that the different Prandtl numbers of the annulus fluid for a heated and cooled annulus are primarily responsible for the large difference in Nusselt numbers.

The results of the friction factor and Colburn j-factor show a similar trend when compared. Figure 5.20 shows a logarithmic plot of the friction factor data as well as the Colburn j-factor for both a heated and cooled annulus.

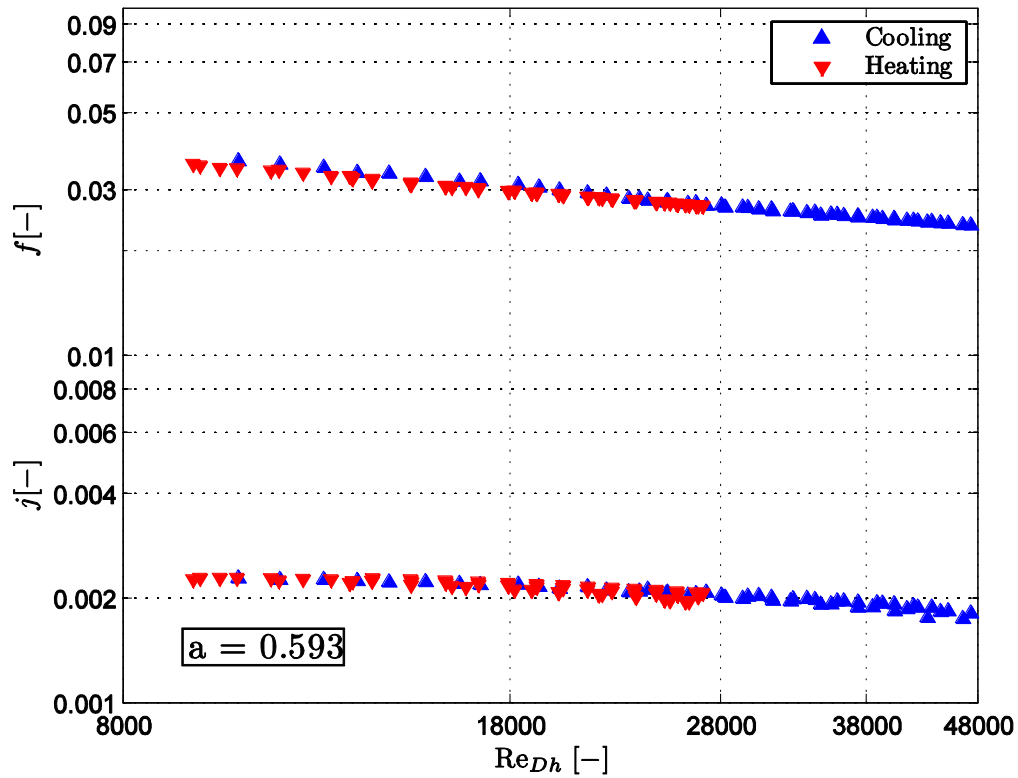


Figure 5.20: Comparison of the friction factor and Colburn  $j$ -factor for a heated and cooled annulus.

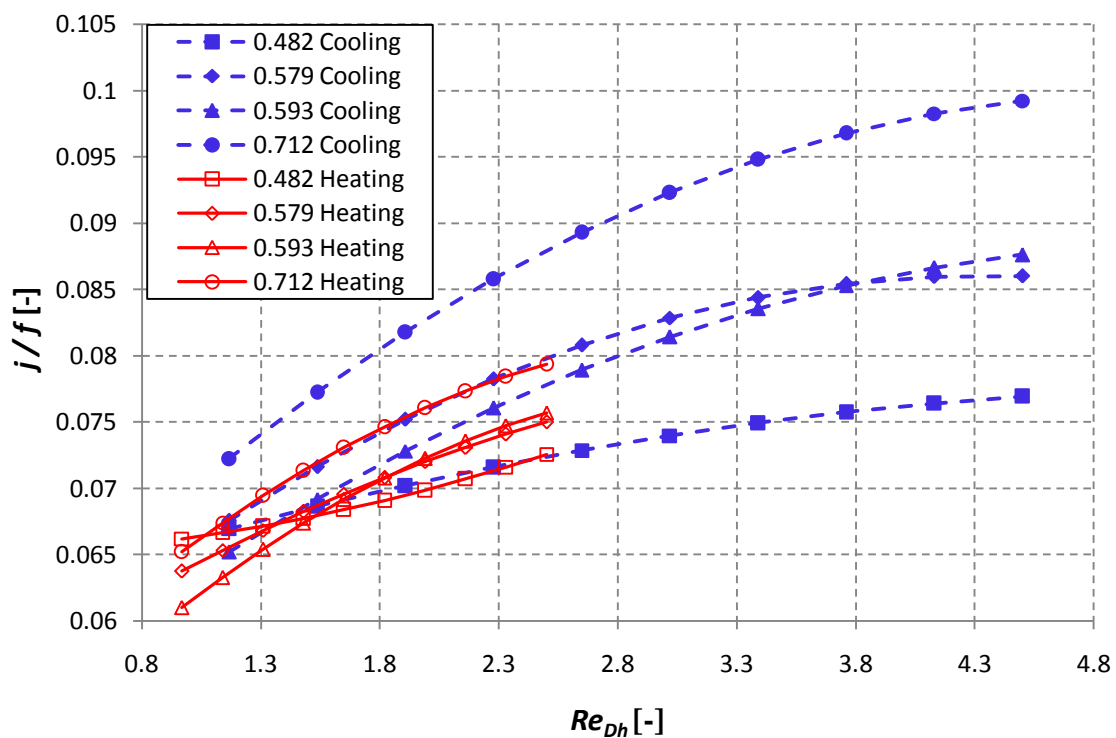
The ratio of the friction factor and Colburn  $j$ -factor was investigated to observe the trend of this ratio across a range of Reynolds numbers. This ratio was calculated for all the annular diameter ratios tested and for convenience is provided in Figure 5.21 in the main text. A polynomial curve was fitted to the results of the ratio of the friction factor and Colburn  $j$ -factor. The polynomial curve fit is of the form:

$$\frac{j}{f} = \tau = C_4 Re_{Dh}^2 + C_5 Re_{Dh} + C_6 \quad (5.8)$$

Constants  $C_4$ ,  $C_5$  and  $C_6$  are provided for all the heat exchanger test sections for both a heated and cooled annulus in Table 5.4.

Table 5.4: Constant  $C_4$ ,  $C_5$  and  $C_6$  used in the polynomial given in Equation (5.8).

Annular diameter ratio ( $a$ )	Cooling			Heating		
	$C_4$	$C_5$	$C_6$	$C_4$	$C_5$	$C_6$
0.482	-5.41e-04	6.05e-03	6.06e-02	-1.14e-03	1.20e-02	6.49e-02
0.579	-1.84e-03	1.59e-02	5.15e-02	-1.42e-03	1.23e-02	5.32e-02
0.593	-1.37e-03	1.45e-02	5.02e-02	-2.80e-03	1.93e-02	4.50e-02
0.712	-1.85e-03	1.86e-02	5.51e-02	-2.72e-03	1.87e-02	4.97e-02


 Figure 5.21: Ratio of Colburn  $j$ -factor to experimental friction factor.

From Figure 5.21 it is observed that with an increase in Reynolds number there is an increase in the friction factor to Colburn  $j$ -factor ratio. The increase in this ratio becomes less at higher Reynolds number ranges, and it seems as though this ratio eventually will become constant. A larger Reynolds number range will need to be tested to confirm this.

## 5.9 Other Test Section Results

Data was gathered for four test sections with annular diameter ratios of 0.482, 0.579, 0.593 and 0.712. In Chapter 5 only the results of the test section with annular diameter ratio were discussed. The detailed results of the other three test sections are provided in Appendix C. A summary of the results of all the test sections is provided in this section.

Table 5.5 provides the average percentage difference between a heated and cooled annulus for:

- Nusselt numbers obtained from the modified Wilson plot method.
- The friction factors obtained directly from the measured pressure drop over the annulus.
- The Colburn  $j$ -factors.

Table 5.5: Percentage difference comparison of  $Nu$ ,  $f$ , and the  $j$ -factor for a heated and cooled annulus.

Annular diameter ratio ( $a$ )	Percentage Difference ( $Nu_{WP}$ ) [%]	Percentage Difference ( $f$ ) [%]	Percentage Difference ( $j$ ) [%]
0.482	24.32	7.15	5.52
0.579	16.45	5.66	5.58
0.593	20.11	6.15	3.08
0.712	20.68	8.22	9.49

To compare the experimental data with existing literature, the Nusselt numbers and friction factors were compared to the Nusselt number and friction factor correlations of Gnielinski (2009). The Nusselt numbers used for the comparison were those obtained from the modified Wilson plot method. In Table 5.6 the Nusselt numbers obtained from the modified Wilson plot method and those predicted by Gnielinski (2009) are compared as an average percentage difference.

Table 5.6: Percentage difference for  $Nu_{WP}$  and  $f$  when compared to the correlations of Gnielinski (2009).

Annular diameter ratio ( $a$ )	$Nu_{WP}$ [%]		$f$ [%]	
	Cooling	Heating	Cooling	Heating
0.482	2.98	15.11	15.17	6.39
0.579	6.76	14.75	5.00	3.24
0.593	6.75	13.04	3.96	1.98
0.712	10.84	11.98	3.51	6.02

The mean and maximum energy balance errors for each of the test sections for a heated and cooled annulus are shown in Table 5.7.

Table 5.7: Mean and maximum energy balances.

Annular diameter ratio ( $a$ )	Cooling		Heating	
	Mean (%)	Maximum (%)	Mean (%)	Maximum (%)
0.482	2.68	4.35	1.65	2.25
0.579	2.81	3.55	0.62	1.53
0.593	1.79	3.68	0.83	1.42
0.712	2.59	4.21	1.08	1.63



## 5.10 Conclusion

Mean Nusselt numbers calculated using experimental techniques were larger than those predicted by existing correlations. Larger Nusselt numbers were obtained for a heated annulus than for a cooled annulus. The effect of the different Prandtl numbers for a heated and cooled annulus has a large influence on the Nusselt number. This is observed by investigating the Colburn j-factor, where a 2.6% larger j-factor is obtained for a heated annulus as opposed to a 35% larger Nusselt number for a heated annulus. The exponent for the Reynolds number in the inner tube was selected and kept constant at 0.8. By altering the inner tube Reynolds number from 0.8 to 0.82 resulted in a 30% and 3% decrease in Nusselt number for the modified Wilson plot and nonlinear regression analysis respectively. Therefore the value of 0.8 presented the most consistent results between the linear and non linear regression methods. Local analyses showed that Nusselt numbers are up to 90% larger towards the inlet of the annulus and decrease towards the outlet of the annulus. Experimental friction factors are larger than predicted by existing correlations. The analyses on both a heated and cooled annulus showed that a cooled annulus produced larger friction factors within the annulus.

# Chapter 6

## Influence of Annular Diameter Ratio

### 6.1 Introduction

The processed experimental results of an annular diameter ratio of 0.593 were presented in Chapter 5. Similar analyses were performed on annular diameter ratios of 0.483, 0.579 and 0.712. Full results for these are presented in Appendix C. All the annular diameter ratios are compared here to observe the effects of altering the diameter ratio on the heat transfer capabilities and friction factors of the test sections.

### 6.2 Mean Heat Transfer

The mean Nusselt numbers for each annular ratio were compared to existing correlations of Dittus and Boelter (1930), Dirker and Meyer (2004) and Gnielinski (2009). Figure 6.2 shows the Nusselt numbers obtained from the various methods for each of the tested annular diameter ratios for a cooled annulus with  $Re_{Dh} = 10\ 000$  and  $Re_i = 20\ 000$ . Figure 6.2 shows a similar plot with  $Re_{Dh} = 25\ 000$  and  $Re_i = 20\ 000$ .

Figure 6.3 is a plot of the Nusselt numbers for the various annular diameter ratios for a heated annulus with  $Re_{Dh} = 10\ 000$  and  $Re_i = 20\ 000$ , and Figure 6.4 a similar plot with  $Re_{Dh} = 25\ 000$  and  $Re_i = 20\ 000$ .

Due to the scatter in the mean LMTD results at larger Reynolds numbers, a linear curve was fitted through these points. The values for the mean LMTD method plotted on Figure 6.1 to Figure 6.4 were the values of the linear curve. This eliminated inconsistencies that were brought about by the scatter in the results.

There is a close agreement with the results of Briggs and Young (1969) and the Khartabil and Christensen (1992) method for a heated and cooled annulus at all tested Reynolds numbers. The trend of the mean LMTD method for both a heated and cooled annulus agreed with the Briggs and Young (1969) and the Khartabil and Christensen (1992) methods. At lower Reynolds numbers for a cooled annulus the mean LMTD method showed close agreement

with the regression methods, for a heated annulus it is at a higher Reynolds number range that the LMTD method agrees with the results of both the regression analyses. The linear regression method, non linear regression method and mean LMTD methods produced Nusselt in agreement with the existing correlations for lower Reynolds numbers. For larger Reynolds numbers the linear regression method, non linear regression method and mean LMTD methods produced larger Nusselt numbers than those predicted by existing correlations.

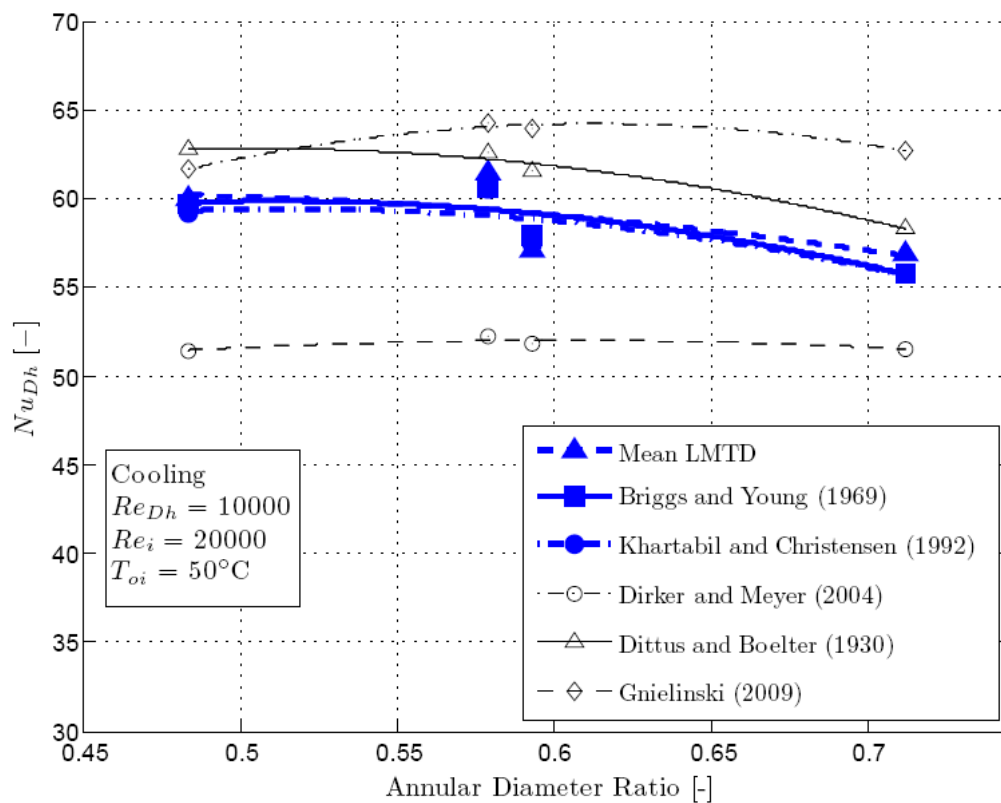


Figure 6.1: Comparison of Nusselt numbers for various annular diameter ratios at  $Re_{Dh} = 10\,000$  for a cooled annulus.

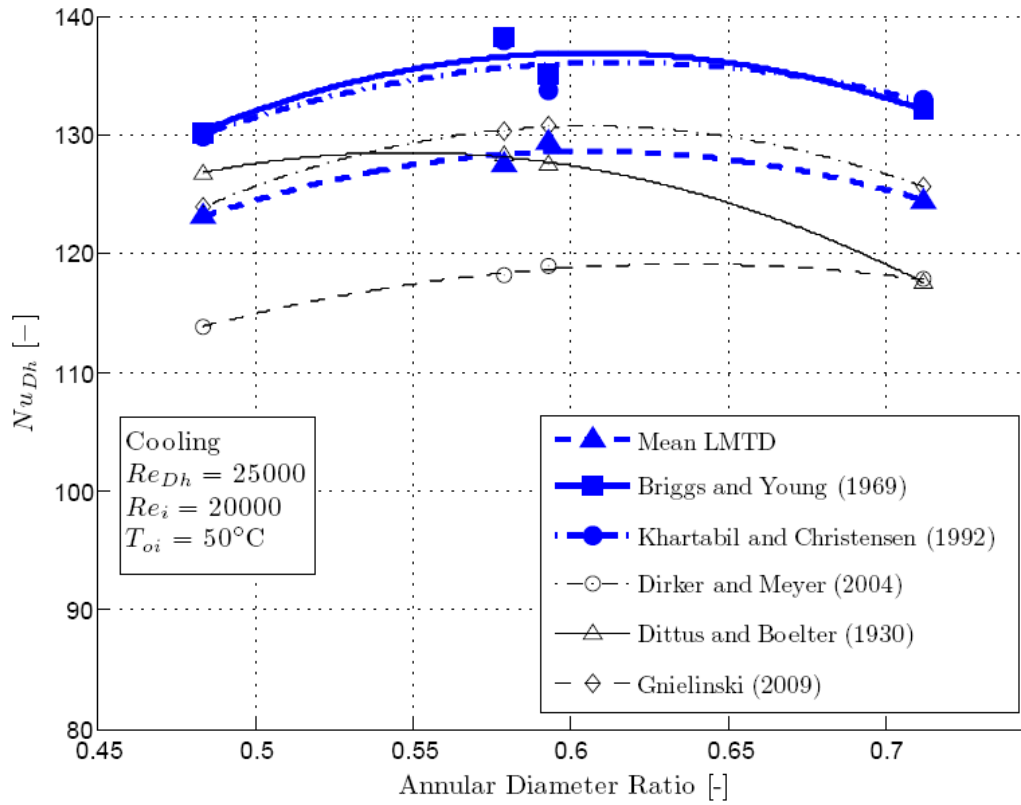


Figure 6.2: Comparison of Nusselt numbers for various annular diameter ratios at  $Re_{Dh} = 25\,000$  for a cooled annulus.

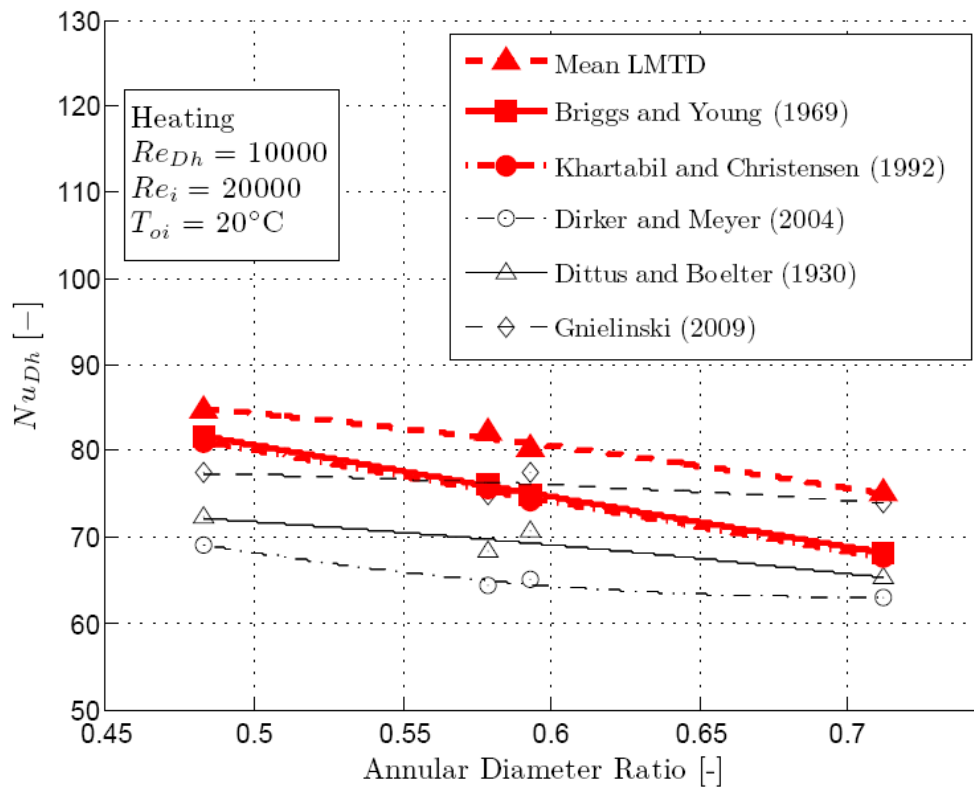


Figure 6.3: Comparison of Nusselt numbers for various annular diameter ratios at  $Re_{Dh} = 10\,000$  for a heated annulus.

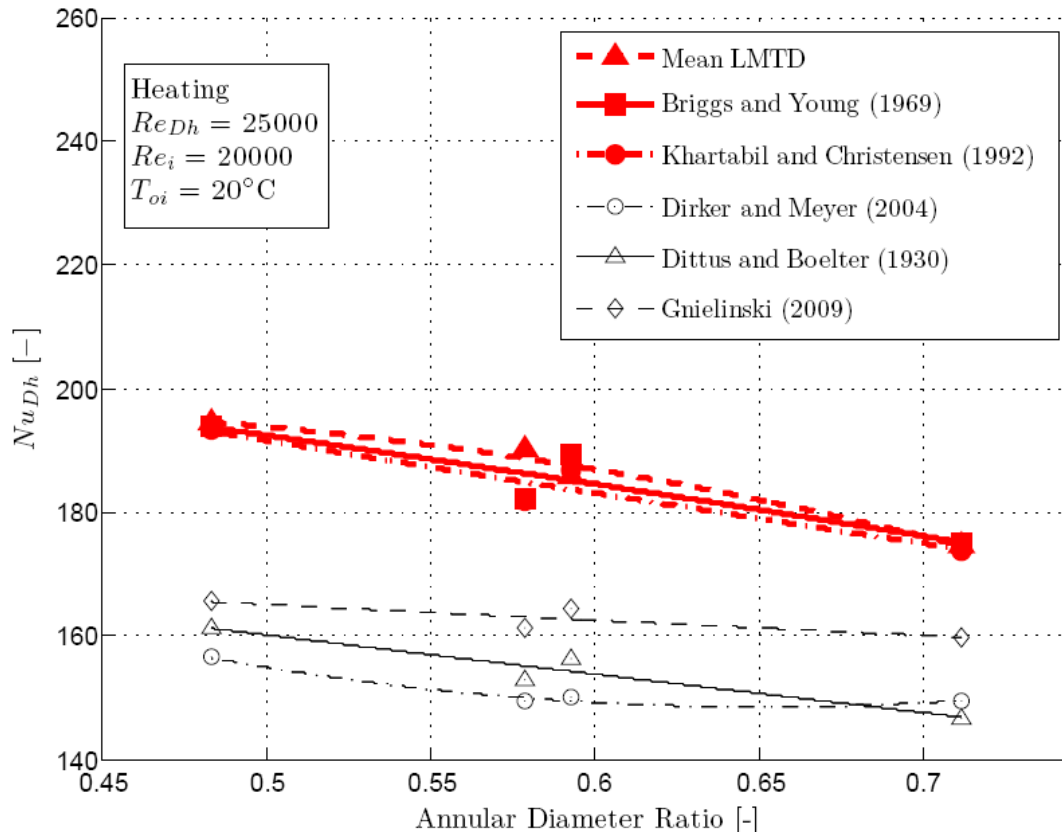


Figure 6.4: Comparison of Nusselt numbers for various annular diameter ratios at  $Re_{Dh} = 25\,000$  for a heated annulus.

It is clear from Figure 6.1 to Figure 6.4 that the Nusselt numbers as a function of annular diameter ratio followed a general trend. For a cooled annulus the Nusselt numbers increased with an increasing annular diameter ratio, with a maximum Nusselt number occurring at  $a = 0.61$ . For  $a > 0.61$ , there is a decrease in Nusselt number with an increase in annular diameter ratio. For the heated annulus there was a steady decrease in Nusselt number with an increase in annular diameter ratio.

Figure 6.5 shows the general trends for the Nusselt numbers as a function of annular diameter ratio for a cooled and heated annulus respectively. The Nusselt number values in Figure 6.5 is only to indicate the approximate ranges of Nusselt numbers and does not represent specific experimental data.

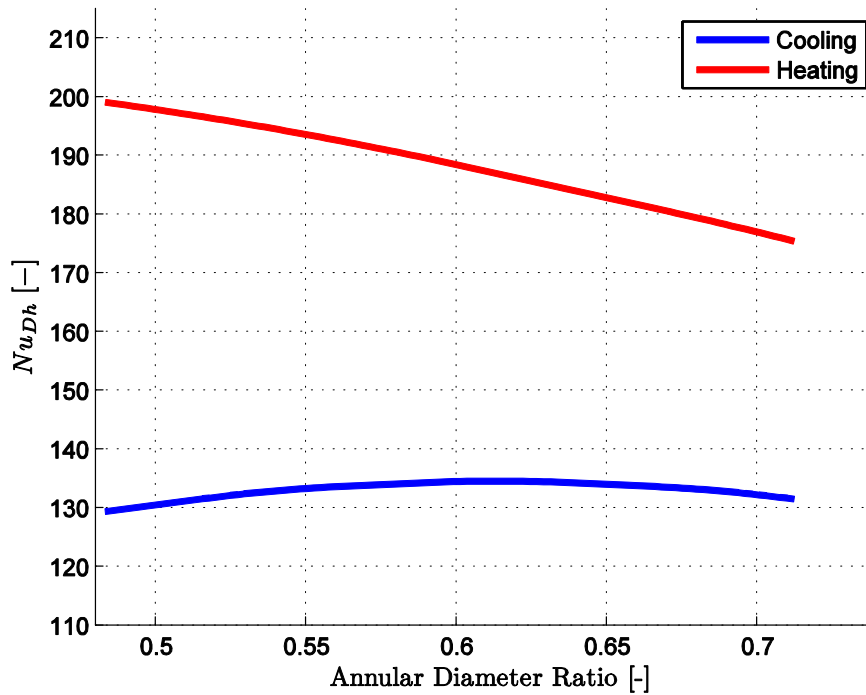


Figure 6.5: General trends present in Nusselt numbers as a function of annular diameter ratio for a heated and cooled annulus.

The Nusselt numbers obtained from the linear regression method for various annular diameter ratios for a heated and cooled annulus with  $Re_{Dh} = 10\,000$  and  $Re_i = 20\,000$  are plotted in Figure 6.6. A similar plot is shown in Figure 6.7 for  $Re_{Dh} = 25\,000$  and  $Re_i = 20\,000$ . For a cooled annulus Figure 6.6 and Figure 6.7 indicate that a maximum Nusselt number exists in the mid range of annular diameter ratio. For a heated annulus, the Nusselt number decreases almost linearly with an increase in annular diameter ratio. The heated annulus shows larger Nusselt numbers than a cooled annulus, the cause of this is discussed in section 5.8.

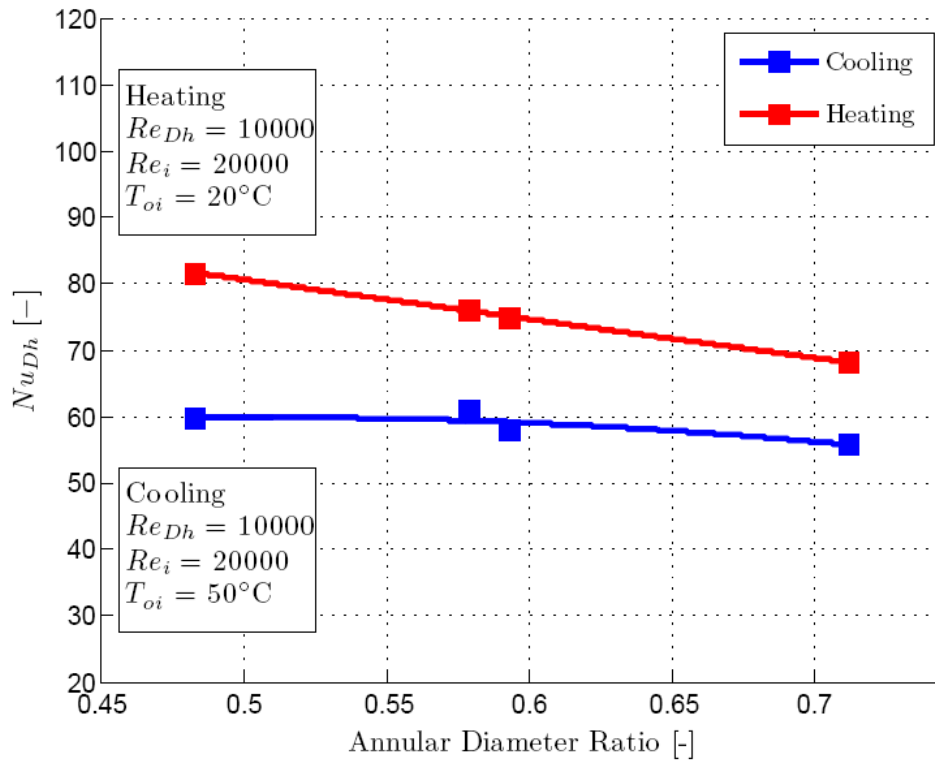


Figure 6.6: Comparison of Nusselt numbers obtained from the modified Wilson plot method for various annular diameter ratios at  $Re_{Dh} = 10\ 000$ , for a heated and cooled annulus.

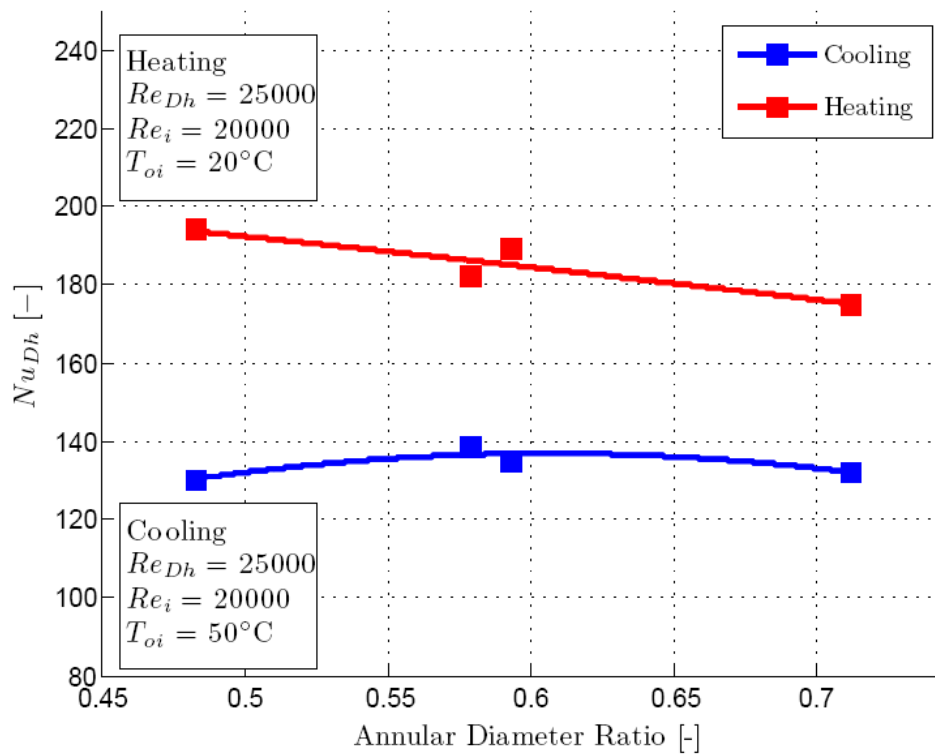


Figure 6.7: Comparison of Nusselt numbers obtained from the modified Wilson plot method for various annular diameter ratios at  $Re_{Dh} = 25\ 000$ , for a heated and cooled annulus.

### 6.3 Friction Factors

Friction factors for the various annular diameter ratios are compared. In Figure 6.8 a heated and cooled annulus are compared to available correlations for  $Re_i = 20\ 000$  and  $Re_{Dh} = 10\ 000$ . Figure 6.9 shows a similar plot for  $Re_i = 20\ 000$  and  $Re_{Dh} = 20\ 000$ . The effect of altering the annular diameter ratio on the friction factor is far greater than that predicted by the existing correlations of Blasius, Gnielinski (2009), Kaneda et al (2008) and Jones and Leung (1981). The friction factor for a test section with an annular diameter ratio of 0.355 presented in Ntuli et al (2010) for a heated annulus is included in Figure 6.8 and Figure 6.9.

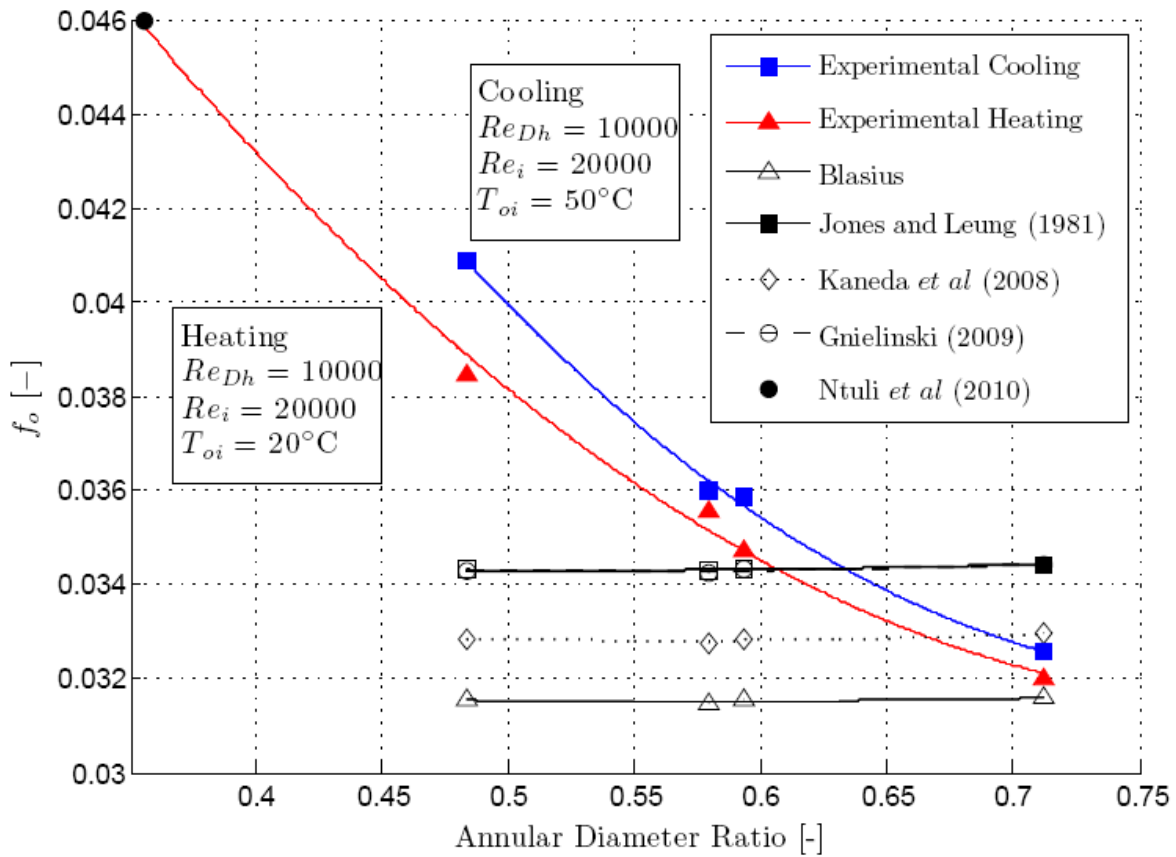


Figure 6.8: Friction factors for various annular diameter ratios for a heated and cooled annulus with  $Re_{Dh} = 10\ 000$  and  $Re_i = 20\ 000$ .

Friction factors for the cooled annulus are larger than those of a cooled annulus. The maximum percentage difference in friction factor between a heated and cooled annulus is 4% with  $Re_{Dh} = 10\ 000$ . With  $Re_{Dh} = 20\ 000$  the maximum difference is 9%, thus the



difference between the friction factor for a cooled and heated annulus increases with an increasing Reynolds number.

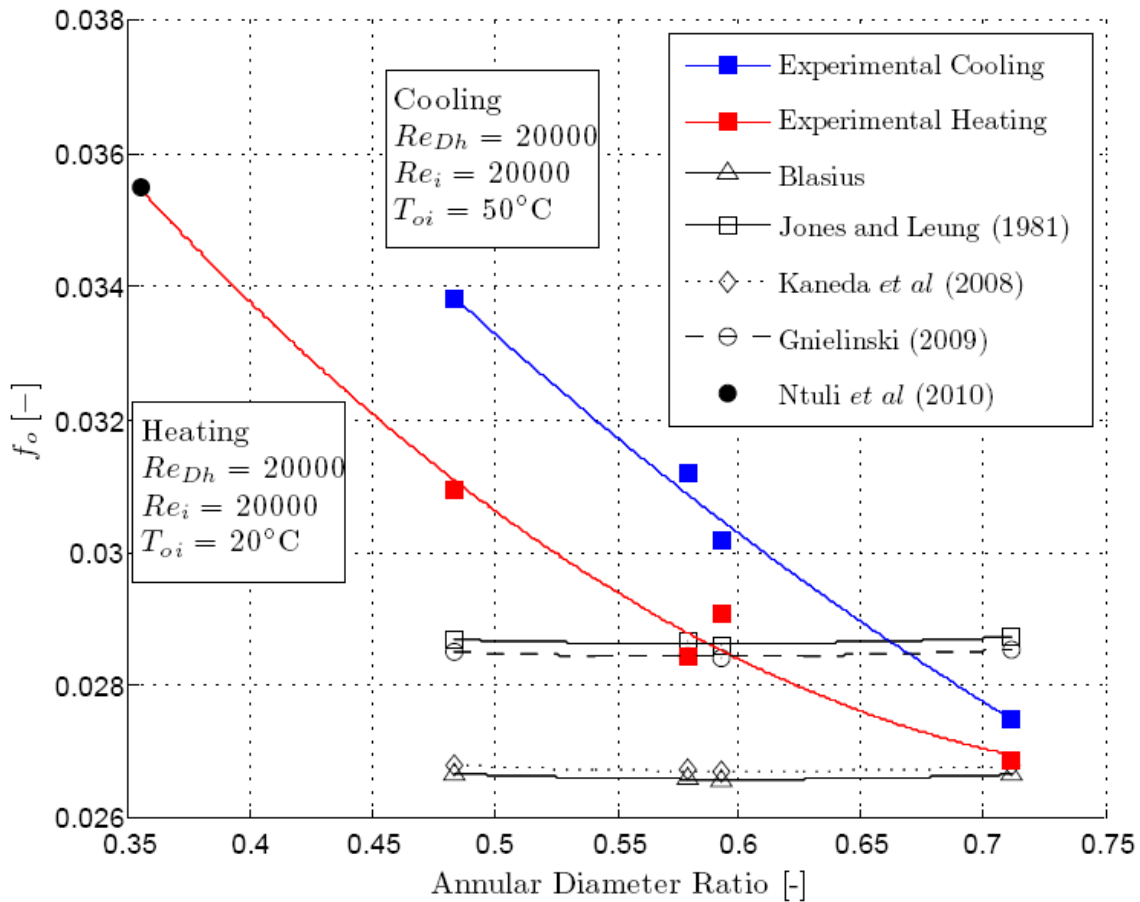


Figure 6.9: Friction factors for various annular diameter ratios for a heated and cooled annulus with  $Re_{Dh} = 20\,000$  and  $Re_i = 20\,000$ .

The curve fitted through the friction factors of the current study for a heated annulus also fits the data point of Ntuli *et al* (2010), where an annular diameter ratio of 0.355 was tested. The data point taken from Ntuli *et al* (2010) was for similar  $Re_{Dh}$  and  $Re_i$  values. This indicates agreement with the study of Ntuli *et al* (2010).

### 6.4 Colburn j-Factor

In section 5.8 the Colburn j-factor is introduced and used to explain the reason for a heated annulus having larger Nusselt numbers. The relationship between the Colburn j-factor and annular diameter ratio is shown in Figure 6.10 to Figure 6.13.

For a cooled annulus Figure 6.10 and Figure 6.11 show the relationship between the Colburn  $j$ -factor and the annular diameter ratio for  $Re_{Dh} = 10\ 000$  and  $Re_{Dh} = 25\ 000$  respectively. The general trend for the  $j$ -factor from Figure 6.10 and Figure 6.11 show a minimum  $j$ -factor in the mid-range of annular diameter ratio. For a cooled annulus there is close agreement between the experimental  $j$ -factors obtained from the linear regression, nonlinear regression and mean LMTD methods. The experimental methods also show an agreement with correlations in the literature.

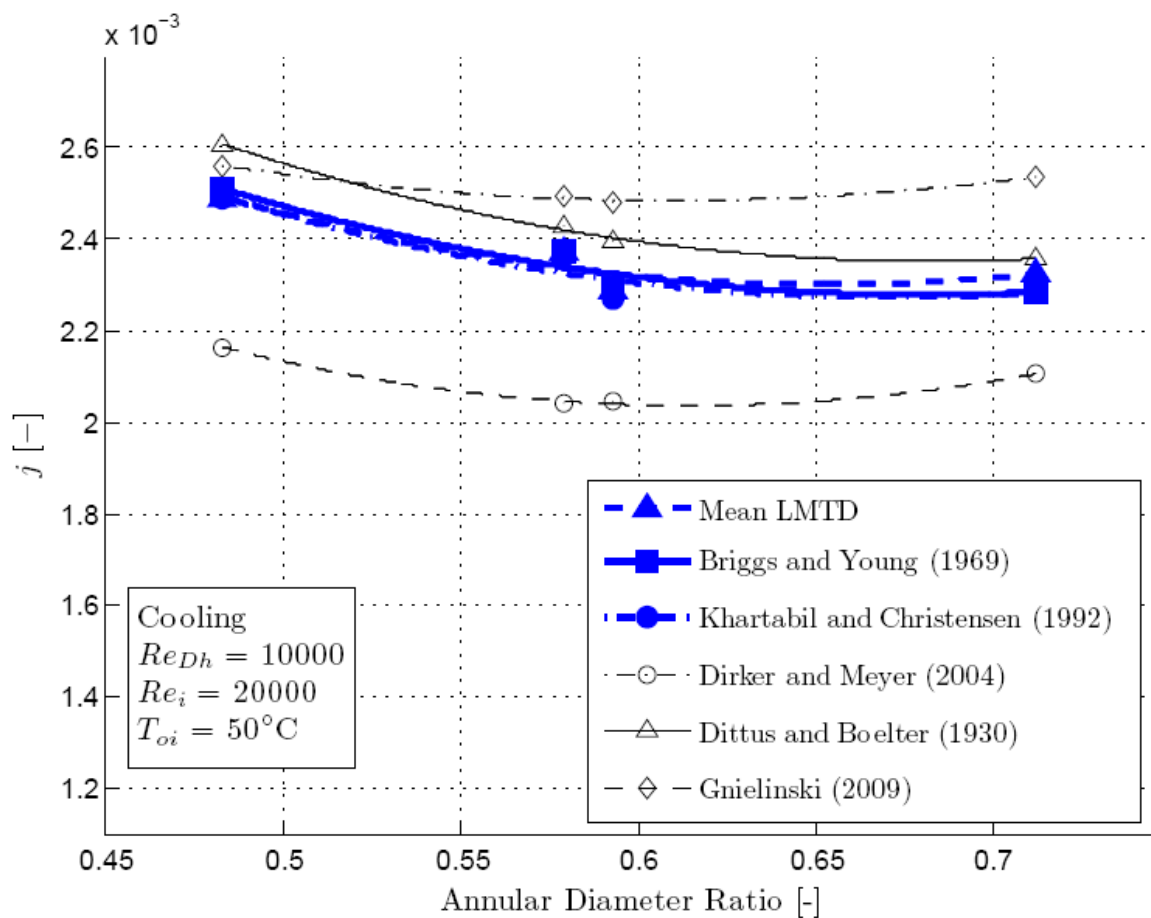


Figure 6.10: The relationship between the Colburn  $j$ -factor and annular diameter ratio for a cooled annulus with  $Re_{Dh} = 10\ 000$ .

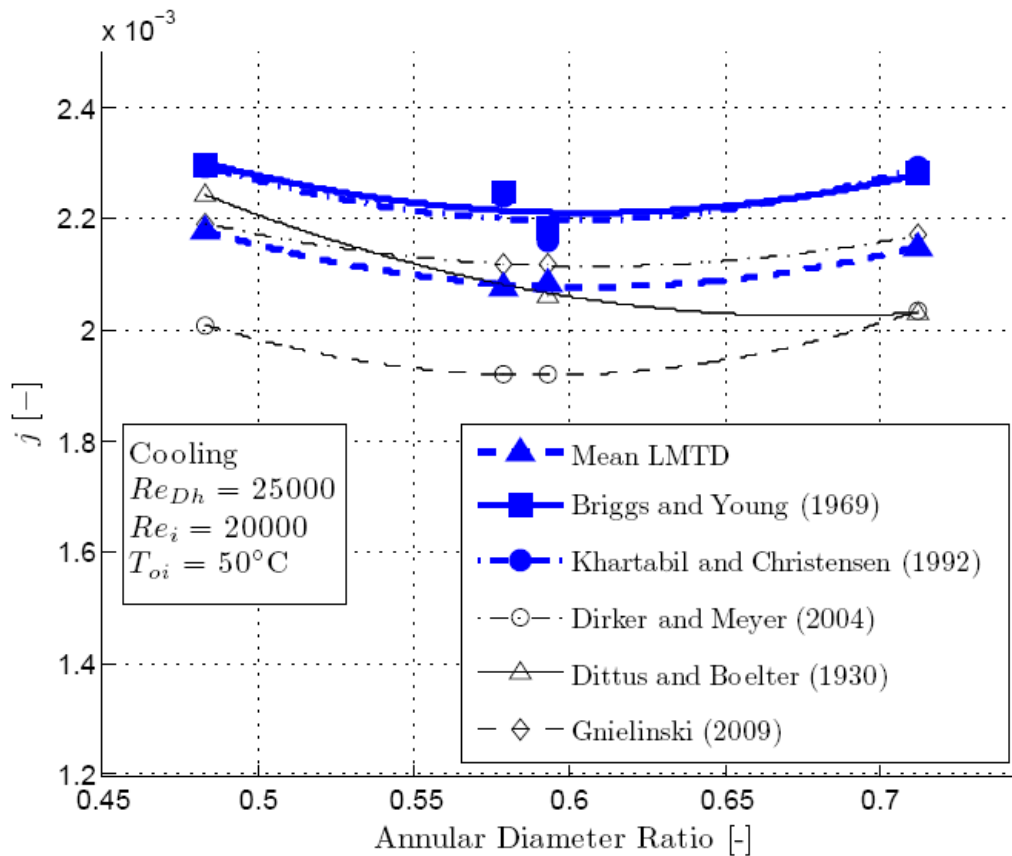


Figure 6.11: The relationship between the Colburn  $j$ -factor and annular diameter ratio for a cooled annulus with  $Re_{Dh} = 25\ 000$ .

Figure 6.12 and Figure 6.13 show the relationship between the Colburn  $j$ -factor and the annular diameter ratio for a heated annulus for  $Re_{Dh} = 10\ 000$  and  $Re_{Dh} = 25\ 000$  respectively. The general trend for the  $j$ -factor from Figure 6.12 and Figure 6.13 show a linear decrease in  $j$ -factor with an increasing annular diameter ratio. A heated annulus shows close agreement between the three experimental methods. For  $Re_{Dh} = 20\ 000$  the experimental results are on average 16% larger than the correlations in the literature predict.

For a heated annulus the correlations of Gnielinski (2009) and Dirker and Meyer (2004) do not follow the linearly decreasing trend seen in the experimental methods. There is close agreement with the experimental methods at higher Reynolds numbers. The experimental methods produce  $j$ -factors that are on average 16% larger than those predicted by the correlations.

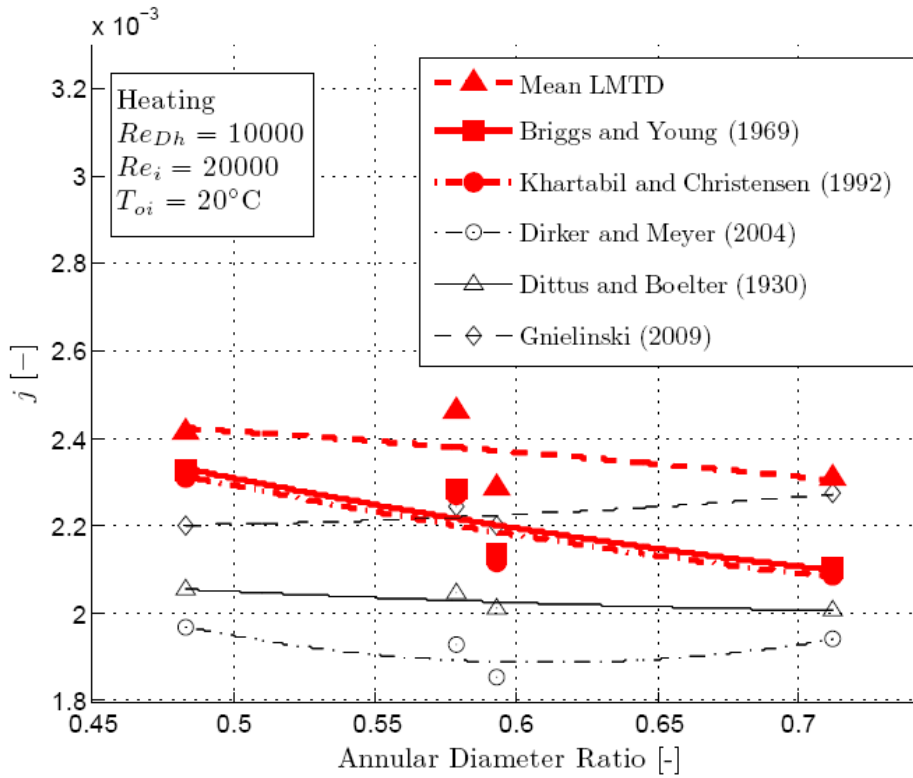


Figure 6.12: The relationship between the Colburn j-factor and annular diameter ratio for a heated annulus with  $Re_{Dh} = 10\ 000$ .

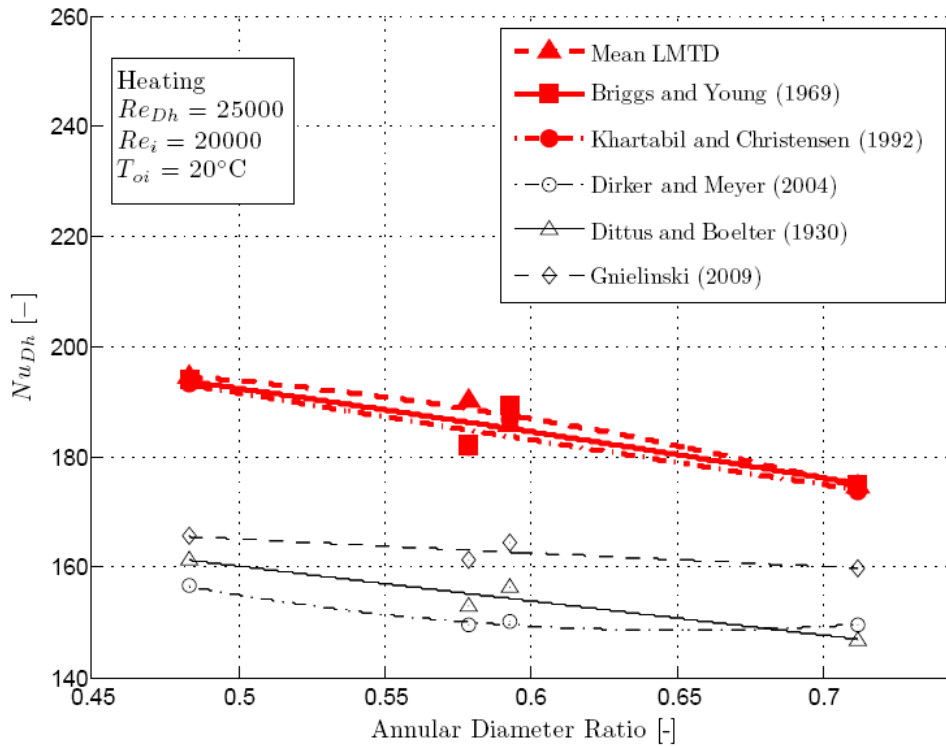


Figure 6.13: The relationship between the Colburn j-factor and annular diameter ratio for a heated annulus with  $Re_{Dh} = 25\ 000$ .

Figure 6.14 uses the results obtained from the modified Wilson plot method to compare the  $j$ -factors for a heated and cooled annulus.

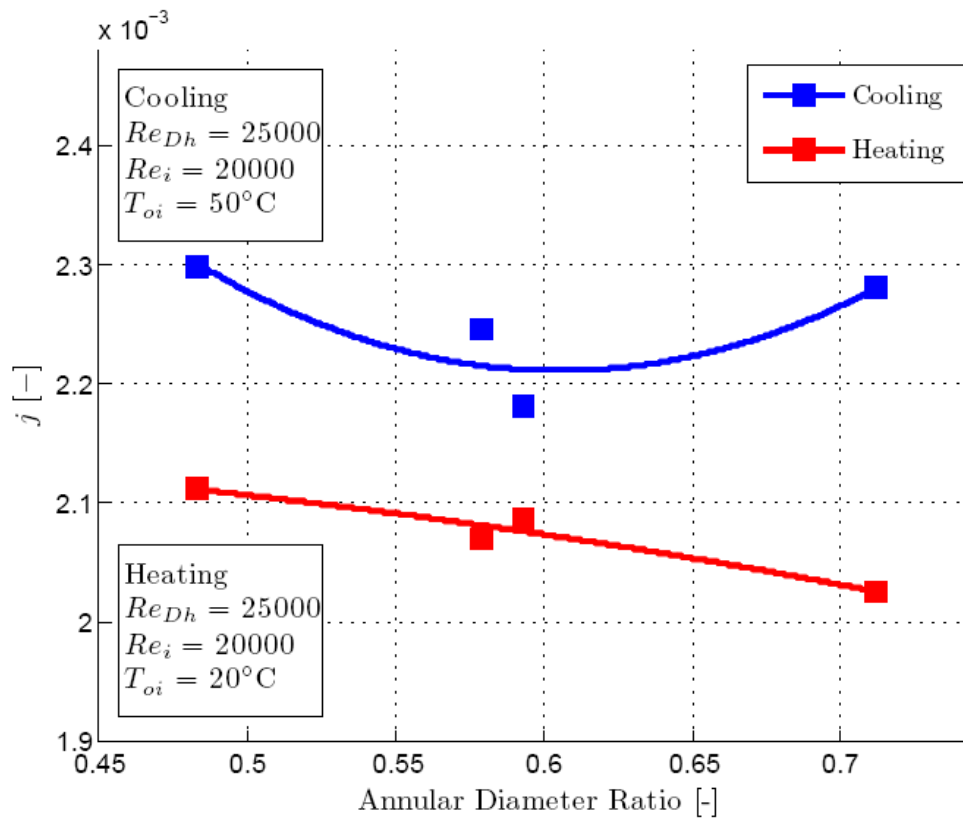


Figure 6.14: Comparison of Colburn  $j$ -factors for a heated and cooled annulus with  $Re_{Dh} = 25\ 000$ .

A cooled annulus produces larger  $j$ -factors than a heated annulus. In section 5.8 the differences in Nusselt numbers and Colburn  $j$ -factors are summarized. It is evident from these results that the difference in Nusselt numbers between a heated and cooled annulus is largely influenced by the different Prandtl numbers as a result of the different fluid temperatures.

## 6.5 Modified Wilson Plot and Khartabil and Christensen Coefficients

The coefficients of the Sieder and Tate type equation obtained from the Briggs and Young (1992) and Khartabil and Christensen (1992) methods differ for each annular diameter ratio.

The Briggs and Young (1969) constants  $C_i$ ,  $C_o$  and  $P$  of Equation (6.1) and Equation(6.2)are plotted in Figure 6.15a), b) and c), for both a heated and cooled annulus. The results of  $C_o$  and  $P$  were compared to the correlation of Dirker and Meyer (2004) given in Equation (2.20).

$$Nu_i = \frac{h_i D_i}{k_i} = C_i Re_i^{0.8} Pr_i^{\frac{1}{3}} \left( \frac{\mu}{\mu_w} \right)_i^{0.14} \quad (6.1)$$

$$Nu_{Dh} = \frac{h_o D_h}{k_o} = C_o Re_{Dh}^P Pr_o^{\frac{1}{3}} \left( \frac{\mu}{\mu_w} \right)_o^{0.14} \quad (6.2)$$

The coefficients  $C_i$ ,  $C_o$  and  $P$  obtained using the Khartabil and Christensen (1992) method are shown in Figure 6.16 a), b) and c). The values of  $C_o$  and  $P$  are again compared to the correlation of Dirker and Meyer (2004).

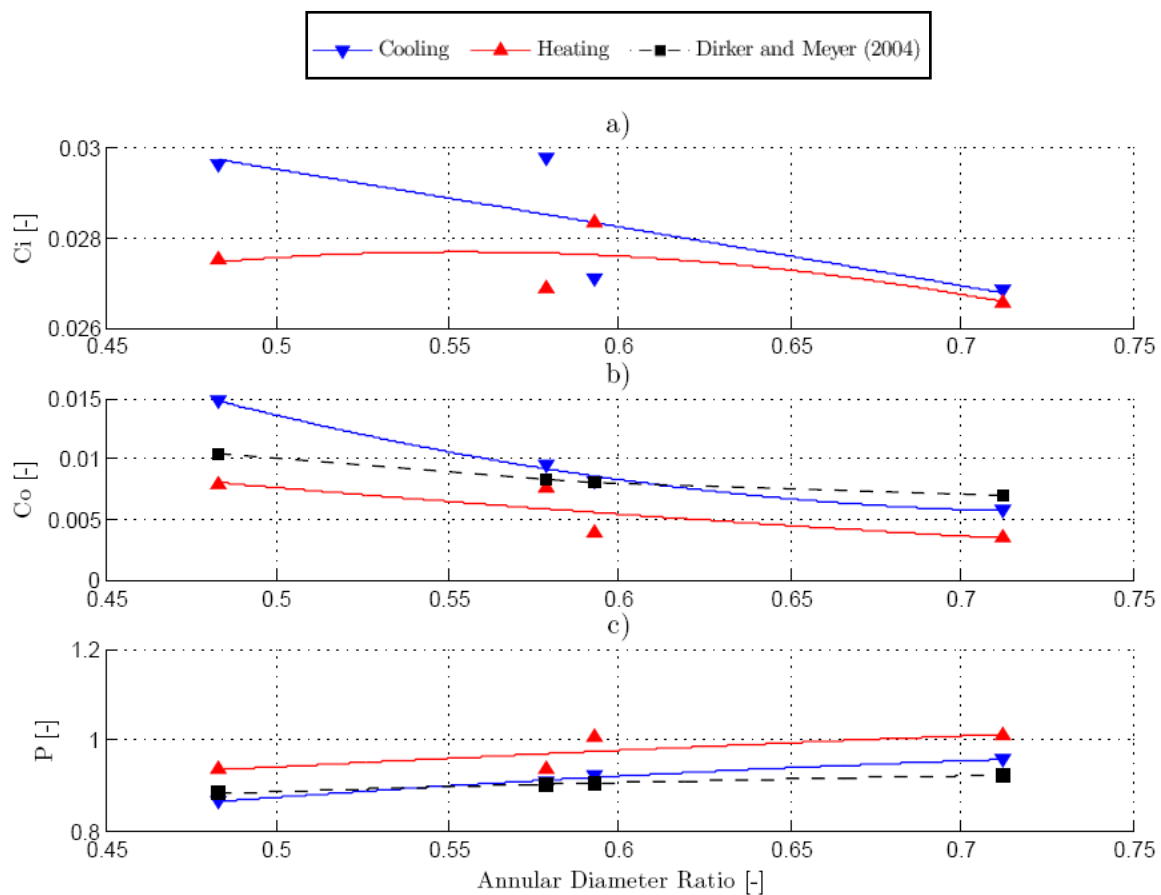


Figure 6.15: Sieder and Tate type equation coefficients a)  $C_i$ , b)  $C_o$ , and c)  $P$ , obtained from the modified Wilson plot technique of Briggs and Young (1969), for various annular diameter ratios for a heated and cooled annulus.

The method of Dirker and Meyer (2004) only considers a heated annulus and did not correlate  $C_i$ . Figure 6.15 and Figure 6.16 indicate that the constants  $C_i$ ,  $C_o$  and  $P$  are dependent on both the annular ratio and direction of heat flux across the inner wall. The coefficients  $C_i$  and  $C_o$  are lower for a heated annulus however the exponent  $P$  is larger for a heated annulus suggesting a greater dependence on  $Re_{Dh}$ .

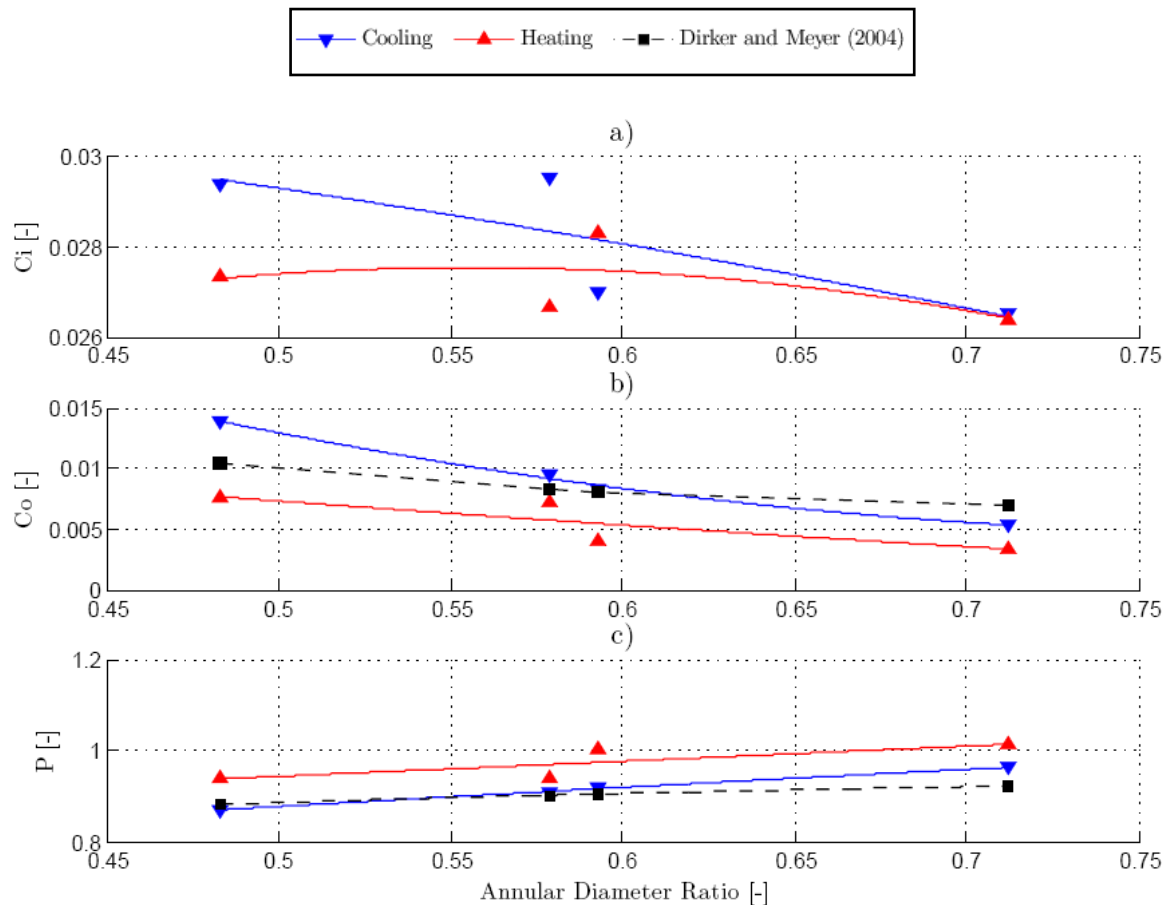


Figure 6.16: Sieder and Tate type equation coefficients a)  $C_i$ , b)  $C_o$ , and c)  $P$ , obtained from the Khartabil and Christensen (1992) method, for various annular diameter ratios for a heated and cooled annulus.

The method of Briggs and Young (1969) and Khartabil and Christensen (1992) show a difference of 8% between the  $C_i$  values for an annular diameter ratio of 0.579 and 0.593. These values should be within close proximity of each other as the annular diameter ratios are similar. The difference between the  $C_i$  values may be attributed to the different annulus sizes, and it may be that the Sieder and Tate constants are also dependent on the actual size of the annulus.

## 6.6 Conclusion

General trends showing the effect of the annular diameter ratio on the Nusselt numbers were similar for the experimental methods and existing correlations. The Colburn  $j$ -factors as a function of annular diameter ratio also followed a general trend. It was evident that the Nusselt numbers and Colburn  $j$ -factors are dependent on the annular diameter ratio.

Altering the annular diameter ratio affects the Sieder and Tate constants  $C_i$ ,  $C_o$  and  $P$  which are obtained from the linear regression and nonlinear regression methods. The influence of the annular diameter ratio on these constants does not agree exactly with results previously presented by Dirker and Meyer (2004), however, similar trends are observed.

The influence of the annular diameter ratio on the measured friction factor is larger than any of the existing correlations predict. For small annular diameter ratios, existing correlations under predict the friction factors and over predict the friction factors for larger diameter ratios. There exists a considerable decrease in friction factor with an increase in annular diameter ratio.



# Chapter 7

## Conclusion

### 7.1 Heat Transfer

Investigations into the turbulent flow regime of annular passages in the past have resulted in correlations being developed for both heat transfer and pressure drop. Due to discrepancies in these correlations, further investigations were required.

Three methods (the mean LMTD method, the linear regression method and a nonlinear regression scheme) were used to obtain the mean Nusselt numbers. These methods were compared to existing correlations. The existing correlations under predicted the mean heat transfer results obtained with these methods for all four test sections used. Nusselt numbers for a heated annulus were larger than those of a cooled annulus due to the different properties of the annulus fluids that existed due to the difference in the fluid temperature. Calculating the Colburn  $j$ -factor removed the effects of the Prandtl number. This gave a clear indication that it was indeed the different Prandtl numbers resulting from the different fluid temperatures that caused the large difference in Nusselt numbers for a heated and cooled annulus.

Two regression models used (the linear regression method and the nonlinear regression scheme) showed very similar mean Nusselt number results for all four test sections used. However, further investigations into these two methods revealed the Wilson Plot method to be more reliable. Average inner wall temperatures predicted by the modified Wilson plot method agreed closely with the averaged measured wall temperatures. Overall heat transfer results of the modified Wilson plot method had small errors when compared to experimentally calculated heat transfer results. The inner tube Reynolds number exponent used in the regression models was assumed to be a constant 0.8. Investigations into the use of other exponents showed a large change in the resulting Nusselt numbers for the linear regression method. This exponent was less influential on the nonlinear regression scheme. Due to the obstructions within the inner tube, the exponent may not be a constant 0.8, however by changing the exponent would result in a disagreement between the linear and

nonlinear regression methods due to the small effect the exponent has on the nonlinear regression method.

Methods of experimentally measuring inner wall temperatures from previous studies have been reported to be inaccurate. A different method was used in this study where the thermocouple junctions were embedded within the inner tube wall. This prevented any fin effects that could result from protrusions present in the thermocouple attachment. The temperature profiles of the inner wall and annulus wall followed a polynomial profile.

Calculations of local properties in these control volumes showed large sensitivities to errors in the wall temperature measurements. Thus, using a polynomial relation for the temperature profiles, the local Nusselt numbers were calculated for control volumes situated along the axial length of the test section. The local analyses showed larger local Nusselt numbers towards the annulus inlet and a decrease towards the annulus outlet. This was observed for all the tested combinations of annular diameter ratios. This was due to the development of the thermal boundary over the heat exchanger length. Thermal entry lengths for the annuli tested were larger than those predicted in the literature for tubes.

The local Nusselt numbers for each control volume were averaged and compared to existing correlations and the mean LMTD method. The averaged local Nusselt numbers agreed closely with existing correlations where similar test section lengths were used, and did not agree with the mean LMTD method. This suggests that the test section length may have an influence on the mean Nusselt numbers.

## 7.2 Friction Factor

The friction factors were calculated directly from pressure drops measured across the annulus pressure drop length. All test sections were tested with both heated and cooled annuli. A cooled annulus (containing warmer water) showed larger friction factors than a heated annulus (containing colder water). This results from the difference in annulus fluid properties which are dependent on the bulk fluid temperature of the annulus fluid. The friction factors obtained in this study for various annular diameter ratios agreed with a friction factor previously obtained in a similar experimental study.

### 7.3 Influence of Annular Diameter Ratio

It is known that the annular diameter ratio influences both the heat transfer and pressure drop characteristics of a heat exchanger. The effects of the diameter ratio need to be considered in correlation derivation for tube-in-tube heat exchangers and it is not sufficiently accurate to base these correlations solely on the hydraulic diameter. Four different test sections were tested and the effects on of the annular diameter ratio on both the Nusselt numbers and friction factors were observed.

The Nusselt number as a function of annular diameter ratio, for both a heated and cooled annulus, showed similar trends for available correlations and all the experimental methods with the exception of the mean LMTD method. The values for all these methods differed, however, the trends were similar.

The friction factors showed that they have a dependence on the annular diameter ratio larger than the existing correlations predict, and thus these correlations do not fit the data for all the annular diameter ratios tested.

## References

- Abu-Eishah, S.I., 2001. Correlations for the Thermal Conductivity of Metals as a Function of Temperature. *International Journal of Thermophysics*, 22(6), pp.1855-68.
- Briggs, D.E. & Young, E.H., 1969. Modified Wilson Plot Techniques for Obtaining Heat Transfer Correlations for Shell and Tube Heat Exchangers. *Chemical Engineering Progress Symposium Series*, 65, pp.35-45.
- Brighton, J.A. & Jones, J.B., 1969. Fully Developed Turbulent Flow in Annuli. *Journal of Basic Engineering*, 86(4), pp.835-42.
- Cengel, Y.A., 2006. *Heat and Mass Transfer: A Practical Approach*. 3rd ed. McGraw-Hill.
- Crookston, R.B., Rothfus, R.R. & Kermod, R.I., 1968. Turbulent Heat Transfer In Annuli With Small Cores. *International Journal of Heat and Mass Transfer*, 11, pp.415-26.
- Davis, E.S., 1943. Heat Transfer and Pressure Drop in Annuli. *Transactions of ASME*, pp.755-60.
- Dirker, J. & Meyer, J.P., 2005. Convection Heat Transfer in Concentric Annuli. *Heat Transfer Engineering*, 26(2), pp.19-29.
- Dittus, F.W. & Boelter, L.M.K., 1930. *Publications on Engineering*, 2, p.443.
- Foust, A.S. & Christian, G.A., 1940. Non-Boiling Heat Transfer Coefficients in Annuli. *American Institute of Chemical Engineers*, 36, pp.541-54.
- Gnielinski, V., 1993. Heat Transfer in a Concentric Annulus. *VDI-Heat Atlas*, VDI-Verlag, Düsseldorf, Germany, Section Gd.
- Gnielinski, V., 2009. Heat Transfer Coefficients for Turbulent Flow in Concentric Annular Ducts. *Heat Transfer Engineering*, 30, pp.431-36.
- Gujarati, D. & Porter, D., 2008. *Basic Econometrics*. 5th ed. McGraw-Hill.
- Jones, O.C. & Leung, J.C.M., 1981. An Improvement in the Calculation of Turbulent Friction in Smooth Concentric Annuli. *Journal of Fluids Engineering*, 103, pp.615-23.

- Kaneda, M., Yu, B., Ozoe, H. & Churchill, S.W., 2003. The Characteristics of Turbulent Flow and Convection in Concentric Circular Annuli. *International Journal of Heat and Mass Transfer*, 46, pp.5045-57.
- Kays, L.M. & Leung, E.Y., 1963. Heat Transfer in Annular Passages-Hydrodynamically Developed Turbulent Flow with Arbitrarily Prescribed Heat Flux. *International Journal of Heat and Mass Transfer*, 6, pp.537-57.
- Khartabil, H.F. & Christensen, R.N., 1992. An Improved Scheme for Determining Heat Transfer Correlations from Heat Exchanger Regression Models with Three Unknowns. *Experimental Thermal and Fluid Science*, 5, pp.808-19.
- Kline, F.J. & McClintock, F.A., 1953. Describing Uncertainties in Single Sample Experiments. *Mechanical Engineering*, 75, pp.2-8.
- Lu, G. & Wang, J., 2008. Experimental Investigation on Heat Transfer Characteristics of Water Flow in a Narrow Annulus. *Applied Thermal Engineering*, 28, pp.8-13.
- McAdams, W.H., 1954. Heat Transmissions. New York. pp.241-44.
- Monrad, C.C. & Pelton, J.F., 1942. Heat Transfer by Convection in Annular Spaces. *American Institute of Chemical Engineers*, 38, pp.593-611.
- Ntuli, M.P., Dirker, J. & Meyer, J.P., 2010. Heat Transfer and Pressure Drop Coefficients for Turbulent Flow in Concentric Annular Ducts. In *CHISA*. Prague, 2010.
- Olson, R.M. & Sparrow, E.M., 1963. Measurement of Turbulent Flow Development in Tubes and Annuli with Square and Rounded Entrances. *American Institute of Chemical Engineers*, 9(6), pp.766-70.
- Pethukov, B.S. & Roizen, L.I., 1964. General Relationships for Heat Transfer in Turbulent Flow of a Gas in Tubes of Annular Section. *High Temperature*, 2, pp.65-68.
- Popiel, C.O. & Wojtkowiak, J., 1998. Simple Formulas for Thermophysical Properties of Liquid Water for Heat Transfer Calculations. *Heat Transfer Engineering*, 19(3), pp.87-101.
- Quarmby, A., 1967. An Experimental Study of Turbulent Flow Through Concentric Annuli. *International Journal of Mechanical Engineering Science*, 9, pp.205-21.

Rothfus, R.R., Monrad, C.C., Sikchi, K.G. & Heideger, W.J., 1955. *Industrial and Engineering Chemistry*, 47.

Shah, R.K., n.d. Assessment of Modified Wilson Plot Techniques for Obtaining Heat Exchanger Design Data. In *9th International Heat Transfer Conference*. Jerusalem Isreal.

Shigley, J., Mischke, C. & Budynas, R., 2006. *Mechanical Engineering Design*. 5th ed. McGraw-Hill.

Sieder, E.N. & Tate, G.E., 1936. Heat Transfer and Pressure Drop of Liquids in Tubes. *Industrial and Engineering Chemistry*, (28), pp.1429-36.

Stein, R.P. & Begell, W., 1958. Heat Transfer to Water in Turbulent Flow in Internally Heated Annuli. *American Institute of Chemical Engineers*, 4(2), pp.127-31.

Swamee, P.K., Aggarwal, N. & Aggarwal, V., 2008. Optimum Design of Double Pipe Heat Exchangers. *International Journal of Heat and Mass Transfer*, 51, pp.2260-66.

Wiegand, J.H., McMillen, E.L. & Larson, R.E., 1945. Annular Heat Transfer Coefficients for Turbulent Flow. *American Institute of Chemical Engineers*, 41, pp.147-53.

Wilson, E.E., 1915. *Transactions of the American Society of Mechanical Engineers*, 37, pp.47-82.

# Appendix A

## The Wilson Plot Method

### Contents

A.1 Introduction .....	A.1
A.2 The Modified Wilson Plot Technique Explained.....	A.1
A.2.1 Experimental Data.....	A.2
A.2.2 Fundamentals of the Modified Wilson Plot Method (Briggs and Young (1969)) .....	A.3
A.2.3 Tube Properties.....	A.6
A.2.4 Fluid Properties .....	A.7
A.2.5 Application of the Briggs and Young (1969) Method for Experimental Data. ....	A.7
A.2.6 Linear Regression plots and Converged Solutions for the Heat Exchangers.....	A.9
A.2.6.1 Annular Diameter Ratio 0.482 .....	A.10
A.2.6.2 Annular Diameter Ratio 0.579 .....	A.11
A.2.6.3 Annular Diameter Ratio 0.593 .....	A.12
A.2.6.4 Annular Diameter Ratio 0.712 .....	A.13
A.3 Comparison of Modified Wilson Plot Wall Temperatures to Measured Wall Temperatures.....	A.14
A.3.1.1 Annular Diameter Ratio 0.482 .....	A.15
A.3.1.2 Annular Diameter Ratio 0.579 .....	A.16
A.3.1.3 Annular Diameter Ratio 0.593 .....	A.17
A.3.1.4 Annular Diameter Ratio 0.712 .....	A.18
A.4 Heat Transfer Coefficient Analysis .....	A.19

## List of Figures

Figure A.1: Dimensional properties of the concentric tube arrangement. ....	A.2
Figure A.2: Linear regression results of X and Y, $X_{shell}$ and $Y_{shell}$ and number of iterations for P to converge for a cooled annulus (annular diameter ratio = 0.482).....	A.10
Figure A.3: Linear regression results of X and Y, $X_{shell}$ and $Y_{shell}$ and number of iterations for P to converge for a heated annulus (annular diameter ratio = 0.482). ....	A.10
Figure A.4: Linear regression results of X and Y, $X_{shell}$ and $Y_{shell}$ and number of iterations for P to converge for a cooled annulus (annular diameter ratio = 0.579). ....	A.11
Figure A.5: Linear regression results of X and Y, $X_{shell}$ and $Y_{shell}$ and number of iterations for P to converge for a heated annulus (annular diameter ratio = 0.579). ....	A.11
Figure A.6: Linear regression results of X and Y, $X_{shell}$ and $Y_{shell}$ and number of iterations for P to converge for a cooled annulus (annular diameter ratio = 0.593). ....	A.12
Figure A.7: Linear regression results of X and Y, $X_{shell}$ and $Y_{shell}$ and number of iterations for P to converge for a heated annulus (annular diameter ratio = 0.593). ....	A.12
Figure A.8: Linear regression results of X and Y, $X_{shell}$ and $Y_{shell}$ and number of iterations for P to converge for a cooled annulus (annular diameter ratio = 0.712). ....	A.13
Figure A.9: Linear regression results of X and Y, $X_{shell}$ and $Y_{shell}$ and number of iterations for P to converge for a heated annulus (annular diameter ratio = 0.712). ....	A.13
Figure A.10: Wall temperature comparisons for the averaged experimentally measured wall temperatures and those predicted by the modified Wilson Plot method (annular diameter ratio of 0.482).....	A.15
Figure A.11: Temperature differences of measured wall temperatures and those predicted by the modified Wilson plot method (annular diameter ratio of 0.482). ....	A.16
Figure A.12: Wall temperature comparisons for the averaged experimentally measured wall temperatures and those predicted by the modified Wilson Plot method (annular diameter ratio of 0.579).....	A.16
Figure A.13: Temperature differences of measured wall temperatures and those predicted by the modified Wilson plot method (annular diameter ratio of 0.579). ....	A.17
Figure A.14: Wall temperature comparisons for the experimentally measured wall temperatures and those predicted by the modified Wilson Plot method (annular diameter ratio of 0.593).....	A.17



Figure A.15: Temperature differences of measured wall temperatures and those predicted by the modified Wilson plot method (annular diameter ratio of 0.593). ..... A.18

Figure A.16: Wall temperature comparisons for the averaged experimentally measured wall temperatures and those predicted by the modified Wilson Plot method (annular diameter ratio of 0.712)..... A.18

Figure A.17: Temperature differences of measured wall temperatures and those predicted by the modified Wilson plot method (annular diameter ratio of 0.712). ..... A.19

Figure A.18: Errors of the rate of heat transfer predicted by the modified Wilson plot for ar0.48 for a) cooled and b) heated annulus..... A.20

Figure A.19: Errors of the rate of heat transfer predicted by the modified Wilson plot for ar0.57 for a) cooled and b) heated annulus..... A.21

Figure A.20: Errors of the rate of heat transfer predicted by the modified Wilson plot for ar0.59 for a) cooled and b) heated annulus..... A.21

Figure A.21: Errors of the rate of heat transfer predicted by the modified Wilson plot for ar0.71 for a) cooled and b) heated annulus..... A.22

## List of Tables

Table A.1: Correlations proposed by Popiel and Wojtkowiak (2001) for determining fluid properties at various temperatures. .... A.8

Table A.2: Wilson Plot Coefficients for the four heat exchangers tested..... A.9

Table A.3: Mean temperature differences of measured wall temperatures and those predicted by the modified Wilson plot method..... A.15

Table A.4: Mean errors for the heat transfer rate predicted by the modified Wilson plot method for all annular diameter ratios and configurations. .... A.22

## Nomenclature

In addition to the nomenclature of the main text body, the following symbols are used in this appendix.

$b$	Intercept of Linear Regression	-
$e$	Percentage Error	%
$m$	Gradient of Linear Regression	-
$r_{cond}$	Conductive Resistance Across Inner Tube Wall	-
$r_{fin}$	Conductive Resistance From Fins	-
$\Delta T$	Temperature Difference	°C
$T_k$	Wall Temperature	K
$U$	Overall Heat Transfer Coefficient	$W/m^2\text{°C}$
$X$	Linear Regression Independent Variable	-
$Y$	Linear Regression Dependent Variable	-

### Subscripts

$shell$	Referring to the Shell Side of the Heat Exchanger
$wp$	Obtained From the Modified Wilson Plot Method
$diff$	Refers to the temperature difference at the inner wall between measured values and those predicted by the linear regression method.

### Other Symbols

$\Delta$	Temperature Difference
----------	------------------------

**Note:** All nomenclature declared in the main text are not repeated here.

## A.1 Introduction

The modified Wilson Plot Method is a numerical approach to obtain wall temperatures of the inner tube, as well as constants used to calculate Nusselt numbers in a tube-in-tube heat exchanger. The method involves an iterative scheme of the fundamental equations of heat transfer to converge to a solution. Experimentally, obtaining these values often poses a problem in that the thermocouples, unless placed on the tube with great care, may result in inaccurate temperature readings. This arises from the disruption in the annulus flow from the thermocouples as well as the development of an increase in surface area around the thermocouple from the solder or other mechanism used to attach the thermocouple to the tube. This effectively acts as a fin resulting in more heat transfer in the vicinity of the thermocouple.

## A.2 The Modified Wilson Plot Technique Explained

To implement the modified Wilson plot method, Matlab 7.6.0 (R2008a) was used. This allowed precision of 16 decimal digits, thus ensuring an accurate solution. The implementation involves an iterative process where an initial guess of the annular Reynolds number exponent,  $P$ , in a Sieder and Tate type equation, and the average wall temperature is supplied by the user and the program iterates until a sufficient convergence is obtained ( $1e^{-06}$  was used in this study). Each iteration of  $P$  produces the coefficients  $C_i$  and  $C_o$  used in the Sieder and Tate type equations given in Equations (A.1) and (A.2). Using the newly obtained values of  $C_i$  and  $C_o$ ,  $P$  is recalculated. This process iterates until convergence of  $P$  is obtained.

The Sieder-Tate type equations for both the inner tube and annulus respectively are:

$$Nu_i = \frac{h_i D_i}{k_i} = C_i Re_i^{0.8} Pr_i^{\frac{1}{3}} \left( \frac{\mu}{\mu_w} \right)_i^{0.14} \quad (\text{A.1})$$

$$Nu_o = \frac{h_o D_h}{k_o} = C_o Re_{D_h}^P Pr_o^{\frac{1}{3}} \left( \frac{\mu}{\mu_w} \right)_o^{0.14} \quad (\text{A.2})$$

## A.2.1 Experimental Data

The first step in the modified Wilson plot procedure is obtaining sufficient and accurate data. For each annular diameter ratio, a new set of data is required. Figure A.1 shows a cross section of the tube arrangement showing all dimensional parameters.

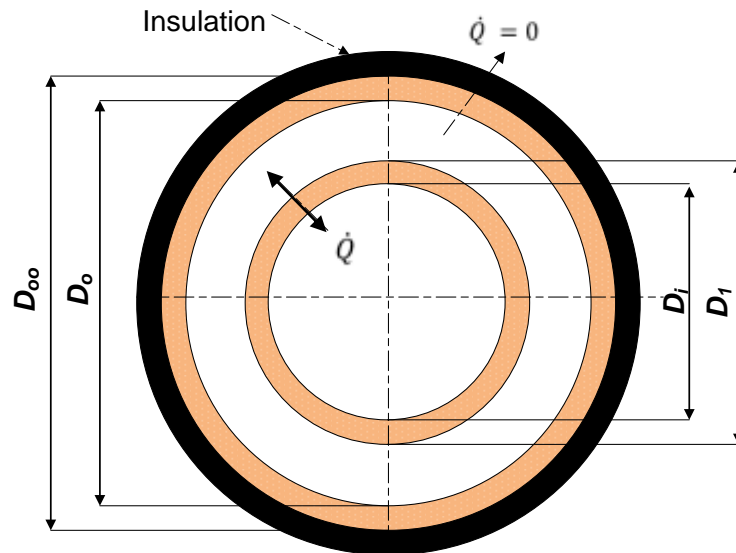


Figure A.1: Dimensional properties of the concentric tube arrangement.

The data required are the inlet and outlet temperatures as well as the mass flow rates for both the annulus and inner tube. Ideally, it is reported by Shah (1990) that the flow rates for the inner tube be kept constant while varying the flow rates in the outer tube. This will promote a quicker convergence and a more accurate result. The more measurement points the more accurate the solution may be, however, it is unreasonable to have an excessive number of data points.

## A.2.2 Fundamentals of the Modified Wilson Plot Method (Briggs and Young (1969))

The modified Wilson plot method proposed here is based on the fundamental equation for the overall heat transfer coefficient shown in Equation (A.3). This equation incorporates both convective heat transfer from the fluid within the tube and conductive heat transfer in the tube itself.

$$\frac{1}{U_o A_{so}} = \frac{1}{h_i A_{si}} + r_{cond} + r_{fin} + \frac{1}{h_o A_{so}} \quad (\text{A.3})$$

Where  $\frac{1}{h_i A_i}$  : Convective heat transfer in the inner tube.

$\frac{1}{h_o A_o}$  : Convective heat transfer in the annulus.

$r_{cond}$  : Conductive resistance across the tube wall given as  $\frac{\ln\left(\frac{D_1}{D_i}\right)}{2\pi L_{hx} k_w}$ .

$r_{fin}$  : Conductive resistance resulting from fins.

As the present study is concerned with smooth tubes  $r_{fin}$  is neglected.

The convective heat transfer coefficients ( $h$ ) for both the inner tube and annulus are calculated using the modified Sieder and Tate equation and the definition of the Nusselt number. The hydraulic diameter is used in the calculation of the annulus given by definition as

$$D_h = D_o - D_1 \quad (\text{A.4})$$

The exponent for  $Re_i$  is taken to be 0.8 (refer to section 5.3). The inner tube and annulus Nusselt numbers are defined in Equation (A.1) and Equation (A.2).

The values of  $C_i$ ,  $C_o$  and  $P$  will differ for different geometry configurations. As discussed in section A.2.5 these will be determined using the modified Wilson plot technique.

Rearranging Equation (A.1) and Equation (A.2); to solve for the convective heat transfer coefficients and substituting these into Equation (A.3) yields

$$\left( \frac{1}{U_o} - \frac{A_{so} \ln\left(\frac{D_1}{D_o}\right)}{2\pi L_{hx} k_w} \right) = \frac{1}{C_o \frac{k_o}{D_h} Re_o^P Pr_o^{\frac{1}{3}} \left(\frac{\mu}{\mu_w}\right)_o^{0.14}} + \frac{A_{so}}{C_i A_{si} \frac{k_i}{D_i} Re_i^{0.8} Pr_i^{\frac{1}{3}} \left(\frac{\mu}{\mu_w}\right)_i^{0.14}} \quad (\text{A.5})$$

To create a linear form of Equation (A.5), it is multiplied by

$$\frac{k_o}{D_h} Re_o^P Pr_o^{\frac{1}{3}} \left( \frac{\mu}{\mu_w} \right)_o^{0.14} \quad (\text{A.6})$$

The multiplication of Equation (A.5) and Equation (A.6) results in Equation (A.7).

$$\left( \frac{1}{U_o} - \frac{A_{so} \ln \left( \frac{D_1}{D_o} \right)}{2\pi L_{hx} k_w} \right) \frac{k_o}{D_h} Re_o^P Pr_o^{\frac{1}{3}} \left( \frac{\mu}{\mu_w} \right)_o^{0.14} = \frac{1}{C_i} \frac{\frac{A_{so} k_o}{A_{si} D_h} Re_o^P Pr_o^{\frac{1}{3}} \left( \frac{\mu}{\mu_w} \right)_o^{0.14}}{\frac{k_i}{D_i} Re_i^{0.8} Pr_i^{\frac{1}{3}} \left( \frac{\mu}{\mu_w} \right)_i^{0.14}} + \frac{1}{C_o} \quad (\text{A.7})$$

This is in the form of a straight line given as

$$Y = mX + b \quad (\text{A.8})$$

Where:

$$Y = \left( \frac{1}{U_o} - \frac{\ln \left( \frac{D_1}{D_o} \right)}{2\pi L_{hx} k_w} \right) \frac{k_o}{D_h} Re_o^P Pr_o^{\frac{1}{3}} \left( \frac{\mu}{\mu_w} \right)_o^{0.14} \quad (\text{A.9})$$

$$X = \frac{\frac{A_{so} k_o}{A_{si} D_h} Re_o^P Pr_o^{\frac{1}{3}} \left( \frac{\mu}{\mu_w} \right)_o^{0.14}}{\frac{k_i}{D_i} Re_i^{0.8} Pr_i^{\frac{1}{3}} \left( \frac{\mu}{\mu_w} \right)_i^{0.14}} \quad (\text{A.10})$$

$$m = \frac{1}{C_i} \quad (\text{A.11})$$

$$b = \frac{1}{C_o} \quad (\text{A.12})$$

To evaluate  $X$  and  $Y$ , an initial estimate of  $P$  and the wall temperature ( $T_w$ ) is required. The initial wall temperature is guessed and used to obtain the initial viscosity at the wall using the methods of section A.2.4. With the value of  $P$  initially guessed a value for  $X$  and  $Y$  is obtained. A linear regression analysis is then performed on these values obtaining both  $C_i$  and  $C_o$ .

A method is used where the average outer wall temperature ( $T_{wo}$ ) is forced to comply with the temperature drop or rise (depending on the heat exchanger configuration) across the wall. This is accomplished by calculating the convective heat transfer coefficient in the inner

tube using Equation (A.1). The temperature at the inner wall is then calculated using Newton's law of cooling rearranged:

$$T_{wi} = T_{bi} + \frac{\dot{Q}_i}{A_{si}h_i} \quad (\text{A.13})$$

The temperature difference across the wall is then calculated as:

$$\Delta T_w = -\bar{Q} \left[ \frac{\ln\left(\frac{D_1}{D_i}\right)}{2\pi L_{hx}k_w} \right] \quad (\text{A.14})$$

The temperature at the outer wall is then given as:

$$T_{wo} = T_{wi} + \Delta T_w \quad (\text{A.15})$$

With new wall temperatures, new fluid properties at the wall are calculated and thus a new value for  $C_i$  and  $C_o$  calculated. This process is completed iteratively until  $C_i$  converges to the appropriate convergence criterion ( $1e^{-06}$  was used in this study).

Attention is then turned to the convective heat transfer coefficient in the annulus. It is calculated using Equation (A.3) rearranged as:

$$h_o = \frac{1}{\frac{1}{U_o} - \frac{A_{so} \ln\left(\frac{D_1}{D_i}\right)}{2\pi L_{hx}k_w} - \frac{A_{so}}{h_i A_{si}}} \quad (\text{A.16})$$

A linear regression as previously performed is now applied to the annulus using the Sieder and Tate expression given in Equation (A.2). This is rearranged into a linear form:

$$\frac{Nu_{Dh}}{Pr_o^{\frac{1}{3}}} = C_{o,shell} Re_{Dh}^P \quad (\text{A.17})$$

Now taking the natural logarithm on either side of Equation (A.17)

$$\ln\left(\frac{Nu_{Dh}}{Pr_o^{\frac{1}{3}} \left(\frac{\mu}{\mu_w}\right)_o^{0.14}}\right) = P \ln(Re_{Dh}) + \ln(C_{o,shell}) \quad (\text{A.18})$$

This is now of the form  $Y_{shell} = m_{shell} X_{shell} + b_{shell}$ .

Where:

$$Y_{shell} = \ln \left( \frac{Nu_{Dh}}{Pr_o^{\frac{1}{3}} \left( \frac{\mu}{\mu_w} \right)_o^{0.14}} \right) \quad (\text{A.19})$$

$$X_{shell} = \ln(Re_{Dh}) \quad (\text{A.20})$$

$$m_{shell} = P \quad (\text{A.21})$$

$$b_{shell} = \ln(C_{o,shell}) \quad (\text{A.22})$$

A linear regression is performed to obtain values for  $C_{o,shell}$  and  $P$ . This process is iterated until convergence for both  $P$  and  $C_{o,shell}$  are reached.

### A.2.3 Tube Properties

To obtain the thermal conductivity of the copper at the various temperatures, a method proposed by Abu-Eishah (2000) was used. This required the average of the wall temperature which is given as:

$$T_{wave} = \frac{T_{wi} + T_{wo}}{2} \quad (\text{A.23})$$

The thermal conductivity ( $k_w$ ) is then obtained using:

$$k_w = a \times T_k^b \times e^{cT_k} \times e^{d/T_k} \quad (\text{A.24})$$

Where:  $T_k = T_{wave} + 273.15$

$$a = 82.56648$$

$$b = 0.262301$$

$$c = -4.06701e-04$$

$$d = 59.72934$$

The thermal conductivity obtained in this way is reported by Abu-Eishah (2000) to have an accuracy of  $\pm 0.1332\%$ .



## A.2.4 Fluid Properties

The fluid properties in both the annulus and inner tubes were determined from correlations proposed by Popiel and Wojtkowiak (1998). The bulk fluid temperature given in Equation (A.25) and Equation (A.26) for the inner tube and annulus respectively, were used to calculate the fluid properties while the wall temperature was used to calculate the fluid properties at the wall.

$$T_{bi} = \frac{T_{ii} + T_{io}}{2} \quad (\text{A.25})$$

and similarly for the annulus:

$$T_{bo} = \frac{T_{oi} + T_{oo}}{2} \quad (\text{A.26})$$

The correlations for the fluid properties are provided in Table A.1.

## A.2.5 Application of the Briggs and Young (1969) Method for Experimental Data.

The logarithmic mean temperature is given in Equation (A.27) for a counter flow heat exchanger.

$$T_{LMTD} = \frac{\Delta T_1 - \Delta T_2}{\ln\left(\frac{\Delta T_1}{\Delta T_2}\right)} \quad (\text{A.27})$$

Where

$$\Delta T_1 = T_{ii} - T_{oo} \quad (\text{A. 28})$$

$$\Delta T_2 = T_{io} - T_{oi} \quad (\text{A. 29})$$

The Reynolds number for both the inner tube and annulus is calculated as

$$Re = \frac{\rho VD}{\mu} \quad (\text{A.30})$$

Where  $D = D_h$  for the annulus and  $D = D_i$  for the inner tube. The fluid properties  $\rho$  and  $\mu$  are calculated at the bulk temperatures, and are calculated as explained in section A.2.4.

Table A.1: Correlations proposed by Popiel and Wojtkowiak (2001) for determining fluid properties at various temperatures.

Fluid property	Correlation	Constants
Density [ $\rho$ ]	$\rho = a + bT + cT^2 + dT^{2.5} + eT^3$	$a = 999.79684$ $b = 0.068317355$ $c = -0.010740248$ $d = 0.000821409$ $e = -2.30310e-05$
Specific Heat at Constant Pressure [ $C_p$ ]	$C_p = a + bT + cT^{1.5} + dT^2 + eT^{2.5}$	$a = 4.2174356000;$ $b = -0.0056181625;$ $c = 0.0012992528;$ $d = -0.000115354;$ $e = 4.14964e-06;$
Thermal Conductivity [ $k$ ]	$k = a + bT + cT^{1.5} + dT^2 + eT^{0.5}$	$a = 82.56648;$ $b = 0.262301;$ $c = -4.06701e-04;$ $d = 59.72934;$ $e = 2.718281828;$
Dynamic Viscosity [ $\mu$ ]	$\mu = \frac{1}{a + bT + cT^2 + dT^3}$	$a = 557.82468;$ $b = 19.408782;$ $c = 0.1360459;$ $d = -3.1160832e-04;$
Prandtl Number [ $Pr$ ]	$Pr = \frac{1}{a + bT + cT^2 + dT^3}$	$a = 0.074763403;$ $b = 0.0029020983;$ $c = 2.8606181e-05;$ $d = -8.1395537e-08;$

The fluid velocity for both the inner tube and annulus is calculated from:

$$V = \frac{\dot{m}}{\rho A} \quad (\text{A.31})$$

Where  $A = A_o$  for the annulus and  $A = A_i$  for the inner tube, with  $A_o$  and  $A_i$  defined as:

$$A_o = \frac{\pi}{4} [D_o^2 - D_i^2] \quad (\text{A.32})$$

$$A_i = \frac{\pi}{4} D_i^2 \quad (\text{A.33})$$

The heat transfer can then be obtained from the experimental results using:

$$\dot{Q} = \dot{m} C_p \Delta T \quad (\text{A.34})$$

Where  $\Delta T = T_{io} - T_{ii}$  for the inner tube and  $\Delta T = T_{oo} - T_{oi}$  for the annulus.

The average heat transfer rate is then calculated as:

$$\bar{Q} = \frac{|\dot{Q}_i| + |\dot{Q}_o|}{2} \quad (\text{A.35})$$

Overall heat transfer coefficients can then be calculated from:

$$U_i = \frac{\bar{Q}}{A_{si} T_{LMTD}} \quad (\text{A.36})$$

$$U_o = \frac{\bar{Q}}{A_{so} T_{LMTD}} \quad (\text{A.37})$$

Here  $U_i$  and  $U_o$  are the overall heat transfer coefficients for the inner tube and annulus respectively. Where  $A_{si} = \pi D_i L$  and  $A_{so} = \pi D_o L$ .

The procedure to calculate the coefficients  $C_i$ ,  $C_o$  and  $P$  as explained in section A.2 is then followed until convergence is obtained.

## A.2.6 Linear Regression plots and Converged Solutions for the Heat Exchangers

The data for the four heat exchangers, for both heating and cooling of the annulus was used in the modified Wilson plot analysis. The linear regression plots of  $X$  vs  $Y$ ,  $X_{shell}$  vs  $Y_{shell}$  and the convergence of  $P$  for each heat exchanger and each configuration is provided in the following sections. Converged values of  $C_i$ ,  $C_o$ ,  $C_{o,shell}$  and  $P$  are provided in Table A.2.

Table A.2: Wilson Plot Coefficients for the four heat exchangers tested.

Annular diameter ratio(a)	Cooling				Heating			
	$C_i$	$C_o$	$C_{o,shell}$	$P$	$C_i$	$C_o$	$C_{o,shell}$	$P$
<b>0.482</b>	0.0296	0.0154	0.0154	0.8598	0.0273	0.0079	0.0079	0.9354
<b>0.579</b>	0.0304	0.0097	0.0097	0.9087	0.0275	0.0077	0.0077	0.9367
<b>0.593</b>	0.0278	0.0095	0.0095	0.9058	0.0288	0.0039	0.0039	1.0070
<b>0.712</b>	0.0273	0.0071	0.0071	0.9322	0.0265	0.0035	0.0035	1.0107

A.2.6.1 Annular Diameter Ratio 0.482

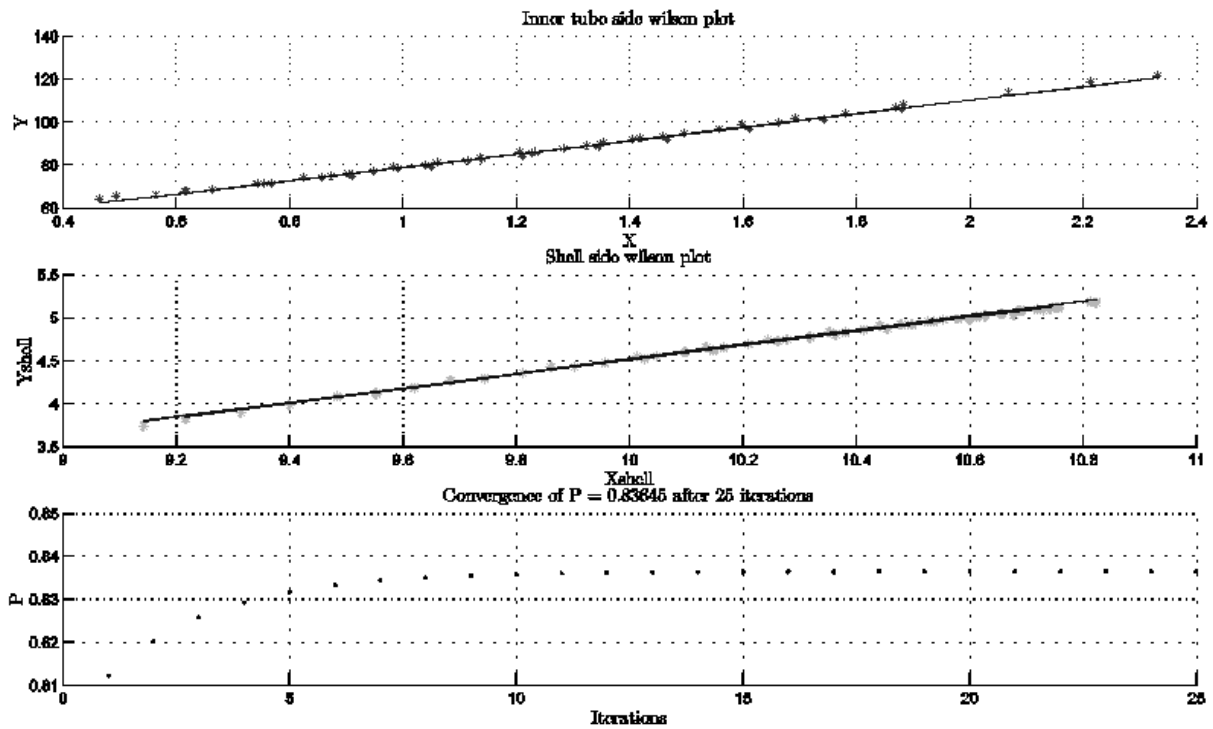


Figure A.2: Linear regression results of  $X$  and  $Y$ ,  $X_{shell}$  and  $Y_{shell}$  and number of iterations for  $P$  to converge for a cooled annulus (annular diameter ratio = 0.482).

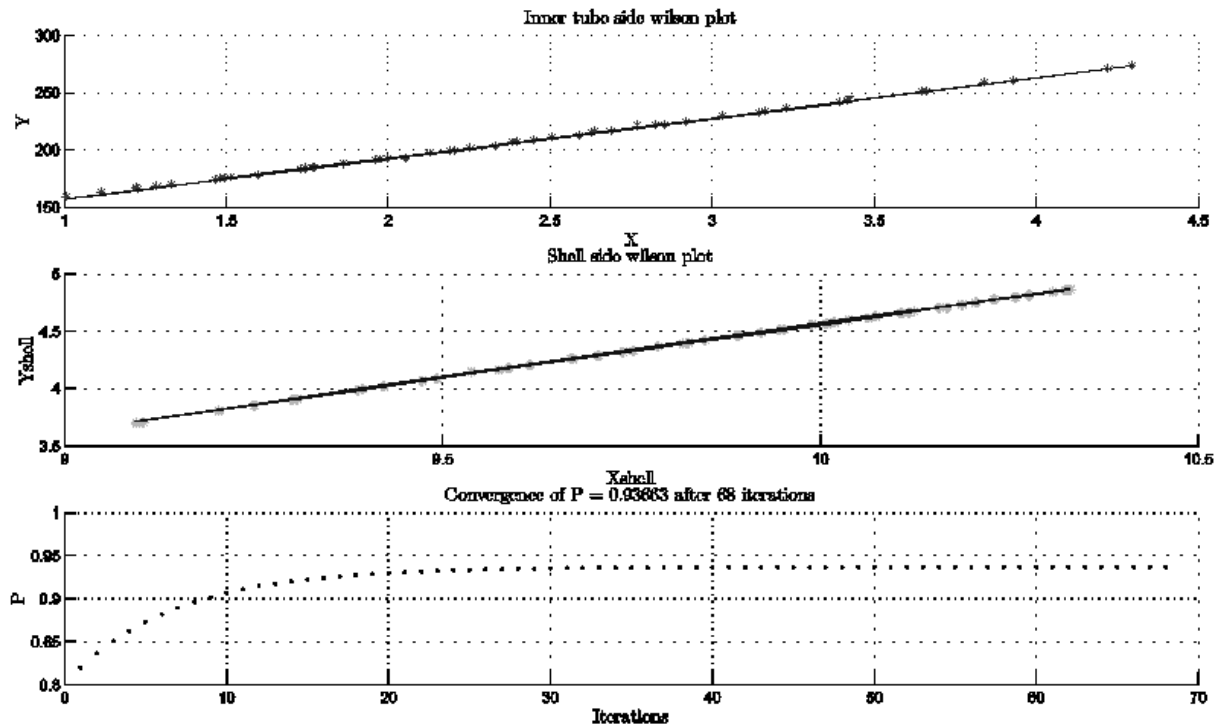


Figure A.3: Linear regression results of  $X$  and  $Y$ ,  $X_{shell}$  and  $Y_{shell}$  and number of iterations for  $P$  to converge for a heated annulus (annular diameter ratio = 0.482).

### A.2.6.2 Annular Diameter Ratio 0.579

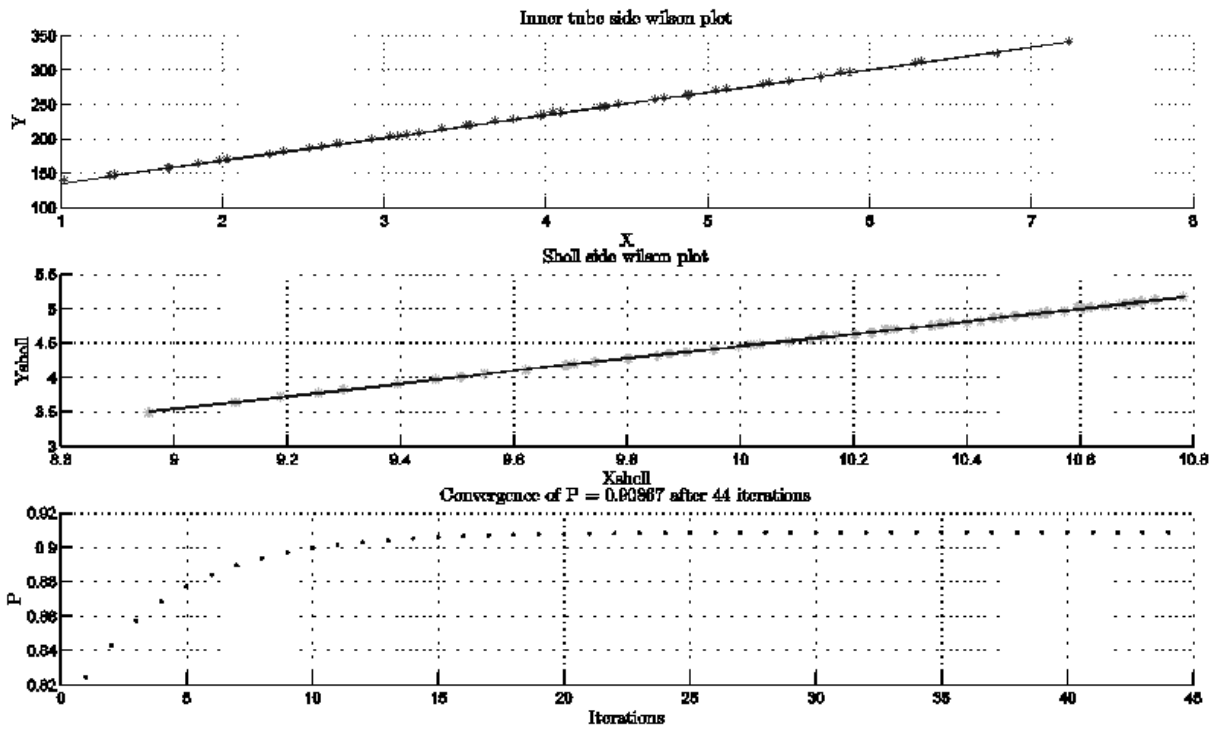


Figure A.4: Linear regression results of  $X$  and  $Y$ ,  $X_{shell}$  and  $Y_{shell}$  and number of iterations for  $P$  to converge for a cooled annulus (annular diameter ratio = 0.579).

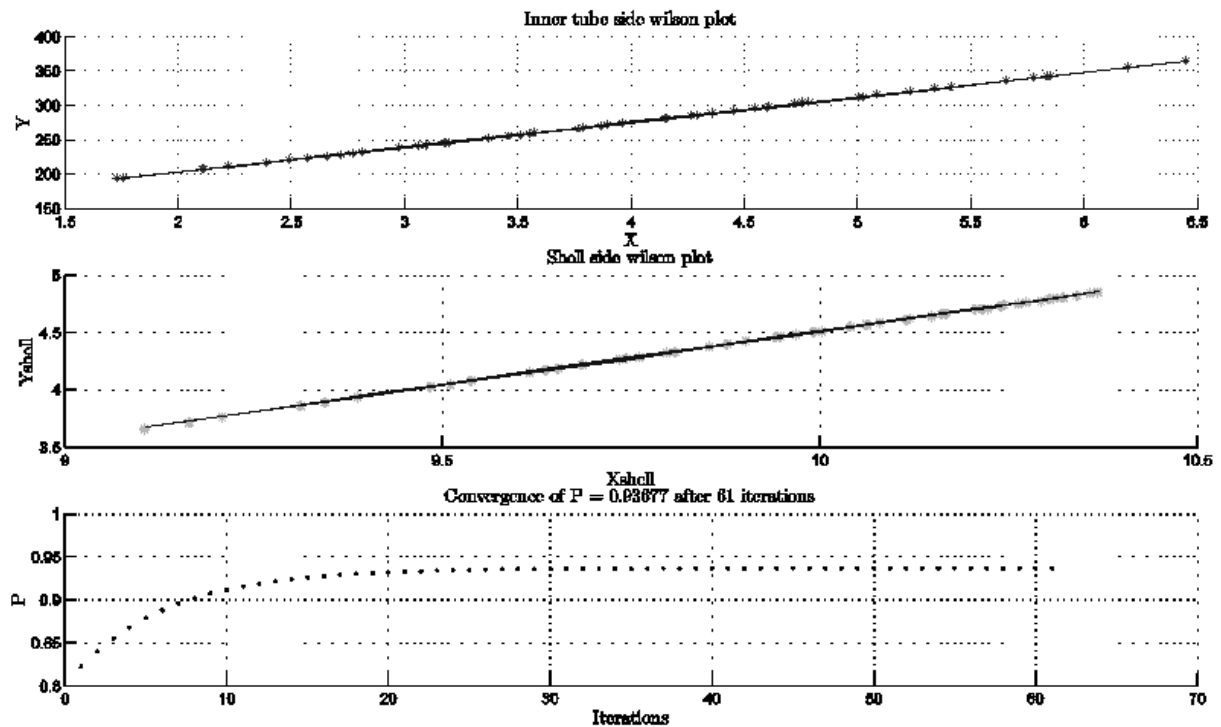


Figure A.5: Linear regression results of  $X$  and  $Y$ ,  $X_{shell}$  and  $Y_{shell}$  and number of iterations for  $P$  to converge for a heated annulus (annular diameter ratio = 0.579).

### A.2.6.3 Annular Diameter Ratio 0.593

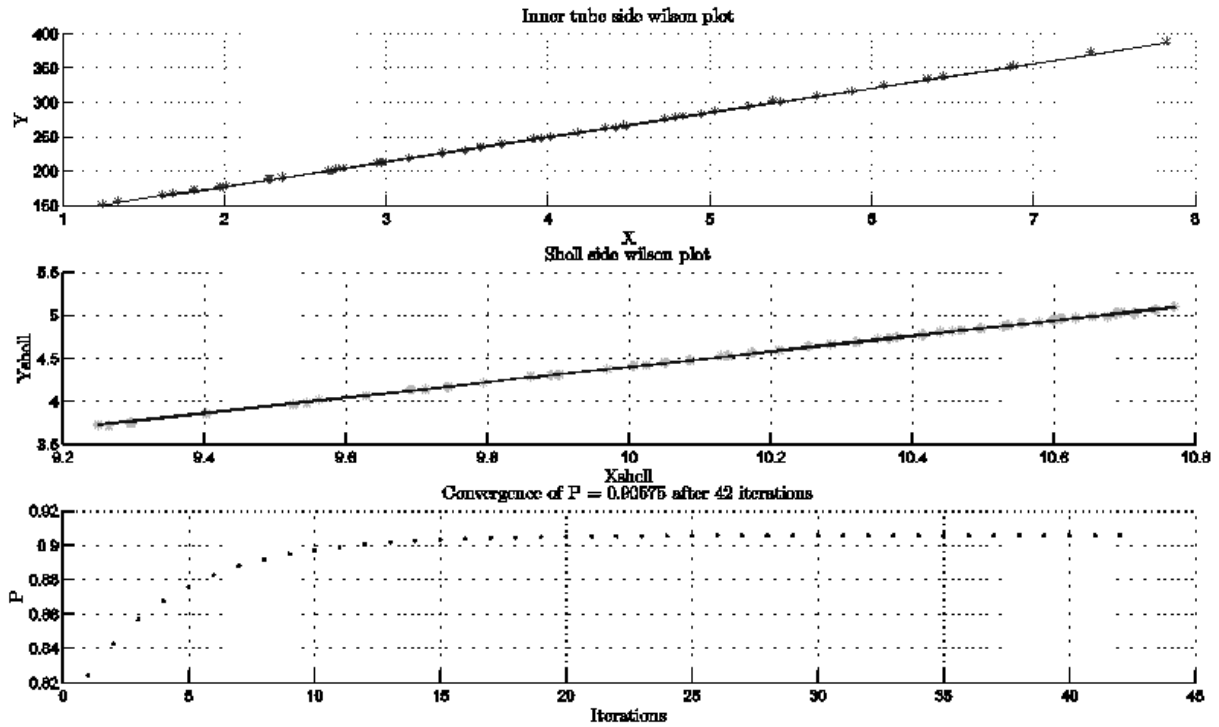


Figure A.6: Linear regression results of  $X$  and  $Y$ ,  $X_{shell}$  and  $Y_{shell}$  and number of iterations for  $P$  to converge for a cooled annulus (annular diameter ratio = 0.593).

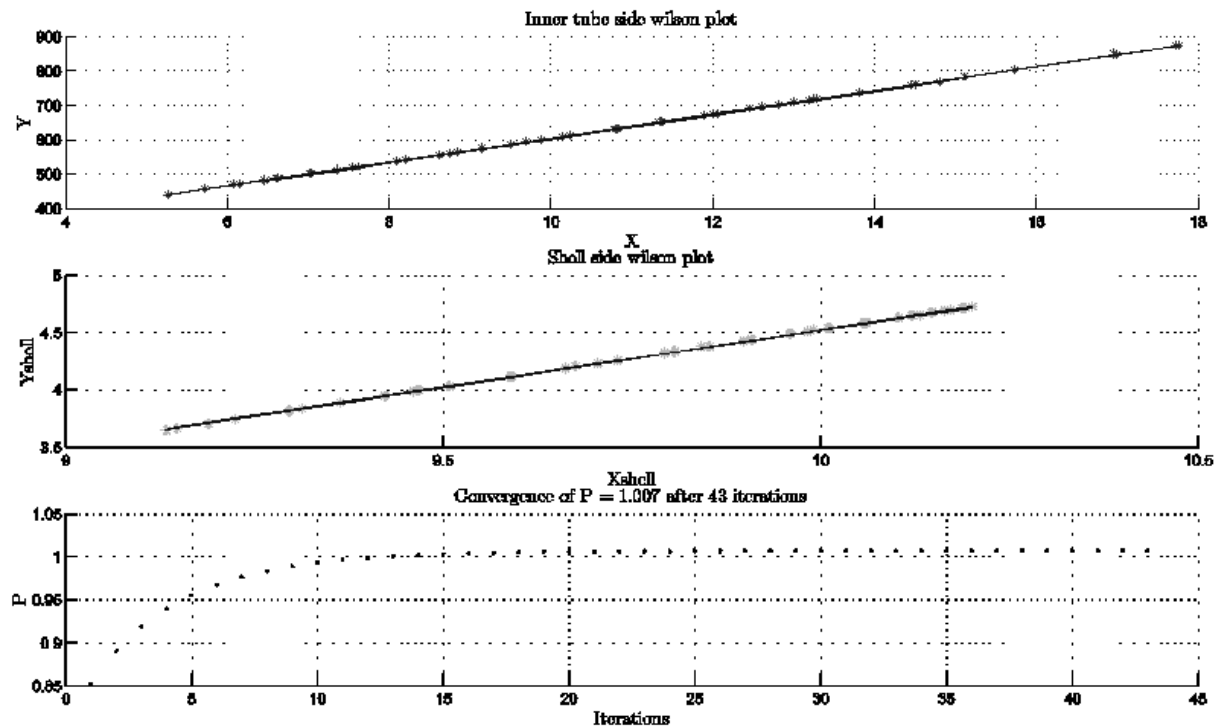


Figure A.7: Linear regression results of  $X$  and  $Y$ ,  $X_{shell}$  and  $Y_{shell}$  and number of iterations for  $P$  to converge for a heated annulus (annular diameter ratio = 0.593).

A.2.6.4 Annular Diameter Ratio 0.712

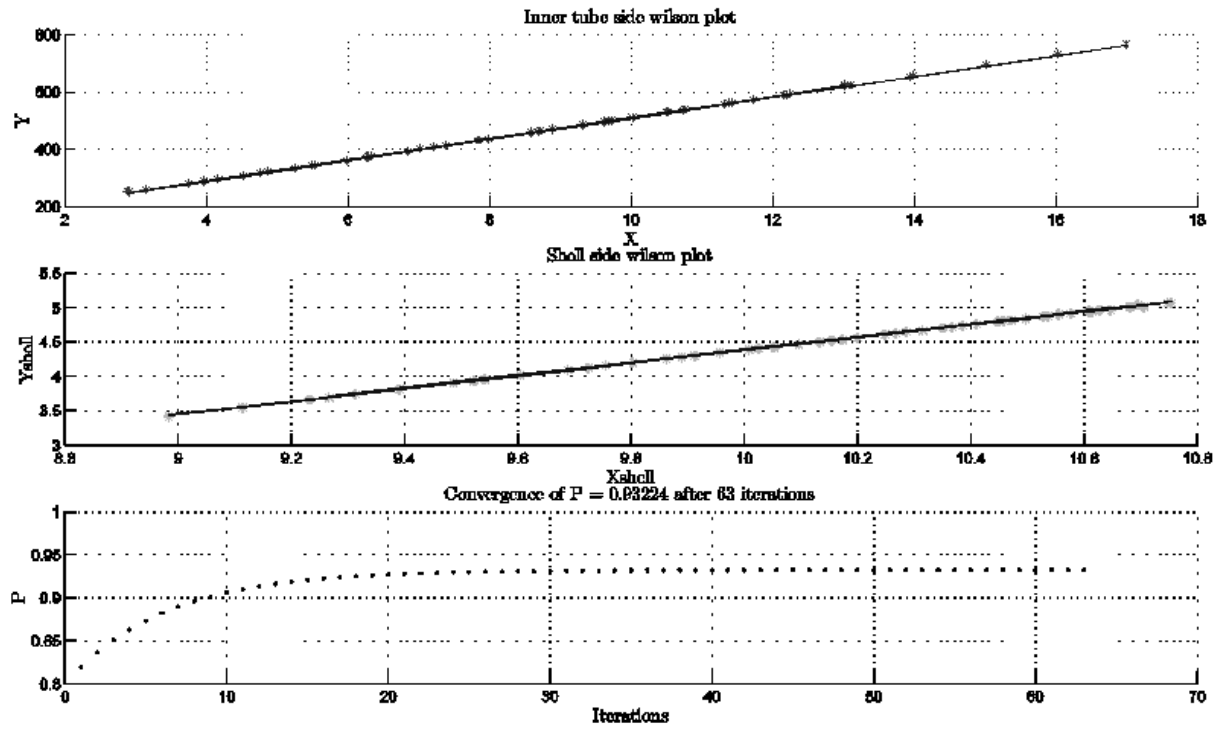


Figure A.8: Linear regression results of  $X$  and  $Y$ ,  $X_{shell}$  and  $Y_{shell}$  and number of iterations for  $P$  to converge for a cooled annulus (annular diameter ratio = 0.712).

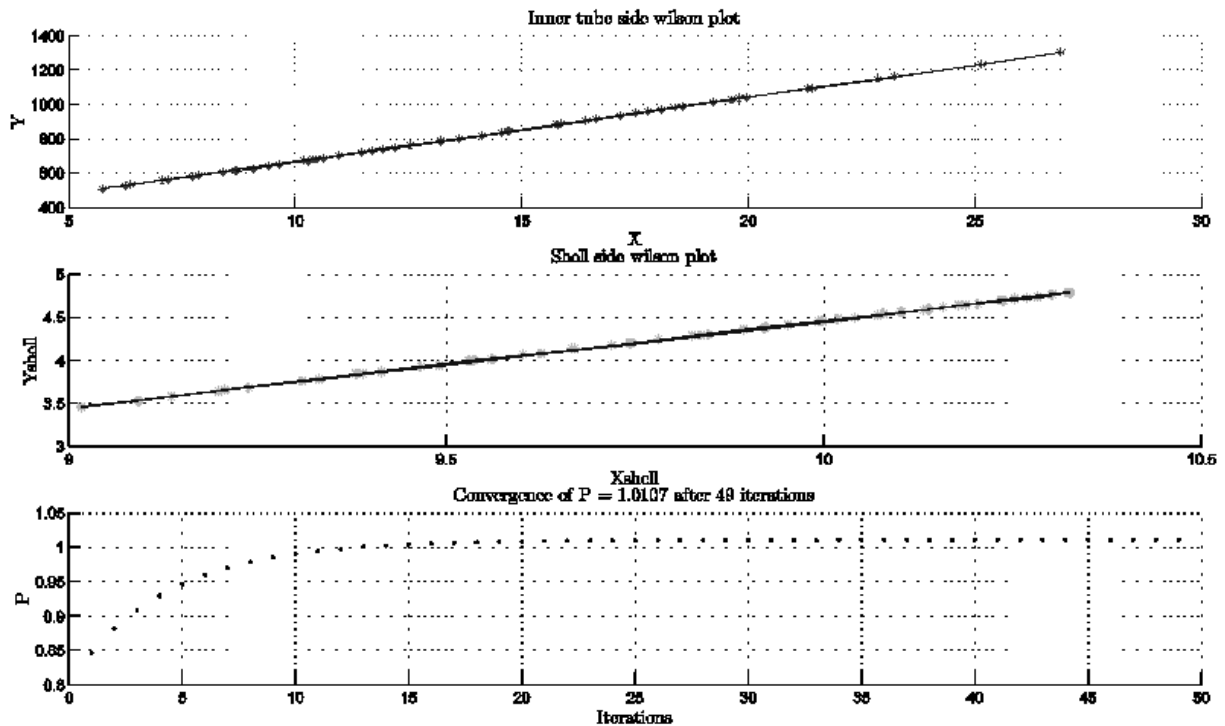


Figure A.9: Linear regression results of  $X$  and  $Y$ ,  $X_{shell}$  and  $Y_{shell}$  and number of iterations for  $P$  to converge for a heated annulus (annular diameter ratio = 0.712).

### A.3 Comparison of Modified Wilson Plot Wall Temperatures to Measured Wall Temperatures

The modified Wilson Plot technique predicts both the average inner and average outer wall temperatures. These temperatures are compared to the experimentally measured wall temperatures averaged across the heat exchanger length, given as:

$$\bar{T}_w = \frac{1}{N_i} \sum_{j=1}^{N_i} T_{i,j} \quad (\text{A.38})$$

Where  $\bar{T}_w$  is the average wall temperature,  $N_i$  the number of thermocouples on the inner wall and  $T_{i,j}$ , thermocouple  $j$  in the wall.

Figure A.10, Figure A.12, Figure A.14 and Figure A.16 are plots of the predicted wall temperatures of the modified Wilson plot technique and the experimentally measured wall temperatures, for all annular ratios 0.412, 0.579, 0.593 and 0.712 respectively.

Equation (A.39) defines the difference of the experimentally measured wall temperatures and the average of the inner and outer wall temperatures of the modified Wilson plot method are plotted in Figure A.11, Figure A.13, Figure A.15 and Figure A.17 for the four respective annular ratios tested.

$$T_{diff} = \bar{T}_w - \left( \frac{T_{wi,wp} + T_{wo,wp}}{2} \right) \quad (\text{A.39})$$

Where the  $\bar{T}_w$  is the measured wall temperatures and  $T_{wi,wp}$  and  $T_{wo,wp}$  are the inner and outer wall temperatures predicted by the modified Wilson plot method. Table A.3 provides the mean temperature differences for the four heat exchangers for both a cooled and heated annulus.



Table A.3: Mean temperature differences of measured wall temperatures and those predicted by the modified Wilson plot method.

Annular diameter ratio  (a)	Temperature difference (°C)	
	Cooling	Heating
<b>0.48</b>	0.306	0.632
<b>0.58</b>	0.772	0.398
<b>0.59</b>	0.671	0.162
<b>0.71</b>	0.722	0.004

### A.3.1.1 Annular Diameter Ratio 0.482

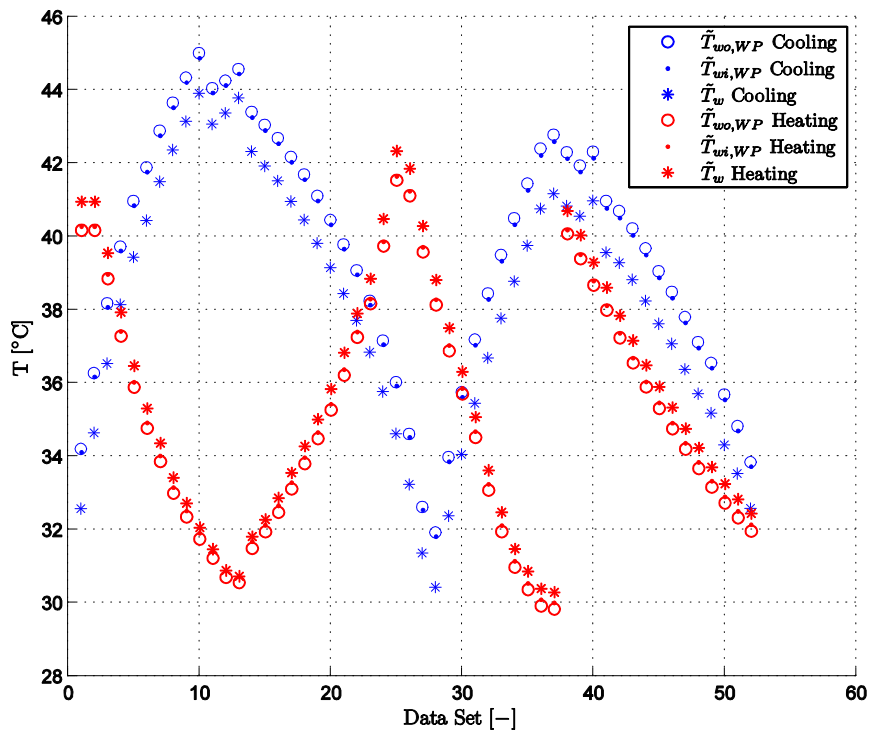


Figure A.10: Wall temperature comparisons for the averaged experimentally measured wall temperatures and those predicted by the modified Wilson Plot method (annular diameter ratio of 0.482).

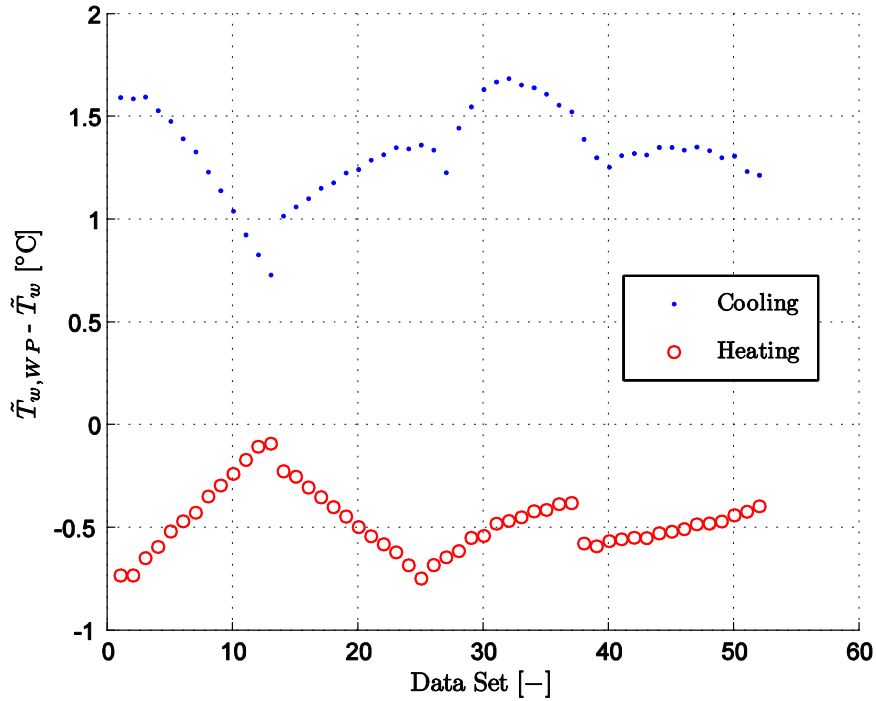


Figure A.11: Temperature differences of measured wall temperatures and those predicted by the modified Wilson plot method (annular diameter ratio of 0.482).

### A.3.1.2 Annular Diameter Ratio 0.579

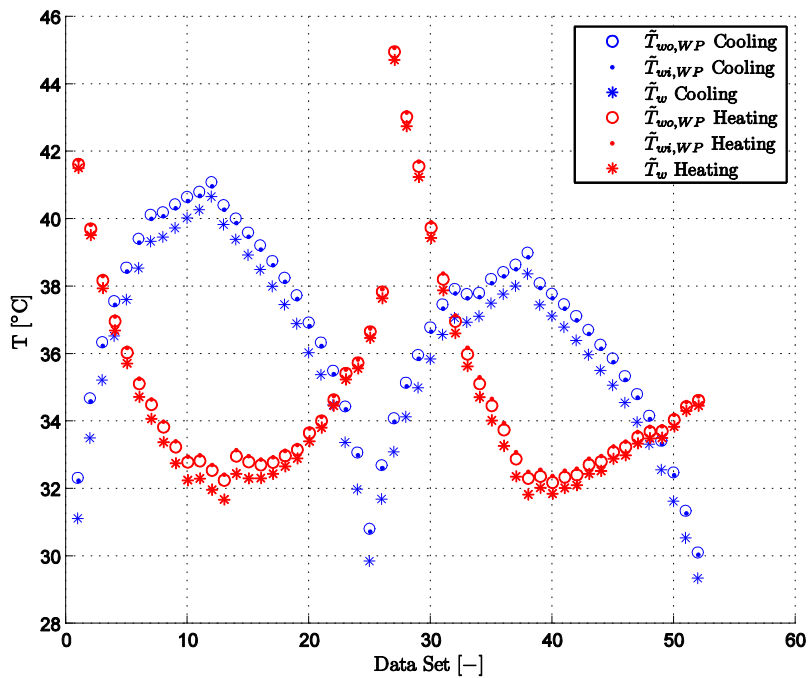


Figure A.12: Wall temperature comparisons for the averaged experimentally measured wall temperatures and those predicted by the modified Wilson Plot method (annular diameter ratio of 0.579).

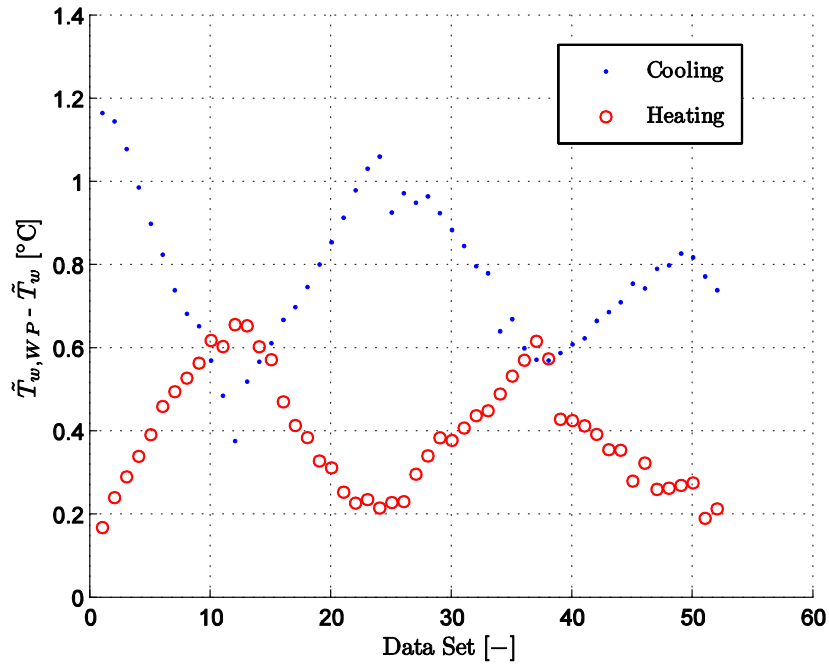


Figure A.13: Temperature differences of measured wall temperatures and those predicted by the modified Wilson plot method (annular diameter ratio of 0.579).

### A.3.1.3 Annular Diameter Ratio 0.593

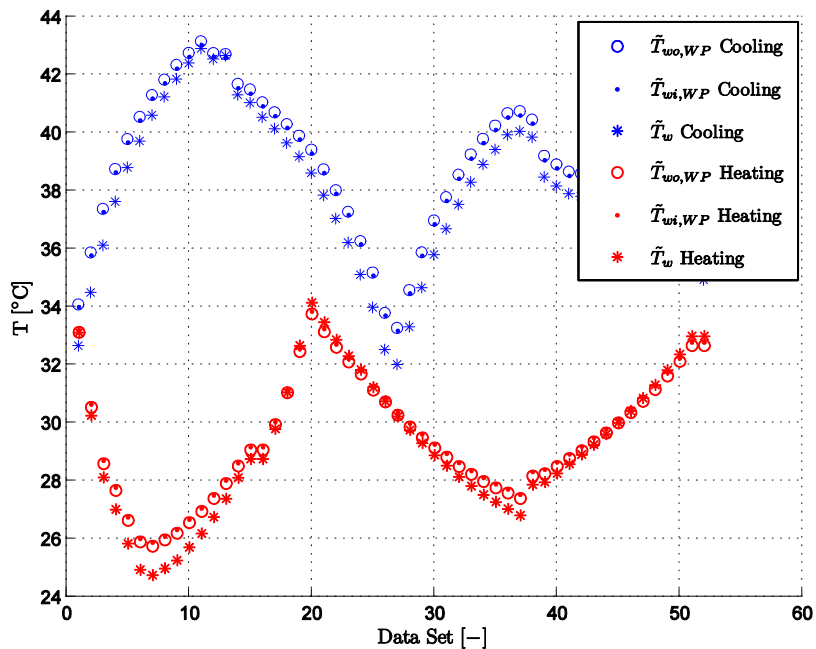


Figure A.14: Wall temperature comparisons for the experimentally measured wall temperatures and those predicted by the modified Wilson Plot method (annular diameter ratio of 0.593).

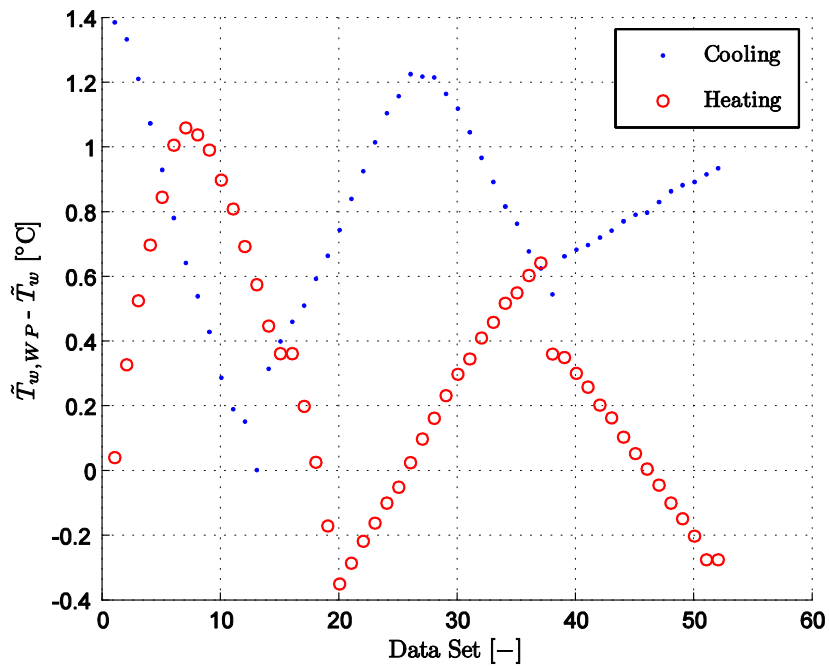


Figure A.15: Temperature differences of measured wall temperatures and those predicted by the modified Wilson plot method (annular diameter ratio of 0.593).

### A.3.1.4 Annular Diameter Ratio 0.712

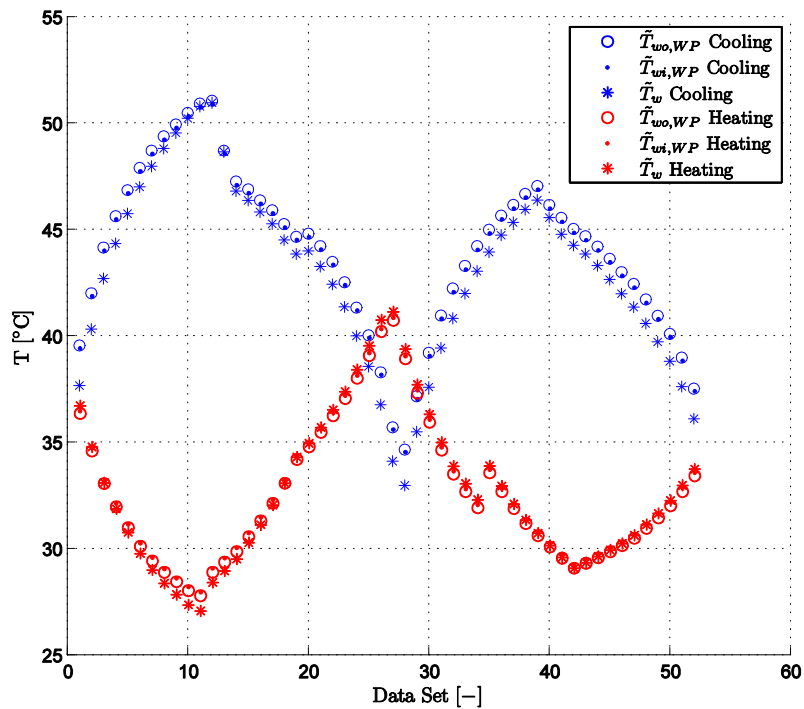


Figure A.16: Wall temperature comparisons for the averaged experimentally measured wall temperatures and those predicted by the modified Wilson Plot method (annular diameter ratio of 0.712).

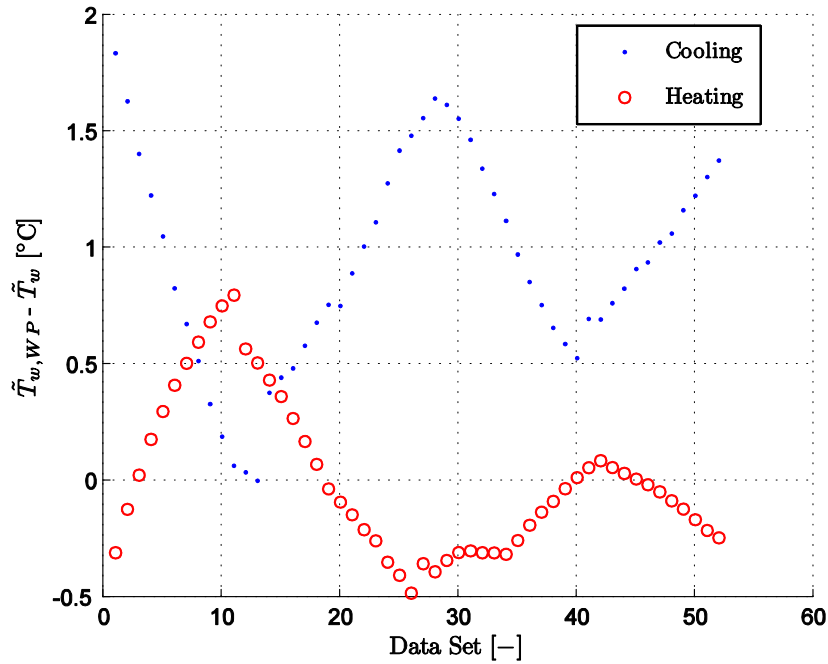


Figure A.17: Temperature differences of measured wall temperatures and those predicted by the modified Wilson plot method (annular diameter ratio of 0.712).

## A.4 Heat Transfer Coefficient Analysis

The accuracy of the heat transfer coefficient predicted by the modified Wilson plot method is investigated here. To determine the accuracy, the overall heat transfer coefficients for both the inner tube and annulus are calculated as

$$U_{i,wp} = \frac{1}{1/h_{i,wp} + A_{si}/A_{so}h_{o,wp}} \quad (\text{A. 40})$$

$$U_{o,wp} = \frac{1}{1/h_{o,wp} + A_{so}/A_{si}h_{i,wp}} \quad (\text{A. 41})$$

With  $h_i$  and  $h_o$  obtained from the modified Wilson plot method. The overall heat transfer coefficients are then used to calculate the heat transfer to both the inner tube and annulus

$$\dot{Q}_{i,wp} = U_{i,wp}A_{si}\Delta T_{LMTD} \quad (\text{A. 42})$$

$$\dot{Q}_{o,wp} = U_{o,wp}A_{so}\Delta T_{LMTD} \quad (\text{A. 43})$$

The heat transfer calculated using experimental values for the inner tube and annulus is given as:

$$\dot{Q}_i = \dot{m}_i C p_i \Delta T_i \quad (\text{A. 44})$$

$$\dot{Q}_o = \dot{m}_o C p_o \Delta T_o \quad (\text{A. 45})$$

Where  $\Delta T_i = T_{ii} - T_{io}$  and  $\Delta T_o = T_{oi} - T_{oo}$ .  $\dot{Q}_{i,wp}$  and  $\dot{Q}_i$  for the inner tube; and  $\dot{Q}_{o,wp}$  and  $\dot{Q}_o$  for the annulus are compared to obtain the error

$$e_{i,wp} = \left| \frac{\dot{Q}_i - \dot{Q}_{i,wp}}{\dot{Q}_i} \right| \times 100 \quad (\text{A. 46})$$

$$e_{o,wp} = \left| \frac{\dot{Q}_o - \dot{Q}_{o,wp}}{\dot{Q}_o} \right| \times 100 \quad (\text{A. 47})$$

The heat transfer rate errors calculated from the modified Wilson plot heat transfer coefficient are shown in Figure A.18 to Figure A.21 for the four respective annular diameter ratios. The mean errors for the annulus and inner tube are also shown on each of these figures.

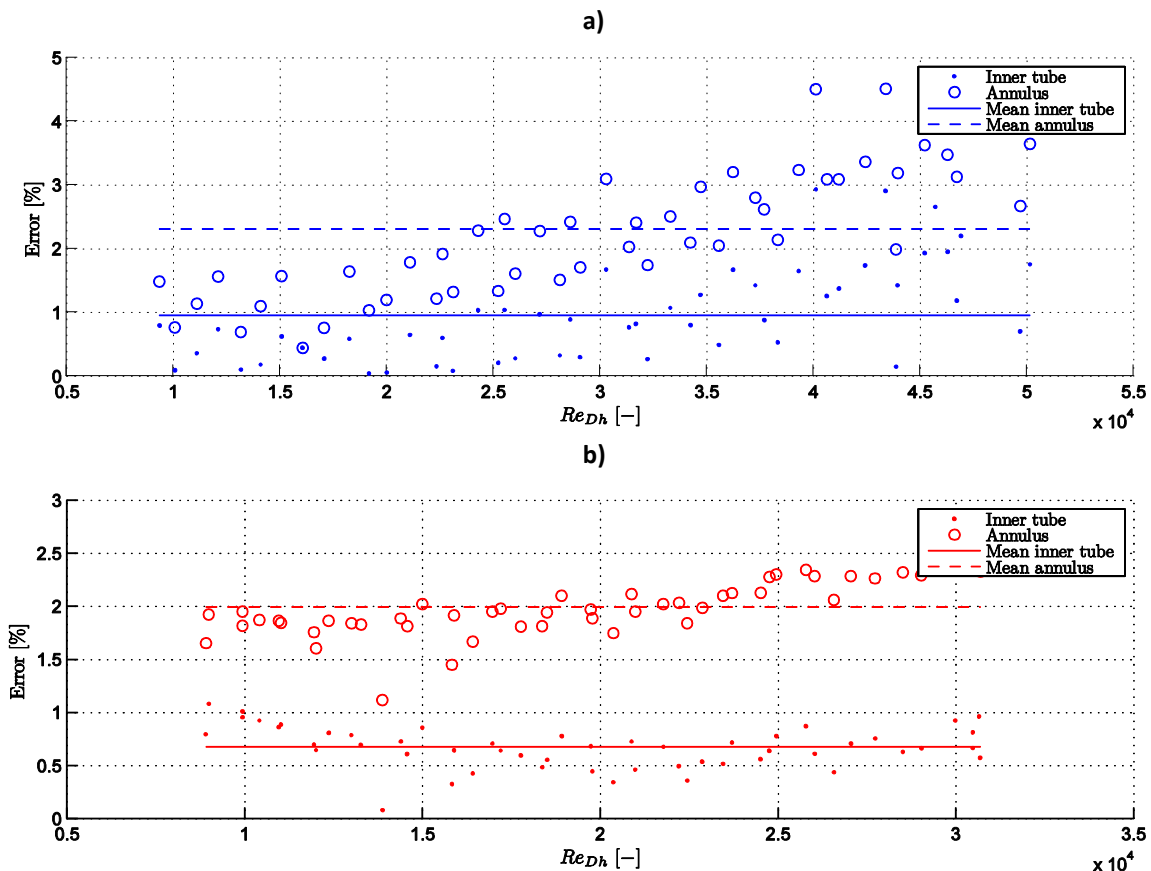


Figure A.18: Errors of the rate of heat transfer predicted by the modified Wilson plot for ar0.48 for a) cooled and b) heated annulus.

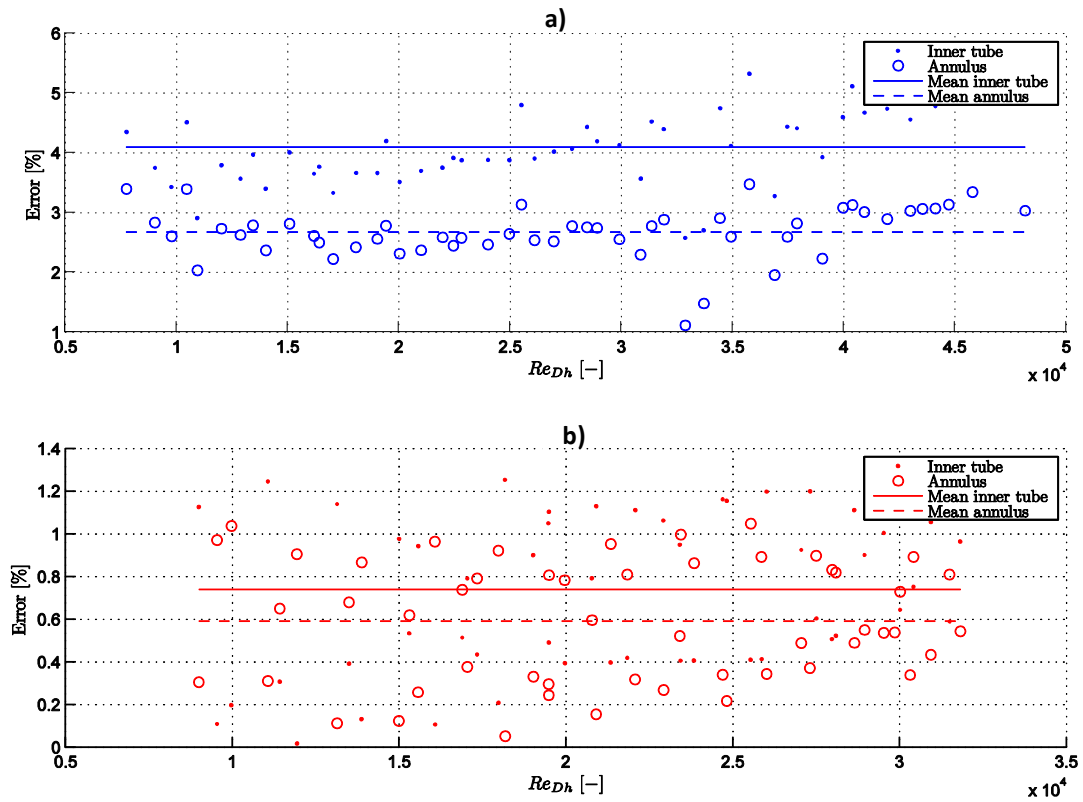


Figure A.19: Errors of the rate of heat transfer predicted by the modified Wilson plot for  $ar=0.57$  for a) cooled and b) heated annulus.

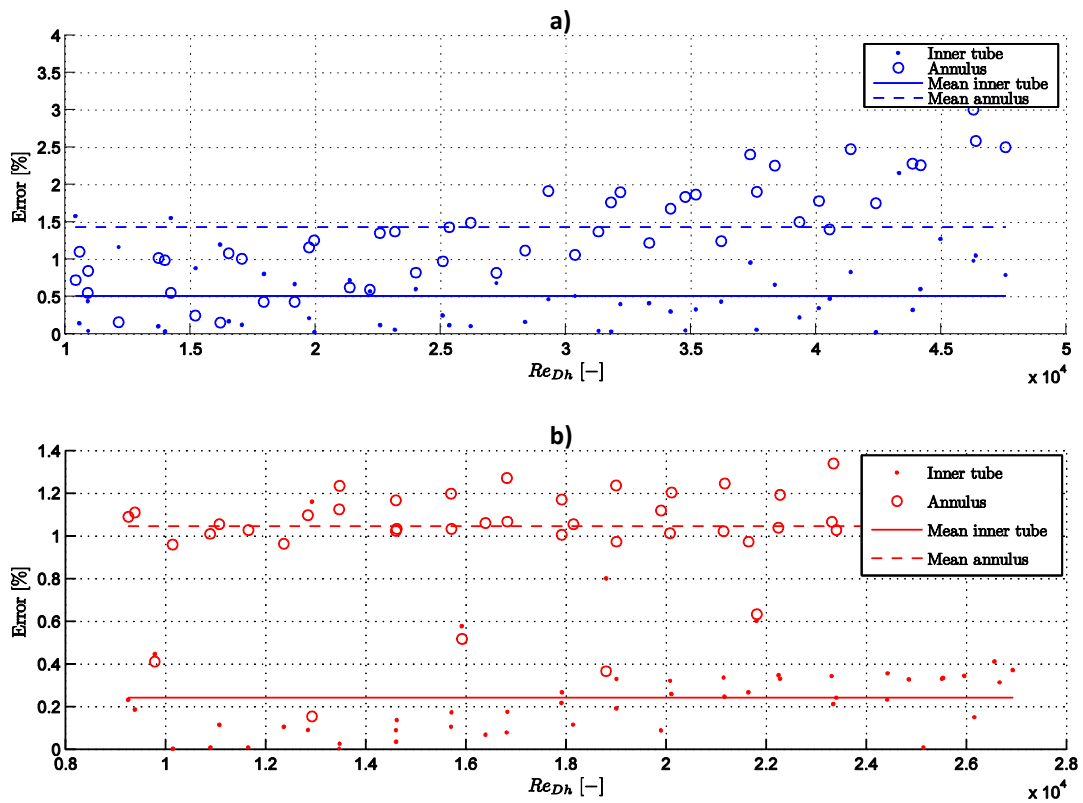


Figure A.20: Errors of the rate of heat transfer predicted by the modified Wilson plot for  $ar=0.59$  for a) cooled and b) heated annulus.

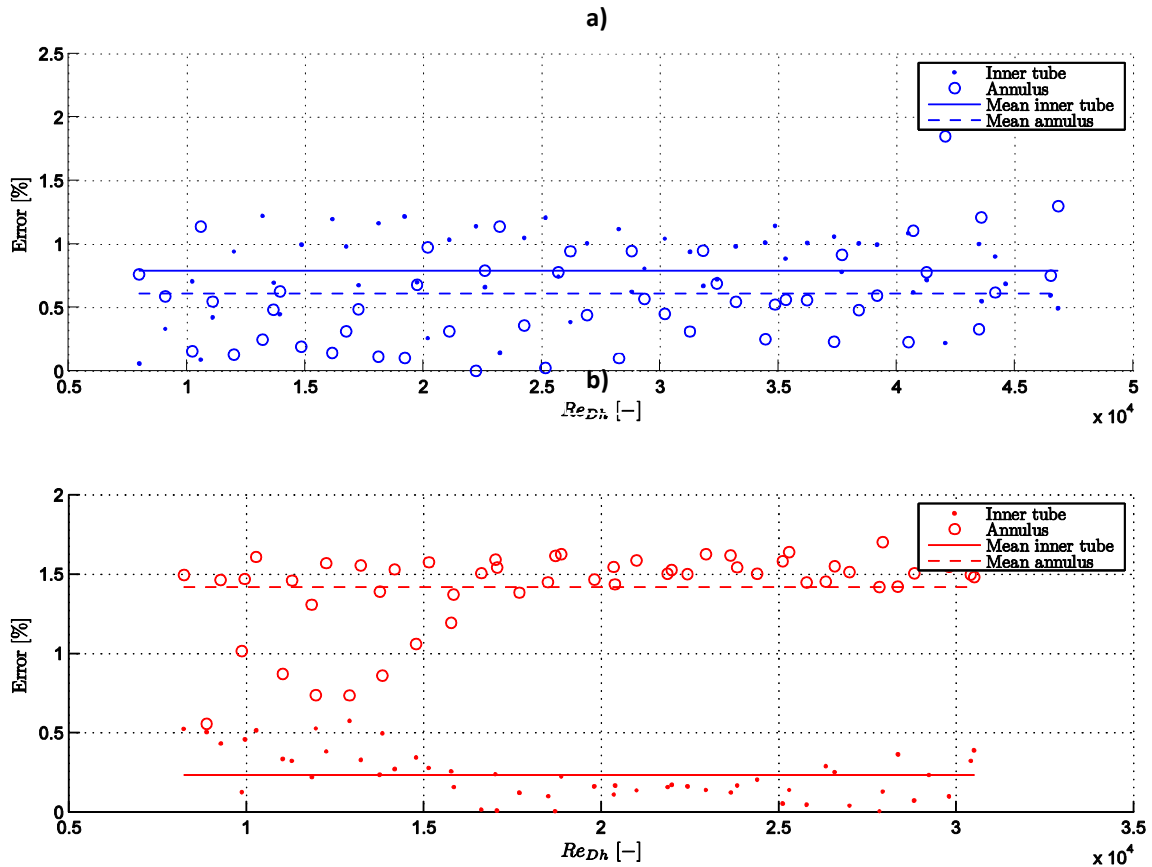


Figure A.21: Errors of the rate of heat transfer predicted by the modified Wilson plot for ar0.71 for a) cooled and b) heated annulus.

Mean errors for all the annular ratios and configurations for both the inner tube and annulus are provided in Table A.4.

Table A.4: Mean errors for the heat transfer rate predicted by the modified Wilson plot method for all annular diameter ratios and configurations.

Annular diameter ratio (a)	$e_{i,wp}(\%)$		$e_{o,wp}(\%)$	
	Cooling	Heating	Cooling	Heating
0.482	0.952	0.674	2.312	1.996
0.579	4.103	0.746	2.675	0.595
0.593	1.446	0.245	0.513	1.059
0.712	0.792	0.234	0.618	1.411



The modified Wilson plot method predicts heat transfer coefficients which produce mean errors reaching a maximum of 4.10 % for all annular diameter ratios and heating or cooling configurations.

## Appendix B

### Khartabil and Christensen Nonlinear Regression

#### Contents

B.1 Introduction .....	B.1
B.2 The Nonlinear Regression method Explained .....	B.1
B.2.1 Fundamentals of the Nonlinear Regression Scheme (Khartabil and Christensen (1992)) .....	B.2
B.2.2 Non Linear Regression Analysis performed on Experimental Data .....	B.6
B.2.2.1 Annular Diameter Ration 0.482.....	B.7
B.2.2.2 Annular Diameter Ration 0.579.....	B.8
B.2.2.3 Annular Diameter Ration 0.593.....	B.9
B.2.2.4 Annular Diameter Ration 0.712.....	B.10
B.3 Comparison of Khartabil and Christensen Wall Temperatures to Measured Wall Temperatures. ....	B.11
B.3.1 Annular Diameter Ratio 0.482 .....	B.12
B.3.2 Annular Diameter Ratio 0.579 .....	B.13
B.3.3 Annular Diameter Ratio 0.593 .....	B.14
B.3.4 Annular Diameter Ratio 0.712 .....	B.15
B.4 Heat Transfer Coefficient Analysis .....	B.16

## List of Figures

Figure B.1: a) Plot of $f(P)$ showing the area of interest where $f(P) = 0$ , as well as b) the convergence obtained using the bisection method for cooling of the annulus (annular diameter ratio 0.482).....	B.7
Figure B.2: a) Plot of $f(P)$ showing the area of interest where $f(P) = 0$ , as well as b) the convergence obtained using the bisection method for heating of the annulus (annular diameter ratio 0.482).....	B.7
Figure B.3: a) Plot of $f(P)$ showing the area of interest where $f(P) = 0$ , as well as b) the convergence obtained using the bisection method for cooling of the annulus (annular diameter ratio 0.579).....	B.8
Figure B.4: a) Plot of $f(P)$ showing the area of interest where $f(P) = 0$ , as well as b) the convergence obtained using the bisection method for heating of the annulus (annular diameter ratio 0.579).....	B.8
Figure B.5: a) Plot of $f(P)$ showing the area of interest where $f(P) = 0$ , as well as b) the convergence obtained using the bisection method for cooling of the annulus (annular diameter ratio 0.593).....	B.9
Figure B.6: a) Plot of $f(P)$ showing the area of interest where $f(P) = 0$ , as well as b) the convergence obtained using the bisection method for heating of the annulus (annular diameter ratio 0.593).....	B.9
Figure B.7: a) Plot of $f(P)$ showing the area of interest where $f(P) = 0$ , as well as b) the convergence obtained using the bisection method for cooling of the annulus (annular diameter ratio 0.712).....	B.10
Figure B.8: a) Plot of $f(P)$ showing the area of interest where $f(P) = 0$ , as well as b) the convergence obtained using the bisection method for heating of the annulus (annular diameter ratio 0.712).....	B.10
Figure B. 9: Comparison of averaged measured wall temperatures and wall temperatures predicted by the Khartabil and Christensen method (annular diameter ratio 0.482).....	B.12
Figure B. 10: Errors of the wall temperatures predicted by the Khartabil and Christensen method compared to the averaged measured wall temperatures (annular diameter ratio 0.482).....	B.12

Figure B. 11: Comparison of averaged measured wall temperatures and wall temperatures predicted by the Khartabil and Christensen method (annular diameter ratio 0.579).....	B.13
Figure B. 12: Errors of the wall temperatures predicted by the Khartabil and Christensen method compared to the averaged measured wall temperatures (annular diameter ratio 0.579).....	B.13
Figure B. 13: Comparison of averaged measured wall temperatures and wall temperatures predicted by the Khartabil and Christensen method (annular diameter ratio 0.593).....	B.14
Figure B. 14: Errors of the wall temperatures predicted by the Khartabil and Christensen method compared to the averaged measured wall temperatures (annular diameter ratio 0.593).....	B.14
Figure B. 15: Comparison of averaged measured wall temperatures and wall temperatures predicted by the Khartabil and Christensen method (annular diameter ratio 0.712).....	B.15
Figure B. 16: Errors of the wall temperatures predicted by the Khartabil and Christensen method compared to the averaged measured wall temperatures (annular diameter ratio 0.593).....	B.15
Figure B. 17: Errors for the rate of heat transfer rate predicted by the Khartabil and Christensen method for ar0.483 for a) cooled and b) heated annulus.....	B.17
Figure B. 18: Errors for the rate of heat transfer rate predicted by the Khartabil and Christensen method for ar0.579 for a) cooled and b) heated annulus.....	B.17
Figure B. 19: Errors for the rate of heat transfer rate predicted by the Khartabil and Christensen method for ar0.593 for a) cooled and b) heated annulus.....	B.18
Figure B. 20: Errors for the rate of heat transfer rate predicted by the Khartabil and Christensen method for ar0.712 for a) cooled and b) heated annulus.....	B.18

## List of Tables

Table B.1: Coefficients $C_i$ , $C_o$ and $P$ used in the Sieder and Tate type equation for the annulus.....	B.6
Table B.2: Mean temperature difference of measured temperatures and those predicted by Khartabil and Christensen (1992).....	B.11
Table B. 3: Mean errors for the heat transfer rate predicted by the Khartabil and Christensen method for all annular diameter ratios and heating or cooling configuration. ..	B.19

## Nomenclature

In addition to the nomenclature used in the main text body, the following symbols are used in this appendix.

$j$	Index	-
$a1 - a4$	Matrix Components	-
$A$	Matrix	-
$b1 - b2$	Matrix Components	-
$B$	Matrix	-
$C$	Matrix	-
$e$	Error	-
$LHS$	Left Hand Side of Equation	-
$n$	Number of Data Points	-
$RHS$	Right Hand Side of Equation	-
$r_{cond}$	Conductive Resistance Across Tube Wall	-
$S$	Sum of squares of deviations.	-

### Greek Symbols

$\phi$	Simplification Variable	-
$\psi$	Simplification Variable	-

### Subscripts

$kc$	Obtained From the Method of Khartabil and Christensen (1992)
------	--

### Other Symbols

$\partial$	Partial Differential	-
$\Delta$	Temperature Difference	-

**Note:** Nomenclature declared in the main text are not repeated here.

## B.1 Introduction

Khartabil and Christensen (1992) propose a nonlinear regression scheme for the analysis of heat exchangers where only one of the fluids' thermal resistances varies. Three unknowns are determined here and this analysis scheme is said to solve similar data sets to that of the modified Wilson plot technique. Khartabil and Christensen (1992) suggest that the modified Wilson plot technique is approximate and may not always converge to an optimum solution. The nonlinear regression analysis used here, according to Khartabil and Christensen (1992), is guaranteed to converge provided a solution exists.

Unlike the modified Wilson plot method; this nonlinear scheme does not separate the model into linear parts.

## B.2 The Nonlinear Regression method Explained

To implement the nonlinear regression scheme, Matlab 7.6.0 (R2008a) was used with a precision of 16 decimals. This is adequate as Khartabil and Christensen (1992) suggest double-precision arithmetic. The method involves iteratively incrementing the  $P$  value of the Sieder Tate type equation and solving for the corresponding constants.

The dataset required to complete the nonlinear regression analysis is similar to that required for the modified Wilson plot technique. Section A.2.1 pertaining to the required data set for the modified Wilson plot technique is also applicable here.

## B.2.1 Fundamentals of the Nonlinear Regression Scheme (Khartabil and Christensen (1992))

Definitions of basic heat transfer relations used in the nonlinear regression scheme are shown; this is followed by the formulation and implementation of the Khartabil and Christensen (1992) method.

With the heat transfer rate of the fluid for both the inner tube and annulus is given as:

$$\dot{Q}_i = \dot{m}_i c_p (T_{ii} - T_{io}) \quad (\text{B.1})$$

$$\dot{Q}_o = \dot{m}_o c_p (T_{oi} - T_{oo}) \quad (\text{B.2})$$

The mean heat transfer rate is then defined as:

$$\bar{Q} = \frac{|\dot{Q}_i| + |\dot{Q}_o|}{2} \quad (\text{B.3})$$

The overall heat transfer coefficient over the heat exchange length is then given as:

$$U_o = \frac{\bar{Q}}{A_{so} \Delta T_{lmtd}} \quad (\text{B.4})$$

Where  $\Delta T_{lmtd}$  is defined as:

$$\Delta T_{lmtd} = \frac{(T_{ii} - T_{oo}) - (T_{io} - T_{oi})}{\ln[(T_{ii} - T_{oo}) / (T_{io} - T_{oi})]} \quad (\text{B.5})$$

The overall heat transfer coefficient is then separated into its constituent components namely the inner tube fluid stream, inner tube wall and annulus fluid stream:

$$\frac{1}{U_o A_{so}} = \frac{1}{h_i A_{si}} + r_{cond} + \frac{1}{h_o A_{so}} \quad (\text{B.6})$$

The method of Khartabil and Christensen(1992) then proceeds to formulate the nonlinear regression by assuming that the heat transfer coefficients within the inner tube and annulus can be correlated using the Sieder and Tate correlation for smooth tubes. Equation (B.7) and (B.8) are the Sieder and Tate type correlations for the inner tube and annulus respectively, where Equation (B.8) is modified using the hydraulic diameter for the annulus.

$$Nu_i = \frac{h_i D_i}{k_i} = C_i Re_i^{0.8} Pr_i^{\frac{1}{3}} \left( \frac{\mu}{\mu_w} \right)_i^{0.14} \quad (\text{B.7})$$

$$Nu_o = \frac{h_o D_h}{k_o} = C_o Re_{D_h}^P Pr_o^{\frac{1}{3}} \left( \frac{\mu}{\mu_w} \right)_o^{0.14} \quad (\text{B.8})$$

Using Equations (B.7) and (B.8), and rearranging Equation (B.6) it can be written that:

$$\frac{1}{U_o A_{so}} = \frac{1}{C_i Re_i^{0.8} Pr_i^{\frac{1}{3}} \left( \frac{k_i A_{si}}{D_i} \right) \left( \frac{\mu_i}{\mu_{wi}} \right)_j^{0.14}} + r_{cond} \frac{1}{C_o Re_{D_h}^P Pr_o^{\frac{1}{3}} \left( \frac{k_o A_{so}}{D_h} \right) \left( \frac{\mu_o}{\mu_{wo}} \right)_j^{0.14}} \quad (\text{B.9})$$

Equation (B.9) is linear with respect to the Sieder Tate constants  $C_i$  and  $C_o$ , and nonlinear with respect to  $P$ . This represents a nonlinear regression model, and it is thus possible to analyze using the method of least squares. The method of least squares will require minimizing the sum of the squares of the deviations between the measured dependant variable (left-hand side of Equation (B.9)) and the fitted variable (right-hand side of Equation (B.9)). The sum of the squares is defined as:

$$S = \sum_{j=1}^n \left[ \left( \frac{1}{U_o A_{so}} \right) - \left( \frac{1}{C_i \phi_j \left( \frac{\mu_i}{\mu_{wi}} \right)_j^{0.14}} \right) - r_{cond} - \left( \frac{1}{C_o Re_{D_h}^P \psi_j \left( \frac{\mu_o}{\mu_{wo}} \right)_j^{0.14}} \right) \right]^2 \quad (\text{B.10})$$

Where  $j$  represents the  $j$ th data point and  $n$  the total number of data points. To simplify the formulation, terms of Equation (B.9) for the inner tube and annulus are grouped together into  $\phi$  and  $\psi$  respectively:

$$\phi = Re_i^{0.8} Pr_i^{\frac{1}{3}} \left( \frac{k_i A_{si}}{D_i} \right) \quad (\text{B.11})$$

$$\psi = Pr_o^{\frac{1}{3}} \left( \frac{k_o A_{so}}{D_h} \right) \quad (\text{B.12})$$

The inner tube wall thermal resistance  $r_{cond}$  is assumed negligible ( $r_{cond} \approx 0$ ). To minimize Equation (B.10) the partial derivatives of  $S$  with respect to the unknowns  $C_i$ ,  $C_o$  and  $P$  are taken and equated to zero. The resulting equations simplify to the normal Equations (B.13), (B.14) and (B.15).



$$\frac{\partial S}{\partial C_i} : \sum_{j=1}^n \frac{\overbrace{\left(\frac{1}{U_o A_{so}}\right)_j}^{b1}}{\phi_j \left(\frac{\mu_i}{\mu_{wi}}\right)_j^{0.14}} = \frac{1}{C_i} \sum_{j=1}^n \frac{\overbrace{1}^{a1}}{\phi_j^2 \left(\frac{\mu_i}{\mu_{wi}}\right)_j^{0.28}} + \frac{1}{C_o} \sum_{j=1}^n \frac{\overbrace{1}^{a2}}{\psi_j \phi_j Re_{Dh,j}^P \left(\frac{\mu_o}{\mu_{wo}}\right)_j^{0.14} \left(\frac{\mu_i}{\mu_{wi}}\right)_j^{0.14}} \quad (B.13)$$

$$\begin{aligned} \frac{\partial S}{\partial C_o} : \sum_{j=1}^n \frac{\overbrace{\left(\frac{1}{U_o A_{so}}\right)_j}^{b2}}{Re_{Dh,j}^P \psi_j \left(\frac{\mu_o}{\mu_{wo}}\right)_j^{0.14}} \\ = \frac{1}{C_i} \sum_{j=1}^n \frac{\overbrace{1}^{a3}}{\psi_j \phi_j Re_{Dh,j}^P \left(\frac{\mu_i}{\mu_{wi}}\right)_j^{0.14} \left(\frac{\mu_o}{\mu_{wo}}\right)_j^{0.14}} + \frac{1}{C_o} \sum_{j=1}^n \frac{\overbrace{1}^{a4}}{Re_{Dh,j}^{2P} \psi_j^2 \left(\frac{\mu_o}{\mu_{wo}}\right)_j^{0.28}} \end{aligned} \quad (B.14)$$

$$\begin{aligned} \frac{\partial S}{\partial P} : \sum_{j=1}^n \frac{\overbrace{\left(\frac{1}{U_o A_{so}}\right)_j \ln(Re_{Dh,j})}^{LHS}}{Re_{Dh,j}^P \psi_j \left(\frac{\mu_o}{\mu_{wo}}\right)_j^{0.14}} \\ = \frac{1}{C_i} \sum_{j=1}^n \frac{\overbrace{\ln(Re_{Dh,j})}^{RHS}}{\psi_j \phi_j Re_{Dh,j}^P \left(\frac{\mu_i}{\mu_{wi}}\right)_j^{0.14} \left(\frac{\mu_o}{\mu_{wo}}\right)_j^{0.14}} + \frac{1}{C_o} \sum_{j=1}^n \frac{\overbrace{\ln(Re_{Dh,j})}^{RHS}}{Re_{Dh,j}^{2P} \psi_j^2 \left(\frac{\mu_o}{\mu_{wo}}\right)_j^{0.28}} \end{aligned} \quad (B.15)$$

Equation (B.13) and (B.14) are nonlinear and can be solved numerically. Khartabil and Christensen (1992) noted that these equations are linear with respect to  $C_i$  and  $C_o$  and nonlinear with respect to  $P$ .  $C_i$  and  $C_o$  are solved using Gauss elimination for an assumed value of  $P$ .

The Gauss elimination is performed by setting up the matrices as follows:

$$\begin{bmatrix} [B] \\ b1 \\ b2 \end{bmatrix} = \begin{bmatrix} [A] \\ a1 & a2 \\ a3 & a4 \end{bmatrix} \begin{bmatrix} [C] \\ 1 \\ C_i \\ 1 \\ C_o \end{bmatrix} \quad (\text{B.16})$$

With the components of  $[A]$  and  $[B]$  available, the process of Gauss elimination is then used to solve for matrix  $[C]$ . Equation (B.15) can be solved numerically by defining Equation (B.17), where  $LHS$  and  $RHS$  are the left and right hand sides of Equation (B.15), and substituting in the calculated  $C_i$  and  $C_o$  values:

$$f(P) = LHS - RHS \quad (\text{B.17})$$

If a solution exists for  $P$ , the function ( $f(P)$ ) will intersect the x-axis ( $f(P) = 0$ ), it is at this point that the solution to the set of equations exists. To obtain the solution for  $P$  various numerical methods can be used; in this instance the bisection method was used. The convergence criterion for the bisection method is  $f(P) \leq 1e^{-12}$ .

To initiate the nonlinear regression it was assumed that the inner wall temperature was equal to the mean temperature of the inner tube fluid, and the outer wall temperature equal to the mean fluid temperature of the annulus or  $T_{wi} = T_{bi}$  and  $T_{wo} = T_{bo}$ . This implies that  $\mu_{wi} = \mu_i$  and  $\mu_{wo} = \mu_o$ . After the first iteration it is possible to calculate both the inner and outer wall temperatures and therefore the wall viscosities ( $\mu_{wi}$  and  $\mu_{wo}$ ). The method employed to calculate the wall temperatures is outlined below:

With the value of  $C_i$  obtained from Gauss elimination it is possible to calculate  $h_i$  using Equation (B.7). The inner wall temperature for a heated annulus is then calculated using:

$$T_{wi} = T_{bi} - \frac{\dot{Q}_i}{h_i A_{si}} \quad (\text{B.18})$$

For a cooled annulus the inner wall is calculated with:

$$T_{wi} = T_{bi} + \frac{\dot{Q}_i}{h_i A_{si}} \quad (\text{B.19})$$

The outer wall temperature is now calculated using:

$$T_{wo} = T_{wi} - \Delta T_w \quad (\text{B.20})$$

Where the temperature difference across the wall  $\Delta T_w$  is given as:

$$\Delta T_w = -\bar{Q} \left( \frac{\ln \left( \frac{D_1}{D_i} \right)}{2\pi k_{cu} L_{hx}} \right) \quad (\text{B.21})$$

## B.2.2 Non Linear Regression Analysis performed on Experimental Data

The method of Khartabil and Christensen (1992) was performed on the set of data obtained from the four heat exchangers. In Figure B.1 to Figure B.8, the plots of  $f(P)$  are provided as well as the convergence of  $f(P)$  showing the number of iterations using the bisection method. The experimentally measured wall temperatures are compared to those predicted by the nonlinear regression analysis.

Table B.1 provides the coefficients  $C_i$ ,  $C_o$ , and  $P$  obtained from the nonlinear regression analysis for all the heat exchangers for both heating and cooling of the annulus.

Table B.1: Coefficients  $C_i$ ,  $C_o$  and  $P$  used in the Sieder and Tate type equation for the annulus.

Annular diameter ratio(a)	Cooling			Heating		
	$C_i$	$C_o$	$P$	$C_i$	$C_o$	$P$
<b>0.48</b>	0.029	0.015	0.866	0.027	0.008	0.939
<b>0.58</b>	0.027	0.009	0.908	0.024	0.007	0.941
<b>0.59</b>	0.027	0.008	0.919	0.028	0.004	1.002
<b>0.71</b>	0.027	0.006	0.943	0.026	0.003	1.013

### B.2.2.1 Annular Diameter Ratio 0.482

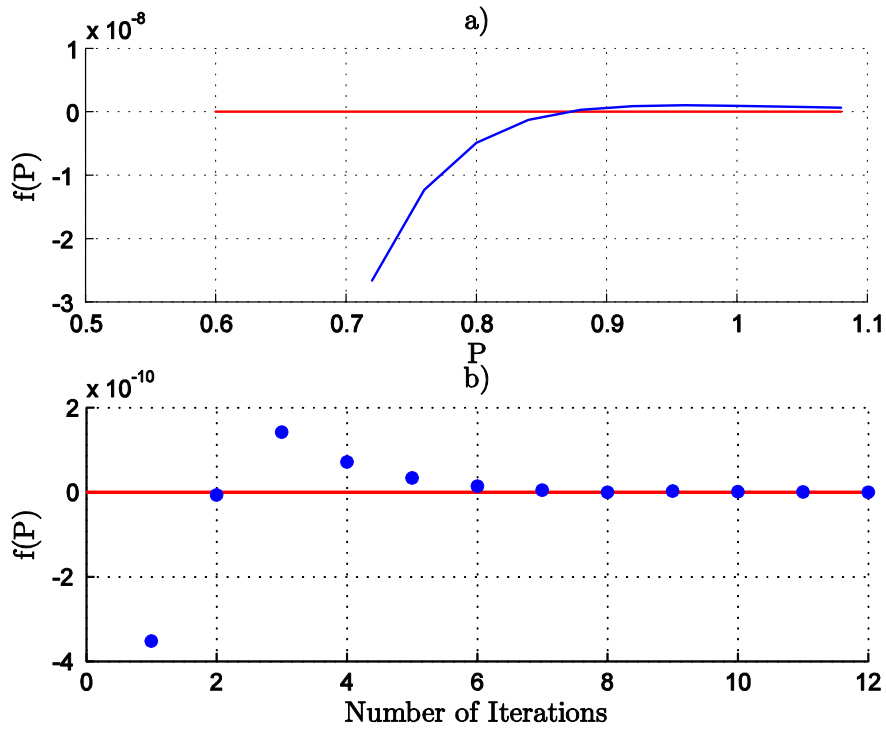


Figure B.1: a) Plot of  $f(P)$  showing the area of interest where  $f(P) = 0$ , as well as b) the convergence obtained using the bisection method for cooling of the annulus (annular diameter ratio 0.482).

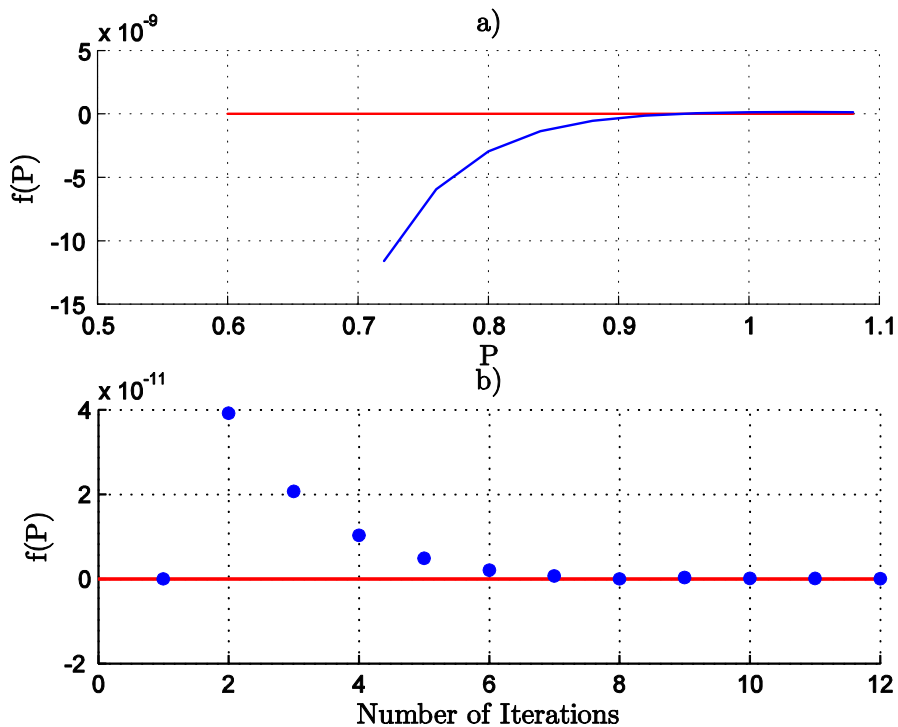


Figure B.2: a) Plot of  $f(P)$  showing the area of interest where  $f(P) = 0$ , as well as b) the convergence obtained using the bisection method for heating of the annulus (annular diameter ratio 0.482).

### B.2.2.2 Annular Diameter Ratio 0.579

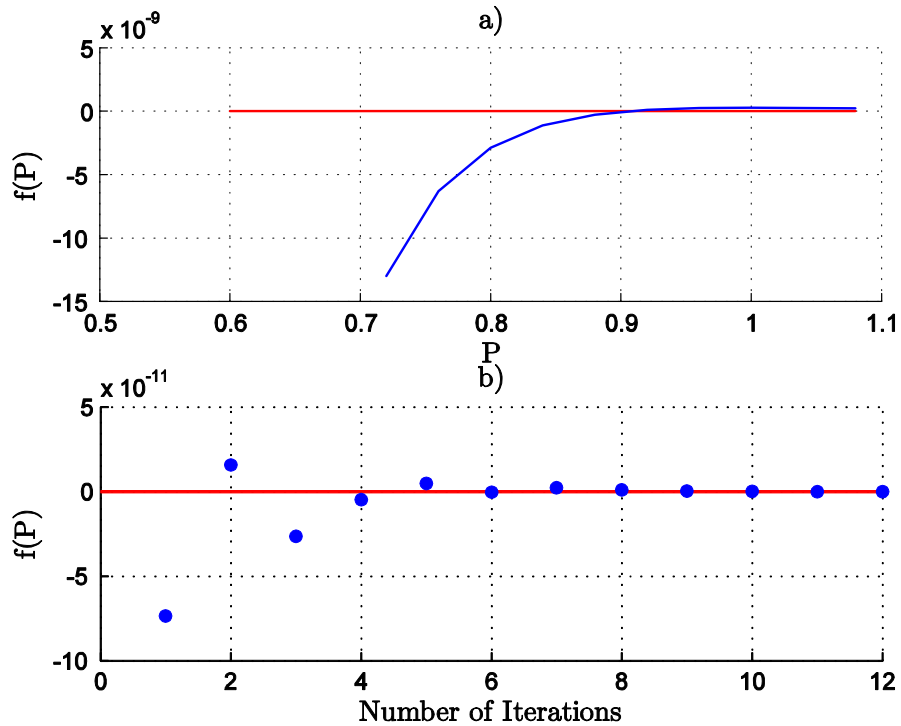


Figure B.3: a) Plot of  $f(P)$  showing the area of interest where  $f(P) = 0$ , as well as b) the convergence obtained using the bisection method for cooling of the annulus (annular diameter ratio 0.579).

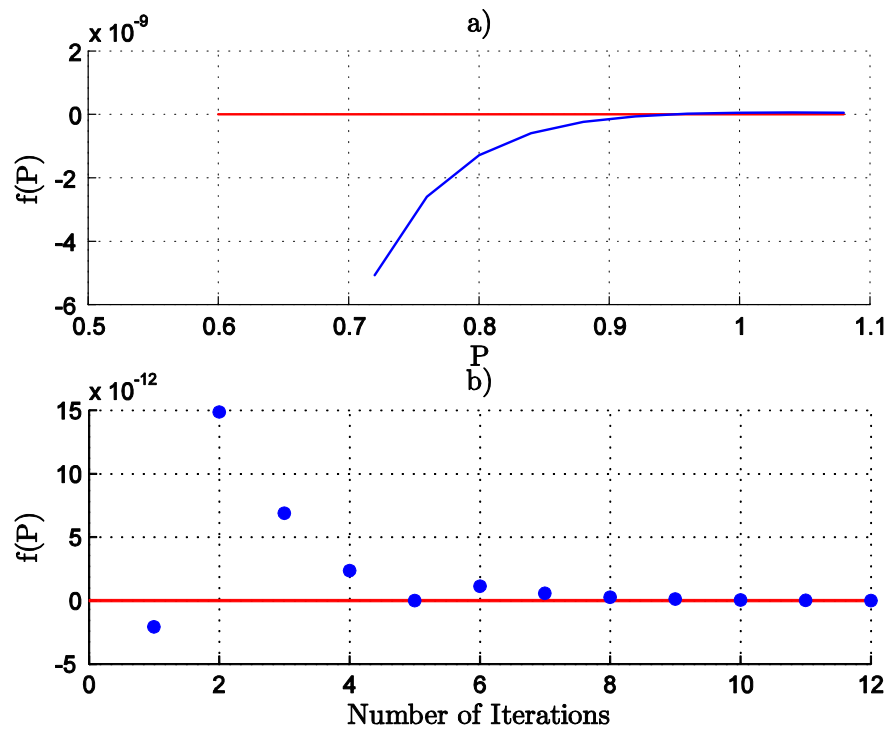


Figure B.4: a) Plot of  $f(P)$  showing the area of interest where  $f(P) = 0$ , as well as b) the convergence obtained using the bisection method for heating of the annulus (annular diameter ratio 0.579).

### B.2.2.3 Annular Diameter Ratio 0.593

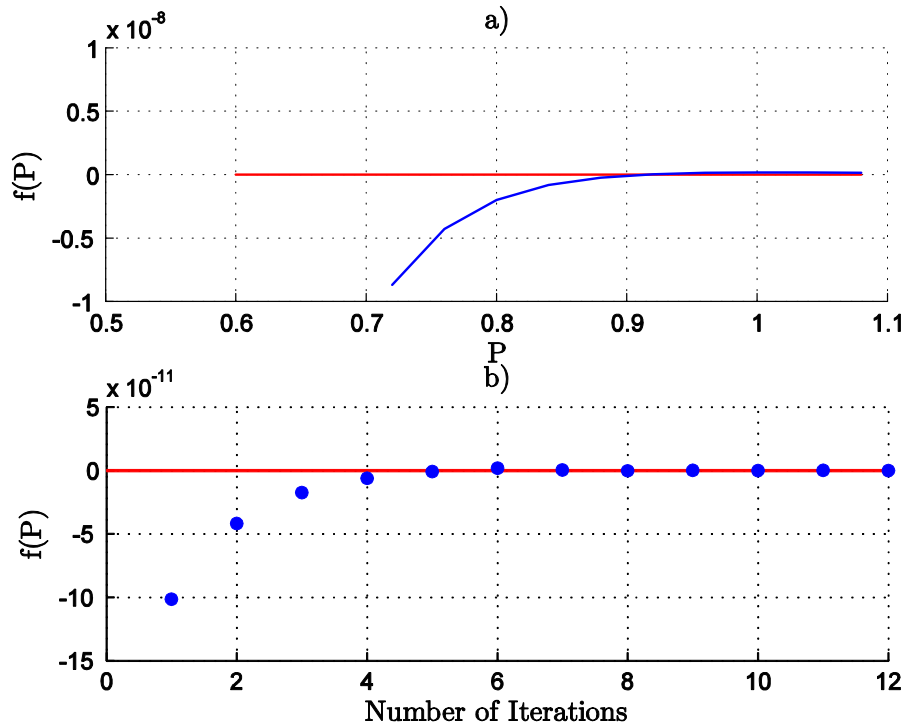


Figure B.5: a) Plot of  $f(P)$  showing the area of interest where  $f(P) = 0$ , as well as b) the convergence obtained using the bisection method for cooling of the annulus (annular diameter ratio 0.593).

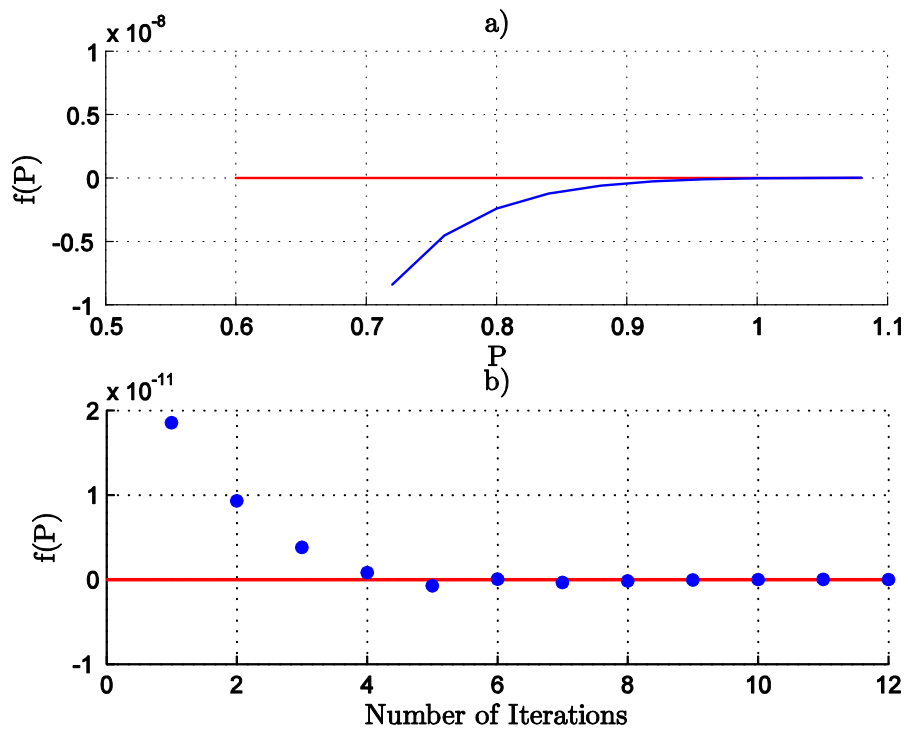


Figure B.6: a) Plot of  $f(P)$  showing the area of interest where  $f(P) = 0$ , as well as b) the convergence obtained using the bisection method for heating of the annulus (annular diameter ratio 0.593).

### B.2.2.4 Annular Diameter Ratio 0.712

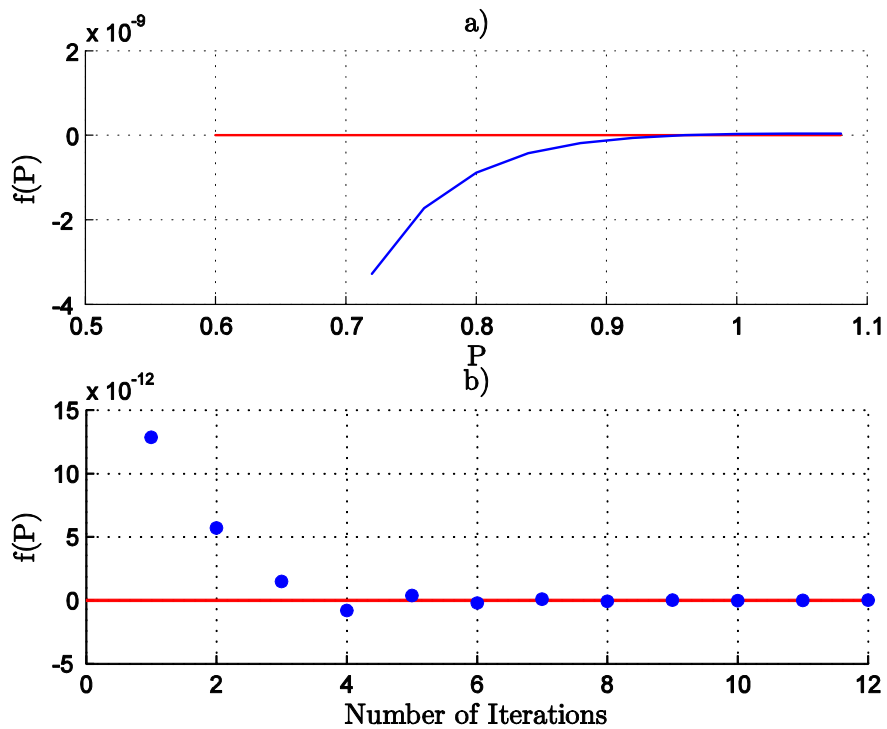


Figure B.7: a) Plot of  $f(P)$  showing the area of interest where  $f(P) = 0$ , as well as b) the convergence obtained using the bisection method for cooling of the annulus (annular diameter ratio 0.712).

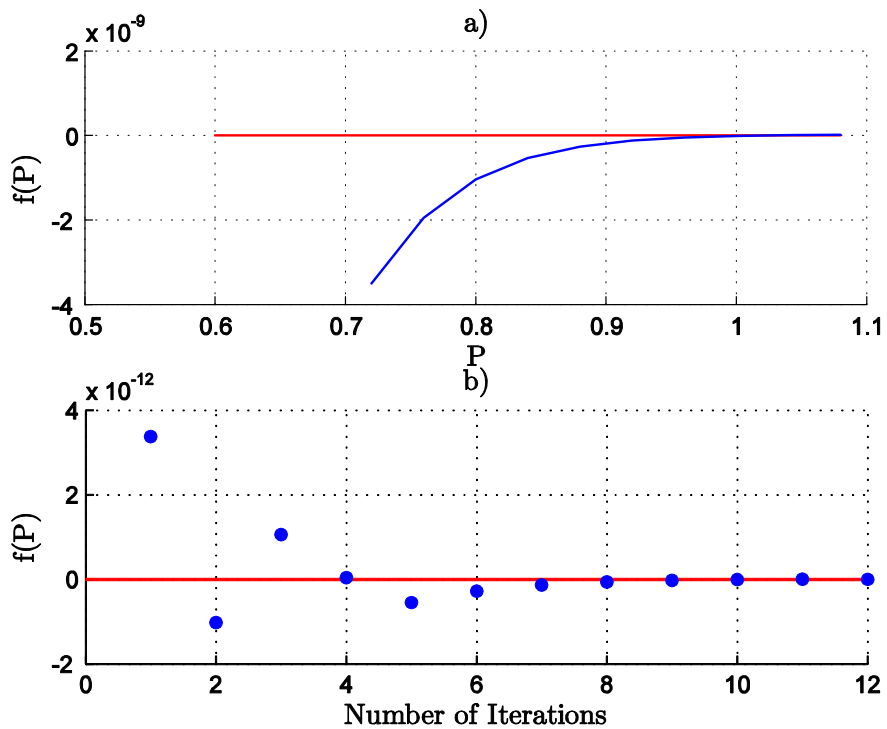


Figure B.8: a) Plot of  $f(P)$  showing the area of interest where  $f(P) = 0$ , as well as b) the convergence obtained using the bisection method for heating of the annulus (annular diameter ratio 0.712).

### B.3 Comparison of Khartabil and Christensen Wall Temperatures to Measured Wall Temperatures.

The method of Khartabil and Christensen predicts both the inner tubes inner wall and outer wall temperatures. These temperatures are compared to the experimentally measured wall temperatures averaged across the heat exchanger length. Percentage errors for all the annular diameter ratios and heat exchanger configuration are provided in the proceeding section.

Equation (B.22) shows the temperature difference of the experimentally measured wall temperatures and the average of the outer and inner wall temperatures predicted by the method of Khartabil and Christensen (1992).

$$T_{diff} = \bar{T}_w - \left( \frac{T_{wi,kc} + T_{wo,kc}}{2} \right) \quad (\text{B.22})$$

Table B.2 provides the mean temperature difference for all four annular ratios and for both a heated and cooled annulus.

**Table B.2: Mean temperature difference of measured temperatures and those predicted by Khartabil and Christensen (1992).**

Annular diameter ratio(a)	Temperature difference (°C)	
	Cooling	Heating
<b>0.482</b>	3.053	-2.541
<b>0.579</b>	2.177	-1.341
<b>0.593</b>	1.797	-0.387
<b>0.712</b>	1.713	-0.578



### B.3.1 Annular Diameter Ratio 0.482

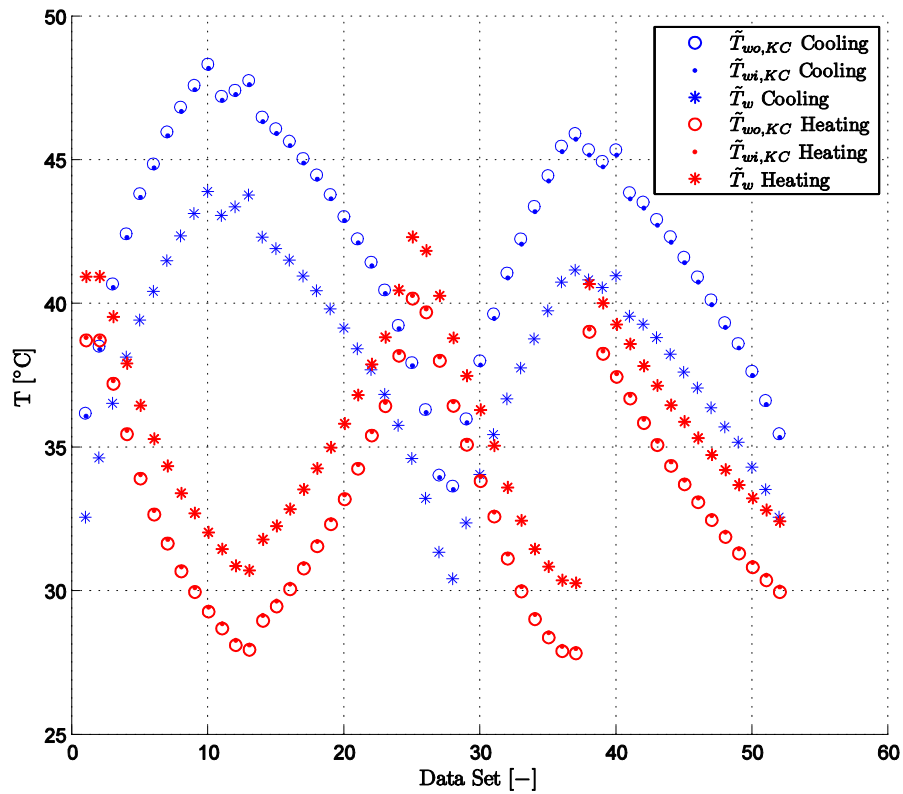


Figure B. 9: Comparison of averaged measured wall temperatures and wall temperatures predicted by the Khartabil and Christensen method (annular diameter ratio 0.482).

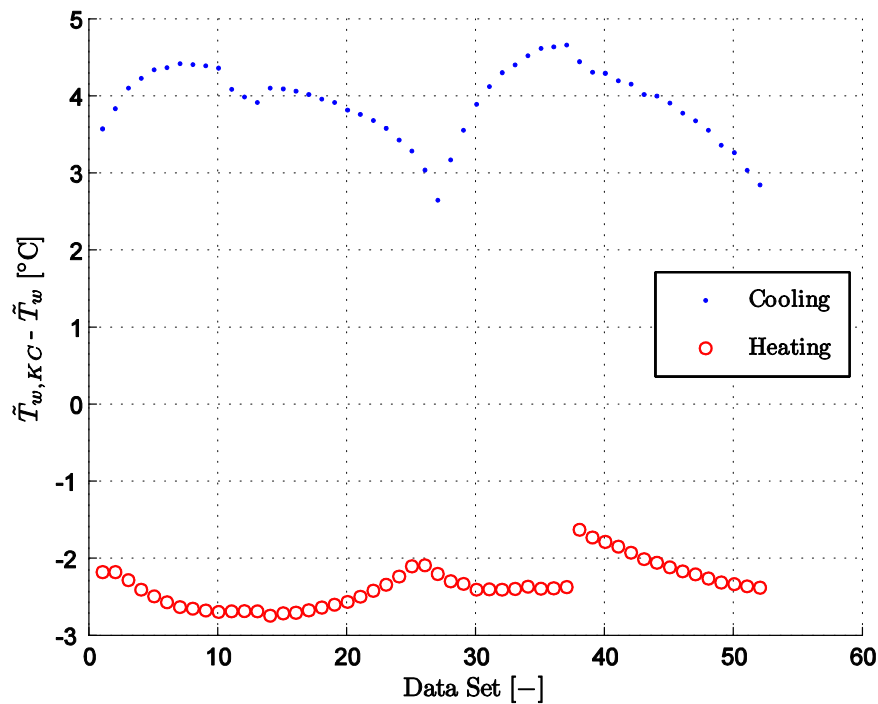


Figure B. 10: Errors of the wall temperatures predicted by the Khartabil and Christensen method compared to the averaged measured wall temperatures (annular diameter ratio 0.482).

### B.3.2 Annular Diameter Ratio 0.579

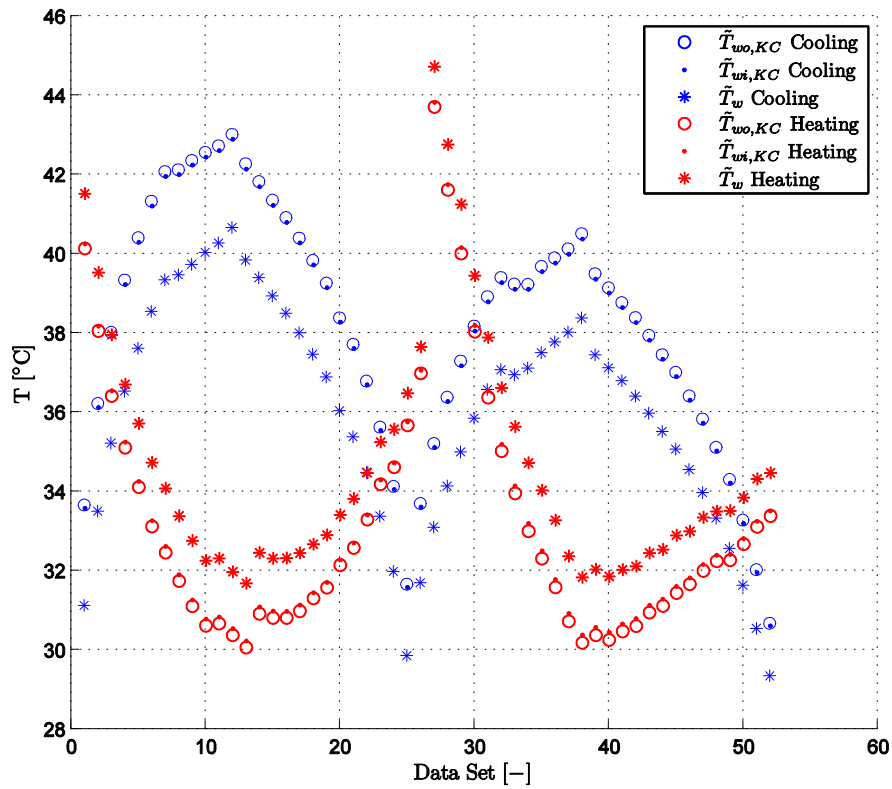


Figure B. 11: Comparison of averaged measured wall temperatures and wall temperatures predicted by the Khartabil and Christensen method (annular diameter ratio 0.579).

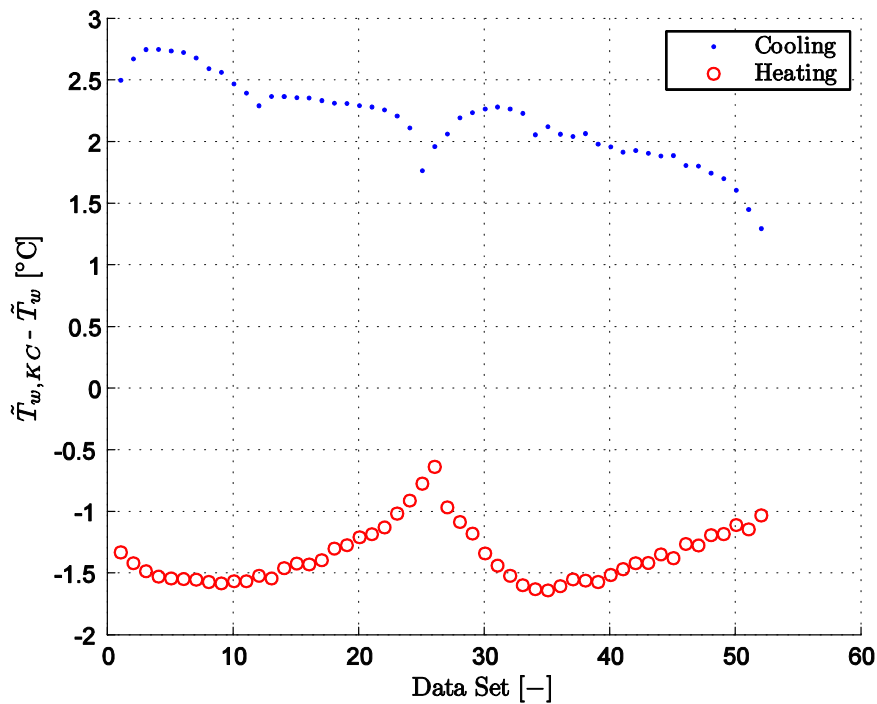


Figure B. 12: Errors of the wall temperatures predicted by the Khartabil and Christensen method compared to the averaged measured wall temperatures (annular diameter ratio 0.579).

### B.3.3 Annular Diameter Ratio 0.593

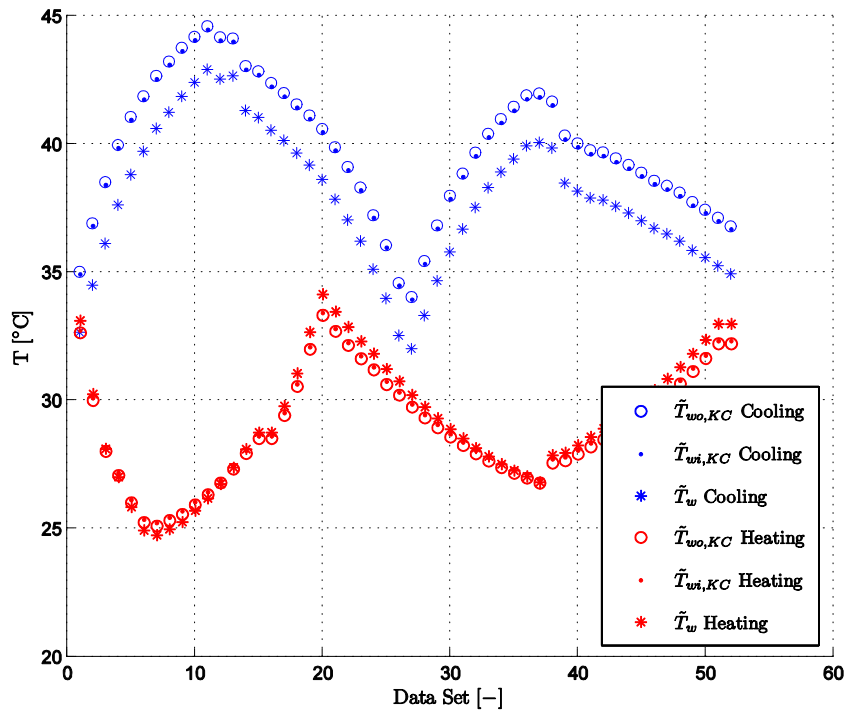


Figure B. 13: Comparison of averaged measured wall temperatures and wall temperatures predicted by the Khartabil and Christensen method (annular diameter ratio 0.593).

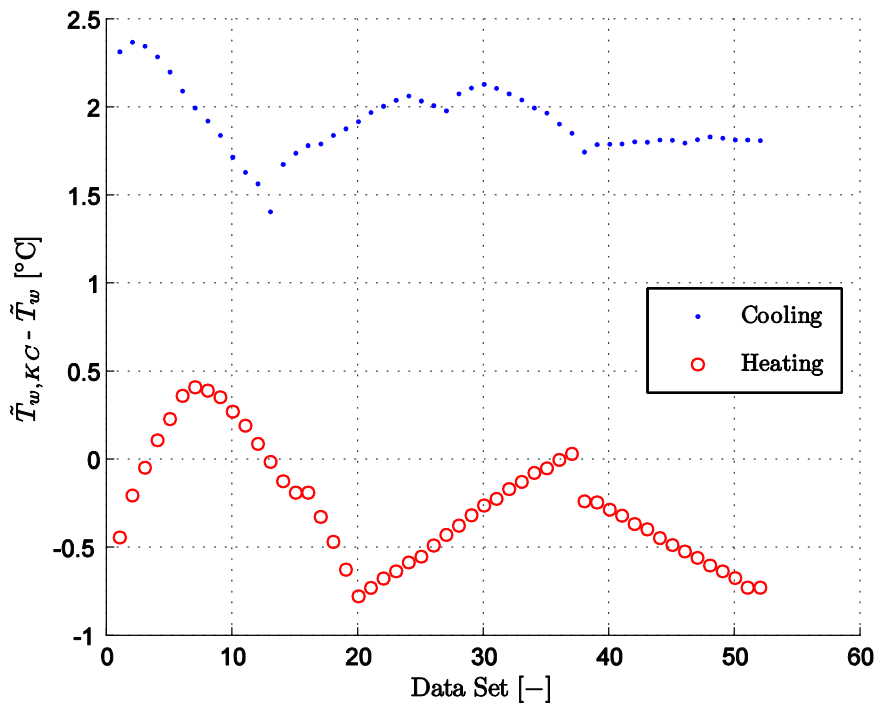


Figure B. 14: Errors of the wall temperatures predicted by the Khartabil and Christensen method compared to the averaged measured wall temperatures (annular diameter ratio 0.593).

### B.3.4 Annular Diameter Ratio 0.712

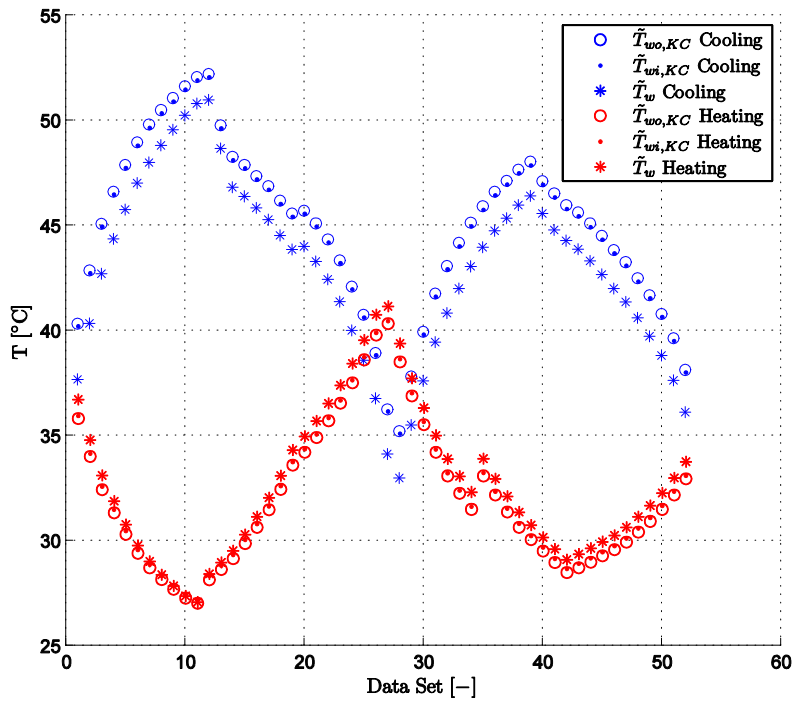


Figure B. 15: Comparison of averaged measured wall temperatures and wall temperatures predicted by the Khartabil and Christensen method (annular diameter ratio 0.712).

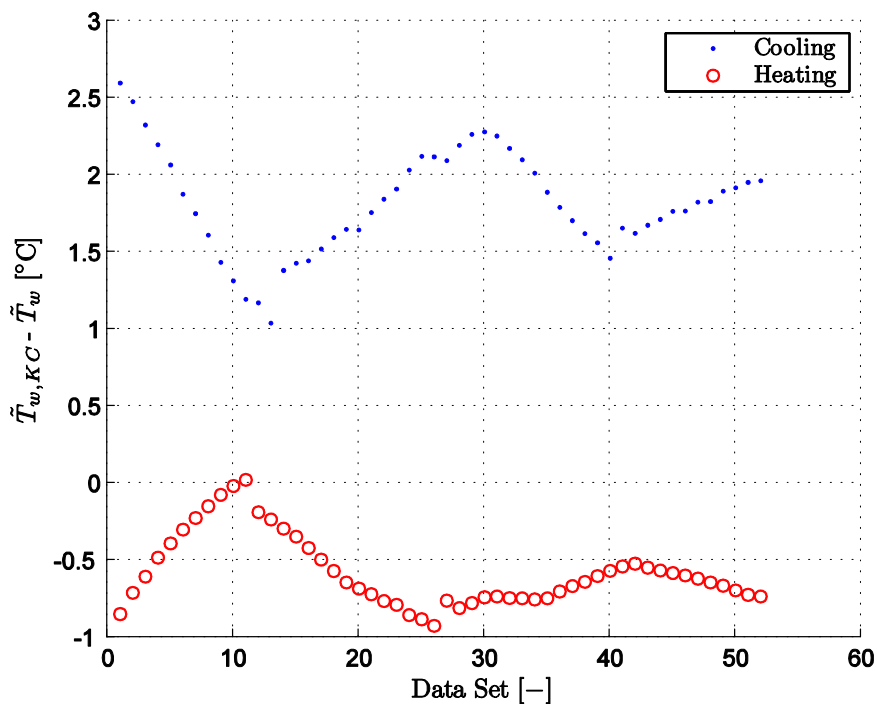


Figure B. 16: Errors of the wall temperatures predicted by the Khartabil and Christensen method compared to the averaged measured wall temperatures (annular diameter ratio 0.593).

## B.4 Heat Transfer Coefficient Analysis

As with the modified Wilson plot method, the accuracy of the heat transfer coefficient predicted by the Khartabil and Christensen (1992) method was investigated by calculating the heat transfer rate and comparing it to the heat transfer rate obtained from experimental methods. This method is explained below:

The overall heat transfer coefficient is obtained from:

$$U_{i,kc} = \frac{1}{1/h_{i,kc} + A_{si}/A_{so}h_{o,kc}} \quad (\text{B.23})$$

$$U_{o,kc} = \frac{1}{1/h_{o,kc} + A_{so}/A_{si}h_{i,kc}} \quad (\text{B.24})$$

The heat transfer to the inner tube and annulus is then:

$$\dot{Q}_{i,kc} = U_{i,kc}A_{si}\Delta T_{LMTD} \quad (\text{B.25})$$

$$\dot{Q}_{o,kc} = U_{o,kc}A_{so}\Delta T_{LMTD} \quad (\text{B.26})$$

The heat transfer calculated using experimental values for the inner tube and annulus is given as:

$$\dot{Q}_i = \dot{m}_i C p_i \Delta T_i \quad (\text{B.27})$$

$$\dot{Q}_o = \dot{m}_o C p_o \Delta T_o \quad (\text{B.28})$$

Where  $\Delta T_i = T_{ii} - T_{io}$  and  $\Delta T_o = T_{oi} - T_{oo}$ .  $\dot{Q}_{i,kc}$  and  $\dot{Q}_i$  for the inner tube; and  $\dot{Q}_{o,kc}$  and  $\dot{Q}_o$  for the annulus are compared to obtain the percentage error:

$$e_{i,kc} = \left| \frac{\dot{Q}_i - \dot{Q}_{i,kc}}{\dot{Q}_i} \right| \times 100 \quad (\text{B.29})$$

$$e_{o,kc} = \left| \frac{\dot{Q}_o - \dot{Q}_{o,kc}}{\dot{Q}_o} \right| \times 100 \quad (\text{B.30})$$

The heat transfer rate errors calculated from the Khartabil and Christensen (1992) heat transfer coefficients are shown in Figure B. 17 to Figure B. 20 for the four respective annular diameter ratios tested.

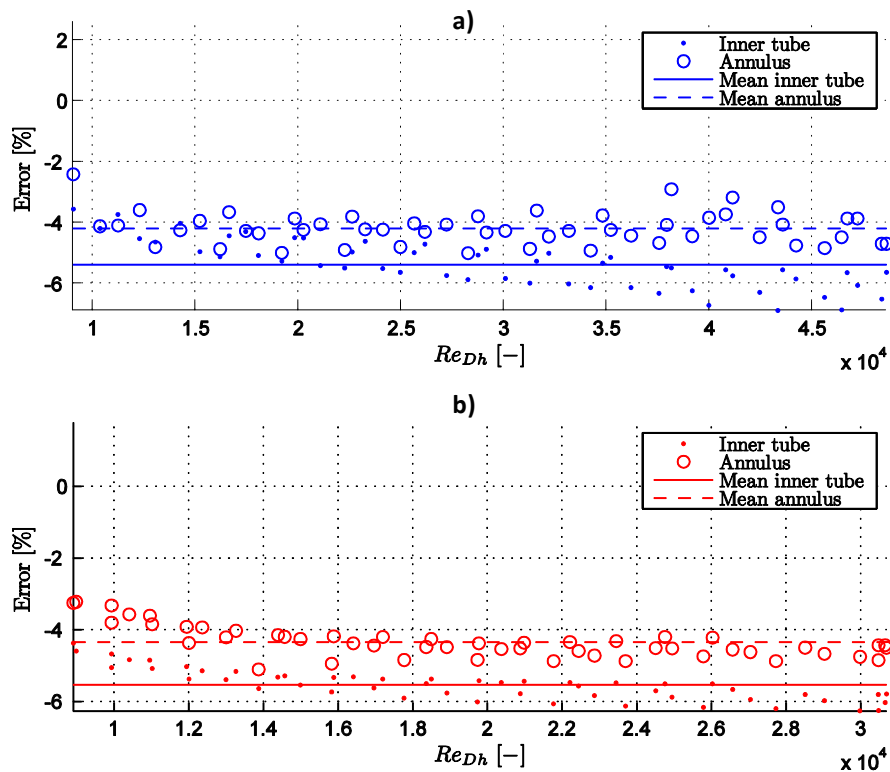


Figure B. 17: Errors for the rate of heat transfer rate predicted by the Khartabil and Christensen (1992) method for ar0.483 for a) cooled and b) heated annulus.

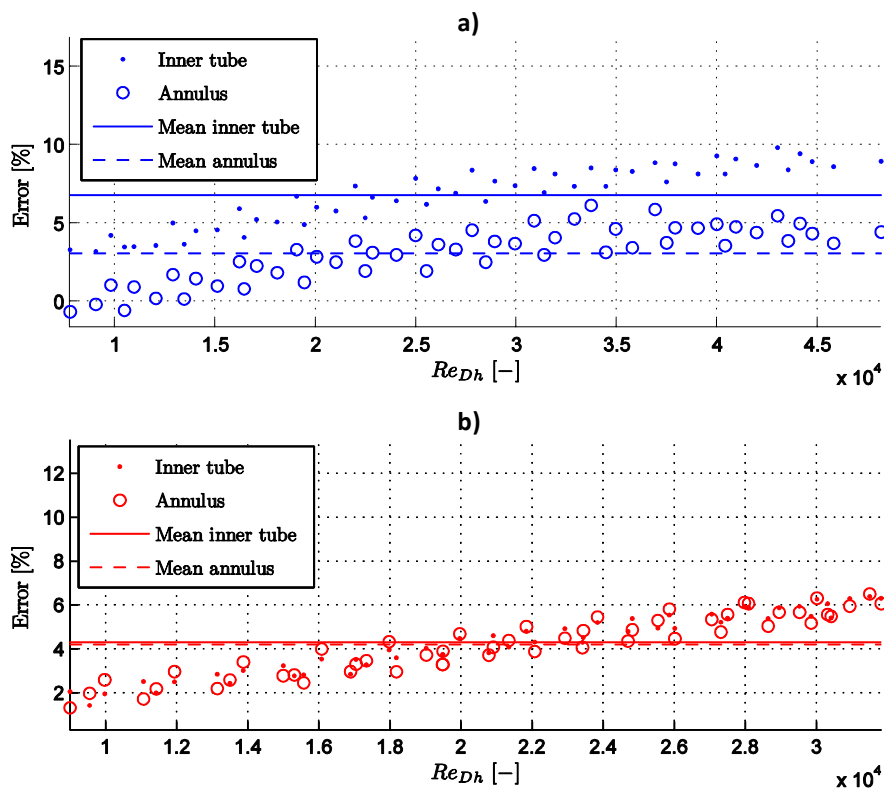


Figure B. 18: Errors for the rate of heat transfer rate predicted by the Khartabil and Christensen (1992) method for ar0.579 for a) cooled and b) heated annulus.

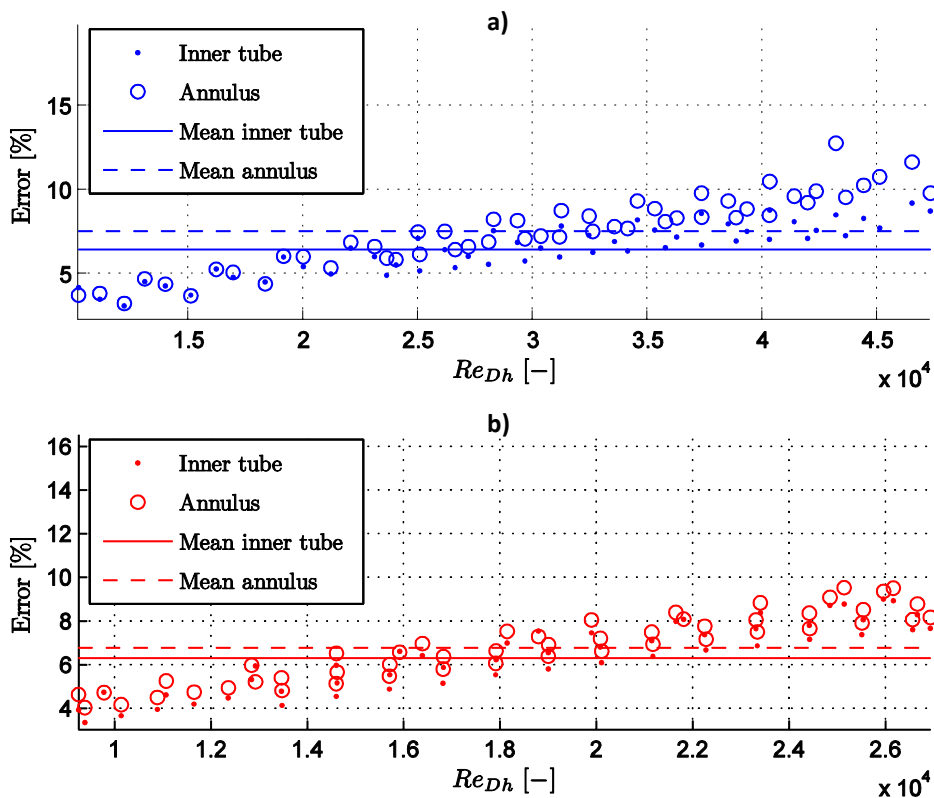


Figure B.19: Errors for the rate of heat transfer rate predicted by the Khartabil and Christensen (1992) method for ar 0.593 for a) cooled and b) heated annulus.

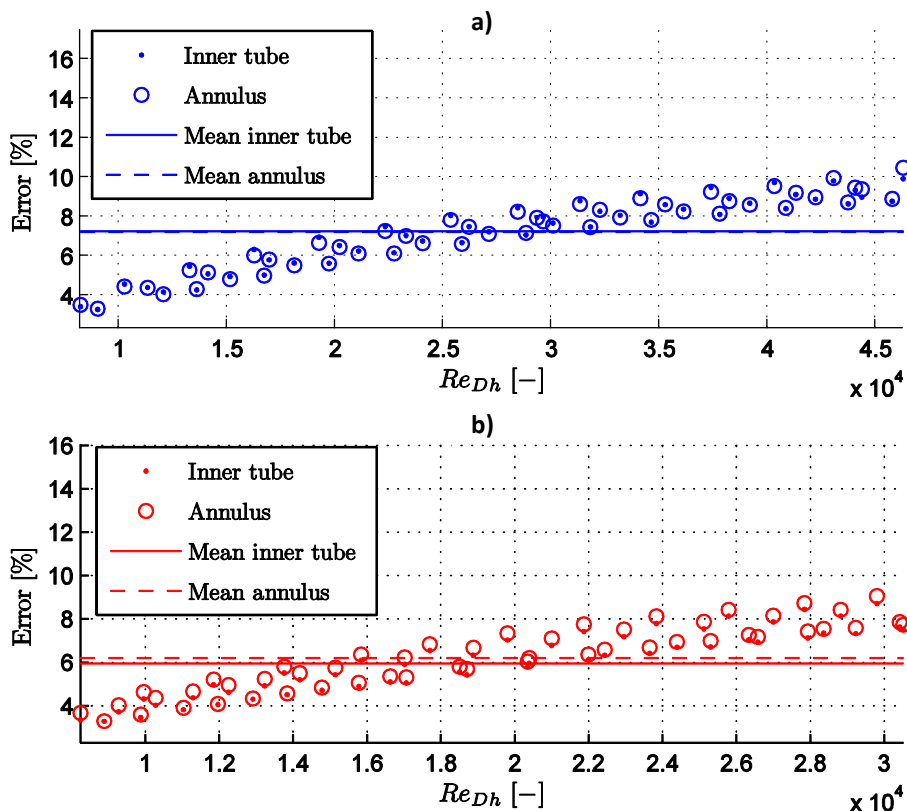


Figure B.20: Errors for the rate of heat transfer rate predicted by the Khartabil and Christensen (1992) method for ar 0.712 for a) cooled and b) heated annulus.

The mean errors for each annular diameter ratio and heating or cooling configuration for both the Inner tube and annulus are provided in Table B. 3.

**Table B. 3:** Mean errors for the heat transfer rate predicted by the Khartabil and Christensen (1992) method for all annular diameter ratios and heating or cooling configuration.

Annular diameter ratio(a)	$e_{i,KC}(\%)$		$e_{o,KC}(\%)$	
	Cooling	Heating	Cooling	Heating
<b>0.482</b>	-5.24	-5.32	-4.13	4.26
<b>0.579</b>	7.06	4.14	4.19	4.11
<b>0.593</b>	5.83	6.18	7.54	6.84
<b>0.712</b>	7.18	6.02	7.16	6.19

The Khartabil and Christensen method predicts heat transfer coefficients which produce mean errors with a maximum error of 12.25% for an annular diameter ratio of 0.593.



# Appendix C

## Test Section Results

### Contents

C.1 Introduction .....	C.1
C.2 Annular Diameter Ratio 0.482.....	C.1
C.2.1 Mean Heat Transfer .....	C.1
C.2.2 Local Heat Transfer .....	C.3
C.2.3 Friction Factor.....	C.6
C.2.4 Colburn j-factor.....	C.6
C.3 Annular Diameter Ratio 0.579.....	C.9
C.3.1 Mean Heat Transfer .....	C.9
C.3.2 Local Heat Transfer .....	C.11
C.3.3 Friction Factor.....	C.14
C.3.4 Colburn j-factor.....	C.14
C.4 Annular Diameter Ratio 0.712.....	C.17
C.4.1 Mean Heat Transfer .....	C.17
C.4.2 Local Heat Transfer .....	C.19
C.4.3 Friction Factor.....	C.22
C.4.4 Colburn j-factor.....	C.22
C.5 Energy Balances.....	C.25
C.6 Summary.....	C.25
C.6.1 Mean Heat Transfer .....	C.25
C.6.2 Friction Factors .....	C.26
C.7 Discussion.....	C.26

## List of Figures

Figure C.1: Inner tube and annulus Reynolds numbers for both a) cooled and b) heated annulus for an annular diameter ratio of 0.482. ....	C.1
Figure C.2: Mean Nusselt numbers calculated using three experimental methods compared to correlations available in the literature for a cooled annulus with annular diameter ratio of 0.482. ....	C.2
Figure C.3: Mean Nusselt numbers calculated using three experimental methods compared to correlations available in the literature for a heated annulus with annular diameter ratio of 0.482. ....	C.2
Figure C.4: Local LMTD Nusselt numbers for control volumes 1-9, compared to the mean LMTD Nusselt numbers and correlations of Dirker and Meyer (2004) and Gnielinski (2009) for a cooled annulus with annular diameter ratio of 0.483. ....	C.4
Figure C.5: Local LMTD Nusselt numbers for control volumes 1-9, compared to the mean LMTD Nusselt numbers and correlations of Dirker and Meyer (2004) and Gnielinski (2009) for a heated annulus with annular diameter ratio of 0.483. ....	C.5
Figure C.6: Diabatic friction factors for both a cooled and heated annulus compared to available correlations for an annular diameter ratio of 0.483. ....	C.6
Figure C.7: Nusselt numbers obtained from the modified Wilson plot method for a heated and cooled annulus. ....	C.7
Figure C.8: Friction factors and Colburn j-factors for a heated and cooled annulus. ....	C.7
Figure C.9: Colburn j-factors for a heated and cooled annulus with a polynomial curve fitted for an annular diameter ratio of 0.482. ....	C.8
Figure C.10: Inner tube and annulus Reynolds numbers for both a) cooled and b) heated annulus for an annular diameter ratio of 0.579. ....	C.9
Figure C.11: Mean Nusselt numbers calculated using three experimental methods compared to correlations available in the literature for a cooled annulus with annular diameter ratio of 0.579. ....	C.10
Figure C.12: Mean Nusselt numbers calculated using three experimental methods compared to correlations available in the literature for a heated annulus with annular diameter ratio of 0.579. ....	C.10
Figure C.13: Local LMTD Nusselt numbers for control volumes 1-9, compared to the mean LMTD Nusselt numbers and correlations of Dirker and Meyer (2004) and Gnielinski (2009) for a cooled annulus with annular diameter ratio of 0.579. ....	C.12
Figure C.14: Local LMTD Nusselt numbers for control volumes 1-9, compared to the mean LMTD Nusselt numbers and correlations of Dirker and Meyer (2004) and Gnielinski (2009) for a heated annulus with annular diameter ratio of 0.579. ....	C.13
Figure C.15: Diabatic friction factors for both a cooled and heated annulus compared to available correlations for an annular diameter ratio of 0.579. ....	C.14
Figure C.16: Nusselt numbers obtained from the modified Wilson plot method for a heated and cooled annulus. ....	C.15
Figure C.17: Friction factors and Colburn j-factors for a heated and cooled annulus. ....	C.15
Figure C.18: Colburn j-factors for a heated and cooled annulus with a polynomial curve fitted for an annular diameter ratio of 0.578. ....	C.16

Figure C.19: Inner tube and annulus Reynolds numbers for both a) cooled and b) heated annulus for an annular diameter ratio of 0.712 .....	C.17
Figure C.20: Mean Nusselt numbers calculated using three experimental methods compared to correlations available in the literature for a cooled annulus with annular diameter ratio of 0.712. ....	C.18
Figure C.21: Mean Nusselt numbers calculated using three experimental methods compared to correlations available in the literature for a heated annulus with annular diameter ratio of 0.712. ....	C.18
Figure C.22: Local LMTD Nusselt numbers for control volumes 1-9, compared to the mean LMTD Nusselt numbers and correlations of Dirker and Meyer (2004) and Gnielinski (2009) for a cooled annulus with annular diameter ratio of 0.712. ....	C.20
Figure C.23: Local LMTD Nusselt numbers for control volumes 1-9, compared to the mean LMTD Nusselt numbers and correlations of Dirker and Meyer (2004) and Gnielinski (2009) for a heated annulus with annular diameter ratio of 0.712. ....	C.21
Figure C.24: Diabatic friction factors for both a cooled and heated annulus compared to available correlations for an annular diameter ratio of 0.712.....	C.22
Figure C.25: Nusselt numbers obtained from the modified Wilson plot method for a heated and cooled annulus. ....	C.23
Figure C.26: Friction factors and Colburn j-factors for a heated and cooled annulus. ....	C.23
Figure C.27: Colburn j-factors for a heated and cooled annulus with a polynomial curve fitted for an annular diameter ratio of 0.712. ....	C.24

## List of Tables

Table C.1: Mean and maximum energy balances. ....	C.25
Table C.2: Averaged percentage differences for experimental mean Nusselt numbers and existing mean Nusselt number correlations. ....	C.26
Table C.4: Averaged percentage differences for experimental friction factors and existing correlations. ....	C.26

## Nomenclature

**Note:** The nomenclature used in the main text body is also used in this appendix.

## C.1 Introduction

The results presented in the main text are for a test section with annular diameter ratio 0.593. Three additional heat exchanger test sections with annular diameter ratios 0.482, 0.579 and 0.712 were also tested. The results include mean annulus heat transfer, local annulus heat transfer and annular friction factors. The dimensions of these heat exchanger test sections are provided in the main text. All calculations and methods used to obtain the respective results are provided in the main text.

## C.2 Annular Diameter Ratio 0.482

The range of inner and annulus Reynolds numbers tested for both a heated and cooled annulus are shown in Figure C.1.

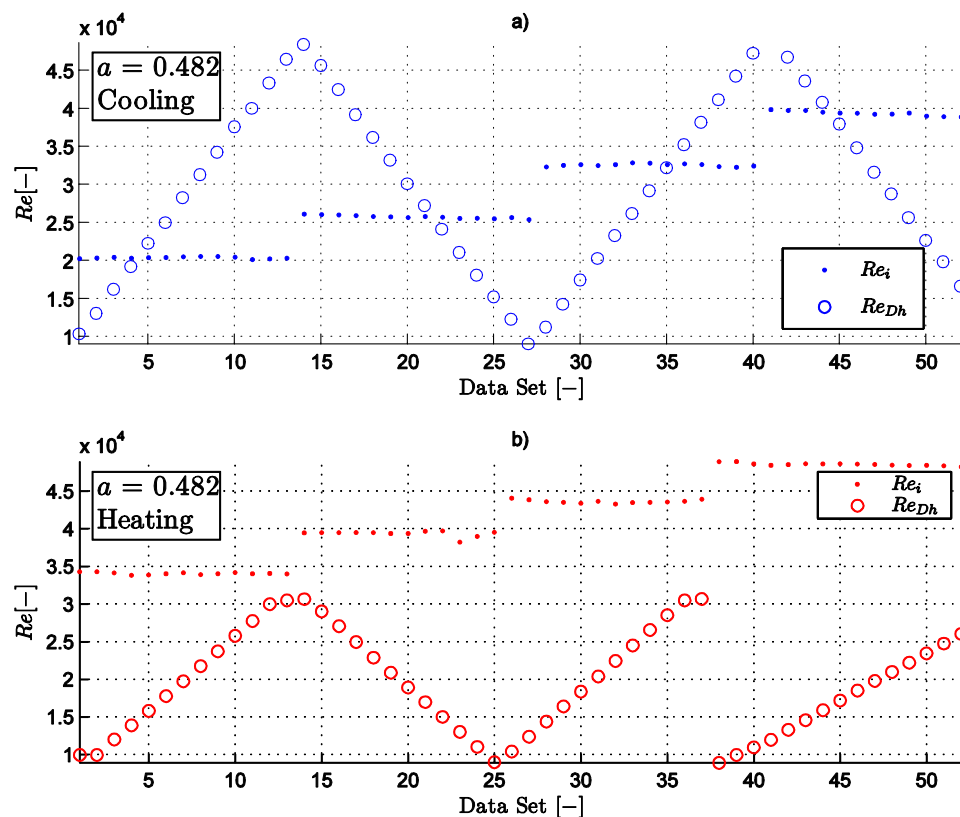


Figure C.1: Inner tube and annulus Reynolds numbers for both a) cooled and b) heated annulus for an annular diameter ratio of 0.482.

### C.2.1 Mean Heat Transfer

The mean heat transfer calculated using the mean LMTD method, modified Wilson plot method of Briggs and Young (1969) and the nonlinear regression method of Khartabil and Christensen (1992) are compared to mean heat transfer results predicted using available correlations in the literature. Figure C.2 and Figure C.3 are for a cooled and heated annulus respectively.

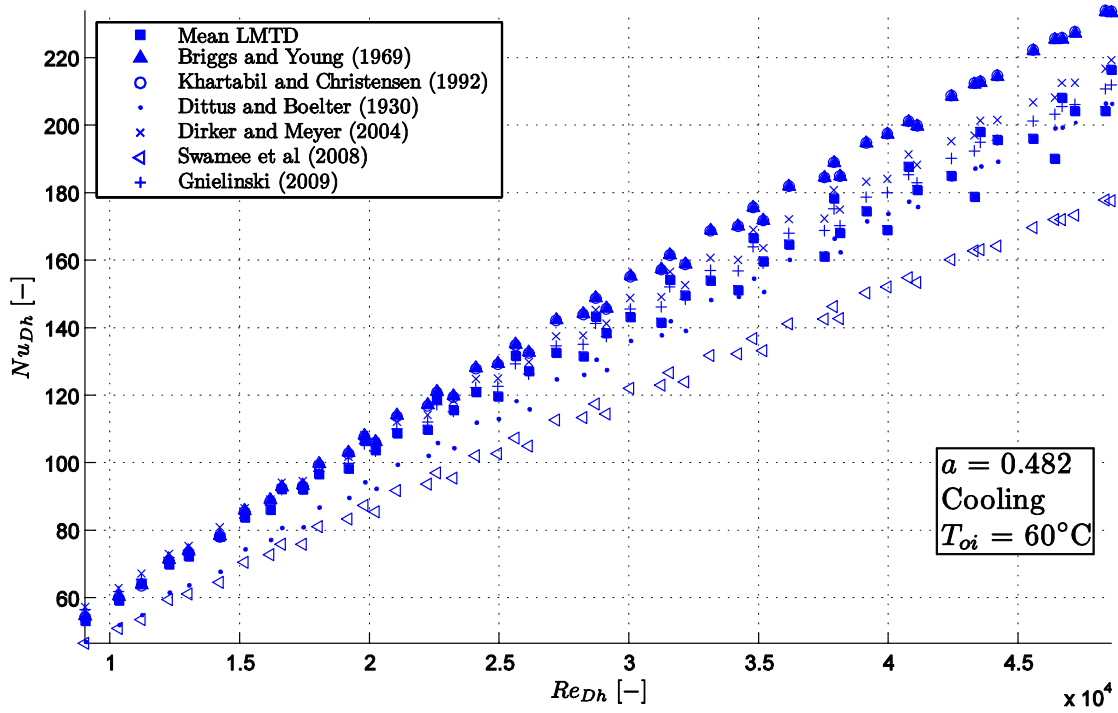


Figure C.2: Mean Nusselt numbers calculated using three experimental methods compared to correlations available in the literature for a cooled annulus with annular diameter ratio of 0.482.

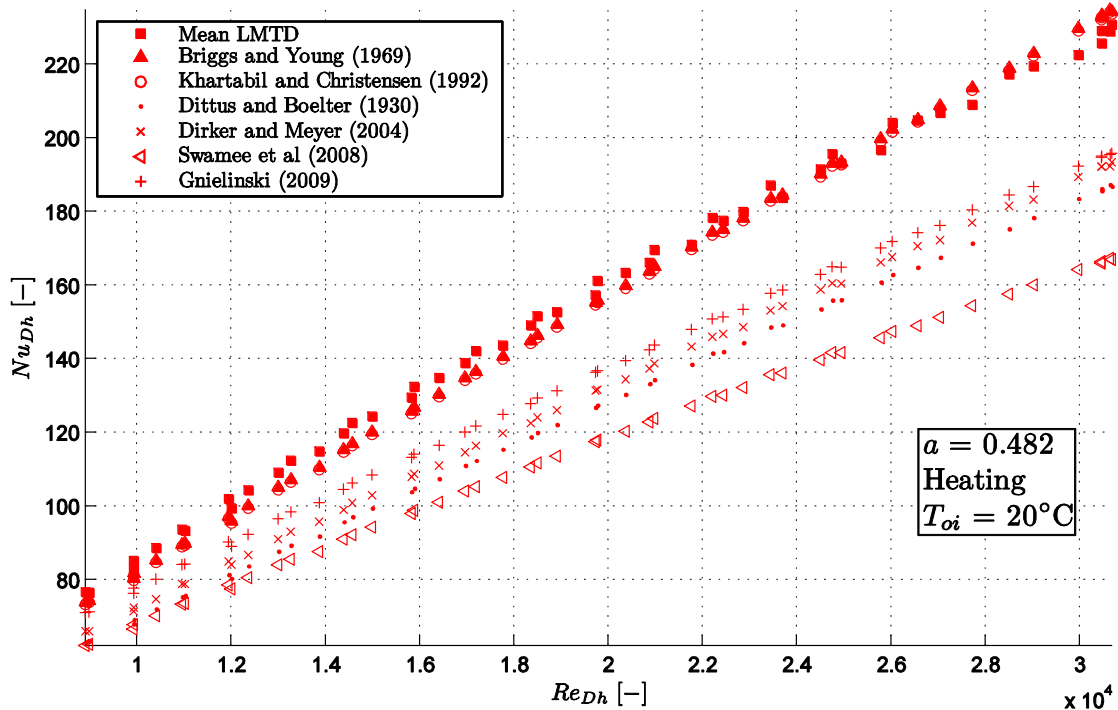


Figure C.3: Mean Nusselt numbers calculated using three experimental methods compared to correlations available in the literature for a heated annulus with annular diameter ratio of 0.482.

Observations on the mean Nusselt numbers are summarized at the end of Appendix C.

## C.2.2 Local Heat Transfer

The local heat transfer for each of the control volumes are compared to the mean LMTD method as well as the correlations of Dirker and Meyer (2004) and Gnielinski (2009). Figure C.4 and Figure C.5 are for a cooled and heated annulus respectively.

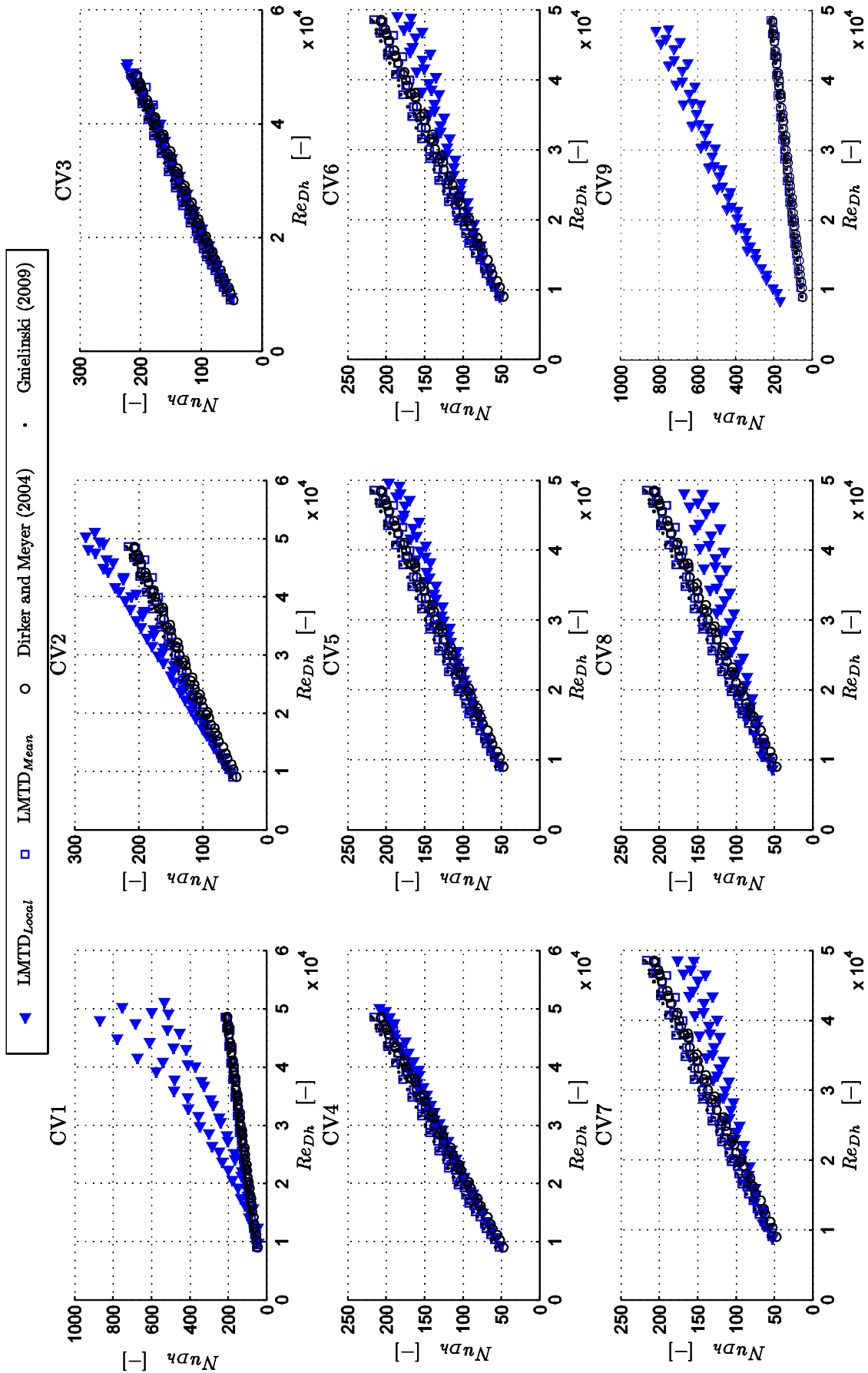


Figure C.4: Local LMTD Nusselt numbers for control volumes 1-9, compared to the mean LMTD Nusselt numbers and correlations of Dirker and Meyer (2004) and Gnielinski (2009) for a cooled annulus with annular diameter ratio of 0.483.

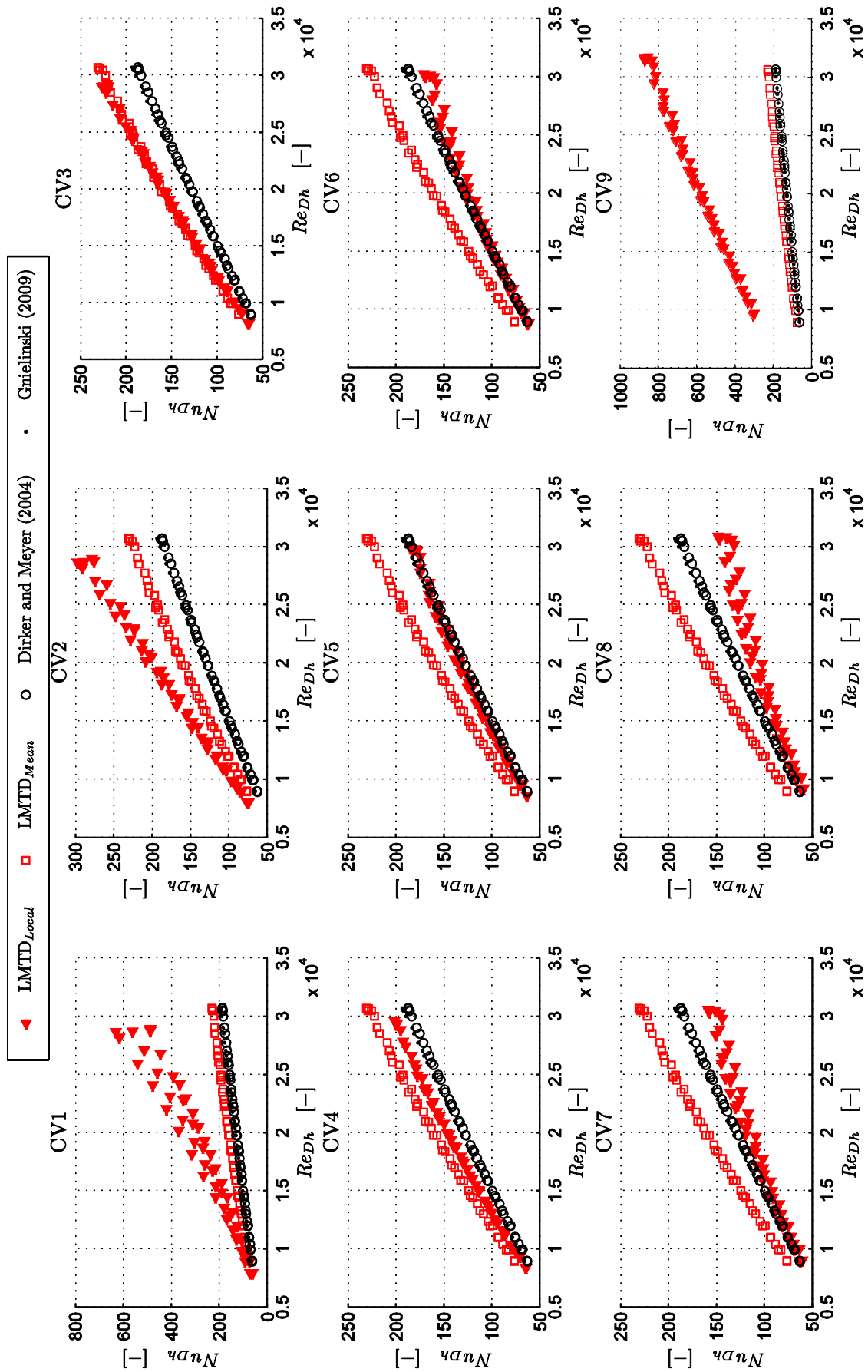


Figure C.5: Local LMTD Nusselt numbers for control volumes 1-9, compared to the mean LMTD Nusselt numbers and correlations of Dirker and Meyer (2004) and Gnielinski (2009) for a heated annulus with annular diameter ratio of 0.483.



### C.2.3 Friction Factor

The friction factors are compared to correlations available in the literature. Figure C.6 shows the friction factor results for both a heated and cooled annulus.

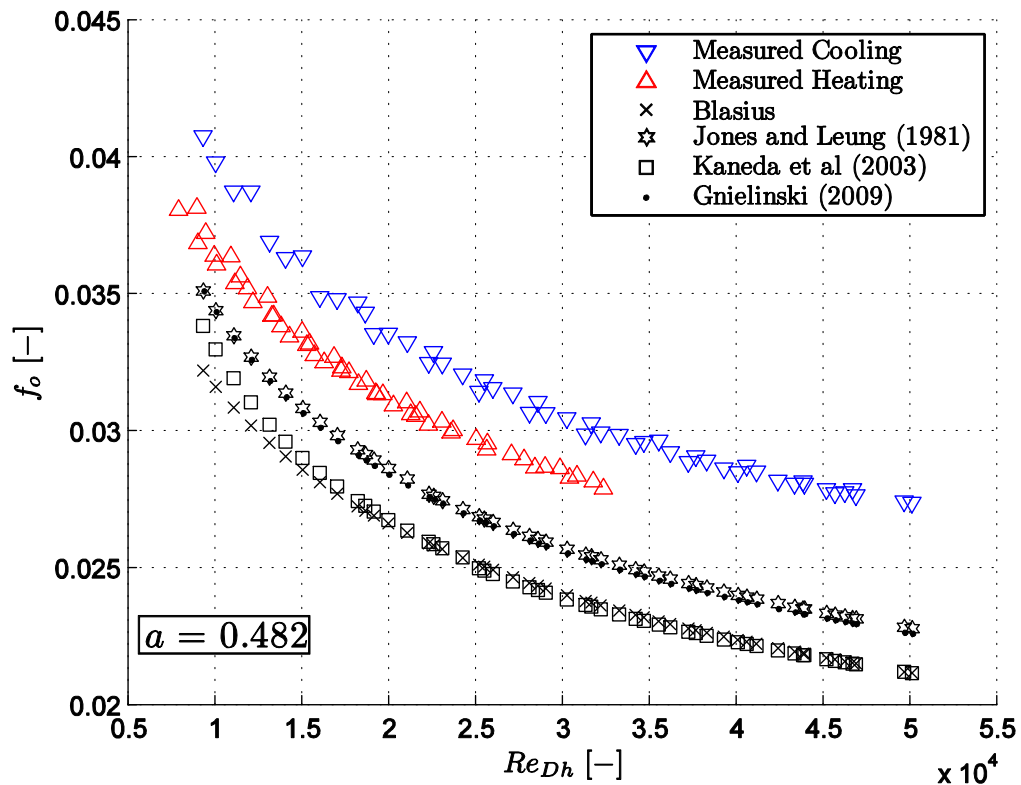


Figure C.6: Diabatic friction factors for both a cooled and heated annulus compared to available correlations for an annular diameter ratio of 0.483.

Observations on the friction factor are provided at the end of Appendix C.

### C.2.4 Colburn j-factor

The results obtained from the modified Wilson plot method for both a heated and cooled annulus are plotted on the same set of axis in Figure C.7.

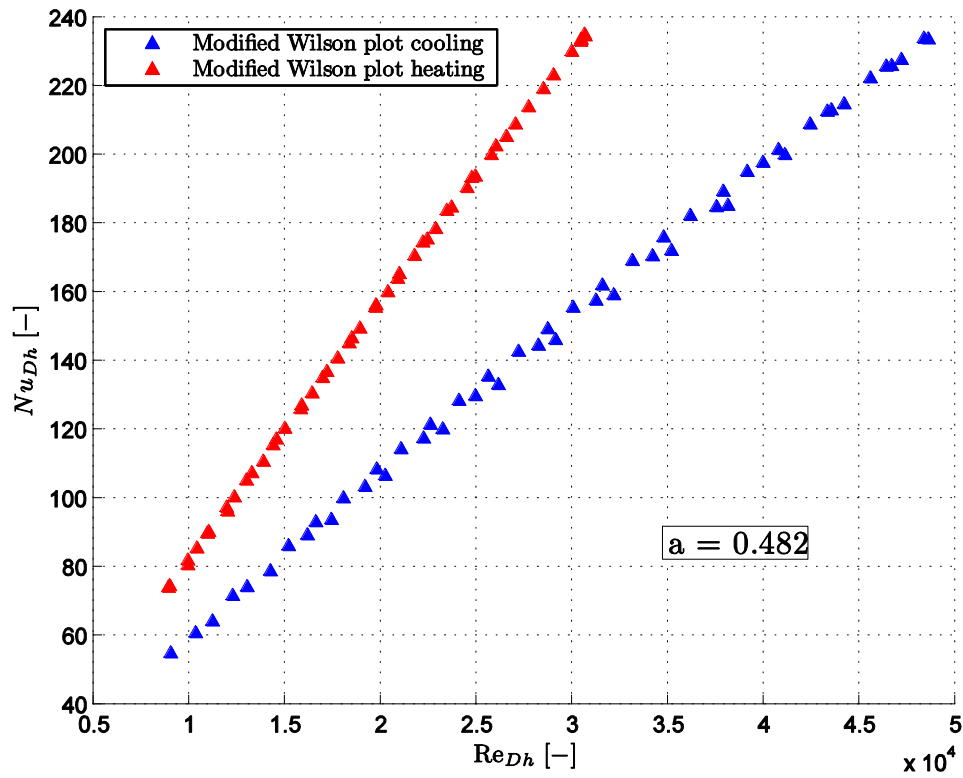


Figure C.7: Nusselt numbers obtained from the modified Wilson plot method for a heated and cooled annulus.

The friction factors and j-factors for a heated and cooled annulus are plotted in Figure C.8.

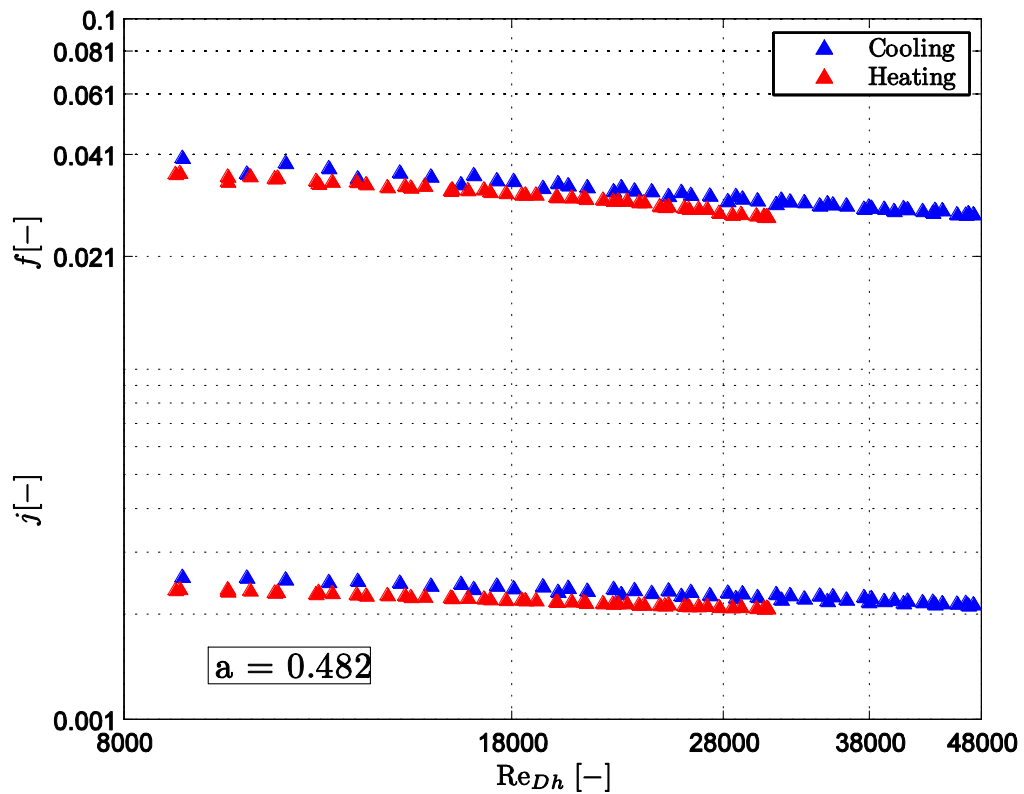


Figure C.8: Friction factors and Colburn j-factors for a heated and cooled annulus.

The Colburn  $j$ -factors obtained from the Nusselt numbers of the modified Wilson plot method are plotted in Figure C.9 for a heated and cooled annulus. A polynomial curve is fitted through the Colburn  $j$ -factors. The constants of the polynomial and description thereof are provided in the main text body in Section 5.8.

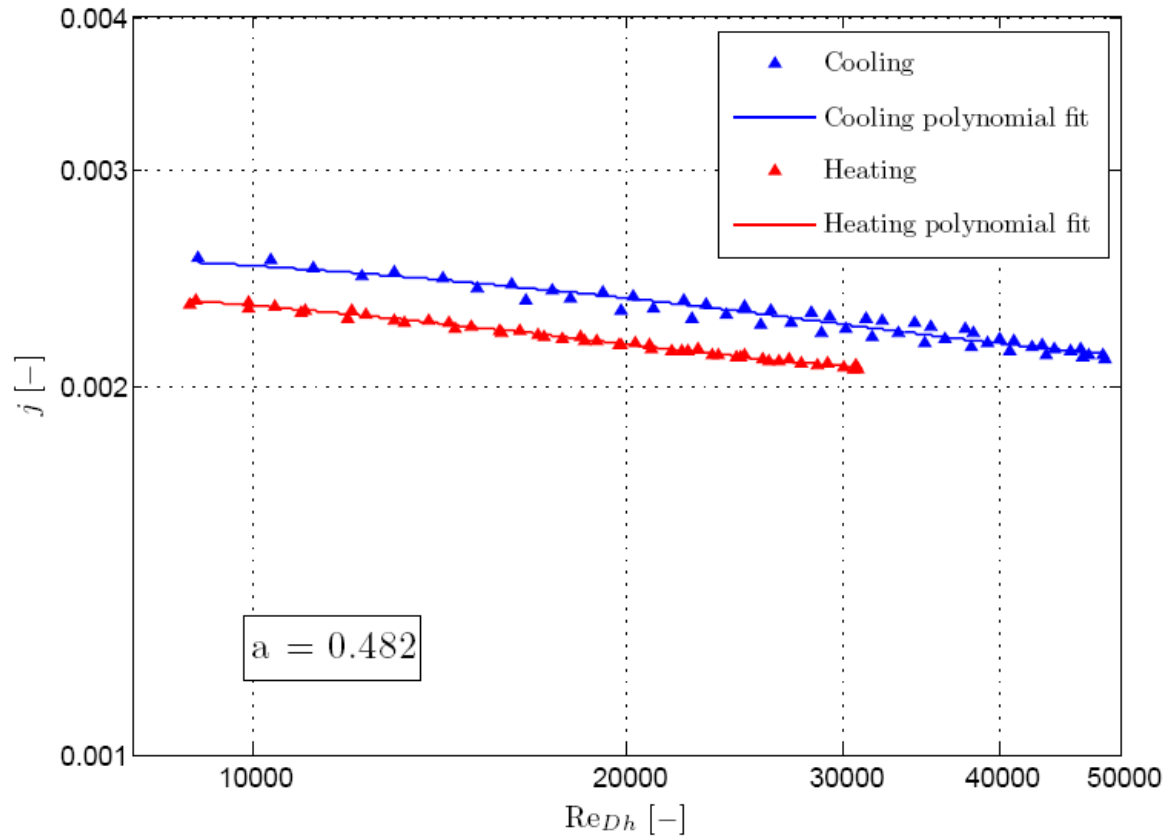


Figure C.9: Colburn  $j$ -factors for a heated and cooled annulus with a polynomial curve fitted for an annular diameter ratio of 0.482.

### C.3 Annular Diameter Ratio 0.579

The range of inner and annulus Reynolds numbers tested for both a heated and cooled annulus are shown in Figure C.10.

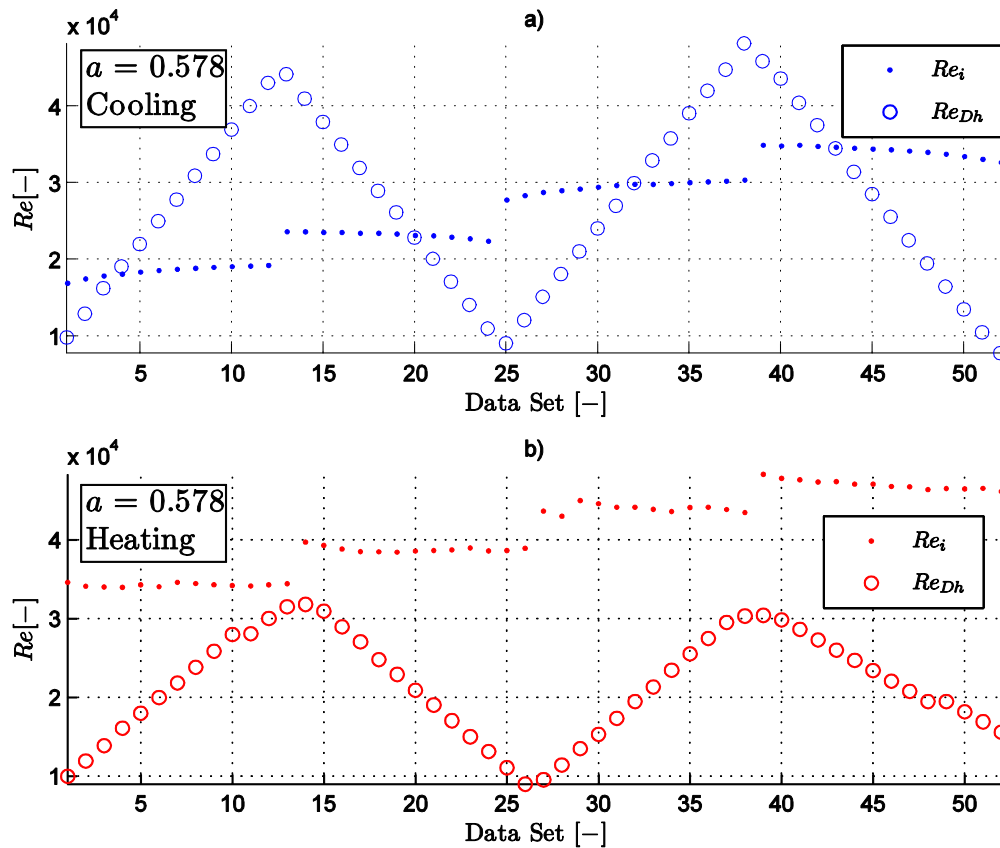


Figure C.10: Inner tube and annulus Reynolds numbers for both a) cooled and b) heated annulus for an annular diameter ratio of 0.579.

#### C.3.1 Mean Heat Transfer

The mean heat transfer calculated using the LMTD, modified Wilson plot method and the nonlinear regression method of Khartabil and Christensen (1992) are compared to mean heat transfer results predicted using available correlations in the literature. Figure C.11 and Figure C.12 are for a cooled and heated annulus respectively.

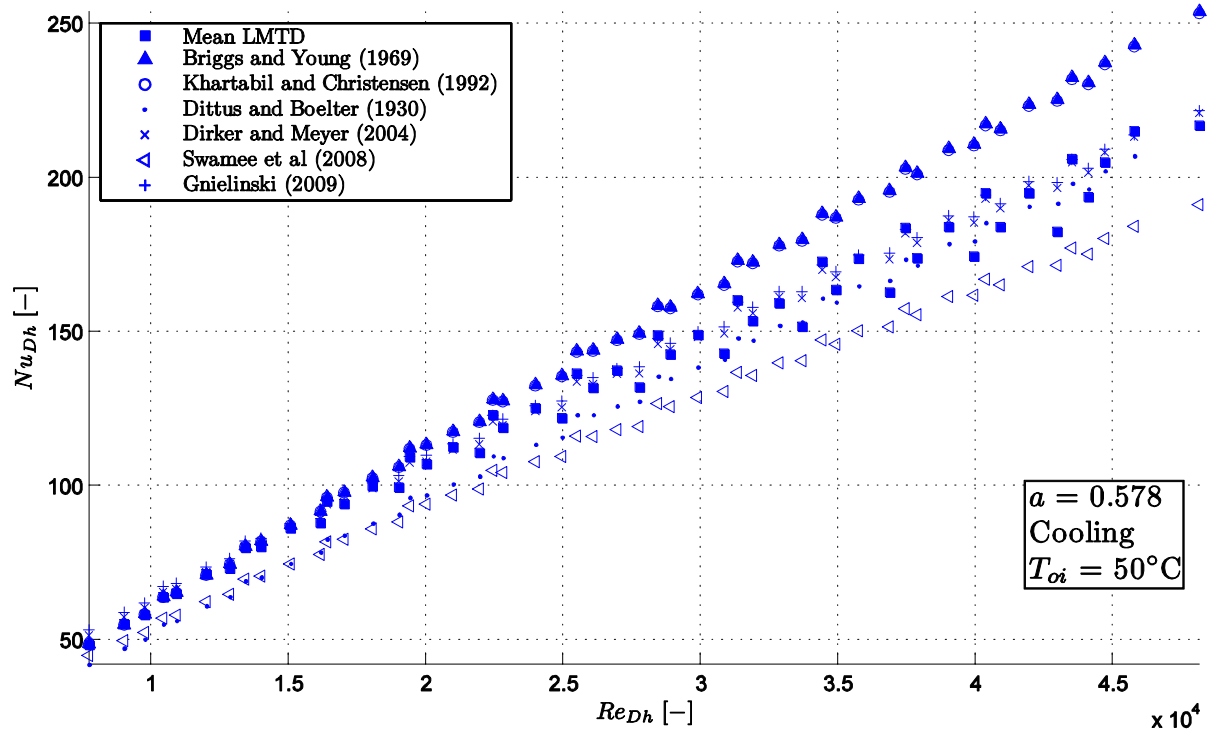


Figure C.11: Mean Nusselt numbers calculated using three experimental methods compared to correlations available in the literature for a cooled annulus with annular diameter ratio of 0.579.

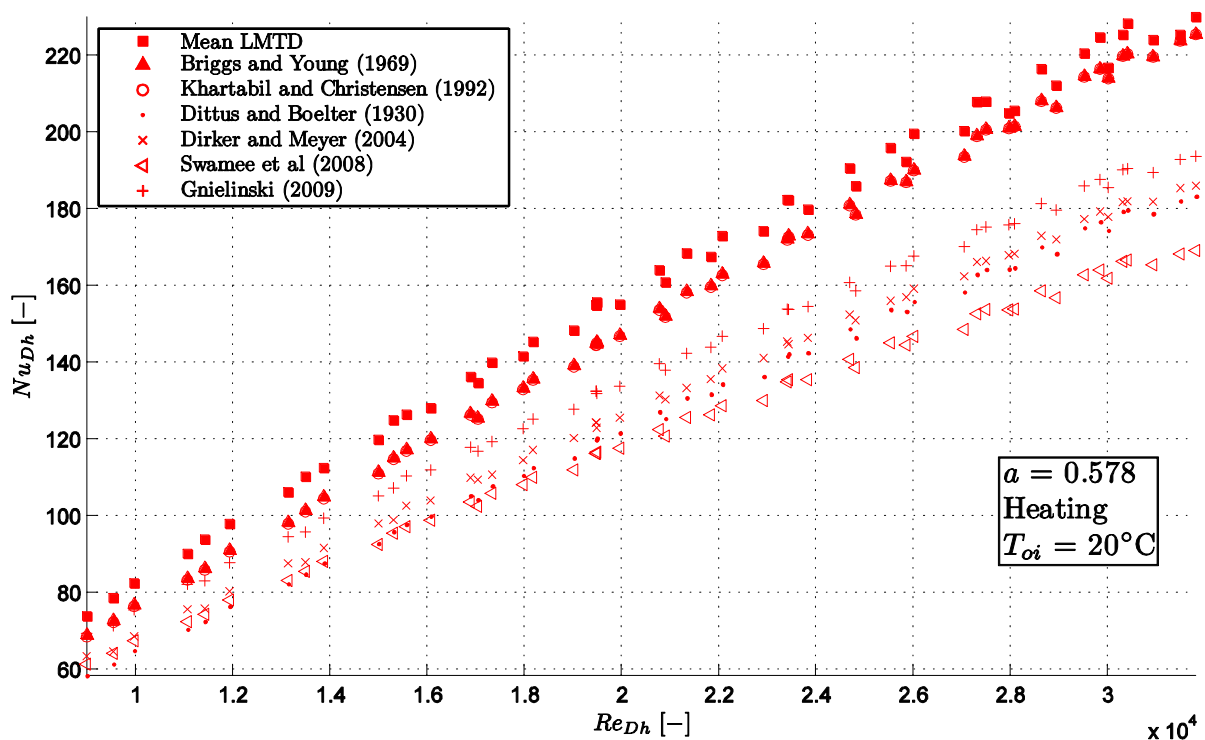


Figure C.12: Mean Nusselt numbers calculated using three experimental methods compared to correlations available in the literature for a heated annulus with annular diameter ratio of 0.579.

Observations on the mean Nusselt numbers are summarized at the end of Appendix C.

### **C.3.2 Local Heat Transfer**

The local heat transfer for each of the control volumes are compared to the mean LMTD method as well as the correlations of Dirker and Meyer (2004) and Gnielinski (2009). Figure C.13 and Figure C.14 are for a cooled and heated annulus respectively.

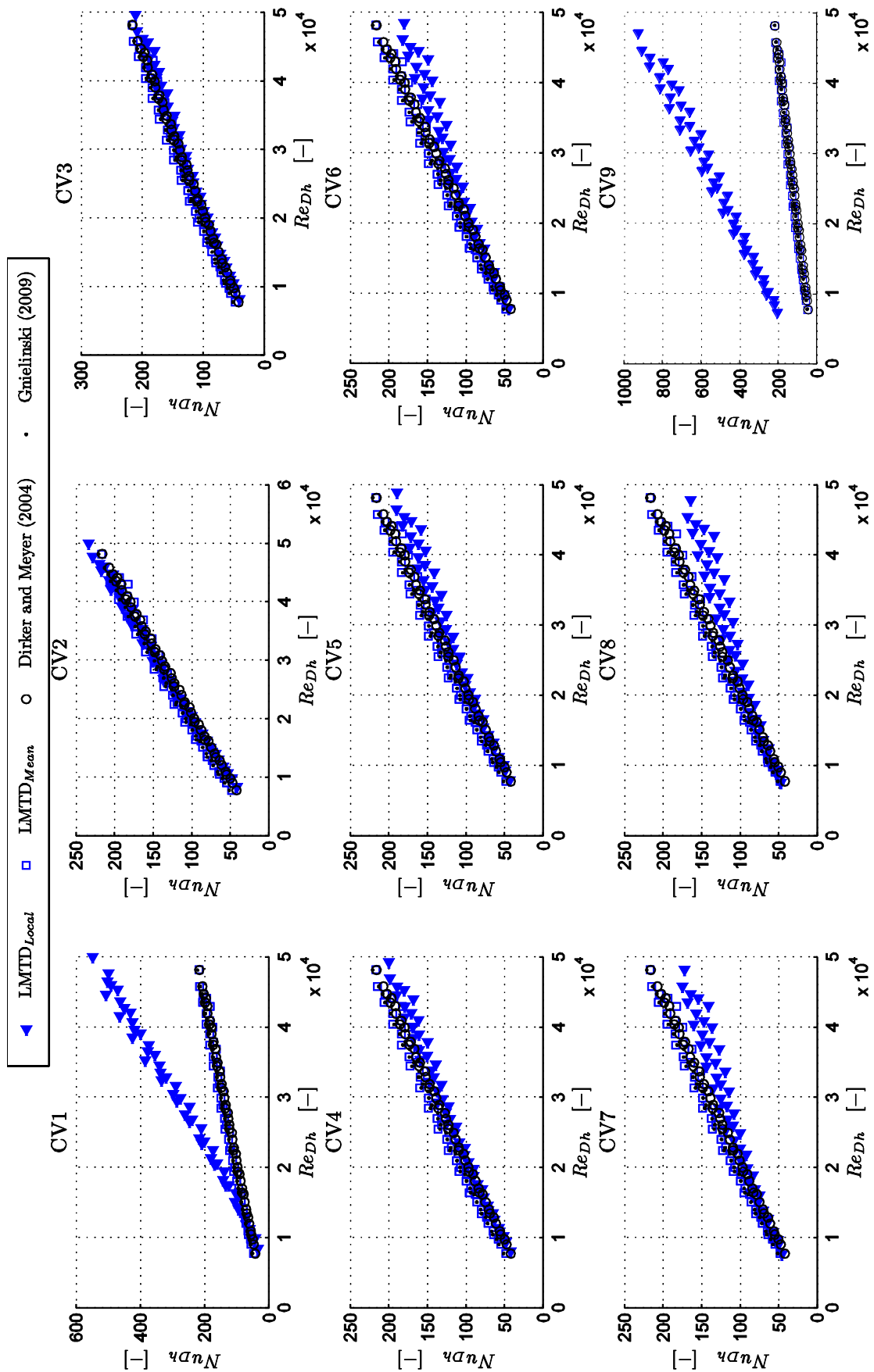


Figure C.13: Local LMTD Nusselt numbers for control volumes 1-9, compared to the mean LMTD Nusselt numbers and correlations of Dirker and Meyer (2004) and Gnielinski (2009) for a cooled annulus with annular diameter ratio of 0.579.

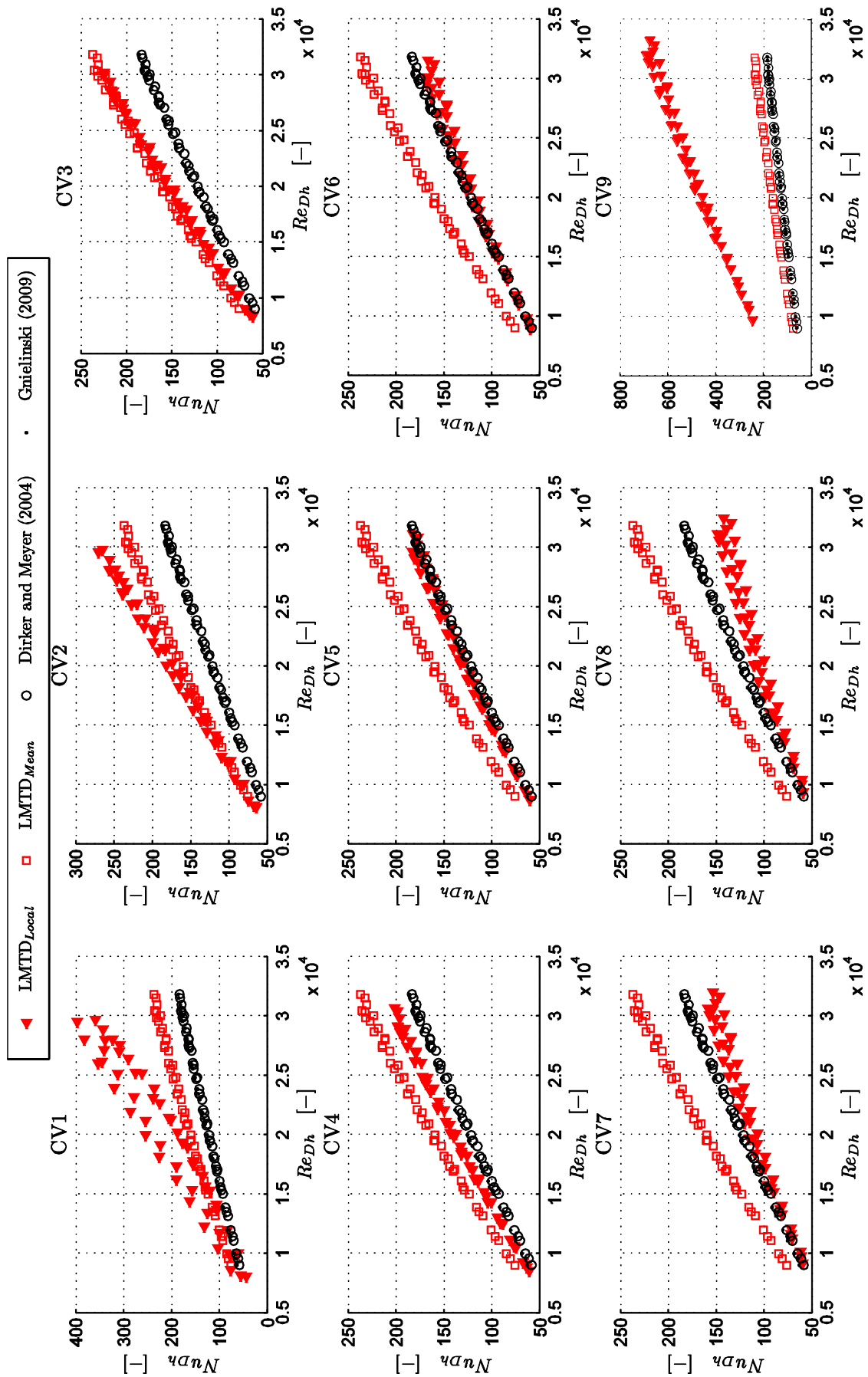


Figure C.14: Local LMTD Nusselt numbers for control volumes 1-9, compared to the mean LMTD Nusselt numbers and correlations of Dirker and Meyer (2004) and Gnielinski (2009) for a heated annulus with annular diameter ratio of 0.579.



### C.3.3 Friction Factor

The friction factors are compared to correlations available in the literature. Figure C.15 shows the friction factor results for both a heated and cooled annulus.

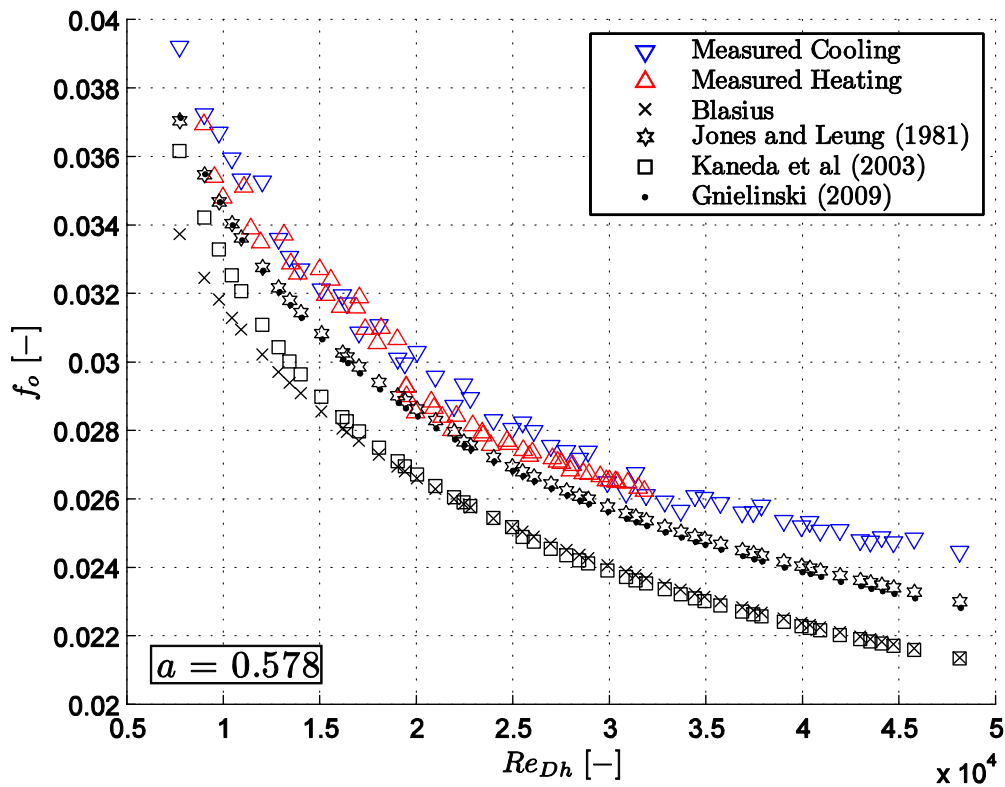


Figure C.15: Diabatic friction factors for both a cooled and heated annulus compared to available correlations for an annular diameter ratio of 0.579.

Observations on the friction factor are provided at the end of Appendix C.

### C.3.4 Colburn j-factor

The results obtained from the modified Wilson plot method for both a heated and cooled annulus are plotted on the same set of axis in Figure C.16.

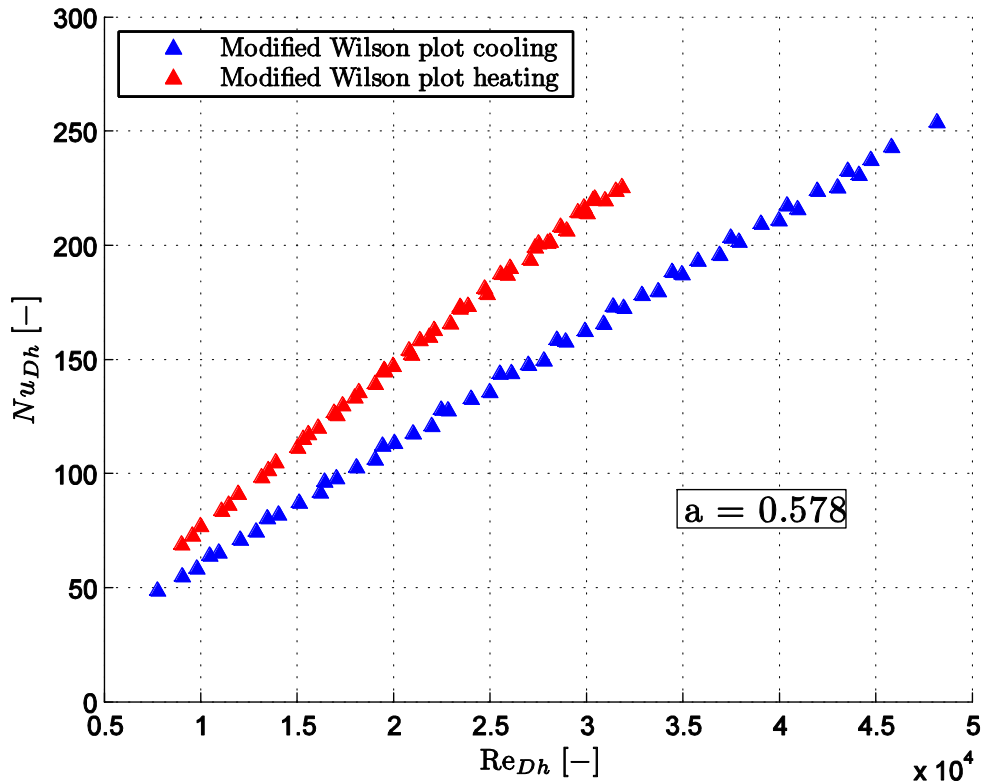


Figure C.16: Nusselt numbers obtained from the modified Wilson plot method for a heated and cooled annulus.

The friction factors and j-factors for a heated and cooled annulus are plotted in Figure C.17.

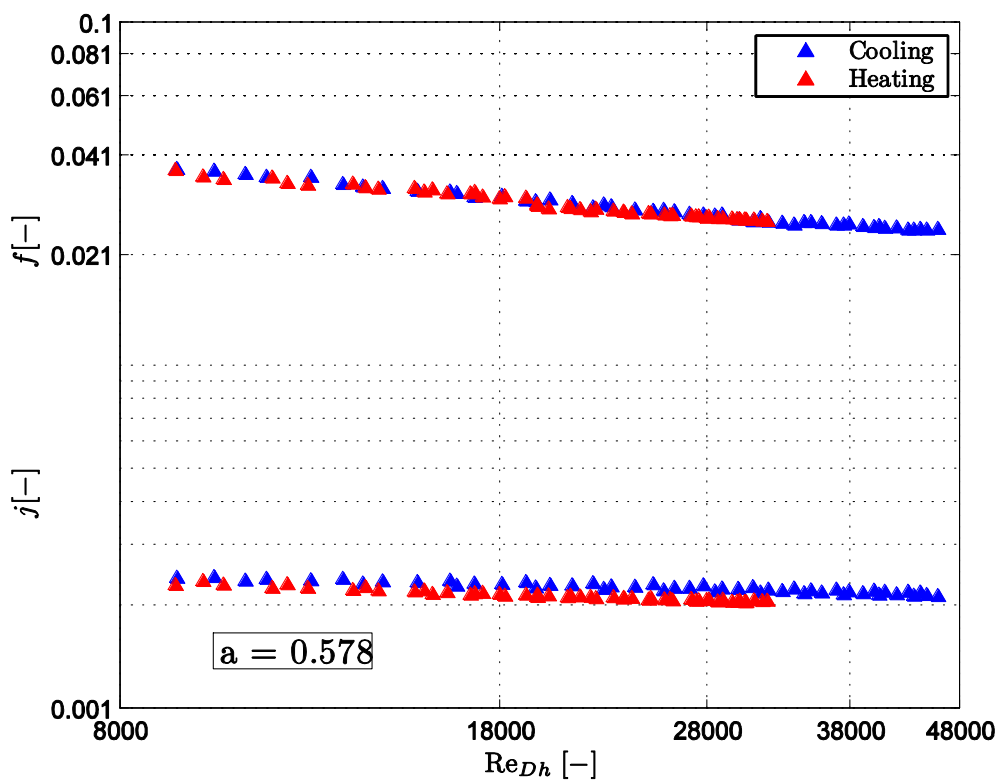


Figure C.17: Friction factors and Colburn j-factors for a heated and cooled annulus.

The Colburn  $j$ -factors obtained from the Nusselt numbers of the modified Wilson plot method are plotted in Figure C.18 for a heated and cooled annulus. A polynomial curve is fitted through the Colburn  $j$ -factors. The constants of the polynomial and description thereof are provided in the main text body in Section 5.8.

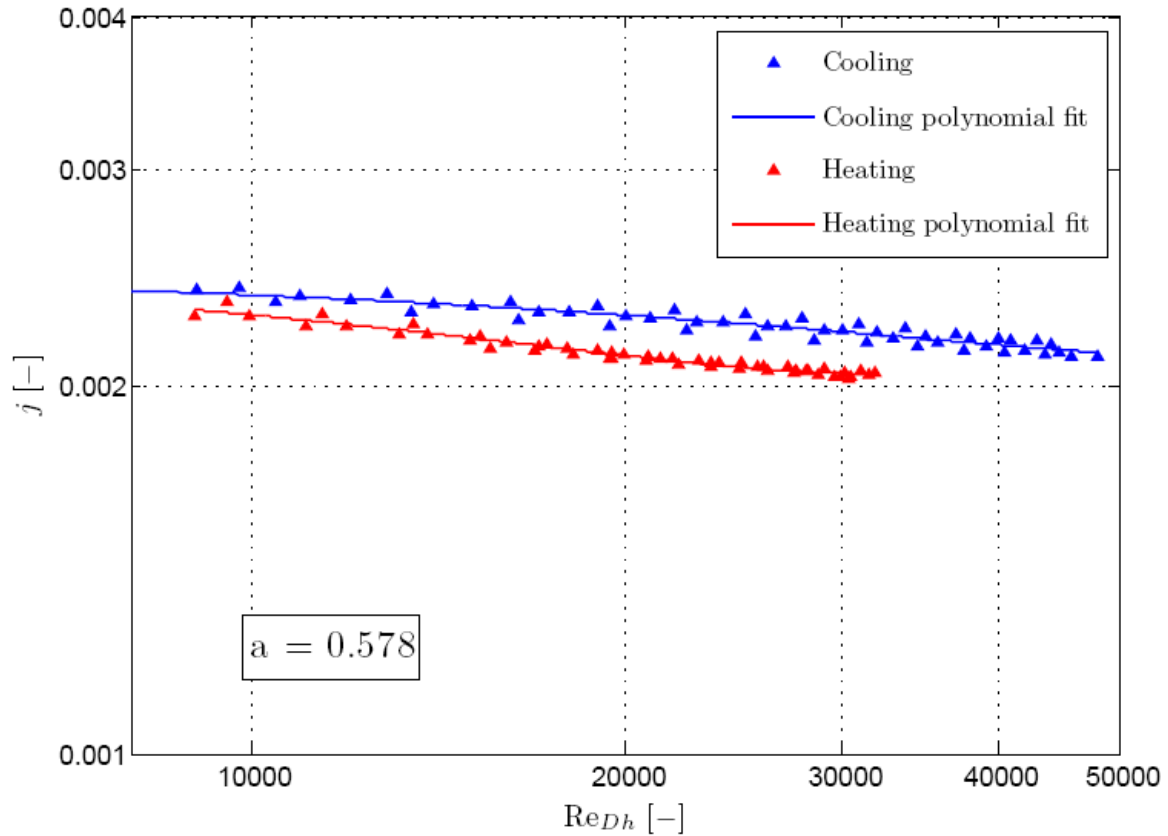


Figure C.18: Colburn  $j$ -factors for a heated and cooled annulus with a polynomial curve fitted for an annular diameter ratio of 0.578.

## C.4 Annular Diameter Ratio 0.712

The range of inner and annulus Reynolds numbers tested for both a heated and cooled annulus are shown in Figure C.19.

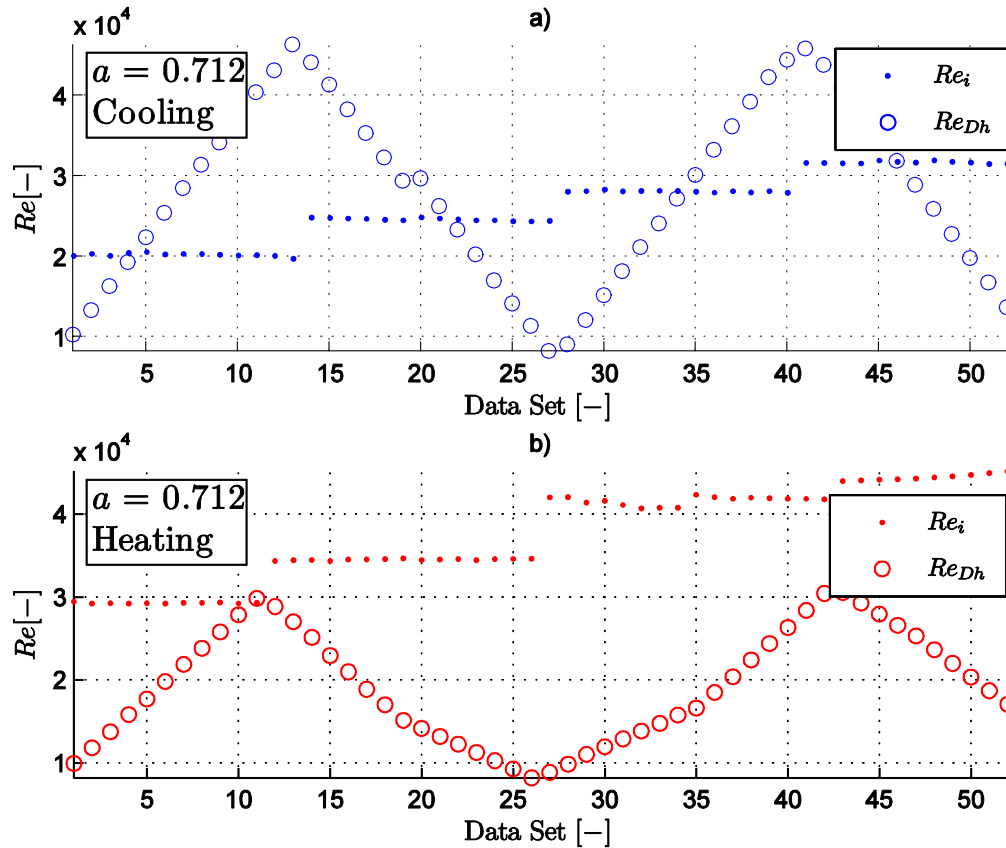


Figure C.19: Inner tube and annulus Reynolds numbers for both a) cooled and b) heated annulus for an annular diameter ratio of 0.712

### C.4.1 Mean Heat Transfer

The mean heat transfer calculated using the LMTD, modified Wilson plot method and the nonlinear regression method of Khartabil and Christensen (1992) are compared to mean heat transfer results predicted using available correlations in the literature. Figure C.20 and Figure C.21 are for a cooled and heated annulus respectively.

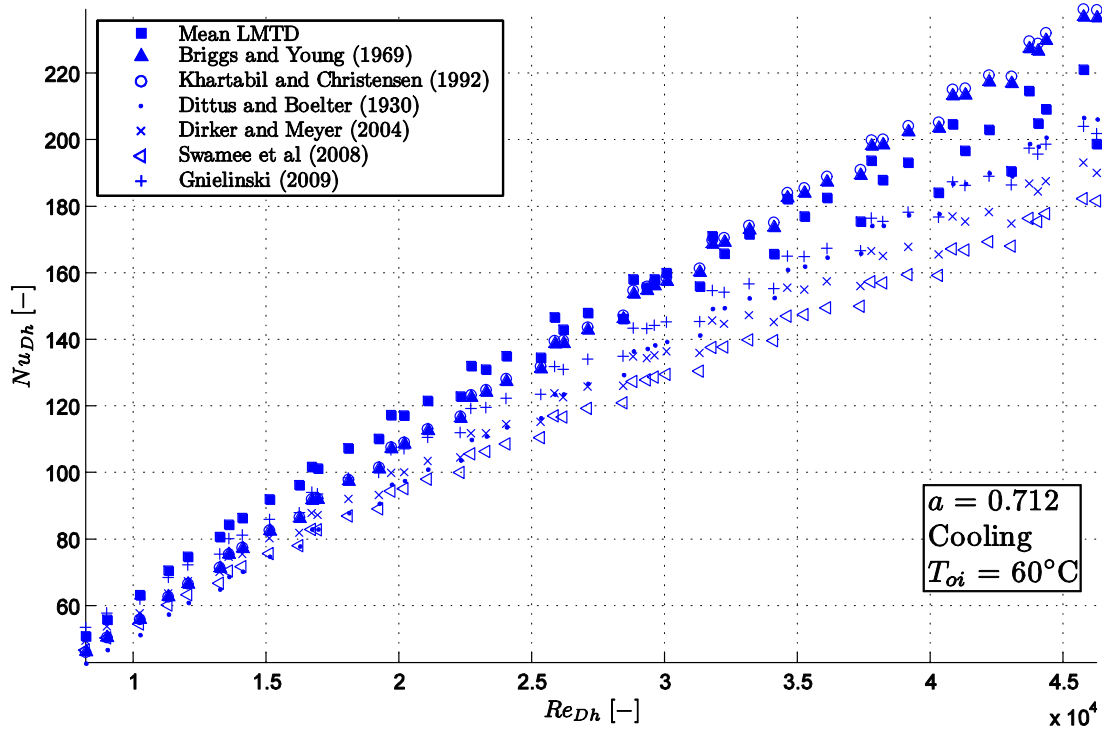


Figure C.20: Mean Nusselt numbers calculated using three experimental methods compared to correlations available in the literature for a cooled annulus with annular diameter ratio of 0.712.

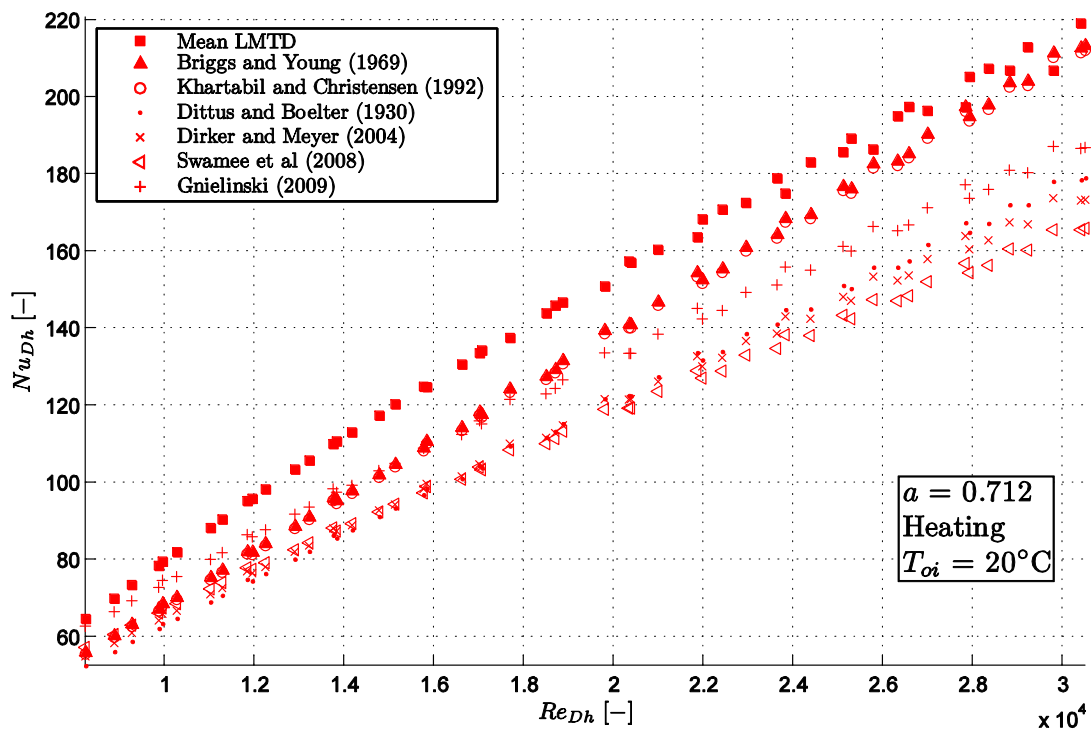


Figure C.21: Mean Nusselt numbers calculated using three experimental methods compared to correlations available in the literature for a heated annulus with annular diameter ratio of 0.712.

Observations on the mean Nusselt numbers are summarized at the end of Appendix C.

## C.4.2 Local Heat Transfer

The local heat transfer for each of the control volumes are compared to the mean LMTD method as well as the correlations of Dirker and Meyer (2004) and Gnielinski (2009). Figure C.22 and Figure C.23 are for a cooled and heated annulus respectively

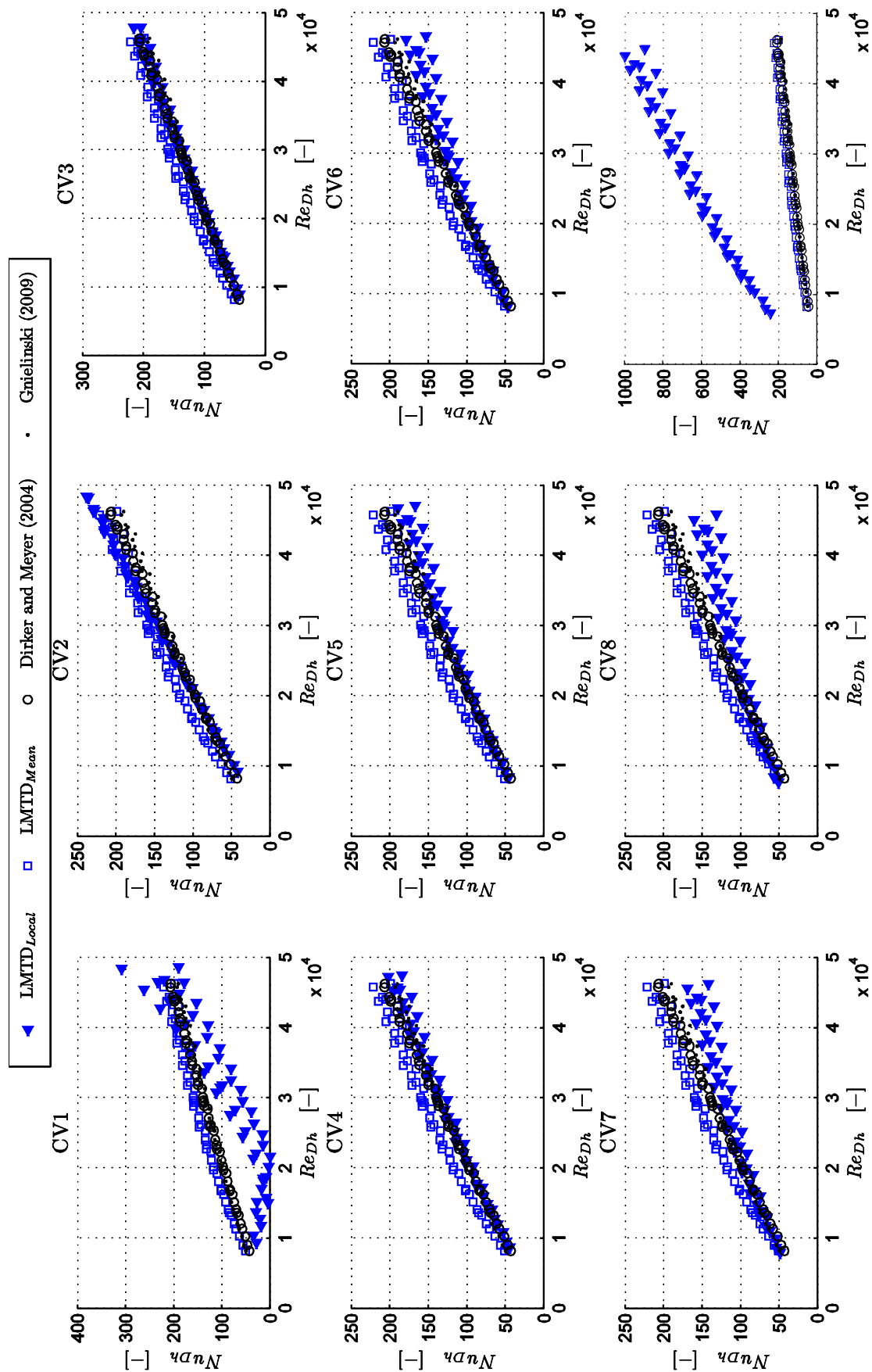


Figure C.22: Local LMTD Nusselt numbers for control volumes 1-9, compared to the mean LMTD Nusselt numbers and correlations of Dirker and Meyer (2004) and Gnielinski (2009) for a cooled annulus with annular diameter ratio of 0.712.

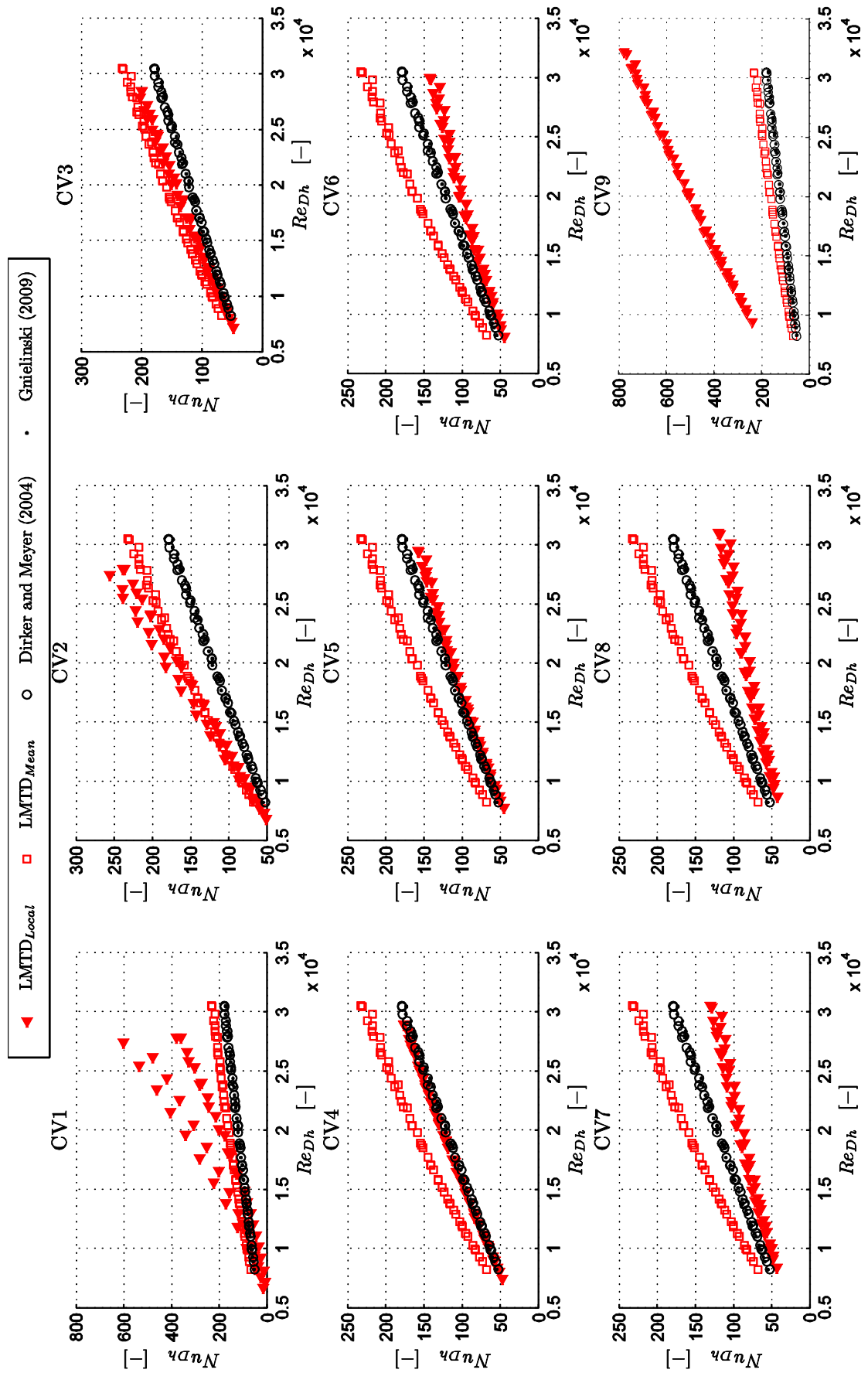


Figure C.23: Local LMTD Nusselt numbers for control volumes 1-9, compared to the mean LMTD Nusselt numbers and correlations of Dirker and Meyer (2004) and Gnielinski (2009) for a heated annulus with annular diameter ratio of 0.712.



### C.4.3 Friction Factor

The friction factors are compared to correlations available in the literature. Figure C.24 shows the friction factor results for both a heated and cooled annulus.

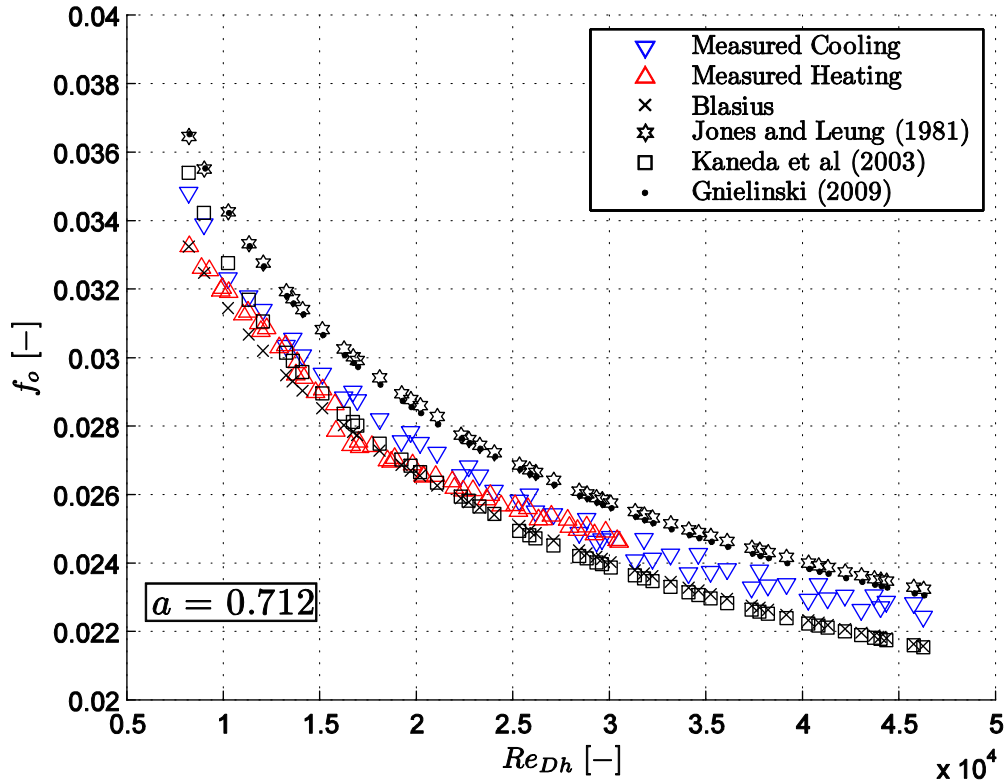


Figure C.24: Diabatic friction factors for both a cooled and heated annulus compared to available correlations for an annular diameter ratio of 0.712.

Observations on the friction factor are provided at the end of Appendix C.

### C.4.4 Colburn j-factor

The results obtained from the modified Wilson plot method for both a heated and cooled annulus are plotted on the same set of axis in Figure C.25.

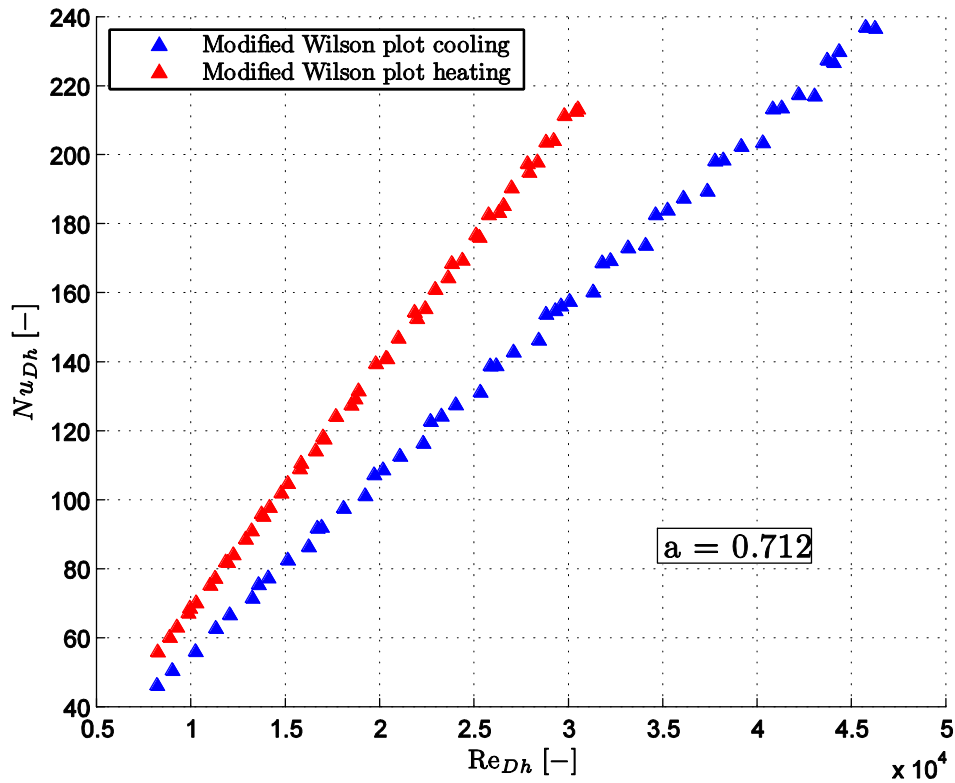


Figure C.25: Nusselt numbers obtained from the modified Wilson plot method for a heated and cooled annulus.

The friction factors and j-factors for a heated and cooled annulus are plotted in Figure C.26 for a heated and cooled annulus.

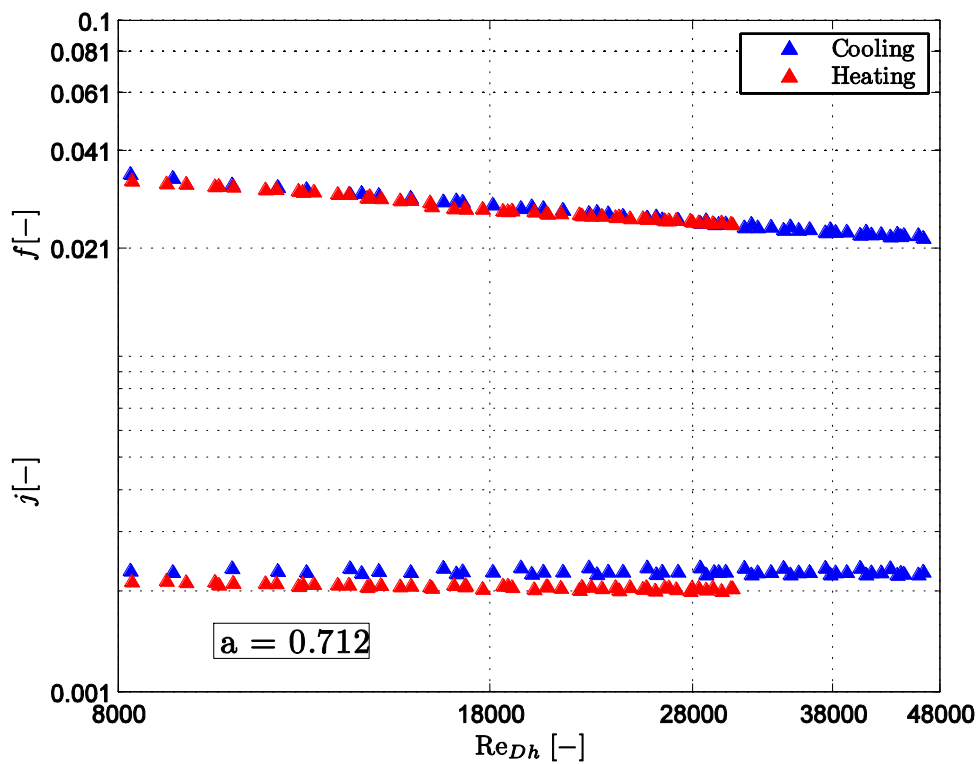


Figure C.26: Friction factors and Colburn j-factors for a heated and cooled annulus.

The Colburn  $j$ -factors obtained from the Nusselt numbers of the modified Wilson plot method are plotted in Figure C.27 for a heated and cooled annulus. A polynomial curve is fitted through the Colburn  $j$ -factors. The constants of the polynomial and description thereof are provided in the main text body in Section 5.8.

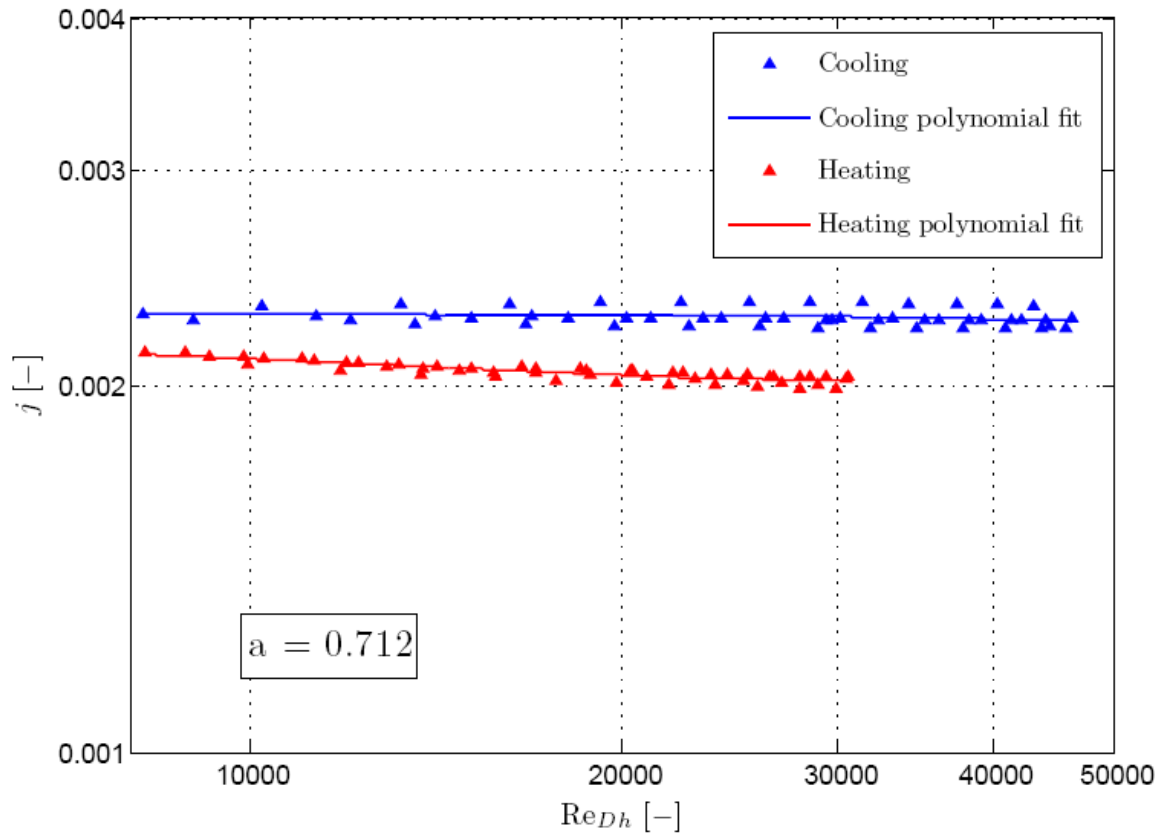


Figure C.27: Colburn  $j$ -factors for a heated and cooled annulus with a polynomial curve fitted for an annular diameter ratio of 0.712.

## C.5 Energy Balances

The mean and maximum energy balances for a heated and cooled annulus for the four heat exchangers tested are provided in Table C.1.

Table C.1: Mean and maximum energy balances.

Annular diameter ratio (a)	Cooling		Heating	
	Mean (%)	Maximum (%)	Mean (%)	Maximum (%)
<b>0.482</b>	2.68	4.35	1.65	2.25
<b>0.579</b>	2.81	3.55	0.62	1.53
<b>0.593</b>	1.79	3.68	0.83	1.42
<b>0.712</b>	2.59	4.21	1.08	1.63

For all the heat exchanger test sections, the cooled annulus has larger energy balances than a heated annulus. This is a result of the large temperature difference between the fluid in the annulus and the ambient surroundings for a cooled annulus.

## C.6 Summary

The observations of all four heat exchanger test sections are summarized here. The observations of the mean and local heat transfer as well as friction factors are included. The results of the Colburn j-factor for all the annular diameter ratios are included in the main text for convenience.

### C.6.1 Mean Heat Transfer

The observations of the mean heat transfer are summarized in Table C.2. Comparisons of the experimental results to existing correlations are performed. Columns 1 – 4 in Table C.2 provide the following averaged percentage difference comparisons for the mean Nusselt numbers:

1. The methods of Briggs and Young (1969) and Khartabil and Christensen (1992).
2. The LMTD method and the method of Briggs and Young (1969).
3. The correlation of Gnielinski (2009) and the method of Briggs and Young (1969).
4. The correlation of Swamee et al (2008) and the method of Briggs and Young (1969).

**Table C.2: Averaged percentage differences for experimental mean Nusselt numbers and existing mean Nusselt number correlations.**

Annular diameter ratio (a)	Column 1 (%)		Column 2 (%)		Column 3 (%)		Column 4 (%)	
	Cooling	Heating	Cooling	Heating	Cooling	Heating	Cooling	Heating
<b>0.482</b>	0.21	0.51	7.11	1.74	2.98	15.11	21.00	23.53
<b>0.579</b>	0.27	0.25	9.02	5.02	6.76	14.75	18.97	20.21
<b>0.593</b>	1.07	1.15	6.71	2.35	6.75	13.04	17.59	19.07
<b>0.712</b>	0.57	0.66	1.47	7.39	10.84	11.98	15.41	12.96

## C.6.2 Friction Factors

The friction factors calculated across the annulus are compared to existing correlations. Columns 1-2 in Table C.3 provide the following averaged percentage difference comparisons:

1. The correlation of Gnielinski (2009).
2. The Blasius equation.

**Table C.3: Averaged percentage differences for experimental friction factors and existing correlations.**

Annular diameter ratio (a)	Column 1 (%)		Column 2 (%)	
	Cooling	Heating	Cooling	Heating
<b>0.482</b>	15.17	6.39	20.65	12.71
<b>0.579</b>	5.00	3.24	11.31	9.67
<b>0.593</b>	3.96	1.98	10.19	8.69
<b>0.712</b>	3.51	6.02	3.40	1.34

## C.7 Discussion

The results of the three heat exchanger test sections not presented in the main text are provided in Appendix C. In the main text an investigation into the test section with annular diameter ratio 0.593 is provided. The conclusions drawn are similar for all four heat exchangers and are provided in the main text. Using the results of all four test sections the main text investigates the effects of the annular diameter ratio on the heat transfer as well as the friction factor of the test sections.

# Appendix D

## Uncertainty Analysis

### Contents

D.1 Introduction .....	D.1
D.2 Cause and Types of Experimental Errors .....	D.1
D.3 Generalized Uncertainty Analysis Methods .....	D.1
D.4 Quantifying Uncertainties .....	D.4
D.4.1 Instruments.....	D.4
D.4.2 Fluid and Tube Properties .....	D.4
D.4.3 Inlet and Outlet Temperature .....	D.5
D.4.4 Inner Wall Average Temperature Uncertainty .....	D.6
D.4.5 Temperature Difference .....	D.6
D.4.6 Logarithmic Mean Temperature Difference.....	D.6
D.4.7 Local Logarithmic Mean Temperature Difference.....	D.7
D.4.8 Heat Transfer Rate .....	D.8
D.4.8.1 Inner Tube.....	D.8
D.4.8.2 Annulus .....	D.9
D.4.8.3 Average Heat Transfer Rate.....	D.9
D.4.9 Annulus Heat Transfer Coefficient.....	D.9
D.4.10 Physical Dimensions .....	D.10
D.4.11 Hydraulic Diameter .....	D.10
D.4.12 Heat Transfer Area .....	D.10

D.4.13 Inner Tube Cross Sectional Area .....	D.11
D.4.14 Annulus Cross Sectional Area .....	D.11
D.4.15 Reynolds Number .....	D.12
D.4.16 Friction Factor .....	D.12
D.4.17 Nusselt Number .....	D.13
D.4.18 Local Nusselt Number .....	D.13
D.4.19 Summary .....	D.15

## List of Tables

Table D.1: Uncertainty properties for the measurement equipment used .....	D.4
Table D.2: Uncertainties of fluid properties from the correlations of Popiel and Wojtkowiak (1991).....	D.5
Table D.3: Uncertainties of properties used to calculate heat transfer and friction factors for low ( $\approx 15\ 000$ ) and high ( $\approx 25\ 000$ ) Reynolds numbers. ....	D.15

## Nomenclature

In addition to the nomenclature in the main text body, the following symbols are used in this appendix. Where there is a symbol clash, the definition given here takes precedence in this appendix.

$B$	Bias	-
$n$	Number of Samples	-
$P$	Precision	-
$R$	Result of a Set of Measurements	-
$x$	Measurement	-

## Greek Symbols

$\delta$	Uncertainty
----------	-------------

## Subscripts

$i$	Measurement Number
-----	--------------------

**Note:** All nomenclature declared in the main text are not repeated here.



## D.1 Introduction

All data captured in this study must include a theoretical quantification of the errors involved in the experimentation. This must take into account all variables that introduce errors into the system. The measurement devices on the experimental facility are the primary source of these errors. The equipment consists of two errors: those that the manufacturers specify as a deviation from the actual measurement, and those that are introduced into the system due to uncontrollable factors.

Uncertainty refers to a possible value that an error may have, and identifies an interval around a measured value in which the true value is expected to lie (Kline and McClintock (1953)).

## D.2 Cause and Types of Experimental Errors

Experimental facilities are inherently subjected to errors from various factors; some are minute while others are critical to the validity of the experimental data. The most basic errors are those introduced into the experimental measurement apparatus through poor instrument manufacture, which may completely invalidate experimental data. The second type of errors are referred to as fixed errors, these cause readings to repeatedly deviate from the actual reading by approximately the same value. Fixed errors are inherent in measurement equipment and are supplied by the manufacturer for the ranges where they apply. The third type of error referred to as random errors may be caused by equipment fluctuations, random electronic fluctuations and various influences of friction (Holman (1989))

## D.3 Generalized Uncertainty Analysis Methods

Uncertainty analysis on the final result may be done using a commonsense analysis or a precise mathematical method. Commonsense methods give rough approximations to the overall error and usually indicate errors based on worst case scenarios. One such method states that the overall error is equal to the maximum error in any parameter used in calculating the result. Another common sense method is to combine all the errors in the

most detrimental way in order to determine the maximum error in the final result (Holman (1989)).

A more precise method that was used in this study is the method of Kline and McClintock (1953). This method is based on careful specification of the uncertainties in the various experimental measurements. Each variable is specified as the measured value plus the uncertainty, and the odds on the uncertainty, written in mathematical form as:

$$x_i = x_i(\text{measured}) \pm \delta x_i \text{ (95\% confidence)}$$

Where  $\delta x_i$  is the uncertainty of variable  $x_i$  with a confidence interval that the measured value is within this uncertainty of 95%. The measured value  $x_i$  represents the observation in a single sample experiment or the mean of a data set in a multi-sample experiment.

In Moffat (1988) the uncertainty is calculated as the Euclidean norm of the bias ( $B_{xi}$ ) or fixed errors, and the precision ( $P_{xi}$ ) or random errors.

$$\delta x_i = \sqrt{B_{xi}^2 + P_{xi}^2} \quad \text{(D.1)}$$

Let R be the result of an experiment calculated from a set of measurements. Let it be a function of  $n$  variables,  $x_1, x_2, \dots, x_n$ , each with their own uncertainty value. Therefore written mathematically:

$$R = f(x_1, x_2, \dots, x_n) \quad \text{(D.2)}$$

Assuming that the uncertainties of  $x_1, x_2, \dots, x_n$  are known, the effect of these uncertainties on the result R is:

$$\delta R_{xi} = \frac{\partial R}{\partial x_i} \delta x_i \quad \text{(D.3)}$$

Here the partial derivative of R is called the sensitivity coefficient of the result R with respect to  $x_i$ . The sensitivity coefficient is the effect that the uncertainty of a single measurement for

the variable  $x_i$ , with the measurement being in error, has on the overall uncertainty of the result. Summing all the uncertainties of  $R$  to obtain a maximum overall uncertainty and using a root-sum-squared method Equation (D.4) is derived.

$$\delta R_x = \left\{ \left( \frac{\partial R}{\partial x_1} \delta x_1 \right)^2 + \left( \frac{\partial R}{\partial x_2} \delta x_2 \right)^2 + \dots + \left( \frac{\partial R}{\partial x_n} \delta x_n \right)^2 \right\}^{\frac{1}{2}} \quad (\text{D.4})$$

Equation (D.4) is referred to as the absolute uncertainty of  $R$  with engineering units of  $R$ . It is only valid under the following conditions:

- i. Each measurement must be an independent variable.
- ii. If measurements were repeated observations would display a Gaussian distribution.
- iii. The uncertainty of each measurement was initially expressed at the confidence level.

If  $\delta x_i^2$  are taken to be variances, then Equation (D.4) holds without the need for Gaussian distributed populations.

Some applications require the uncertainty estimate as a relative uncertainty of the result. This approach is simplified if the equation describing the result is of product form as in Equation (D.5).

$$R = x_1^a x_2^b x_3^c \dots x_n^m \quad (\text{D.5})$$

The relative uncertainty can then be found directly from:

$$\frac{\delta R}{R} = \left\{ \left( a \frac{\delta x_1}{x_1} \right)^2 + \left( b \frac{\delta x_2}{x_2} \right)^2 + \dots + \left( \left( m \frac{\delta x_n}{x_n} \right)^2 \right) \right\}^{\frac{1}{2}} \quad (\text{D.6})$$

The relative uncertainty of  $R$  is expressed as a percentage. In this formulation the exponent of  $x_i$  becomes the sensitivity coefficient (Moffat 1988).

## D.4 Quantifying Uncertainties

Using the method of Kline and McClintock (1953) uncertainties of each of the instruments are calculated for their usable ranges. The formulation of the equations used to calculate the uncertainties of all the calculated parameters according to the method of Kline and McClintock (1953) is shown in the proceeding section.

### D.4.1 Instruments

The three instruments used, namely the thermocouples, coriolis flow meters and pressure transducers each had manufacturer specified accuracy which was the bias. The precision was obtained by capturing 100 data points. The standard deviation was found using these points and multiplied by two to fall within the 95% confidence interval. Table D.1 provides all the instruments with their ranges, bias, precision and total uncertainty.

Table D.1: Uncertainty properties for the measurement equipment used

Property	Range	Bias	Precision	Uncertainty
<b>Thermocouple</b>	-200 - 350°C	0.1°C <sup>a</sup>	0.036°C	0.11°C
<b>Coriolis Flow Meter</b>				
<i>Inner Tube</i>	0.015 - 0.603 kg/s	0.1% <sup>b</sup>	0.05%	0.11%
<i>Annulus</i>	0.047 - 1.883 kg/s	0.1% <sup>b</sup>	0.09%	0.14%
<b>Pressure Transducers</b>				
<i>Low Range</i>	0-21kPa	0.25% <sup>c</sup>	2.51%	2.53%
<i>Mid Range</i>	0-35kPa	0.25% <sup>c</sup>	2.71%	2.74%
<i>High Range</i>	0-140kPa	0.25% <sup>c</sup>	3.39%	3.42%

<sup>a</sup> Calibrated with a PT 100 with an uncertainty of 0.01°C.

<sup>b</sup> Percentage of reading.

<sup>c</sup> Percentage of full scale value.

### D.4.2 Fluid and Tube Properties

All fluid properties and their associated uncertainties were calculated from the methods of Popiel and Wojtkowiak (1998). The uncertainties are supplied in Table D.2.

The thermal conductivity of the copper tube was calculated using the method of Abu-Eishah (2001). The uncertainty of this method is given as 0.13%.

**Table D.2: Uncertainties of fluid properties from the correlations of Popiel and Wojtkowiak (1991).**

Fluid Property	Uncertainty
Density	0.04%
Viscosity	1.00%
Specific Heat	0.06%
Thermal Conductivity	2.00%

### D.4.3 Inlet and Outlet Temperature

The inlet and outlet temperatures for both the annulus and inner tube will be obtained using four thermocouples located around the periphery. The temperature will then be taken as the average of these four thermocouple measurements, or written mathematically as:

$$\bar{T}_{ii} = \frac{T_{ii,1} + T_{ii,2} + \dots + T_{ii,n}}{n} \quad (\text{D.7})$$

The uncertainty for the inner inlet is:

$$\delta\bar{T}_{ii} = \left\{ \left( \frac{\delta T_{ii,1}}{n} \right)^2 + \left( \frac{\delta T_{ii,2}}{n} \right)^2 + \dots + \left( \frac{\delta T_{ii,n}}{n} \right)^2 \right\}^{\frac{1}{2}} \quad (\text{D.8})$$

As all the thermocouples are supplied by the same manufacturer, all the uncertainties are equal, therefore:

$$\delta T_{ii,1} = \delta T_{ii,2} = \dots = \delta T_{ii,n} = \delta T \quad (\text{D.9})$$

Equation (D.10) is then simplified further:

$$\delta \bar{T}_{ii} = \sqrt{\frac{1}{4}} \delta T \quad (\text{D.10})$$

A similar result is obtained for the uncertainties for the inner outlet, outer inlet and outer outlet temperatures.

#### D.4.4 Inner Wall Average Temperature Uncertainty

Two thermocouples were used to measure the inner tube wall temperature at nine separate stations along the axial length of the tube. Therefore the average measured outer wall temperature is the average of 18 thermocouple measurements. With a similar derivation to Equation (D.10), the result is:

$$\delta \bar{T}_{iwo} = \sqrt{\frac{1}{18}} \delta T \quad (\text{D.11})$$

#### D.4.5 Temperature Difference

In calculating the experimental heat transfer, the temperature difference over the heat exchanger for both the inner tube and annulus are required. With the temperature difference over the inner tube given as:

$$\Delta T_i = \bar{T}_{ii} - \bar{T}_{io} \quad (\text{D.12})$$

The uncertainty for the temperature difference of the inner tube is:

$$\delta \Delta T_i = \sqrt{\delta \bar{T}_{ii}^2 + \delta \bar{T}_{io}^2} \quad (\text{D.13})$$

The uncertainty for the temperature difference of the annulus is obtained in a similar manner.

#### D.4.6 Logarithmic Mean Temperature Difference

The logarithmic mean temperature difference is defined as:

$$\Delta T_{LMTD} = \frac{(\bar{T}_{ii} - \bar{T}_{oo}) - (\bar{T}_{io} - \bar{T}_{oi})}{\ln\left(\frac{(\bar{T}_{ii} - \bar{T}_{oo})}{(\bar{T}_{io} - \bar{T}_{oi})}\right)} \quad (D.14)$$

With its uncertainty being determined by:

$$\delta T_{LMTD} = \left\{ \left( \frac{\partial T_{LMTD}}{\partial \bar{T}_{ii}} \delta \bar{T}_{ii} \right)^2 + \left( \frac{\partial T_{LMTD}}{\partial \bar{T}_{oo}} \delta \bar{T}_{oo} \right)^2 + \left( \frac{\partial T_{LMTD}}{\partial \bar{T}_{io}} \delta \bar{T}_{io} \right)^2 + \left( \frac{\partial T_{LMTD}}{\partial \bar{T}_{oi}} \delta \bar{T}_{oi} \right)^2 \right\}^{\frac{1}{2}} \quad (D.15)$$

Expanding this results in:

$$\begin{aligned} \delta T_{LMTD} = & \left[ \left( \left\{ \frac{1}{\ln\left(\frac{(\bar{T}_{ii} - \bar{T}_{oo})}{(\bar{T}_{io} - \bar{T}_{oi})}\right)} - \frac{(\bar{T}_{ii} - \bar{T}_{oo}) - (\bar{T}_{io} - \bar{T}_{oi})}{\ln\left(\frac{(\bar{T}_{ii} - \bar{T}_{oo})}{(\bar{T}_{io} - \bar{T}_{oi})}\right)^2 (\bar{T}_{ii} - \bar{T}_{oo})} \right\} \delta \bar{T}_{ii} \right)^2 \right. \\ & + \left( \left\{ -\frac{1}{\ln\left(\frac{(\bar{T}_{ii} - \bar{T}_{oo})}{(\bar{T}_{io} - \bar{T}_{oi})}\right)} + \frac{(\bar{T}_{ii} - \bar{T}_{oo}) - (\bar{T}_{io} - \bar{T}_{oi})}{\ln\left(\frac{(\bar{T}_{ii} - \bar{T}_{oo})}{(\bar{T}_{io} - \bar{T}_{oi})}\right)^2 (\bar{T}_{ii} - \bar{T}_{oo})} \right\} \delta \bar{T}_{oo} \right)^2 \\ & + \left( \left\{ -\frac{1}{\ln\left(\frac{(\bar{T}_{ii} - \bar{T}_{oo})}{(\bar{T}_{io} - \bar{T}_{oi})}\right)} + \frac{(\bar{T}_{ii} - \bar{T}_{oo}) - (\bar{T}_{io} - \bar{T}_{oi})}{\ln\left(\frac{(\bar{T}_{ii} - \bar{T}_{oo})}{(\bar{T}_{io} - \bar{T}_{oi})}\right)^2 (\bar{T}_{io} - \bar{T}_{oi})} \right\} \delta \bar{T}_{io} \right)^2 \\ & \left. + \left( \left\{ \frac{1}{\ln\left(\frac{(\bar{T}_{ii} - \bar{T}_{oo})}{(\bar{T}_{io} - \bar{T}_{oi})}\right)} - \frac{(\bar{T}_{ii} - \bar{T}_{oo}) - (\bar{T}_{io} - \bar{T}_{oi})}{\ln\left(\frac{(\bar{T}_{ii} - \bar{T}_{oo})}{(\bar{T}_{io} - \bar{T}_{oi})}\right)^2 (\bar{T}_{io} - \bar{T}_{oi})} \right\} \delta \bar{T}_{oi} \right)^2 \right]^{\frac{1}{2}} \quad (D.16) \end{aligned}$$

#### D.4.7 Local Logarithmic Mean Temperature Difference

The local logarithmic mean temperature difference is defined as:

$$\Delta T_{LMTD,Local} = \frac{(\bar{T}_{oi} - \bar{T}_{oo})}{\ln\left(\frac{(\bar{T}_{iw} - \bar{T}_{oo})}{(\bar{T}_{iw} - \bar{T}_{oi})}\right)} \quad (D.17)$$

With its uncertainty being determined by:

$$\delta T_{LMTD} = \left\{ \left( \frac{\partial T_{LMTD}}{\partial \bar{T}_{oi}} \delta \bar{T}_{oi} \right)^2 + \left( \frac{\partial T_{LMTD}}{\partial \bar{T}_{oo}} \delta \bar{T}_{oo} \right)^2 + \left( \frac{\partial T_{LMTD}}{\partial \bar{T}_{iw}} \delta \bar{T}_{iw} \right)^2 \right\}^{\frac{1}{2}} \quad (D.18)$$

Expanding this results in:

$$\begin{aligned} \delta T_{LMTD,Local} = & \left[ \left( \left\{ \frac{1}{\ln \left( \frac{\bar{T}_{iw} - T_{oo}}{\bar{T}_{iw} - T_{oi}} \right)} - \frac{(T_{oi} - T_{oo})}{\ln \left( \frac{\bar{T}_{iw} - T_{oo}}{\bar{T}_{iw} - \bar{T}_{oi}} \right)^2 (\bar{T}_{iw} - T_{oi})} \right\} \delta T_{oi} \right)^2 \right. \\ & + \left( \left\{ -\frac{1}{\ln \left( \frac{\bar{T}_{iw} - T_{oo}}{\bar{T}_{iw} - T_{oi}} \right)} + \frac{(T_{oi} - T_{oo})}{\ln \left( \frac{\bar{T}_{iw} - T_{oo}}{\bar{T}_{iw} - T_{oi}} \right)^2 (\bar{T}_{iw} - T_{oo})} \right\} \delta T_{oo} \right)^2 \\ & \left. + \left( \left\{ \frac{(T_{oi} - T_{oo})}{\ln \left( \frac{\bar{T}_{iw} - T_{oo}}{\bar{T}_{iw} - T_{oi}} \right)^2 (\bar{T}_{iw} - T_{oo})} \right\} \delta \bar{T}_{iw} \right)^2 \right]^{\frac{1}{2}} \end{aligned} \quad (D.19)$$

## D.4.8 Heat Transfer Rate

### D.4.8.1 Inner Tube

The heat transfer rate of the inner tube is calculated as:

$$\dot{Q}_i = \dot{m}_i c_{p,i} (\bar{T}_{ii} - \bar{T}_{io}) = \dot{m}_i c_{p,i} \Delta T_i \quad (D.20)$$

With the uncertainties being determined by:

$$\begin{aligned} \delta \dot{Q}_i &= \left\{ \left( \frac{\partial \dot{Q}_i}{\partial \dot{m}_i} \delta \dot{m}_i \right)^2 + \left( \frac{\partial \dot{Q}_i}{\partial c_{p,i}} \delta c_{p,i} \right)^2 + \left( \frac{\partial \dot{Q}_i}{\partial \Delta T_i} \delta \Delta T_i \right)^2 \right\}^{\frac{1}{2}} \\ &= \left\{ (c_{p,i} \Delta T_i \delta \dot{m}_i)^2 + (\dot{m}_i \Delta T_i \delta c_{p,i})^2 + (\dot{m}_i c_{p,i} \delta \Delta T_i)^2 \right\}^{\frac{1}{2}} \end{aligned} \quad (D.21)$$



### D.4.8.2 Annulus

The mean heat transfer rate of the annulus is calculated as:

$$\dot{Q}_o = \dot{m}_o C_{p,o} (\bar{T}_{oi} - \bar{T}_{oo}) = \dot{m}_o C_{p,o} \Delta T_o \quad (\text{D.22})$$

With the uncertainties being determined by:

$$\begin{aligned} \delta \dot{Q}_o &= \left\{ \left( \frac{\partial \dot{Q}_o}{\partial \dot{m}_o} \delta \dot{m}_o \right)^2 + \left( \frac{\partial \dot{Q}_o}{\partial C_{p,o}} \delta C_{p,o} \right)^2 + \left( \frac{\partial \dot{Q}_o}{\partial \Delta T_o} \delta \Delta T_o \right)^2 \right\}^{\frac{1}{2}} \\ &= \left\{ (C_{p,o} \Delta T_o \delta \dot{m}_o)^2 + (\dot{m}_o \Delta T_o \delta C_{p,o})^2 + (\dot{m}_o C_{p,o} \delta \Delta T_o)^2 \right\}^{\frac{1}{2}} \end{aligned} \quad (\text{D.23})$$

A similar calculation is used for the local annulus heat transfer rate where all mean properties are substituted for local properties.

### D.4.8.3 Average Heat Transfer Rate

The average heat transfer rate for the inner tube and annulus is given by:

$$\dot{Q}_{avg} = \frac{\dot{Q}_i + \dot{Q}_o}{2} \quad (\text{D.24})$$

With the uncertainties being determined by:

$$\delta \dot{Q}_{avg} = \left\{ \left( \frac{\partial \dot{Q}_{avg}}{\partial \dot{Q}_i} \delta \dot{Q}_i \right)^2 + \left( \frac{\partial \dot{Q}_{avg}}{\partial \dot{Q}_o} \delta \dot{Q}_o \right)^2 \right\}^{\frac{1}{2}} \quad (\text{D.25})$$

### D.4.9 Annulus Heat Transfer Coefficient

The mean annulus heat transfer coefficient is defined as:

$$h_o = \frac{\dot{Q}_o}{A_{so} \Delta T_{LMTD}} \quad (\text{D.26})$$

With the uncertainties obtained from:

$$\begin{aligned} \delta h_o &= \left\{ \left( \frac{\partial h_o}{\partial \dot{Q}_o} \delta \dot{Q}_o \right)^2 + \left( \frac{\partial h_o}{\partial A_{so}} \delta A_{so} \right)^2 + \left( \frac{\partial h_o}{\partial \Delta T_{LMTD}} \delta \Delta T_{LMTD} \right)^2 \right\}^{\frac{1}{2}} \\ &= \left\{ \left( \frac{1}{A_{so} \Delta T_{LMTD}} \delta \dot{Q}_o \right)^2 + \left( -\frac{\dot{Q}_o}{A_{so}^2 \Delta T_{LMTD}} \delta A_{so} \right)^2 \right\}^{\frac{1}{2}} \\ &\quad + \left( -\frac{\dot{Q}_o}{A_{so} \Delta T_{LMTD}^2} \delta \Delta T_{LMTD} \right)^2 \end{aligned} \quad (D.27)$$

A similar calculation is used for the local annulus heat transfer rate where all mean properties are substituted for local properties.

#### D.4.10 Physical Dimensions

All physical dimensions measured with a vernier caliper had uncertainties of 20 $\mu$ m (these included all diameter measurements). The larger dimensions measured with a measuring tape had uncertainties of 1mm (these included all dimensions measured along the axial length of the heat exchanger).

#### D.4.11 Hydraulic Diameter

The hydraulic diameter is defined as:

$$D_h = D_o - D_1 \quad (D.28)$$

With the uncertainties obtained from:

$$\begin{aligned} \delta D_h &= \left\{ \left( \frac{\partial D_h}{\partial D_o} \delta D_o \right)^2 + \left( \frac{\partial D_h}{\partial D_1} \delta D_1 \right)^2 \right\}^{\frac{1}{2}} \\ &= \{ (\delta D_o)^2 + (-\delta D_1)^2 \}^{\frac{1}{2}} \end{aligned} \quad (D.29)$$

#### D.4.12 Heat Transfer Area

The inner heat transfer area is defined by:

$$A_{si} = \pi D_i L_h \quad (D.30)$$

With the uncertainties obtained from:

$$\begin{aligned}\delta A_{si} &= \left\{ \left( \frac{\partial A_{si}}{\partial D_i} \delta D_i \right)^2 + \left( \frac{\partial A_{si}}{\partial L_h} \delta L_h \right)^2 \right\}^{\frac{1}{2}} \\ &= \{ (\pi L_h \delta D_i)^2 + (\pi D_i \delta L_h)^2 \}^{\frac{1}{2}}\end{aligned}\quad (\text{D.31})$$

Similarly for the outer heat transfer area:

$$\delta A_{so} = \{ (\pi L_h \delta D_1)^2 + (\pi D_1 \delta L_h)^2 \}^{\frac{1}{2}} \quad (\text{D.32})$$

### D.4.13 Inner Tube Cross Sectional Area

The cross sectional area is defined as:

$$A_i = \frac{\pi}{4} D_i^2 \quad (\text{D.33})$$

With the uncertainties obtained from:

$$\begin{aligned}\delta A_i &= \left\{ \left( \frac{\partial A_i}{\partial D_i} \delta D_i \right)^2 \right\}^{\frac{1}{2}} \\ &= \left( \frac{\pi}{2} D_i \delta D_i \right)\end{aligned}\quad (\text{D.34})$$

### D.4.14 Annulus Cross Sectional Area

The annulus cross sectional area is defined as:

$$A_o = \frac{\pi}{4} (D_o^2 - D_i^2) \quad (\text{D.35})$$

With the uncertainties obtained from:

$$\begin{aligned}\delta A_o &= \left\{ \left( \frac{\partial A_o}{\partial D_o} \delta D_o \right)^2 + \left( \frac{\partial A_o}{\partial D_i} \delta D_i \right)^2 \right\}^{\frac{1}{2}} \\ &= \left\{ \left( \frac{\pi}{2} D_o \delta D_o \right)^2 + \left( \frac{\pi}{2} D_i \delta D_i \right)^2 \right\}^{\frac{1}{2}}\end{aligned}\quad (\text{D.36})$$

### D.4.15 Reynolds Number

The Reynolds number in the inner tube is defined as:

$$Re_i = \frac{\dot{m}_i D_i}{A_i \mu_i} \quad (\text{D.37})$$

With the uncertainties obtained from:

$$\begin{aligned} \delta Re_i &= \left\{ \left( \frac{\partial Re_i}{\partial \dot{m}_i} \delta \dot{m}_i \right)^2 + \left( \frac{\partial Re_i}{\partial D_i} \delta D_i \right)^2 + \left( \frac{\partial Re_i}{\partial A_i} \delta A_i \right)^2 + \left( \frac{\partial Re_i}{\partial \mu_i} \delta \mu_i \right)^2 \right\}^{\frac{1}{2}} \\ &= \left\{ \left( \frac{D_i}{A_i \mu_i} \delta \dot{m}_i \right)^2 + \left( \frac{\dot{m}_i}{A_i \mu_i} \delta D_i \right)^2 + \left( -\frac{\dot{m}_i D_i}{A_i^2 \mu_i} \delta A_i \right)^2 + \left( -\frac{\dot{m}_i D_i}{A_i \mu_i^2} \delta \mu_i \right)^2 \right\}^{\frac{1}{2}} \end{aligned} \quad (\text{D.38})$$

A similar formulation is used for the Reynolds number in the annulus and given below:

$$\delta Re_{Dh} = \left\{ \left( \frac{D_h}{A_o \mu_o} \delta \dot{m}_o \right)^2 + \left( \frac{\dot{m}_o}{A_o \mu_o} \delta D_h \right)^2 + \left( -\frac{\dot{m}_o D_h}{A_o^2 \mu_o} \delta A_o \right)^2 + \left( -\frac{\dot{m}_o D_h}{A_o \mu_o^2} \delta \mu_o \right)^2 \right\}^{\frac{1}{2}} \quad (\text{D.39})$$

### D.4.16 Friction Factor

The friction factor in the annulus is defined as :

$$f = \frac{2D_h \Delta P \rho_o A_o^2}{L_{dp} \dot{m}_o^2} \quad (\text{D.40})$$

With the uncertainties obtained from:

$$\begin{aligned}
 \delta f &= \left\{ \left( \frac{\partial f}{\partial D_h} \delta D_h \right)^2 + \left( \frac{\partial f}{\partial \Delta P} \delta \Delta P \right)^2 + \left( \frac{\partial f}{\partial \rho_o} \delta \rho_o \right)^2 + \left( \frac{\partial f}{\partial A_o} \delta A_o \right)^2 \right. \\
 &\quad \left. + \left( \frac{\partial f}{\partial L_{dp}} \delta L_{dp} \right)^2 + \left( \frac{\partial f}{\partial \dot{m}_o} \delta \dot{m}_o \right)^2 \right\}^{\frac{1}{2}} \\
 &= \left\{ \left( \frac{2\Delta P \rho_o A_o^2}{L_{dp} \dot{m}_o^2} \delta D_h \right)^2 + \left( \frac{2D_h \rho_o A_o^2}{L_{dp} \dot{m}_o^2} \delta \Delta P \right)^2 + \left( \frac{2D_h \Delta P A_o^2}{L_{dp} \dot{m}_o^2} \delta \rho_o \right)^2 \right. \\
 &\quad + \left( \frac{4D_h \Delta P \rho_o A_o}{L_{dp} \dot{m}_o^2} \delta A_o \right)^2 + \left( -\frac{2D_h \Delta P \rho_o A_o^2}{L_{dp}^2 \dot{m}_o^2} \delta L_{dp} \right)^2 \\
 &\quad \left. + \left( -\frac{4D_h \Delta P \rho_o A_o^2}{L_{dp} \dot{m}_o^3} \delta \dot{m}_o \right)^2 \right\}^{\frac{1}{2}} \tag{D.41}
 \end{aligned}$$

#### D.4.17 Nusselt Number

The Nusselt number in the annulus is defined as:

$$Nu_{Dh} = \frac{h_o D_h}{k_o} \tag{D.42}$$

With the uncertainties obtained from:

$$\begin{aligned}
 \delta Nu_{Dh} &= \left\{ \left( \frac{\partial Nu_{Dh}}{\partial h_o} \right)^2 + \left( \frac{\partial Nu_{Dh}}{\partial D_h} \right)^2 + \left( \frac{\partial Nu_{Dh}}{\partial k_o} \right)^2 \right\}^{\frac{1}{2}} \\
 &= \left\{ \left( \frac{D_h}{k_o} \delta h_o \right)^2 + \left( \frac{h_o}{k_o} \delta D_h \right)^2 + \left( -\frac{h_o D_h}{k_o^2} \delta k_o \right)^2 \right\}^{\frac{1}{2}} \tag{D.43}
 \end{aligned}$$

#### D.4.18 Local Nusselt Number

The local Nusselt number is defined as:

$$Nu_{Dh,Local} = \frac{h_{o,Local} D_h}{k_{o,Local}} \tag{D.44}$$

With the uncertainties obtained from:

$$\begin{aligned}
 \delta Nu_{Dh,Local} &= \left\{ \left( \frac{\partial Nu_{Dh,Local}}{\partial h_{o,Local}} \right)^2 + \left( \frac{\partial Nu_{Dh,Local}}{\partial D_h} \right)^2 + \left( \frac{\partial Nu_{Dh,Local}}{\partial k_{o,Local}} \right)^2 \right\}^{\frac{1}{2}} \\
 &= \left\{ \left( \frac{D_h}{k_{o,Local}} \delta h_{o,Local} \right)^2 + \left( \frac{h_{o,Local}}{k_{o,Local}} \delta D_h \right)^2 + \left( -\frac{h_{o,Local} D_h}{k_{o,Local}^2} \delta k_{o,Local} \right)^2 \right\}^{\frac{1}{2}} \quad \text{(D.45)}
 \end{aligned}$$

The averaged local Nusselt numbers uncertainty is obtained from:

$$\delta Nu_{Dh,LocalAverage} = \sqrt{\frac{1}{7}} \delta Nu_{Dh} \quad \text{(D.46)}$$

### D.4.19 Summary

Table D.3 provides the uncertainties of the values discussed. The values for a heated and cooled annulus are provided. The uncertainties are calculated at a low  $Re_{Dh}$  and a high  $Re_{Dh}$ . Inner tube uncertainties are calculated at a low  $Re_i$  and high  $Re_i$ .

**Table D.3: Uncertainties of properties used to calculate heat transfer and friction factors for low and high Reynolds numbers.**

Property	Cooling		Heating	
	Low Re (Re = 15 000)	High Re (Re = 25 000)	Low Re (Re = 15 000)	High Re (Re = 25 000)
$\bar{T}_{ii}, \bar{T}_{io}, \bar{T}_{oi}, \bar{T}_{oo}$	0.053°C	0.053°C	0.053°C	0.053°C
$\bar{T}_{iw}$	0.075°C	0.075°C	0.075°C	0.075°C
$T_{ow}$	0.106°C	0.106°C	0.106°C	0.106°C
$\Delta T_i, \Delta T_o$	0.075°C	0.075°C	0.075°C	0.075°C
$\Delta T_{LMTD}$	0.272°C	0.172°C	0.121°C	0.043°C
$\Delta T_{LMTD,Local}$	0.738°C	0.738°C	0.738°C	0.738°C
$\dot{Q}_i$	0.086%	0.085%	0.103%	0.088%
$\dot{Q}_o$	0.086%	0.086%	0.104%	0.090%
$\dot{Q}_{avg}$	0.061%	0.061%	0.073%	0.063%
$\dot{Q}_{o,Local}$	0.502%	0.317%	0.119%	0.125%
$h_o$	0.222%	0.090%	0.105%	0.091%
$h_{o,Local}$	3.411%	6.966%	3.204%	4.071%
$D_h$	0.003%	0.003%	0.003%	0.003%
$A_{si}$	0.001%	0.001%	0.001%	0.001%
$A_{so}$	0.001%	0.001%	0.001%	0.001%
$A_i$	0.003%	0.003%	0.003%	0.003%
$A_o$	0.003%	0.003%	0.003%	0.003%
$Re_i$	1.003%	1.003%	1.003%	1.005%
$Re_{Dh}$	1.055%	1.017%	1.068%	1.021%
$f$	1.666%	1.571%	1.175%	0.727%
$Nu_{Dh,LMTD}$	2.019%	2.002%	2.003%	2.002%
$Nu_{Dh,Local}$	4.080%	7.493%	3.904%	4.668%